2012

Poverty Shelf, New Zealand from the Holocene to Present: Stratigraphic Development and Event Layer Preservation in Response to Sediment Supply, Tectonics and Climate

Lila Eve Rose Pierce
College of William and Mary - Virginia Institute of Marine Science

Poverty Shelf, New Zealand from the Holocene to Present: Stratigraphic Development and Event Layer Preservation in Response to Sediment Supply, Tectonics and Climate

---

A Dissertation

Presented to

The Faculty of the School of Marine Science

The College of William & Mary

In Partial Fulfillment

Of the Requirements for the Degree of

Doctor of Philosophy

By

Lila Eve Rose Pierce

2012

APPROVAL SHEET

This dissertation is submitted in partial fulfillment of
the requirements for the degree of

Doctor of Philosophy

Lila Eve Rose Pierce

Approved, by the Committee, August 2012

Steven A. Kuehl, Ph.D.
Committee Chair/Advisor

Elizabeth A. Canuel, Ph.D.

Courtney K. Harris, Ph.D.

James E. Perry, III, Ph.D.

Alan R. Orpin, Ph.D.
National Institute of Water & Atmospheric Research (NIWA)
Wellington, N.Z.

DEDICATION

To my wonderful family and amazing husband.
To run a marathon, you need the motivation to start and to finish.
Mom, Dad and Katie, you motivated me to hit the pavement and work hard.
Walter, you helped me keep on pressing, you made me laugh in the face of mental and physical adversity, and you motivated me to finish mile 26.2.

TABLE OF CONTENTS

CHAPTER 2

Modern Event Layers on the Waipaoa Continental Shelf: Characteristics, Preservation and Possible Modes of Initiation

CHAPTER 3

Event Layer Frequency, Characteristics and Preservation on the Waipaoa Continental Shelf Throughout the Holocene

ACKNOWLEDGEMENTS

First, I must thank Dr. H. Allen Curran, my undergraduate Smith advisor, for introducing me to Marine Geology! No turning back after an Al-led field trip to San Sal and the first time I dipped my head underwater with a snorkel. After that, traveling to Belize twice for my thesis was an incredible, life-changing experience. Thank you, Al!!! And also, thank you to Dr. Lisa Greer for being an unofficial undergraduate advisor – you were the person who recommended I apply to VIMS!

Of course, a huge thanks to my graduate advisor, Dr. Steven Kuehl, who has been a model scientist and teacher. He is the finest advisor and I know all others hold him as the epitome of a great mentor. He is also my yoga master and dear friend. Steve, thank you for showing me how to lash myself down to the deck to keep coring through gale force winds, for teaching me to be a broad-thinking scientist, for patiently editing and reminding me to say things only once ('cause I like to say things twice), and for adjusting my downward dog, for now it is a resting pose.

Dr. Alan Orpin has made an especially strong and much appreciated effort to be of assistance. He offers well-meaning critical advice, direction and suggestions that I hold in the highest esteem. His addition to my committee has not been hampered by us literally always being 180° of longitude apart. Thank you, Alan. You are just peachy!

I am indebted to the rest of my committee for guidance, suggestions and support. Drs. Elizabeth Canuel, Courtney Harris and James Perry, III, all of whom were on my MS thesis committee too, have been on this road with me from the beginning. Liz, your Marine Organic Geochemistry class was my favorite at VIMS. Courtney, your sage advice has really made me think about shelf circulation in expanded ways. Jim, although I'm not a biologist, you've provided extra time to me via a 698, and have motivated me to press on, always with a sense of humor.

With almost 8 years as a VIMSer, the number of people to thank for helping me seems almost as endless as writing one's dissertation. I would be in academic probational purgatory without the assistance of Cindy Hornsby, Cynthia Harris and Sue Presson. Seriously, I don't know what I'd do without you. Thank you.

I could not have sanely gotten through an M.S. and a Ph.D. without some freakin' incredible friends. Lynn, you are the Earth's example of friendship. You're my shoulder and ear, you bake tasty lemon bars, and thus are the best Bad Friend a girl could dream of having. Meg, Lisa, Sally and Heidi have provided strength, loving and realistic advice. Julia, Cielomar, and Mary supported me in and out of the lab. And to friends, old and new, Barry, Sharon and Ray (The Kid's Table), Tori and JC, Ann and Kevin, I say thank you. You have each supported me in a unique and wonderful way.

Thank you to my loving, caring and supportive family, who never tired of this lengthy process. Mom and Dad, you are my foundation. Katie, you are the coolest, bestest sis in the universe. To my Best Dog, Izzy, my stoic furry companion. It's crazy how much you've supported me in your doggieness. And of course, thanks to Ima, the nutjob dog who makes me laugh and Doug, the badass kitty.

And finally, to my brilliant, supportive, awesome husband, Walter, without whom I would literally be a mess. You've picked me up when I was down, you made me strong when I was weak, you've given me love with all your heart. You're holding my hand as we cross the finish line together. I love you.

LIST OF TABLES

LIST OF FIGURES

CHAPTER 3

ABSTRACT

The small, high sediment yield Waipaoa River is located on the tectonically active, mountainous Poverty Margin on the east coast of the North Island, New Zealand. In contrast to sedimentary sequences on passive margin shelves, active margins, such as the Poverty Margin, can preserve continuous records of changing geological and environmental conditions at the land-sea interface during rapid sea-level rise. Two subsiding mid-shelf basins on the Poverty Shelf contain thick transgressive sequences which provide a record of evolving river, climate, landscape, and oceanographic conditions since the Last Glacial Maximum (LGM).

This dissertation investigates the stratigraphic development of Poverty Shelf, including event layer preservation, over the last ~14ka using geochemical proxies and physical properties analyses of the sedimentary record. The work herein was conducted under the auspices of the MARGINS Source-to-Sink program, a multi-national, interdisciplinary study focused on understanding sediment routing, transformation and fate through the Waipaoa Sedimentary System (WSS) from catchment sources to final sinks on the adjacent Poverty Shelf and Slope. A suit of five giant piston cores and eight box cores were retrieved from Poverty Shelf during two cruises to address long (Holocene) and short (modern) timescales, respectively, of deposition. Geochronological, geochemical and sedimentological profiles from the giant piston cores are used to reconstruct the processes that influenced shelf infilling during this critical period of recent earth history. Accumulation rate analyses from high-resolution radiocarbon profiles and tephrachronology, along with X-radiographic facies analysis, enable tracking of rapidly shifting loci of deposition from the slope to mid-shelf depocenters. Grain size profiles and $\delta^{13}C$ values reveal sympathetic changes that track the waxing and waning influences of sediment supply via the Waipaoa River as sea level rose to maximum flooding at ~7ka, subsequent Poverty Bay shoreline reorganization and changing shelf accommodation, and, in the last ~1ka, a strong anthropogenic signal.

Imprinted upon this record is evidence for temporal and spatial changes in event layer frequency and type throughout the Holocene. Event layers may be produced by extreme and episodic storms, floods, earthquakes and other perturbative events that punctuate background marine sedimentation with large additions of terrestrial sediment. Event layers can be identified by unique textural and geochemical characteristics. An event layer, likely emplaced via hyperpycnal flow, attributed to Cyclone Bola (1988), the most severe modern cyclone on record in this location, serves as a modern benchmark for other storm events in the Poverty Shelf records. Examination of X-radiographs and lithostratigraphy, textural and isotopic variability reveal that the Poverty Shelf stratigraphic record preserves evidence of exceptional event sedimentation in the past and present that can be distinguished from shifts in supply, transport, and accumulation of sediments due to longer-time scale perturbations related to climate, sea level, and tectonics. A period of increased fidelity of the event record in the mid-Holocene is observed associated with increased accommodation within rapidly flooded depocenters.

AUTHOR'S NOTE

The primary research chapters in this dissertation were prepared for journal submission as listed below. Therefore, the chapters were written as stand-alone entities requiring some common background material. Appendices are inclusive for the entire dissertation.

Chapter 1:

Rose, L.E., Kuehl, S.A., Orpin, A.R., Alexander, C. R., Palmer, A.S. In Prep. Complete, High-Resolution Shelf Record of Changes in Sediment Supply, Eustacy, Tectonics and Climate from LGM-Present, Poverty Shelf, N.Z. ***Marine Geology***

Chapter 2:

Rose, L.E., and S. A. Kuehl. In Prep. Modern Event Layers on the Waipaoa Continental Shelf: Characteristics, Preservation and Possible Modes of Initiation. ***Continental Shelf Research Special Issue: Event Sediment Transport and Sedimentation: Insights from Measurements and Modeling***

Chapter 3:

Rose, et al. – Authorship TBD. In Prep. Event Layer Frequency, Characteristics and Preservation on the Waipaoa Continental Shelf Throughout the Holocene. ***Continental Shelf Research***

POVERTY SHELF, NEW ZEALAND FROM THE HOLOCENE TO PRESENT: STRATIGRAPHIC DEVELOPMENT AND EVENT LAYER PRESERVATION IN RESPONSE TO SEDIMENT SUPPLY, TECTONICS AND CLIMATE

CHAPTER 1

Complete, High-Resolution Shelf Record of Changes in Sediment Supply, Eustacy, Tectonics and Climate from LGM-Present, Poverty Shelf, N.Z.

Abstract

Geochronological, geochemical and sedimentological analysis of a suite of 5 giant piston cores from Poverty Margin off the Waipaoa River, New Zealand provide an unparalleled continuous record of changing geological and environmental conditions at the land-sea interface during rapid sea-level rise since the Last Glacial Maximum. Accumulation rate trends from high-resolution radiocarbon profiles and tephrachronology, along with facies analysis and $\delta^{13}C$ measurements, enable tracking of rapidly shifting depocenters from the slope onshore to tectonically controlled shelf depocenters. Shelf break and slope locations show a dramatic shift towards more ^{13}C-enriched (marine) values and finer texture after 12ka, reflecting the shift from shelf bypassing to shelf trapping during a rapid phase of sea-level rise that progressively shut down sediment supply to the outer shelf and slope. Two differentially subsiding mid-shelf basins, bordered on their seaward edge by emergent anticlines, subsequently record waning and waxing phases of Waipaoa River influence as sediment initially became trapped in a coastal embayment near the maximum transgression, followed by progressively increased bypassing to the shelf. A temporal offset in the phasing between the two basins of about 1ka reflects the role of differential subsidence and accommodation. The onset of El Niño-Southern Oscillation ca. 4ka is recorded as a pronounced coarsening in both shelf depocenters and is coincident with a distinct facies change. A strong anthropogenic signal is evident in the upper core sections as a reversal to fining upwards, reflecting a 6-fold increase in fine terrigenous input to the shelf. In contrast with sedimentary sequences in many passive margin settings, active margins such as the Poverty

Margin investigated herein can preserve continuous records of changing geological and environmental conditions at the land-sea interface during a rapid sea-level rise.

1. Introduction

Sedimentary sequences on continental margins develop as competing sedimentological, glacio-eustatic and tectonic drivers act with varying influence, spatially and temporally, on land and seascapes (Hedges and Keil, 1995; Rabouille et al., 2001; deHaas et al., 2002; Walsh and Nittrouer, 2009). Textural and geochemical proxies can be used to reconstruct the processes which have shaped present continental margins, however complete sedimentary sequences are rare on passive margin shelves since the Last Glacial Maximum (LGM) as a result of rapid sea level rise, associated shoreline transgression and reduction in sediment supply, all of which preclude development of a continuous record of rapidly changing earth and environmental conditions.

Active margins with high-yield rivers play a disproportionate role in supplying sediment and associated terrestrial carbon globally to the coastal ocean and continental shelf compared with passive margins (Milliman and Syvitski, 1992; Mulder and Syvitski, 1995; Lyons et al., 2002; Syvitski et al., 2005). Furthermore, tectonically-induced subsidence rates for active margins can be sufficiently high to enhance accommodation. Together, local subsidence and high sediment supply on active margins may result in a more complete stratigraphic record of Late Quaternary history, even during rapid sea-level rise, compared to passive margin settings (Lewis, 1973; Fleming et al., 1998; Prothero and Schwab, 1996; Gerber et al., 2010).

This study focuses on Poverty Margin, North Island, New Zealand (Figure 1) in an effort to extract high-resolution records of changing geological and environmental conditions at the land-sea interface since the LGM. High rates of sediment supply from the nearby Waipaoa River and dynamic climatic forcings coupled with continued accommodation space from active tectonic deformation renders it a prime location to examine temporal and spatial variations in relation to naturally and anthropogenically influenced environmental change. Several giant piston cores retrieved from Poverty Margin provide records useful for interpreting the complex interplay between sea level rise and evolving shelf accommodation during the Late Quaternary. Our main objective is to interpret the shift from slope- to shelf-dominated sediment dispersal while highlighting the competing controls of tectonic deformation, sediment supply and climate on strata formation and paleofacies environments on this active margin during this critical period of recent earth history.

2. The Poverty Margin: Geologic, Climatologic, and Tectonic Setting

The Poverty Margin lies at the boundary between the Pacific and Australian plates off the northeastern coast of New Zealand (Figure 1), where oblique subduction and mountain building combine with a vigorous temperate maritime climate to produce some of the highest sediment yields in the world (Walling and Webb, 1996; Hicks et al., 2000, 2004). The margin is within a zone of active deformation with ubiquitous faulting above a Neogene forearc basin (e.g., Lewis, 1980; Lewis and Pettinga, 1993), where subduction-related underplating drives uplift at an estimated rate of 3 mm y^{-1} (e.g., Reyners and McGinty, 1999). Coseismic deformation generated by large earthquakes produce numerous uplifted terraces on the East Cape (EC; Figure 1A), exposing Quaternary fluvial sequences and marine transgressive sequences (Ota et al., 1988; Berryman et al., 1989; Berryman, 1993; Berryman et al., 2000; Litchfield et al., 2010). Over the last 6ka five large magnitude earthquakes (>7.5) have been identified that impacted the Waipaoa Sedimentary System (WSS; Berryman, 1993; Brown, 1995). A major tectonic transition runs shore-perpendicular through Poverty Bay and across the Poverty Shelf, calculated from uplift rates in transgressive terrace deposits (Ota et. al., 1988; Brown, 1995). This "pivotal" zone between an eastern uplifting region and a western area of subsidence (Figure 1B) highlights the local tectonic complexity, which is presumably reflected in the nature of strata formation offshore during the Holocene. The proximity of the active Taupo Volcanic Zone (Figure 1), 120 km to the northwest, has resulted in the presence of numerous tephras punctuating the lacustrine and marine sedimentary records of the EC and provides excellent chronostratigraphic markers. Over the last 6ka at least seven known volcanic eruptions have emplaced tephras in the Poverty Bay region, including: Kaharoa, 0.636ka; Taupo, 1.717ka; Mapara, 2.075ka; Waimihia, 3.410ka; Whakatane, 5.530ka and Tuhua, 7.005ka (Alloway et al., 2007; Lowe et al., 2008). These tephras form strong, laterally continuous seismic reflections, that provide excellent chronostratigraphic control on the Poverty Shelf and Slope (Gerber et al, 2010; Carter et al, 2002; Orpin, 2004; Lowe et al., 2008).

In general, throughout the Quaternary, documentations of Indo-Pacific sea level rise and fall have been nearly synchronous with global observations (Suggate, 1990; Lui et al., 2004; Figure 1D). Since the Last Glacial Maximum (LGM) at

~24ka, global sea level has risen from a low of 125±5 meters below sea level (mbsl) to present highstand due to global reduction in ice volume (Fleming et al., 1998; Figure 1D). During the LGM, WSS sediments presumably bypassed the modern shelf, as the low stand shore line was near the location of the modern shelf break (now 150mbsl) and were deposited on the continental slope (Orpin et al., 2006; Alexander et al., 2010). Rates of post-glacial sea level rise for the Western Pacific show marked variability through time (Liu et al., 2004; Figure 1D). In New Zealand, sea level rapidly rose after the LGM (Suggate, 1990) and again 14ka (mwp-1a, Figure 1D) during the most intense period of late glacial warming, and decreased during the Younger Dryas (12-11ka, Figure 1D). Globally, the past 7ka years has a continuous and uniform rise of 3-5m (Fleming et al., 1998). For the EC, maximum transgression culminates between 8.7 and 5.5ka (Figure 1C), after which, the rate of sea level rise became more subdued (Ota et al., 1988) with essentially stable sea level for the last 4ka (Ota et al., 1988; Brown, 1995, Figure 1D, inset). Post-glacial warming, melting ice and sea level rise, caused greater connectivity of water masses and weakening of temperature gradients globally (Carter, 2001). In the Southwest Pacific, the Subtropical Convergence (STC), Antarctic Circumpolar Current (ACC), East Cape Current (ECC) and predominant Westerlies saw post-glacial reductions in strength, and pole-ward and landward movement of the ACC and ECC, respectively, however none of these shifts directly impacted or significantly changed circulation on the Poverty Margin; Holocene shelf and upper slope circulation off the Waipaoa River appears to have been similar to modern conditions (Carter et al., 2002; Figure 1A).

The Poverty Shelf is mantled with a post-glacial sedimentary sequence that exceeds 45m thickness in two prominent mid-shelf basins and a shelf break depocenter, underlain by a low stand erosional surface (Lewis, 1973; Foster and Carter, 1997; Gerber et al., 2010). These mid-shelf basins are constrained at their seaward edges by the emergent Lachlan and Ariel anticlinal ridges (Figure 1B; Foster and Carter, 1997; Orpin et al., 2006; Gerber et al, 2010) and are natural candidates for expanded post-glacial sequences. Basin fill in the Northern Depocenter exhibits progradational, seaward-dipping reflectors in seismic section (Gerber et al., 2010), indicating limited accommodation space, in contrast to reflectors from the Southern Depocenter which are concave-up, lapping onto the emergent Lachlan anticlinal ridge, suggesting subsidence has kept pace or exceeded supply.

The modern Waipaoa River has a sediment load of 13-15 X 10^6t yr^{-1} and is the main source of sediment to Poverty Shelf (Griffiths, 1982; Hicks et al, 2000). During normal fair-weather conditions, sediment enters Poverty Bay and becomes entrained in a counterclockwise gyre before reaching the shelf (Stephens et al., 2001; Brackley, 2010; Bever, 2010). Hyperpycnal flows, defined as those exceeding 40g L^{-1}, are produced at an estimated 40-year recurrence interval (Mulder and Syvitski, 1995; Hicks et al., 2004). Mean ambient shelf currents are to the northeast, presumably the extension of the Wairarapa Coastal Current (WCC; Chiswell, 2000). Shelf currents can be intensified by southern storm swell (Chiswell, 2000; Stephens et al., 2001). Seaward of the shelf break, on the Poverty Slope, mean currents are reversed as warm water from the Tasman Front and subtropical gyre flows to the south, forming the saline ECC (Carter, 2001; Carter et al., 2002; Chiswell, 2005; Figure 1A). The ECC meets cold, subantarctic water moving north at the Chatham rise, where both flows are deflected 90° and converge as the STC (Carter, 2001; Figure 1A).

Onset of El Niño-Southern Oscillation (ENSO) in Polynesia commenced ~4 ka evidenced in speleothems and peat-bogs in New Zealand record increasing wetness at this time (Hellstrom et al., 1998; McGlone and Wilmshurst, 1999). This period is associated with increased storminess and large-magnitude rainstorms that result in a transition to landsliding as the dominant form of hillslope erosion (Gomez et al., 2004). Previous studies on the East Coast of the North Island, including a late Holocene record from a single core on the continental shelf off the Waipaoa River (MD97 2122, Figure 1) and another located on the slope adjacent to Hawkes Bay, several hundred kilometers south of Poverty Margin, (MD97 2121; Carter et al., 2002) reveal low frequency, large magnitude signals related to glacio-eustatic sealevel, volcanism, increased erosion, storminess and intensification of ENSO ca. 4ka (Gomez et al., 2004).

A remarkable record of anthropogenic change through deforestation is also evidenced on the shelf in a fining-upwards signature after the first occurrence of Polynesian settlers ca. 0.5-0.7ka (Wilmshurst, 1997; Gomez et al., 2004; Gomez et al, 2007). Current Waipaoa sediment load is 15MT yr^{-1}, compared to an estimated pre-human load of 2.3MT yr^{-1} (Kettner et al., 2007; Gerber et al., 2010, Miller and Kuehl, 2010). Modern, rapid sediment supply is apparent from the presence of ^{7}Be in surface sediments shelf-wide and accumulation rates from ^{210}Pb geochronology of up to 0.59cm y^{-1} on the outer shelf (Miller and Kuehl, 2010; Rose and Kuehl, 2010). In modern sediments, three shelf facies are found that are radially distributed from the

Waipaoa Mouth, ranging from physically laminated nearshore sands to heavily bioturbated outershelf muds (Rose and Kuehl, 2010). Bulk density and radioisotopic (^{7}Be, ^{210}Pb) patterns delineate clear centers of deposition within two mid-shelf depocenters and on the shelf break (Miller and Kuehl, 2010; Rose and Kuehl, 2010).

3. Materials and Methods

3.1 Core Collection

In January-February 2006 aboard the R/V Marion DuFresne (MD), 7 giant piston "Calypso" cores (12.83-25.34m; Proust et al., 2006) were collected representing a cross section of shelf environments including: three distinct shelf depocenters (Northern, Southern and Shelf Break) and two slope basins, identified from a previous seismic reflection survey (Figure 1B). Five of these cores are discussed at length in this study (Figure 1B, Table 1). Onboard processing of MD cores included splitting and visual/digital logging of core properties (grain size, color, layering, contact types, incidence of wood/shells, etc.). Continuous down-core geophysical properties were measured using a Geotek® Multi-Sensor Core Logger (MSCL) and cores were then subsampled at a coarse resolution (every meter) for elemental and isotopic carbon.

Subsequent MD sediment processing in August 2007 included digital X-radiography, grain size analyses and collection of over 200 whole and large fragment gastropods, scaphopods and wood samples for ^{14}C dating. Macro- and microscopic tephra layers were detected with visual inspection of core halves, X-radiography and magnetic susceptibility profiles from MSCL. Glass shard analysis allowed for identification of Taupo, Waimihia and Whakatane tephras (performed by microprobe at Victoria University of Wellington, A.S. Palmer). Published data for marine cores ODP 181-1124 (Carter et al., 1999) and MD97-2121 (Carter et al., 2002; Alloway et al., 2007) from northeastern New Zealand report a robust, linear correlation between AMS-radiocarbon and tephra dates to core depth.

3.2 Radiocarbon

Radiocarbon ages for 94 samples were determined from 75 gastropod and scaphopod shells, 4 wood samples and 15 assemblages of foraminifera tests. Samples were kept frozen until sonified and washed prior to shipment to the Woods Hole NOSAMS facility and GNS Science Rafter Laboratory (New Zealand) for AMS analysis. All ages herein are in calibrated years before present (yr BP), using the MARINE09.14 calibration curve (Reimer et al., 2009) in CALIB Rev 6.0 (Stuiver et al., 1998), with a delta-R (-5) and delta-R standard deviation (57). Raw plots of age versus depth revealed 12 age reversals. Reversals were removed that could be attributed to the following: (1) two samples that were extremely close in age within the core (within the error of the ^{14}C) [3]; (2) a shell fragment that could not be relied upon as *in situ* [2]; (3) a date found for wood surrounded by only whole shells [2]; (4) two samples that were extremely close in depth [1]; and (5) core disturbance [1]. One sample fit both criteria 1 and 3. This left two reversals that can not be removed using the above criteria. These two were averaged for the sake of age model integrity.

3.3 Stable Carbon Isotopes

Stable carbon isotopes were used in this study to quantify the relative contribution of terrigenous and marine sources of organic carbon (Fry and Sherr, 1984; Hedges and Keil, 1995; Hedges et al., 1997). Bulk sediment samples from MD3003, MD3004, MD3006 and MD3007 (1cm in thickness) were collected and frozen onboard for carabon content and isotopic compositions (Tables 1 and 2, Figure 3). Frozen samples were dried, ground and acidified in muffled scintillation vials with 10% HCL for 4 days in random order. They were then redried and weighed into tin capsules previously rinsed with methanol. The UC Davis Stable Isotope Facility processed the samples using a continuous flow Isotope Ratio Mass Spectrometer (IRMS).

3.4 Grain Size

Down-core bulk-sample grain size was measured at 25cm intervals. Standard wet sieve and pipette methods were used to separate the sand, silt and clay fractions of each sample. The sand fraction (coarser than 63μm) was determined by wet-seiving at quarter-phi intervals, whereas the silt and clay fraction was determined using a Sedigraph® 5100, which relates x-ray beam attenuation in a settling cell to grouped size classification (performed at Skidaway Institute of Oceanography).

4. Results and Discussion

4.1. Age Model and Accumulation Rates

High-resolution age models for each core, based on a suite of 94 radiocarbon age dates and three distinct tephras, allowed us to examine variations in accumulation rates for the Poverty Shelf and Slope over the Late Quaternary. Trendline and "point-to-point" analysis of the radiocarbon ages provided smoothed and "instantaneous" accumulation rates, respectively (Figures 2A-D). Tephra ages allow an independent assessment of sedimentation rates over well-established age intervals (Figure 2E) and have been used previously across the margin to assess volumetric (Gerber et al., 2010) and vertical (Gomez et al., 2007) change. As described below, distinct changes in accumulation rates are observed over time, which are later interpreted with respect to variations in sediment supply, tectonics, and climate forcing.

Trendline analysis shows accumulation rate for the Slope Core (MD3003) is moderate at 0.14cm y^{-1} before 14ka, after which it decreases to a low and relatively uniform rate of ~0.06cm yr^{-1} to the present (Figure 2A). On the Shelf Break (MD3006) the opposite trend is observed, with relatively low accumulation of 0.06cm yr^{-1} before 7ka, followed by a four-fold increase in accumulation to ~0.28cm yr^{-1} over the mid-late Holocene (Figure 2A). The Southern Depocenter (MD3004) is characterized by a relatively steady accumulation rate throughout the Holocene (average of 0.14 cm yr^{-1}), with the exception of an uptick in accumulation rate between ~7-6ka (Figure 2B). By comparison, the accumulation rates are elevated in the Northern Depocenter (MD3007, MD3001) at 0.28-0.33cm yr^{-1} from 10ka through ~4ka, after which they decrease by a factor of two (Figure 2C).

Point-to-point accumulation rates were also determined to provide "instantaneous" record of sedimentation rate between adjacent radiocarbon ages (Figure 2D). This method allows us to distinguish periods of relatively high or low variability both within and between cores. Viewed from this perspective, accumulation at the Slope Core (MD3003) is similar to that of the average trendline - relatively uniform over time, with a slightly higher accumulation rate prior to 14ka. In contrast, dramatic swings in short-term accumulation rates for shelf cores (MD3001, MD3007, MD3004) indicate periods of highly variable or episodic sedimentation. Between 7-5ka, these cores are characterized by large fluctuations in accumulation rate from point-to-point, after which, both accumulation and variability decrease until the last 1ka, which shows a rapid rise in accumulation rate. Accumulation rates at the Shelf Break location (MD3006) generally trend upward from 7-4ka, after which they fall until just after 1ka, when a dramatic increase is seen in the most recent interval. Using the three prominent mid-late Holocene tephra layers (Whaketane, Waimahea, Taupo) found in the shelf cores (MD3004, MD3007, MD3006), the surface of each core and the depth at 10ka based on ^{14}C dating, accumulation rates over four time periods were determined: I) 10.0-5.5 ka (Pre-Whaketane tephra); II) 5.5-3.4 ka (Whaketane to Waimahea tephras); III) 3.4-1.7 ka (Waimahea to Taupo tephras); and IV) 1.7ka-present (Post-Taupo; Figure 2E). Compatible with trendline analysis, during pre-Whaketane (Period I), the highest accumulation rates for the Northern and Southern Depocenters (MD3007, MD3004) are recorded, while the lowest accumulation overall is measured at the Shelf Break (MD3006; Figure 2E). Decreasing accumulation rates are recorded in each subsequent time period in the Northern Depocenter (MD3007) to the present. In contrast, accumulation rate in the Southern Depocenter (MD3004) drops dramatically in Period II, and then gradually increases in Period III and IV. Shelf Break (MD3006) accumulation rates increase dramatically after Period I, falling slightly but remaining greater than 0.2cm yr^{-1} through the Holocene.

4.1.1 Interpretation of Accumulation Rates over Space and Time

Abrupt changes in trendline slopes provide information on the timing of important events and coincide with and highlight major shifts in sediment supply and accommodation on Poverty Shelf. On the slope (MD3003, Figure 2A), moderate accumulation rate (0.14cm y^{-1}) prior to 14ka (Figure 1D) reflects more proximal sedimentation when the coast was closer to the shelf break and rivers bypassed the present-day shelf depocenters. Following 14ka, as sea level rose and the shoreline rapidly retreated landward, supply to the slope decreased as observed accumulation rates are halved (to 0.06cm yr^{-1}). On the Shelf Break (MD3006, Figure 2A), the rapid shoreline retreat is also reflected in the low accumulation rate (0.06cm yr^{-1}). As the shoreline retreated behind the emergent anticlinal ridges (mwp-1a, Figure 1D), sediment trapping in the Northern and Southern Depocenters dramatically reduces the sediment supply offshore. After the maximum transgression at 7ka, Shelf Break accumulation rates increase by a factor of four to 0.28cm yr^{-1}, heralding the regressive phase and progradation of the Poverty Coast with concomitant sediment bypassing to the outer shelf. Higher accumulation rates at the Shelf Break following the maximum transgression are also clearly evident in the point-to-point and tephra-derived accumulation rates (Figure 2 D-E).

Accumulation rates derived from trendline and tephra data show that the Southern Depocenter (MD3004; Figure 2B) experiences a relatively steady rate of basin infilling (0.12-0.16 cm yr^{-1}) throughout the Holocene. A single exceptional increase ca. 7ka to 0.41cm yr^{-1} that persists for ~1ka is prominent in the trendline data (Figure 2B), and probably also explains the relatively higher accumulation rate represented in Period I (Figure 2E). This peak in accumulation could be the result of major earthquake activity (subsidence and/or increased catchment erodability) and/or increased erosion due to volcanic activity; the oldest terraces found in the region date to ca. ~7ka, and a major eruption occurred ca. 7ka (Tuhua tephra), both of which could increase sediment supply. On the whole, accumulation rates in the Southern Depocenter (MD3004) show that accommodation has not been outpaced by supply, supported by seismic evidence which shows onlapping reflectors over the emergent Lachlan anticline, which flanks the outer Southern Depocenter (Gerber et al., 2010).

In contrast to the Southern Depocenter, the Northern Depocenter (MD3001, MD3007, Figure 2C) shows a progressive decrease in sediment accumulation rate after the mid-Holocene, suggesting either sediment supply or accommodation space was also simultaneously decreasing (Figure 2E). The decrease is particularly dramatic after 4ka, when trendline accumulation rates decrease from between 0.28-0.33cm yr^{-1} to 0.07-0.09cm yr^{-1}. If insufficient accommodation existed, as suggested by Gerber et al. (2010), lower accumulation rates would be expected as water depths shoal and the depositional loci shift away from the Northern Depocenter. Taken together, these observations suggest differential shelf infilling caused by tectonically controlled accommodation space. Three distinct tectonic zones mapped by Ota et al. (1988) and Brown (1995) show a pivotal zone bisecting Poverty Flats and presumably continuing offshore (Figure 1B), separating areas of uplift in the north from subsidence in the south. This is further supported by isopachs showing greater Holocene thickness offshore (Figure 1B; Gerber et al., 2010).

Point-to-point accumulation rates in both the shelf depocenters reveal a dramatic shift after ~4.5ka from a period of high variability to one of lower variability (Figure 2D). After this transition, accumulation rates for the Shelf Break (MD3006) increase as the accumulation rates in the Northern and Southern Depocenters decrease (Figure 2A-D). The cause(s) for these shifts are unclear, but may be related to a combination of infilling and oceanographic changes. Increasing storm intensity with the onset of ENSO along with shoaling of the depocenters together would effectively enable more frequent disturbance of seafloor sediment by energetic waves and currents. Because wave energy decreases with depth, this may have increased the dispersion of sediment offshore via winnowing and resuspension. Also, more frequent resuspension on the innershelf and nearshore could act to reduce the preservation of river flood pulses there, helping to explain the reduced variability in point-to-point accumulation rates for the Southern and Northern Depocenters. All Poverty Shelf cores show an increase in point-to-point accumulation rate in the recent past (< 0.5ka), clearly coinciding with known human disturbance and associated ~6-fold increase in sediment supply from the Waipaoa watershed.

Previous results reported from MD2122 (Figure 1B) reveal rates of vertical accumulation for tephra time periods II, II and IV within the same order of magnitude as our results (Figure 2E; Gomez et al., 2004). MD2122 is situated between the three primary Poverty Shelf basins, at the nose of the Lachlan Anticline in an area of modern sediment bypassing (Orpin et al., 2006). Unlike our cores, no obvious trend in accumulation between tephra time periods is observed for MD2122, perhaps because it was located furthest from areas of high accumulation over the mid- to late-Holocene.

4.2 Poverty Shelf Facies

Downcore facies changes in all shelf cores were qualitatively determined based on X-radiograph descriptions, including primary structures, extent of structure preservation, degree of mottling and shell occurrence. After visual identification of facies, average geochemical and textural properties were calculated for each facies (Table 2). Four dominant facies are identified on the Poverty Shelf, although not all facies are present in each core, each of which is described below and summarized in Table 2, with X-radiographic examples in Figure 4.

4.2.1 Facies 1

Facies 1 is characterized by a high degree of bioturbation, with most primary layers partially or almost completely obliterated. This is the most recent facies and is present on the shelf in the Northern and Southern Depocenters, extending from modern surface sediment to ~3.5ka (Table 2, Figure 4A). Facies 1 is the result of syn- and post-depositional biological processes which rework and partially obscure physically emplaced layers on the seabed. X-radiographs from the Northern Depocenter show that this facies is relatively uniform in character, while X-radiographs are more variable in the Southern Depocenter, which exhibits better preservation of primary structure. Facies 1 has the highest sand content (nearly 50%) of all facies on the shelf, possibly due to reworking of tephras. However, during the Late Holocene, as the shelf shoaled with continued infilling, wave resuspension of fines and bypassing likely aided in producing the coarse texture of Facies 1. Furthermore, there is a difference of 1phi between the mean grain size of the Northern and Southern Depocenters; the Southern Depocenter being coarser (Table 2). Model simulations have shown that during storm conditions, Waipaoa River plume may switch to a more southerly route (Bever, 2010). The higher sand content within Facies 1 in the Southern Depocenter is consistent with this explanation. Isotopic carbon signatures in the Southern Depocenter also confirm this interpretation, as $\delta^{13}C$ is significantly more depleted than in the Northern Depocenter, providing further evidence that more terrestrial material was sequestered in the Southern Depocenter over the last 4ka, than in the Northern Depocenter.

In the Northern Depocenter, the Facies 1 lower boundary corresponds to a marked decrease in accumulation rate ~4ka (MD3007, MD3001; Figure 2A). A similar change in trendline slope is not seen in the Southern Depocenter, which displays relatively steady sediment supply and corresponding accumulation throughout the Holocene (Figure 2B). The age of the base of Facies 1 corresponds to the onset of ENSO intensification in the Indo-Pacific, and despite differences between the north and south, both exhibit increased sand content in Facies 1 (Table 2), which is consistent with the idea that ENSO intensification brought increased erosion and intensified shelf circulation.

4.2.2 Facies 2

Facies 2 underlies Facies 1 (Table 2), and is characterized by intact to partially intact primary structures such as physical layers and laminations as well as significant biogenic disturbance such as burrows, tubes, and mottling (Figure 9B). Cross-bedding is observed within thicker sandy laminae and thick units (>1cm) comprised of high-density material rhythmically inter-bedded with low density units. Degree of primary sedimentary structure preservation is much higher than in Facies 1. Fully or partially preserved sandier, high-density layers in this facies may indicate periods of increased sediment discharge, enhanced bottom currents, and/or storm layers.

The base of Facies 2 corresponds roughly with the timing of maximum transgression, so this facies records a transitional period during which trapping was enhanced, basin-fill progressed and the Poverty Bay shoreline advanced (Wolinski et al., 2010). High and quite variable point-to-point accumulation rates are observed throughout this time period, possibly influenced by shifting loci of deposition that would have also encouraged preservation of structure (Figure 2D). A major relative increase in accumulation is recorded in the Southern Depocenter (MD3004; Figure 2B). Geochemically, sediments in this facies are similar in $\delta^{13}C$ relative to Facies 1, revealing a strong terrestrial component. In all cores, Facies 2 is significantly finer overall (>0.7 phi units), with less than half the sand content of Facies 1. Multiple causes could produce this - limited sand input due to trapping in Poverty Bay or infrequent storminess, a less energetic wave regime on the shelf or at the coastline (Bever, 2010), and deeper water depth.

4.2.3 Facies 3

Facies 3 is the oldest facies retrieved from MD3004 and MD3001, found between ~6800ka before present to the base of each core, and the second oldest from MD3007, where it terminates at 9.5ka (Table 2). It is also the main facies present at the Shelf Break Depocenter (MD3006). Facies 3 is comprised of mainly homogeneous, mottled and bioturbated muds resulting in near complete destruction and loss of any visible primary physical sedimentary structures (Figure 4). Evidence of bioturbation includes burrows and burrow remnants and tubes, which create a mottled character. The most frequent burrows are of a distinct ichnofabric seen exclusively in Facies 3, described by irregular, curved and kinked thin, high bulk density burrows (Figure 4, inset). In other portions of this facies, mottles aren't present and X-radiographic images show homogeneous mud, with these same few burrows randomly distributed. High and steady sediment accumulation is recorded on the shelf during Facies 3 development, precluding a low accumulation/high bioturbation scenario (Figure 2A-C), and it is finer grained than all other shelf facies. Within both depocenters, a fining signature is recorded as Facies 3 develops (Figures 3D and 3E) and the $\delta^{13}C$ signature of sediments within Facies 3 is the most ^{13}C-enriched of all facies, indicative of a more marine-dominated carbon input.

The time period represented in Facies 3 coincides with the most rapid Holocene sea level rise and shoreline transgression on the Poverty Shelf (Figure 1C), when the margin was starved of coarse material as the proto-Poverty Bay shoreline retreated and course material was trapped within the growing Waipaoa embayment (Figure 1D). No scour, erosion surface or truncate bedding is visible in X-radiographs of Facies 3, indicating an environment less frequently disturbed by storm conditions. During development of Facies 3, sea level rose ~30m (Figure 1C) and using an average shelf accumulation rate of 0.25cm yr^{-1} (Figure 2 A-C) over the time period 11.8-6.4ka (Table 2), approximately 14m of sediment may have accumulated. Although tectonic history is speculative, using the highest recorded yearly modern uplift of 0.04cm it is possible that there has been uplift on the order of ~5m since the beginning of Facies 3. Relative sea level, then, was deeper on the shelf than present day and climate was overall less stormy (pre-ENSO) then present; Facies 3 is thus depauperate of evidence of storm resuspension, reworking or winnowing suggesting that it was likely deposited below the mud-activating storm weather wave base, which has been shown by Wood et al. (2006) to be ~50m at present.

4.2.4 Facies 4

This facies is found at the deepest portion of the Shelf Break (MD3006) and Northern Depocenter (MD3007) cores, below 11.8ka and 9.5ka, respectively (Table 2). Facies 4 is characterized by highly bioturbated muds with remnant lenticular layers that display wavy and diffuse contacts as well as high and low density laminae with sharp contacts (Figure 4) and is significantly coarser than Facies 3 (by 3 phi in

MD3006), directly above it, although percent sand is relatively similar (Table 2B). It is more terrestrial in nature by as evidenced by $\delta^{13}C$ values that are depleted by more than 0.5‰ at both core sites (Table 2B). Another striking characteristic is that in the shelf break location shell and shell fragments were found concentrated at the bottom of the core; 71% of all shell and shell fragments in the core were found below 9.89ka, or the oldest 13% of the core. This facies is indicative of a shallow water environment, and representative of rapid sedimentation from a source position that must be changing in response to eustacy; it corresponds stratigraphically to a period of rapid short bursts in sea level rise from ~100mbsl 14.5ka to ~35mbsl 9.5ka (Fleming et al., 1998; Figure 1D). As such, we suspect this facies represents the transgressive deposits formed when the Waipaoa River mouth shifted from a shelf break locality to landward of the modern Ariel and Lachlan Anticlines.

4.3 Strata Development During the Last 14ka

Sediment accumulation rates, textures, bulk sediment $\delta^{13}C$, and facies progression from the five giant piston cores from the Poverty Margin reveal dramatic and coherent changes over the Late Quaternary in response to sea level and climate change, sediment supply from marine and terrestrial sources, tectonic activity, and land-use practices as discussed below.

4.3.1 Late Pleistocene – Early Holocene

During the LGM, sea level was at ~120mbsl, nearly at the modern shelf break, and riverine sediment from the Raukumara Peninsula presumably bypassed the modern shelf (Figures 1A, B and D). At this time, the STC (shaded gray, Figure 1A) was strengthened and located north relative to its present-day intensity and position, closer to (but still south of) Poverty Margin (Nelson et al., 2000; Carter, 2001). Sediments debouched onto the modern slope through a network of upper-slope gully systems and incised submarine canyons located on the Poverty Margin and were captured in slope basins and fans (Lewis et al., 1998; Orpin et al., 2006; Alexander et al., 2010). As glacial melting commenced, sea level rose episodically in the Western Pacific (Figure 1D; Lui et al., 2004 and references therein). The Slope Core (MD3003) has relatively coarse sediment (average of 5.5 phi, solid vertical black bar) and high textural variability before ~13ka (Figure 3B) reflective of episodic turbidite deposition and characteristic of LGM sediments. Prior to 14ka, the Slope Core also has an enhanced terrestrial $\delta^{13}C$ component and higher accumulation than elsewhere in this core, further indication that it received more proximally sourced terrestrial sediments during lowstand conditions. After this period, accumulation decreased considerably and remained low through the mid-to-late-Holocene. Other investigators noticed a similar decrease in accumulation from a deep sea core (P69) collected offshore of the southern North Island which they attributed to pole-ward contraction of strong westerly winds and associated aeolean transport of sediment at ~14.7ka (Stewart and Neall, 1984; Figure 1A). Aeolian dust likely played a role in transport of sediment to P69, positioned several hundred kilometers to the South, deeper (>2000m water depth) and further offshore than MD3003. However, atmospheric circulation is not likely the main contribution of sediment to Poverty Slope as it received direct input from the point-source of the proto-Waipaoa in the

Late Quaternary. At 14.7ka, when the sediment record fines in both our MD3003 and P69, Western Pacific sea level rose abruptly from ~100mbsl to 70mbsl (Figure 1D, mwp-1a). Given that compared to P69, the Slope Core (MD3003) is located in shallower water, closer to land, has a direct riverine sediment source, and is farther from the STC, we favor the simpler explanation that sea level rise and shelf trapping can explain the observed trends.

Large quantities of shell material preserved within Facies 4 in the Northern (MD3007) and Shelf Break (MD3006) Depocenters between 14.7 and 9.5ka, along with highly depleted $\delta^{13}C$, similar to the trend seen in the Slope Core (3003), indicate deposition in a shallow water environment with a proximal terrestrial source. A dramatic fining from silt- to clay-size texture occurs after about 13ka in the Slope Core when mean grain size decreases to 5.5 to 7.8 phi in the upper core section (Figure 3B). The likely cause is an abrupt Late Pleistocene (~14ka) acceleration in sea level rise from when the coastline went from ~100mbsl to ~79mbsl which flooded the shelf and encouraged trapping of coarse sediment (Figure 1D; i.e., mwp-1a; Suggate, 1990; Liu et al, 2004). A similarly significant, yet more gradual, textural shift occurs at the Shelf Break Depocenter, fining from an average of 4.8 to 7.8 phi after 12ka, correlating with mwp-1b (Figures 1D, 3C). During the rapid rise in sea level from ~12ka to the early Holocene at 30mbsl (Fleming et al., 1998), the shoreline offshore of the Waipaoa would have likely withdrawn landward of the Ariel and Lachlan anticlines (which presently both outcrop at ~50mbsl), shifting the locus of river sediment deposition from the present-day outer shelf and slope to the inner shelf. Accumulation rates decreased markedly and remained low on the slope after

14.5ka and remain low at the shelf break location (0.06cm yr^{-1} in both locations, Figure 2A). As transgression progressed, bulk sediment $\delta^{13}C$ for the Slope and Shelf Break reveal abrupt gross enrichments, shifting more than 1.5‰ towards marine signatures on the Slope (15ka) and 1‰ on the Shelf Break (~11ka). Terrestrial input to the outer shelf and slope would rapidly decrease with increased nearshore trapping as sea level continued to rise; inner shelf basin fill presumably accelerated at this point.

4.3.2 Shelf Inundation to Maximum Flooding

After 11ka, a continued shift towards more enriched (marine sourced) $\delta^{13}C$ in Slope (MD3003) and Shelf Break (MD3006) sediments occurs and can be tracked in the progression from Facies 4 through Facies 3 (Figures 3A, B, D, and E and Table 2) as the shoreline moved landward during transgression. The Shelf Break Depocenter shows continued and progressive fining to ~7ka. This suggests that the reduction of terrestrial input occurred more gradually here than at the location of the Slope Core, which is reasonable given its proximity to the river mouth and location seaward of the gap between the outer shelf anticlines. At 10ka, Southern Depocenter (MD3004) sediments have a significantly enriched marine $\delta^{13}C$ signature in comparison to the Northern Depocenter (MD3007), perhaps indicating that the Southern Depocenter was positioned further from the proto-Waipaoa River mouth.

A fining upwards signature in shelf depocenters from the base of the Holocene tracks the progress of sea level rise with progressively greater trapping of coarse material in the proto-Poverty Bay. At maximum flooding the Waipaoa mouth was situated at its furthest inland position, 12km landward of the present shoreline, and a large protected embayment occupied the modern Waipaoa River floodplain in an area now known as Poverty Bay flats (Brown, 1995; Figure 1C). The maximum fining in the Southern and Northern Depocenters show a temporal offset, peaking at 6.7 and 7.8 ka, respectively, implicating differential tectonic accommodation or infilling while the rate of sea level rise became more subdued on the East Cape (Ota et al., 1998; Figures 4D and E). Both the Southern and Northern Depocenters (MD3004, MD 3007) have highly enriched $\delta^{13}C$ signatures up to maximum flooding, roughly 7ka, with the Southern Depocenter consistently displaying a slightly more enriched signature (Figures 3A, D, and E). Depocenter sediment $\delta^{13}C$ values become increasingly terrestrial in nature after 7ka.

4.3.3 Prograding Shoreline and Sea Level Stabilization

The transgressive fining trend in the midshelf depocenters reverses after maximum flooding and textures show progressive coarsening upwards until ~3.5ka (Figure 3D and E). As the rate of sea level rise slowed after 7ka, Poverty Bay flats developed, trapping Waipaoa River sediments within the elongated estuary created as the river valley was infilled. The trapping efficiency waned towards the present as the embayment was infilled, modern Poverty Bay shoreline developed, and sediments bypassed to the shelf in progressively greater quantities with time. Consistent with this scenario, the $\delta^{13}C$ record from the inner shelf depocenters (Figure 3 D and E) is dominated by marine signatures (~ -24‰) in the early Holocene sections of the cores before about 7ka. Following ~7ka, bulk sediment $\delta^{13}C$ values become highly depleted, indicative of a burgeoning terrestrial input.

As shoreline regression ensued, Northern (MD3007) and Southern (MD3004) Depocenter accumulation rates were high (Figure 2B, C). This signal is enhanced at the Shelf Break Core (MD3006), where, after maximum transgression, accumulation increases 2-3 times (Figure 2A). Interestingly, in both Facies 3 and Facies 2, the Southern Depocenter is always coarser and has higher percent sand than in the Northern Depocenter. This suggests that coarse sediment flux, likely associated with storm events, from the Waipaoa favored a southern route, similar to modern circulation and sediment transport regimes (Bever, 2010). The shift to more terrestrially sourced $\delta^{13}C$ in the Southern Depocenter is also more pronounced and has a greater range after maximum transgression in comparison to the Northern Depocenter (Figures 3D and 3E), suggesting disproportionate transport of terrestrial material to the south. It follows that higher signal fidelity in the South and/or enhanced signal destruction/less sediment retained in the North is possible, especially as the transition to an "overfilled" Northern Depocenter is approached at the end of Facies 2. Increased preservation of primary structures in Facies 2 (~7ka to ~ 3.5ka, Table 2) provides evidence that more events were captured during this phase of enhanced shelf infilling. The Southern Depocenter is also deeper and more sheltered than the Northern Depocenter, decreasing the likelihood that preferential reworking or removal of fine sediments from the Southern Depocenter is a possible mechanism for the observed trends.

4.3.4 4ka to Present – ENSO and Anthropogenic Influences

In both the Southern Depocenter (MD3004) and Northern Depocenter (MD3007) the coarsening trend that began after maximum transgression (~7ka), abruptly intensifies after ~4ka. This near-synchronous textural signal results in an increase in mean particle size of about 1 phi unit. In the Southern Depocenter this coincides with an enrichment of $\delta^{13}C$ values, indicating an increasing marine influence, with a peak at ~1ka. Sea level remains constant within this time period (Figure 1D). Previous studies of marine and terrestrial cores from the East Coast of the North Island postulate a link between prominent coarsening after 4ka and landscape erosion and climate change from the Mid-Holocene due to ENSO (Gomez et al., 2004, 2007). The soil mantle in the Waipaoa catchment contains little clay and is not extensively weathered (Preston and Crozier, 1999), therefore they postulate that increased landsliding liberates a preponderance of silt and sand relative to other hill slope erosion processes such as gullying and deep-seated earth-flows (which generate finer material), implicating a climate-enhanced textural coarsening.

The transition between Facies 2 and Facies 1 on the shelf coincides with ENSO intensification at 4ka, corroborating climate change, in the form of textural changes, as the primary cause for this final facies progression. Interestingly, there is no increase in accumulation rates corresponding to the onset of ENSO (Figure 2D) and no X-radiographic evidence of increased storm event preservation during this time. In fact, the highest accumulation rates in the depocenters correspond to the time period prior to 4ka, the most variability in accumulation is found within Facies 3 between ~9-5ka, and the greatest incidence of layer preservation is found within

Facies 2, all well before the onset of ENSO (Table 2, Figure 4). In the Northern Depocenter, a 4-fold decrease in accumulation rate, commencing at ~4ka, is recorded (0.28 to 0.07cm yr^{-1} in MD3007 and 0.33 to 0.09cm yr^{-1} in MD3001, Figure 2C), which clearly supports the "overfilled" scenario as described previously, corroborated by seismic reflection studies (Gerber et al., 2010). While, the Southern Depocenter does not appear to be accommodation-limited, there is no increase in accumulation as might be expected associated with ENSO-related erosion and increased sediment supply.

We suggest that changes in oceanographic conditions associated with the onset of ENSO are the main drivers for textural and isotopic observations on Poverty Shelf, not increases in climate-associated delivery from the landscape. More energetic conditions (i.e., storms) brought on by ENSO could drive the observed trends in coarsening (Figure 3D and E, Table 2). As the carbon signature is largely contained within the fine sediment fraction (Keil et al., 1997), we suggest that the ^{13}C-enriched $\delta^{13}C$ values consequently reflect a lower relative input of terrestrial fines (rather than an increase in the absolute contribution of marine sediment). In addition, increased marine productivity may also influence the $\delta^{13}C$ enrichment, as nutrient flux presumably intensified post-ENSO onset.

A major textural and isotopic excursion is recorded in the Northern and Southern Depocenters between 1 and 0.5ka (Figures 3D and 3E). This abrupt fining and reversal to significantly more terrestrially sourced $\delta^{13}C$ reflects the massive influx of fine river sediment following changes in landscape erosion and sediment supply linked with human habitation of the Waipaoa watershed. A fining in texture is also seen in the Shelf Break Core, albeit less dramatic than seen in shelf depocenters (Figure 3C). Large-scale removal of the native forest and conversion to pasture has dramatically changed hill slope erosion processes, especially since European habitation when gulley erosion became the dominant control on sediment production resulting in a dramatic increase in fine sediment supply by the river (Wilmshurst, 1997; Gomez et al., 2004). All shelf records record an increase in point-to-point accumulation rates post 1ka (Figure 2D).

Literature Cited

Alexander, C.R., Walsh, J.P., Orpin, A.R. 2010. Modern sediment dispersal and accumulation on the outer Poverty continental margin. *Marine Geology*, 270: 213-226.

Alloway, B.V., Lowe, D.J., Barrell, D.J.A., Newnham, R.M., Almond, P.C., Augustinus, P.C., Bertler, N.A.N., Carter, L., Litchfield, N.J., McGlone, M.S., Shulmeister, J., Vandergoes, M.J., Williams, P.W., NZ-INTIMATE members. 2007. Towards a climate event stratigraphy for New Zealand over the past 30,000 years. *Journal of Quaternary Science*, 22: 9-35.

Berryman, K. 1993. Age, height, and deformation of Holocene marine terraces at Mahia Peninsula, Hikurangi Subduction Margin, New Zealand. *Tectonics*, 12: 1347-1364.

Berryman, K.B., Marden, M., Eden, D., Mazengarb, C., Ota, Y., Moriya, I. 2000. Tectonic and paleoclimatic significance of Quaternary river terraces of the Waipaoa River, east coast, North Island, New Zealand. *The New Zealand Journal of Geology and Geophysics*, 43: 229-245.

Berryman, K.B, Ota, Y., Hull, A.G. 1989. Holocene paleoseismicity in the fold and thrust belt of the Hikurangi subduction zone, eastern North Island, New Zealand. *Tectonophysics*, 163: 185-195.

Bever, A. 2010. Integrating Space-and-Time-Scales of Sediment Transport for Poverty Bay, New Zealand. Ph.D. Dissertation, College of William and Mary. 262 pp.

Brackley, H.L., Blair, N.E., Trustrum, N.A., Carter, L., Leithold, E.L., Canuel, E.A., Johnston, J.H., Tate, K.R. 2010. Dispersal and transformation of organic carbon across an episodic, high sediment discharge continental margin, Waipaoa Sedimentary System, New Zealand. *Marine Geology*, 270: 202-212.

Brown, L.J. 1995. Holocene shoreline depositional processes at Poverty Bay, a tectonically active area, Northeastern North Island, New Zealand. *Quaternary International*, 26: 21-33.

Carter, L. 2001. Currents of change: the ocean flow in a changing world. *NIWA Water and Atmosphere*, 4: 15-17.

Carter, R.M., McCave, I.N., Richter, C., Carter, L., shipboard party. 1999. Leg 181 Summary: southwest Pacific paleoceanography: Proceedings of the Ocean Drilling Program, Initial Reports Vol. 181. Including original data from ODP Janus Web Database: www-odp.tamu.edu/publications/181_IR/181ir.htm.

Carter, L., Manighetti, B., Elliot, M., Trustrum, N., Gomez, B. 2002. Source, sea level and circulation effects on the sediment flux to the deep ocean over the past 15 ka off eastern New Zealand. *Global and Planetary Change*, 33: 339-355.

Chiswell, S.M. 2000. The Wairarapa Coastal Current. *New Zealand Journal of Marine and Freshwater Research*, 40: 303-315.

Chiswell, S.M. 2005. Mean and Variability in the Wairarapa and Hikurangi Eddies, New Zealand. *New Zealand Journal of Marine and Freshwater Research*, 39: 121-134.

Fleming, K., Johnston, P., Zwartz, D., Yokoyama, Y., Lambeck, K., Chappel, J. 1998. Refining the eustatic sea-level curve since the Last Glacial Maximum using far- and intermediate-field sites. *Earth and Planetary Science Letters*, 163: 327-342.

Foster, G. and L. Carter. 1997. Mud sedimentation on the continental shelf at an accretionary margin – Poverty Bay, New Zealand. *New Zealand Journal of Geology and Geophysics,* 40: 157-173.

Fry, B. and E.B Sherr. 1984. ^{13}C Measurements as indicators of carbon flow in marine and freshwater ecosystems. *Contributions In Marine Science*, 27: 13-47.

Gerber, T., Pratson., L., Kuehl, S., Walsh, J.P., Alexander, C., Palmer, A. 2010. The influence of post-glacial sea level rise and tectonics on sediment storage along the high-sediment supply Waipaoa continental shelf. *Marine Geology*, 270: 139-159.

Gomez, B., Carter, L., Trustrum, N.A., Palmer, A.S., Roberts, A.P. 2004. El Nino – Southern Oscillation signal associated with middle Holocene climate change in intercorrelated terrestrial and marine sediment cores, North Island, New Zealand. *Geology*, 32: 653-656.

Gomez, B., Carter, L., Trustrum, N.A. 2007. A 2400 yr record of natural events and anthropogenic impacts in intercorrelated terrestrial and marine sediment cores: Waipaoa sedimentary system, New Zealand. *Geological Society of America Bulletin*, 119: 1415–1432.

Griffiths, G.A. 1982. Spatial and temporal variability in suspended sediment yields of North Island basins, New Zealand. *Water Resources Bulletin,* 8: 575-583.

de Haas, H., van Weering, T.C.E., de Stigter, H. 2002. Organic carbon in shelf seas: sinks or sources, processes and products. *Continental Shelf Research*, 22: 691-717.

Hedges, J.I. and R.G. Keil. 1995. Sedimentary organic matter preservation: an assessment and speculative synthesis. *Marine Chemistry*, 49: 81-115.

Hedges, J.I., Keil, R.G., Benner, R. 1997. What happens to terrestrial organic matter in the ocean? *Organic Geochemistry*, 27: 195-212.

Hellstrom, J., McCulloch, M., Stone, J. 1998. A detailed 31,000-year record of climate and vegetation change from the isotope geochemistry of two New Zealand speleothems. *Quaternary Research*, 50: 167-178.

Hicks, D.M., Gomez, B., Trustrum, N.A. 2000. Erosion thresholds and suspended sediment yields, Waipaoa River Basin, New Zealand. *Water Resources Research*, 36: 1129-1142.

Hicks, D.M., Gomez, B., Trustrum, N.A. 2004. Event suspended sediment characteristics and the generation of hyperpycnal plumes at river mouths: East Coast Continental Margin, North Island, New Zealand. *Journal of Geology*, 112: 471-485.

Kettner, A.J., Gomez, B., Syvitski, J.P.M. 2007. Modeling suspended sediment discharge from the Waipaoa river system, New Zealand: The last 3000 years. *Water Resources Research*, 43: W07411, doi: 10.1029/2006WR005570.

Keil, R.G., Mayer, L.M., Quay, P.D., Richey, J.E., Hedges, J.I. 1997. Loss of organic matter from riverine particles in deltas. Geochemica et Cosmochimica Acta, 61: 1507-1511.

Lewis, K.B. 1980. Quaternary sedimentation on the Hikurangi oblique-subduction and transform margin: *In* Sedimentation in a Oblique-Slip Mobile Zones Vol. 4., P.F. Balance and H.G. Reading Eds., International Association of Sedimentologists, Special Publication. pp. 171-189.

Lewis, K.B. 1973. Erosion and deposition on a tilting continental shelf during Quaternary oscillations of sea level. *New Zealand Journal of Geology and Geophysics*, 16: 281-301.

Lewis, K.B. and J.R. Pettinga. 1993. The emerging, imbricate frontal wedge of the Hikurangi margin. *In* South Pacific Sedimentary Basins. Sedimentary Basins of the World. Vol. 2, P.F. Balance Eds. Elsevier Science Publishers, Amsterdam. pp. 225-250.

Lewis, K.B., Collot, J-Y., Lallemand, S.E. 1998. The dammed Hikurangi Trough: a channel-fed trench blocked by subducting seamounts and their wake avalanches (New Zealand-France GeodyNZ Project): *Basin Research*, 10: 441-468.

Litchfield, N., Wilson, K., Berryman, K., Wallace, L. 2010. Coastal uplift mechanisms at Pakarae River mouth: Constraints from a combined Holocene fluvial and marine terrace dataset. *Marine Geology*, 270: 72-83.

Lowe, D.J., Shane, P.A.R., Alloway, B.V., Newnham, R.M. 2008. Fingerprints and age models for widespread New Zealand tephra marker beds erupted since 30,000 years ago: a framework for NZ-INTIMATE. *Quaternary Science Reviews*, 27: 95-126.

Lui, J.P., Milliman, J.D., Gao, S., Cheng, P. 2004. Development of the Yellow River's subaqueous delta, North Yellow Sea. *Marine Geology*, 209: 45-67.

Lyons, W.B., Nezt, C.A., Carey, A.E., Hicks, D.M. 2002. Organic carbon fluxes to the ocean from high-standing islands. *Geology*, 30: 443-446.

McGlone, M.S. and J.M. Wilmshurst. 1999. A Holocene record of climate, vegetation change and peat bog development, east Otago, South Island, New Zealand. *Journal of Quaternary Science*, 14: 239-254.

Miller, A.J, and S.A. Kuehl. 2010. Shelf sedimentation on a tectonically active margin: A modern sediment budget for Poverty continental shelf, New Zealand. *Marine Geology*, 270: 175-187.

Milliman, J. and J.P.M. Syvitski. 1992. Geomorphic/tectonic control of sediment discharge to the ocean: the importance of small mountainous rivers. *Journal of Geology*, 100: 525-544.

Mulder, T. and J.P.M. Syvitski. 1995. Turbidity currents generated at river mouths during exceptional discharges to the world oceans. *Journal of Geology*, 103: 285-299.

Nelson, C.S., Hendy, I.L., Neil, H.L., Hendy, C.H., Weaver, P.P.E. 2000. Last glacial jetting of cold waters through the Subtropical Convergence zone in the Southwest Pacific off eastern New Zealand, and some geological implications. *Palaeogeography, Palaeoclimatology, Palaeoecology*, 156: 103-121.

Orpin, A.R., Alexander, C., Carter, L., Kuehl, S., Walsh, J.P. 2006. Temporal and spatial complexity in post-glacial sedimentation on the tectonically active, Poverty Bay continental margin of New Zealand. *Continental Shelf Research*, 26: 2205-2224.

Orpin, A.R. 2004. Holocene sediment deposition on the Poverty-slope margin by the muddy Waipaoa River, East Coast New Zealand. *Marine Geology*, 209: 69-90.

Ota, Y., Berryman, K.B, Hull, A.G., Miyauchi, T., Iso, N. 1988. Age and height distribution of Holocene transgressive deposits in eastern North Island, New Zealand. *Palaeogeography, Palaeoclimatology, Palaeoecology*, 68: 135-151.

Preston, N.J. and M.J. Crozier. 1999. Resistance to shallow landslide failure through root-derived cohesion in east coast hill country soils, North Island, New Zealand. *Earth Surface Processes and Landforms*, 24: 665-675.

Prothero, D.R. and F. Schwab, eds. Sedimentary Geology. New York: W. H. Freeman and Company, 1996. 600 pp.

Proust, J.N., Lamarche, G., Migeon, S., Neil, H., and the shipboard scientific party. 2006. Les Rapport de campagnes a la mer, MD152/MATACORE, Institute Polaire Francais, Plouzane, France, 107 pp.

Rabouille, C., Mackenzie, F.T., Ver, L.M. 2001. Influence of the human perturbation on carbon, nitrogen, and oxygen biogeochemical cycles in the global coastal ocean. *Geochimica et Cosmochimica Acta*, 65: 3615-3641.

Reimer, P.J., Baillie, M.G.L., Bard, E., Bayliss, A., Beck, J.W., Blackwell, P.G., Ramsey, C.B., Buck, C.E., Burr, G.S., Edwards, R.L., Friedrich, M., Grootes, P.M., Guilderson, T.P., Hajdas, I., Heaton, T.J., Hogg, A.G., Hughen, K.A., Kaiser, K.F., Kromer, B., McCormac, F.G., Manning, S.W., Reimer, R.W., Richards, D.A., Southon, J.R., Talamo, S., Turney, C.S.M., van der Plicht, J., Weyhenmeye, C.E. 2009. INTCAL09 and MARINE09 radiocarbon age calibration curves, 0- 50,000 years cal. BP. *Radiocarbon*, 51: 1111-1150.

Reyners, M. and P. McGinty. 1999. Shallow subduction tectonics in the Raukumara Peninsula, New Zealand, as illuminated by earthquake focal mechanisms. *Journal of Geophysical Research*, 104: 3025-3034.

Rose, L.E. and S.A. Kuehl. 2010. Recent sedimentation patterns and facies distribution on the Poverty Shelf, New Zealand. *Marine Geology*, 270: 160-174.

Stephens, S.A., Bell, R.G., Black, K.P. 2001. Complex circulation in a coastal embayment: shelf current, wind and density-driven circulation in Poverty Bay, New Zealand. *Journal of Coastal Research Special Issue*, 34: 45–59.

Stuart, R.B. and V.E. Neall. 1984. Chronology of palaeoclimatic change at the end of the last glaciation. *Nature*, 311: 47-48.

Stuiver, M., Reimer, P.J., Bard, E., Beck, J.W., Burr, G.S., Hughen, K.A., Kromer. B., McCormac, F.G., v.d. Plicht, J., Spurk, M. 1998. INTCAL 98 radiocarbon age calibration 24,000–0 cal BP. *Radiocarbon*, 40: 1041-1083.

Suggate, R.P. 1990. Late Pliocene and Quaternary Glaciations of New Zealand. *Quaternary Science Reviews*, 9: 175-197.

Syvitski, J.P.M., Vorosmarty, C.J., Kettner, A.J., Green, P.G. 2005. Impact of humans on the flux of terrestrial sediment to the global coastal ocean. *Science*, 308: 376-380.

Walling, D.E. and B.W. Webb. 1996. Erosion and sediment yield: a global overview. *International Association of Hydrological Sciences Publications*, 236: 3-19.

Walsh, J.P. and C.A. Nittrouer. 2009. Understanding fine-grained river-sediment dispersal on continental margins. *Marine Geology*, 263: 34-45.

Wilmshurst, J.M. 1997. The impact of human settlement on vegetation and soil stability in Hawke's Bay New Zealand. *New Zealand Journal of Botany*, 35: 97-111.

Wolinsky, M.A., Swenson, J.B., Litchfield, N., McNinch, J.E. 2010. Coastal progradation and sediment partitioning in the Holocene Waipaoa Sedimentary System, New Zealand. *Marine Geology*, 270: 94-107.

Wood, M.P. 2006. Sedimentation on a high input continental shelf at the active Hikurangi margin, Poverty Bay, New Zealand. Unpublished M.S. thesis, Victoria University of Wellington. 141 pp. plus appendices.

Table 1

Marion DuFresne core location, length, water depth and age information.

Core	Location	Latitude	Longitude	Length (m)	Water Depth (mbsl)	Oldest ^{14}CAge
MD3007	N. Depocenter	38 43.58 S	178 13.99 E	23.47	61	10179 ±71
MD3001	N. Depocenter	38 44.31 S	178 13.08 E	22.57	59	9577 ±85
MD3004	S. Depocenter	38 51.49 S	178 04.90 E	16.36	52	10035 ±107
MD3006	Shelf Break Depocenter	38 57.60 S	178 10.92 E	25.34	122	14354.5 ±216
MD3003	Slope	39 02.79 S	178 32.17 E	12.88	1398	16937 ±122

Table 2

Facies distribution by core including age and average textural and stable isotopic information.

FACIES 1				
Core (MD)	Age (kya)	Mean Phi	% Sand	Mean $\delta^{13}C$
3007, N Depo	Surface - 3940	6.72 ± 0.49	24.21	-24.44 ± 0.59
3001, N Depo	Surface - 3417	6.86 ± 0.64	23.71	--
3004, S Depo	Surface - 3507	5.83 ± 0.45	49.78	-25.10 ± 0.94

FACIES 2				
Core (MD)	Age (kya)	Mean Phi	% Sand	Mean $\delta^{13}C$
3007, N Depo	3940 - 6351	7.40 ± 0.29	6.36	-24.62 ± 0.20
3001, N Depo	3417 - 6894	7.57 ± 0.38	7.13	--
3004, S Depo	3507 - 6410	7.37 ± 0.38	14.80	-24.85 ± 0.72

FACIES 3				
Core (MD)	Age (kya)	Mean Phi	% Sand	Mean $\delta^{13}C$
3007, N Depo	6351 - 9533	7.84 ± 0.33	4.40	-24.21 ± 0.13
3001, N Depo	6894 - 9577 (core end)	7.99 ± 0.30	4.41	--
3004, S Depo	6410 - 10896 (core end)	7.44 ± 0.53	10.44	-24.02 ± 0.33
3006, Shelf Break	Surface - 11821	7.81 ± 0.37	7.8	-23.50 ± 0.13

FACIES 4				
Core (MD)	Age (kya)	Mean Phi	% Sand	Mean $\delta^{13}C$
3007, N Depo	9533 – 10630 (core end)	7.19 ± 0.40	7.59	-24.84 ± 0.15
3006, Shelf Break	11821 – 14649 (core end)	4.98 ± 0.63	57.53	-24.36 ± 0.01

Chapter 1 Figure Legend

Figure 1.
A. North Island, New Zealand with study area indicated by red box. TVZ = Taupo Volcanic Zone. RP = Raukumara Peninsula. EC = East Cape. ECC = East Cape Curent. STC = Subtropical Convergence. HB = Hawkes Bay. P69 and star = approximate core location from Stewart and Neall (1984). Gray shaded region denotes location of warm surface currents associated with the Subtropical Gyre (after Carter, 2001). **B.** Poverty Margin location map with Marion Dufresne (MD) cores indicated and underlying tectonics and tectonic subregions after Brown, 1995. Holocene sediment thickness is shown in overlay (after Gerber et al., 2010). W = Waipaoa River Mouth **C.** Interpretation of Poverty Bay shoreline position through time modified from Brown (1995) and Gerber et al. (2010). **D.** Post glacial sea level rise in the Western Pacific modified from Lui et al. (2004). Inset (red box) is Holocene sea level rise, modified from Cochran et al. (2006) and Gerber et al. (2010). Grey lines in inset highlight tephra occurrence. Mwp = meltwater pulse.

Figure 2.
A. Slope (3003) and Shelf Break (3006) age model accumulation rates (AR) with major slope changes indicated (black lines) and trendline ARs with 95% confidence intervals associated with the rates (in cm yr^{-1}) labeled. **B.** Southern Depocenter (3004) age model as above. **C.** Northern Depocenter (3001, 3007) age model as above. **D.** Point-to-point ARs over time. **E.** Tephra time periods by location. MD2122 after Gomez et al., 2004.

Figure 3.
A. Shelf and slope $\delta^{13}C$ results plotted by age. **B.** Slope, 3003, $\delta^{13}C$ and grain size (mean phi, ϕ) results plotted by age. **C.** Shelf Break Depocenter, 3006, $\delta^{13}C$ and grain size results plotted by age. **D.** Southern Depocenter, 3004, $\delta^{13}C$ and grain size results plotted by age. E. Northern Depocenter, 3007 $\delta^{13}C$ and 3007 and 3001 GS results plotted by age.

Figure 4.
Examples of Facies 1-4. Images are X-radiographic negatives; light hues are higher density material, darker hues are lower density. The width of each X-ray is 30cm. Zoomed-in box from Facies 3 is a close up of characteristic high bulk density ichnofabric.

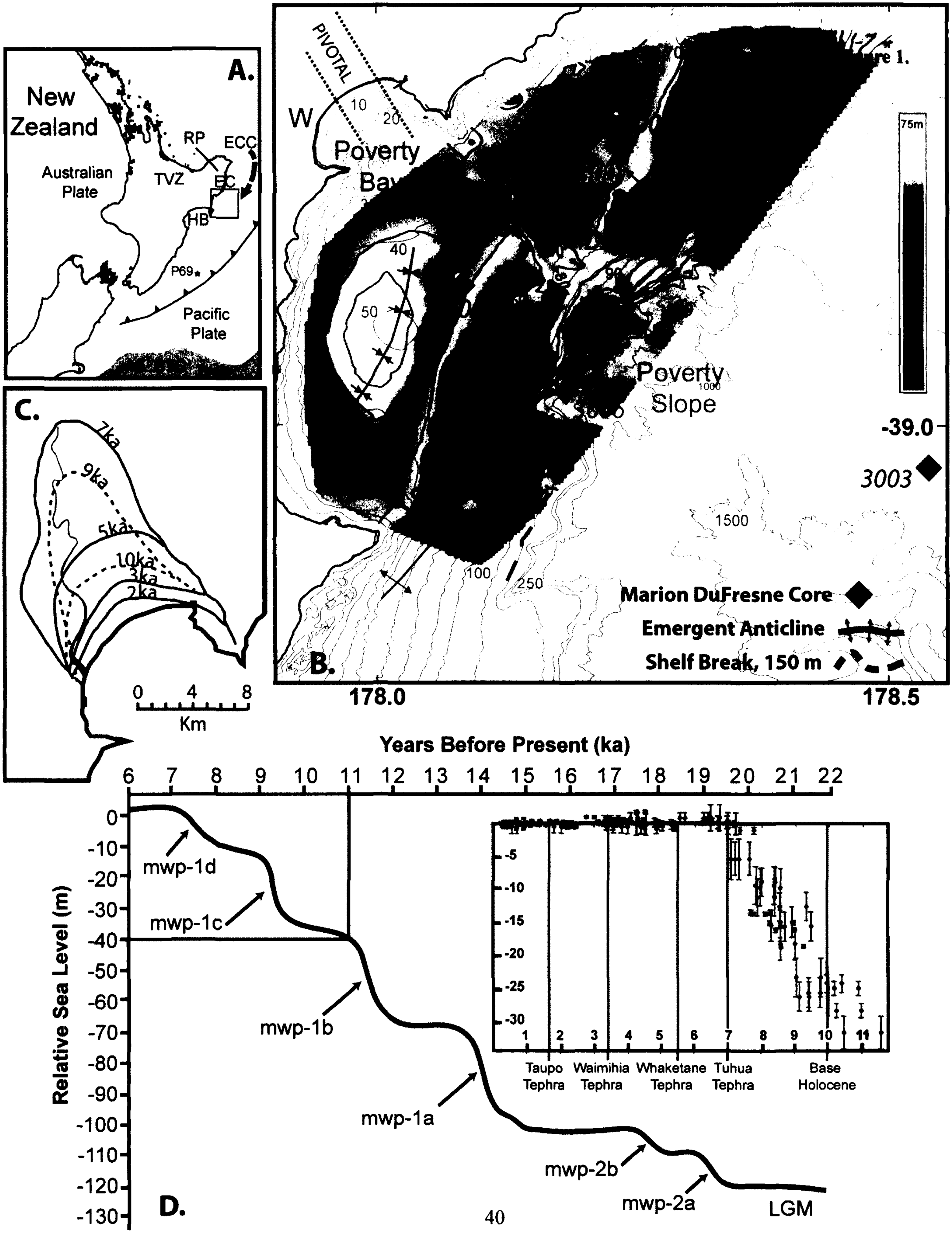
A.
New Zealand
Australian Plate
TVZ
RP
ECC
EC
HB
P69
Pacific Plate
B.
PIVOTAL
W
Poverty Bay
10
20
40
50
90
100
250
500
1000
1500
Poverty Slope
75m
-39.0
3003
Marion DuFresne Core
Emergent Anticline
Shelf Break, 150 m
178.0
178.5
C.
7ka
9ka
5ka
10ka
3ka
2ka
0 4 8
Km
Years Before Present (ka)
6 7 8 9 10 11 12 13 14 15 16 17 18 19 20 21 22
Relative Sea Level (m)
0
-10
-20
-30
-40
-50
-60
-70
-80
-90
-100
-110
-120
-130
mwp-1d
mwp-1c
mwp-1b
mwp-1a
mwp-2b
mwp-2a
LGM
D.
-5
-10
-15
-20
-25
-30
1 2 3 4 5 6 7 8 9 10 11
Taupo Tephra
Waimihia Tephra
Whaketane Tephra
Tuhua Tephra
Base Holocene

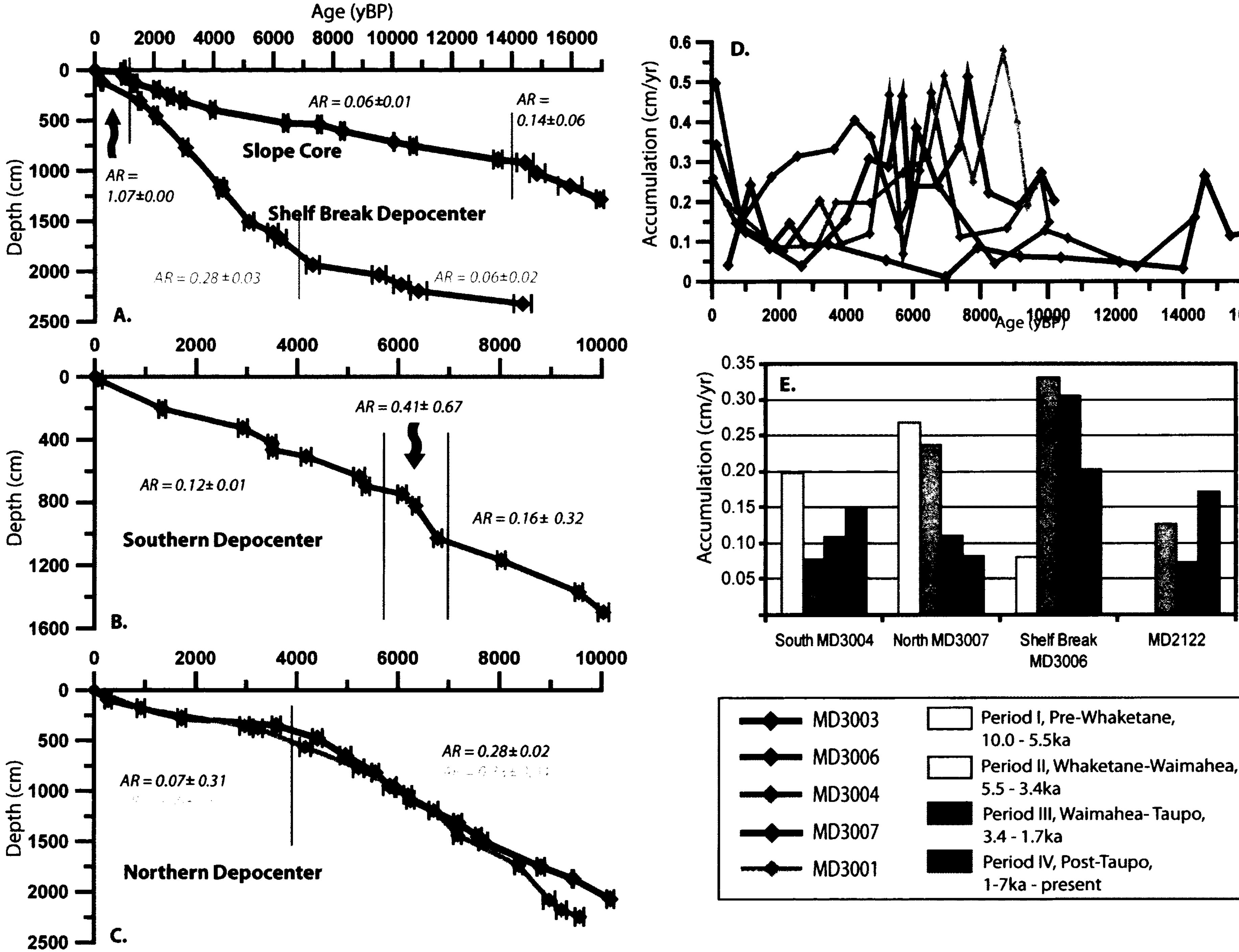
Age (yBP)
AR = 0.06±0.01
AR = 0.14±0.06
Slope Core
AR = 1.07±0.00
Shelf Break Depocenter
AR = 0.28 ± 0.03
AR = 0.06±0.02
Depth (cm)
A.
AR = 0.41± 0.67
AR = 0.12± 0.01
AR = 0.16± 0.32
Southern Depocenter
B.
AR = 0.28± 0.02
AR = 0.07± 0.31
Northern Depocenter
C.
D.
Accumulation (cm/yr)
Age (yBP)
E.
South MD3004
North MD3007
Shelf Break MD3006
MD2122
MD3003
MD3006
MD3004
MD3007
MD3001
Period I, Pre-Whaketane, 10.0 - 5.5ka
Period II, Whaketane-Waimahea, 5.5 - 3.4ka
Period III, Waimahea- Taupo, 3.4 - 1.7ka
Period IV, Post-Taupo, 1-7ka - present

Figure 2.

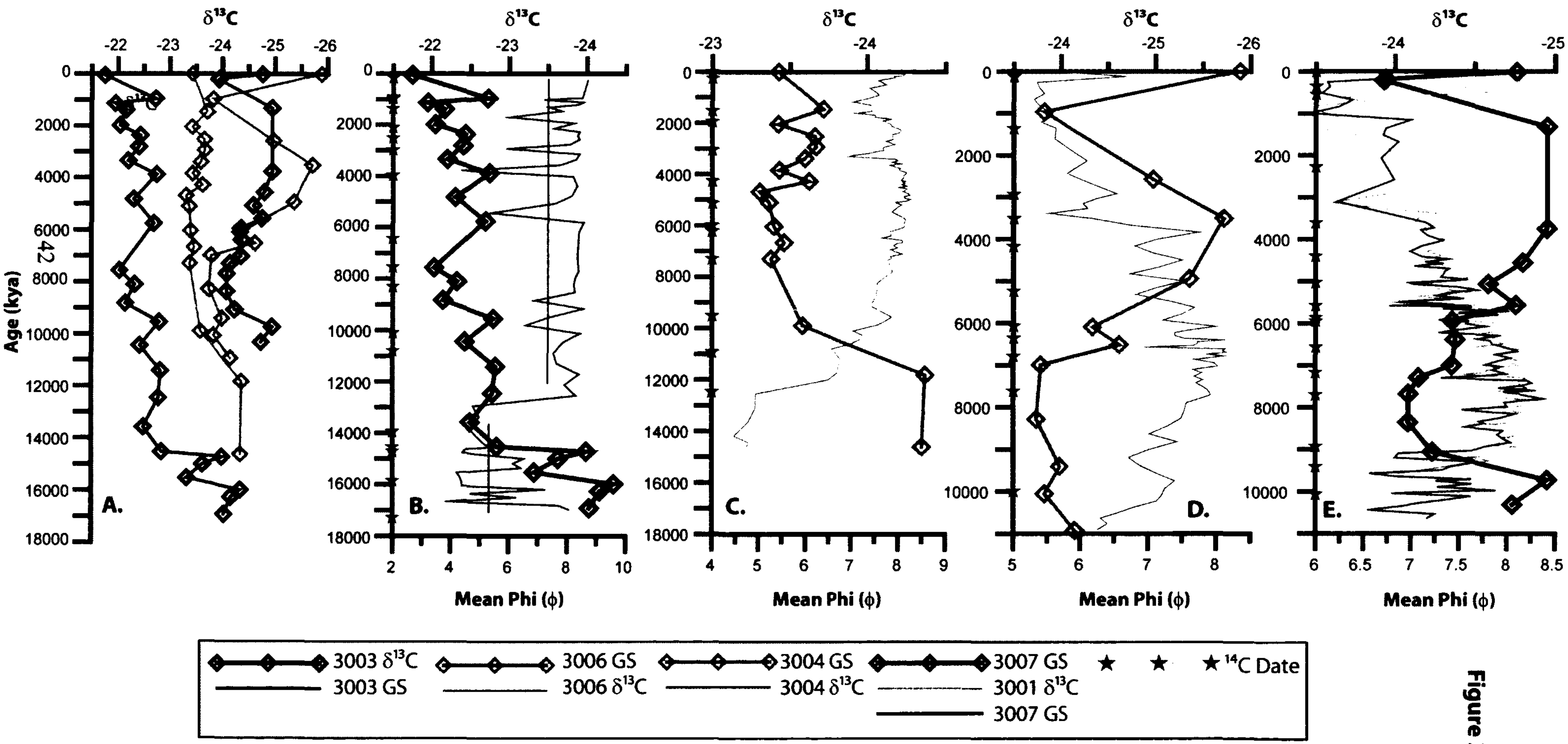
δ13C
Age (kya)
Mean Phi (ϕ)
A.
B.
C.
D.
E.
3003 δ13C
3003 GS
3006 GS
3006 δ13C
3004 GS
3004 δ13C
3007 GS
3001 δ13C
3007 GS
14C Date

Figure 3.

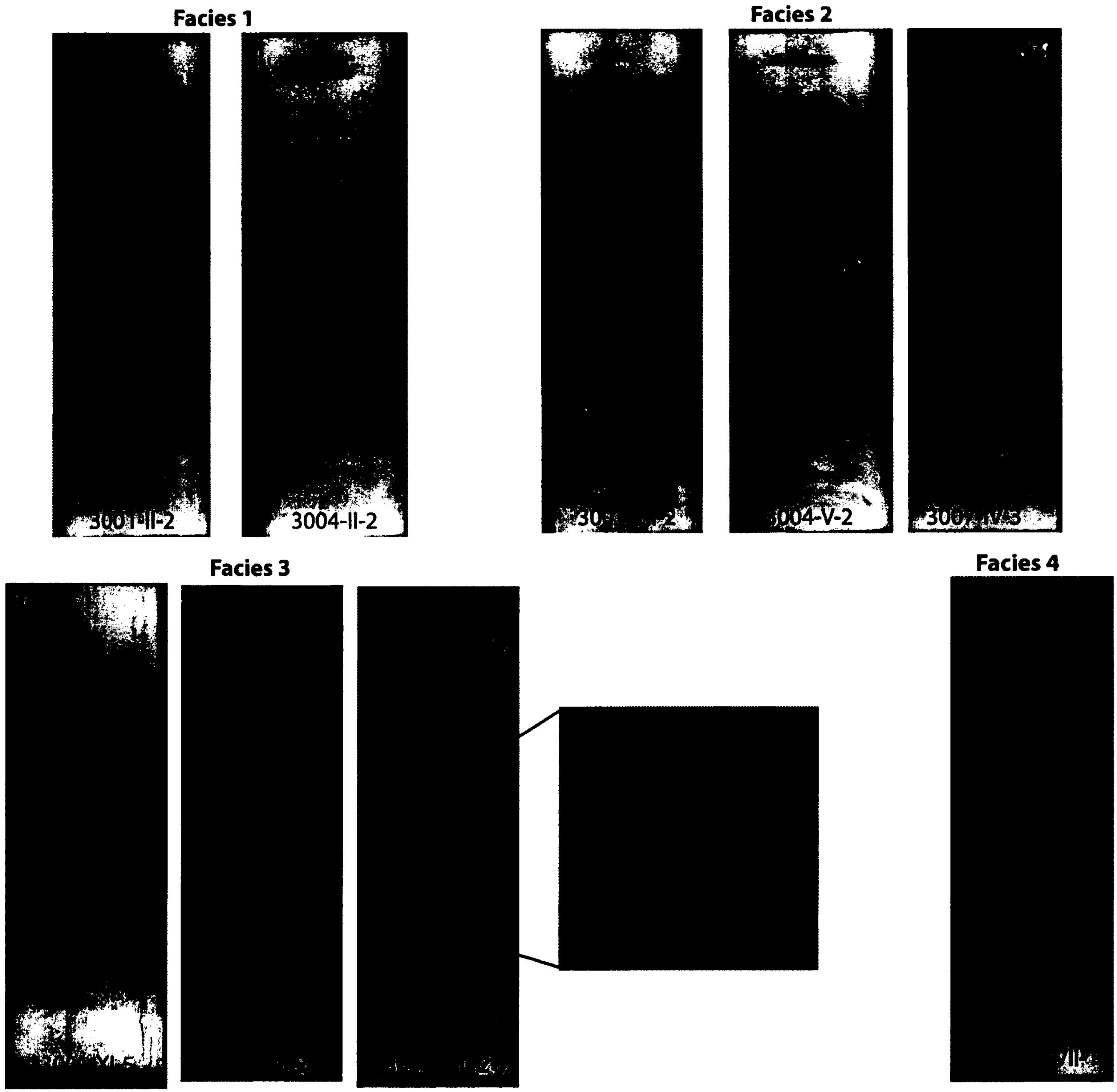

Figure 4.

CHAPTER 2

Modern Event Layers on the Waipaoa Continental Shelf: Characteristics, Preservation and Possible Modes of Initiation

Abstract

Event layer producing perturbations, such as extreme rainfall and wave resuspension events, mass flows, cyclones, volcanoes and earthquakes can punctuate normal background marine water column sedimentation with large, potentially hyperpycnal additions of terrestrial sediment carrying unique textural and geochemical characteristics. Analysis and comparison of eight box cores from the continental shelf adjacent to the small, high-yield Waipaoa River, New Zealand, a MARGINS Source-to-Sink focus area, provide high-resolution records of modern stochastic event sedimentation and preservation. Analysis of detailed stable and radioisotopic, geochemical and physical properties of these cores document the unique characteristics of event sedimentation spatially on the shelf. Cyclone Bola, the most severe tropical storm on record in this region, is identified in seven of the eight box cores and provides a modern benchmark for comparison to other prominent layers in core stratigraphy. High-resolution sampling reveals density and grain size changes within an event layer reflective of waxing and waning flood stages and shelf energy. These are correlated with stable and radioisotopic fluctuations, and ensemble, indicate that hyperpycnal event layer emplacement was the dominant form of sediment transport on the inner and mid-shelf during Cyclone Bola. Striking distinctions are revealed between a northern and southern shelf depocenter, highlighting potential differences in mode of transport and sediment sources for these locations.

1. Introduction

One of the fundamental questions in event stratigraphy is determining how a signal propagates through a sedimentary system and to what degree it is (or isn't) preserved within each segment as material is transferred from its source to site of burial. The MARGINS Source-to-Sink (S2S) program mission is to investigate continental shelf strata in order to better understand how landscape evolution impacts the formation and preservation of events (Margins Science Plans, 2003). In lieu of this goal, it is important to explore the impact of exceptional stochastic events in both the terrestrial and marine environments because such events can be responsible for changes in supply, transport, accumulation, and preservation of material in the short term (individual events) and on longer timescales (regime shifts).

Several processes including surface hypopycnal and hyperpycnal plumes, high wind and wave resuspension events produce signatures that may be preserved, recognizable, and geochemically distinguishable in the stratigraphic record (e.g. Bouma sequences and hyperpycnites; Bouma, 1962; Mulder et al., 2003; Eden and Page, 1998; Kuehl et al., 1995; Shanmugam, 2000; Leithold and Hope, 1999; Wheatcroft and Borgeld, 2000; Wheatcroft and Drake, 2003; Geyer et al., 2000, 2004). Exceptional storm events initiating oceanic flood sedimentation, as described on the Eel River margin (Wheatcroft, 2000; Wheatcroft and Drake, 2003), can provide a disproportionately large fraction of sediment discharged to the shelf (Wheatcroft, 2000). The geochemical, textural, and radioisotopic character of these events depend on a variety of hydrodynamic, physical, and biological factors operating over time and space (Guinasso and Schink, 1975; Nittrouer and Sternberg, 1981; Kuehl et al., 1995; Wheatcroft and Drake, 2003).

By determining the elemental and isotopic carbon content of sedimentary layers, the influence of terrigenous versus marine carbon sources can be revealed (Hedges et al., 1997), and along with the textural identity of sedimentary layers, the provenance or mode of initiation of the sediment that produced the layer can be determined. Distinct event layer characteristics have the potential to clarify not only their trigger (i.e. wet storm event, earthquake, wind/wave resuspension) but can help address questions about the magnitude of specific events within the catchment, the likelihood of modern and past analogues to be preserved, and the ubiquity of regional changes in frequency and/or intensity over time with relation to natural (climate-scope) and anthropogenic influences. This study provides a modern record of sedimentation on the continental shelf off the Waipaoa Sedimentary System (WSS), North Island, New Zealand – a known repository for WSS sediments and most probable area for event signal preservation in the system's marine record (Figures 1A and B).

Geochemical and physical characteristics from over 200 sediment cores collected on the continental shelf adjacent to the small, high-yield Waipaoa River during a January 2005 cruise aboard the R/V Kilo Moana (KM) were used to help identify sites of likely preservation of storm event layers (Miller and Kuehl, 2010; Rose and Kuehl, 2010, Figure 1A, B). From these cores, a suite of eight box cores representing a diverse cross-section of shelf environments (from inner shelf to shelf break, depocenter to by-passing zone), six of which were prominently layered, were subsequently selected and sampled for further and more detailed stratigraphy, with emphasis on constraining geochemical differences within and between layers (Figure 1B).

1.1 Regional Setting - The Waipaoa Sedimentary System (WSS)

The Waipaoa River and WSS located on the East Cape of the North Island of New Zealand empties into Poverty Bay, near Gisborne, and supplies suspended sediment to the adjacent Poverty Margin continental shelf and slope (Figure 1A, B; Griffiths, 1982; Hicks et al., 2004). The Waipaoa River catchment is small (2205km^2), and similar in size to the North American Eel River of Northern California, has a comparatively short sediment transfer time from source to continental shelf sink (Blair et al., 2004). The WSS is thus labeled as roughly "bypassing," as lengthy storage of Waipaoa catchment sediment in successive catchment reservoirs is not significant, especially with the construction of extensive stopbank structures and levees in the lowest reaches of the post-1940 catchment (Brackley, 2006). Gullying and landsliding are the most common erosion regimes in the catchment, and coupled with the steep grade and relatively short mainstem of the river, act as an effective conduit of sediment and organic matter to the Waipaoa, with delivery directly into Poverty Bay and the adjacent shelf setting (Hicks et al., 2004; Brackley, 2006; Brackley et al., 2010). This is supported by the occurrence of ancient, terrestrially sourced carbon (kerogen) even in offshore sites (Brackley, 2006; Leithold et al., 2006). The rapid transfer of sediment from source to sink enhances the possibility of high fidelity signals to be rapidly transferred from land segments of the WSS to the continental shelf.

The Poverty Margin lies at the boundary between the Pacific and Australian plates (Figure 1A), where oblique subduction and mountain building (up to 4mm yr^{-1}) render catchment lithologies highly erodible, and combined with a vigorous temperate maritime climate, produce 6800 t km^{-2} yr^{-1} of sediment, one of the highest sediment yields in the world (Walling and Webb, 1996; Hicks et al., 2000, 2004). The adjacent continental shelf is semi-enclosed by the coastline-parallel, actively deforming Lachlan and Arial anticlinal ridges which flank the seaward edge of two prominent mid-shelf basins, containing sedimentary sequences dating to the Late Pleistocene (Figure 1B; Lewis, 1973; Foster and Carter, 1997; Gerber et al., 2010; Miller and Kuehl, 2010; Rose and Kuehl, 2010; Rose et al., In Prep). ^{7}Be and ^{210}Pb patterns of accumulation and Chirp seismic reflection surveys reveal that these mid-shelf depocenters along with a shelf break depocenter capture at least 35% of modern Waipaoa River flux to the shelf (Figure 1B; Gerber et al., 2010; Miller and Kuehl, 2010; Rose and Kuehl, 2010). Rapid, modern sediment supply is apparent from the presence of ^{7}Be in surface sediments shelf-wide and accumulation rates of up to 0.59cm y^{-1} on the outer shelf (Table 1; Miller and Kuehl, 2010; Rose and Kuehl, 2010). A sandier zone of little net modern accumulation bisects the two shelf depocenters (Kuehl et al, 2006; Orpin et al., 2006; Miller and Kuehl, 2010; Rose and Kuehl, 2010).

The WSS has a remarkable history of anthropogenic change via deforestation. From the earliest Maori (Polynesian) settlers' deforestation by burning (ca 0.9ka) to

European colonization and conversion of scrubland to pasture, humans have increased the susceptibility of the landscape to mass failures and accelerated rates of erosion (Wilmshurst et al., 1997; Foster and Carter, 1997; Eden and Page, 1998; Page et al., 2001; Gomez et al., 2004; Gomez et al, 2007). Currently, only 3% of the Waipaoa catchment retains its original native forest (Page et al., 2001) which influences the quality and quantity of sediment available. Today, the Waipaoa sediment load is ~15Mt yr^{-1}, compared to an estimated pre-human Waipaoa load of 2.3Mt yr^{-1}, and modern shelf sedimentation rates are 6-8 times greater than prior to anthropogenically initiated landscape changes (Wilmshurst et al., 1997; Page et al., 2001; Gomez et al., 2007; Kettner et al., 2007; Gerber et al., 2010, Miller and Kuehl, 2010).

During normal fair-weather conditions, sediment enters Poverty Bay and becomes entrained in an anticlockwise gyre before reaching the shelf (Stephens et al., 2001; Brackley, 2006; Bever, 2010). Hyperpycnal flows, defined as those exceeding 40g L^{-1}, are produced at an estimated 40-year recurrence interval (Foster and Carter, 1997; Wadman and Mcninch, 2008; Hicks et al., 2000). Mean ambient shelf currents are to the northeast, perhaps an extension of the Wairapara Coastal Current (WCC; Chiswell, 2000). Shelf currents can be intensified by southern storm swell (Chiswell, 2000; Stephens et al., 2001). On the Poverty Slope, seaward of the shelf break at 150 meters below sea level (mbsl), warm water from the Tasman Front and subtropical gyre flows to the south, as the saline East Cape Current (Carter et al., 1996; Carter, 2001; Chiswell, 2005).

1.2 Event Sedimentation on Active Margins

Event layer producing perturbations, such as extreme rainfall and wave resuspension events, earthquakes, mass flows, cyclones, and volcanoes can punctuate normal marine water column sedimentation with large additions of terrestrial sediment or produce secondary structures due to reworking. Both initial deposition and secondary processes associated with these perturbations may impart unique textural and geochemical signatures that can be preserved in the stratigraphic record. Several mechanisms have been described that create event sediment deposits that are texturally distinguishable from "background," non-event suspension settling, including, but not limited to, the classic Bouma sequence (turbidites), hyperpycnites and contourites (Kuehl et al., 1995; Eden and Page, 1998; Leithold and Hope, 1999; Geyer et al., 2000; Shanmugam, 2000; Wheatcroft and Borgeld, 2000; Mulder et al., 2003; Wheatcroft and Drake, 2003; Geyer et al., 2004; Goldfinger et al., 2008). Sediment texture is essential in identifying the presence of flood event layers, as they have been found to be extremely fine-grained in comparison with "normal," non-event driven deposition (Leithold and Hope, 1999; Wheatcroft and Borgeld, 2000; Wheatcroft and Drake, 2003).

Numerous hydrodynamic, physical, biological, and environmental factors operating over time and space influence the probability that sediment layers will persist until they are buried below the zone of sediment mixing in the zone of preservation, a horizon unalterable by physical and biological processes, on a continental shelf. Such processes, in turn, may impart new, or change the existing, geochemical, textural, and radioisotopic properties of strata (Guinasso and Schink, 1975; Nittrouer and Sternberg, 1981; Kuehl et al., 1995; Wheatcroft and Drake, 2003). Conditions will favor preservation of stochastic sediment pulses if accumulation rates are high and/or subsequent depositional events rapidly follow the original pulse (effectively increasing the short term accumulation rate). Preservation is also favored when event layers are thick and when physical and biological mixing is minimal (Guinasso and Schink, 1975; Nittrouer and Sternberg, 1981; Kuehl et al., 1995; Wheatcroft and Drake, 2003; Wheatcroft et al., 2007). On longer timescales, mainly beyond the scope of this investigation, the cumulative effects of time (i.e. hiatus in deposition, compaction, erosion, etc.) may render a sedimentary sequence incomplete (Sadler, 1981). However, if preserved within the marine stratigraphy, textural and geochemical signatures of extreme episodic flood events, along with other seabed perturbations (i.e. tectonically generated gravity flows, wind and wave resuspension), may be identified and traced back to their mode of initiation.

Sedimentologically distinct event layers and their preservation have been documented and described in active margin continental shelf marine sediments off the Eel River shelf for wet storms (Leithold and Hope, 1999; Wheatcroft and Borgeld, 2000; Wheatcroft and Drake, 2003) and earthquake triggered (turbidites) sequences along the California margin and Poverty Margin (Goldfinger et al., 2003, 2007; Pouderoux et al., 2011). Wheatcroft (2000) showed that oceanic floods, caused by extreme rainfall events that produce atypical discharge from small rivers, may generate characteristic event layers in the marine environment which can be used to interpret the stratigraphic record. Wet storms are defined as those with concomitant rain on land and elevated wave action on the continental shelf (Wheatcroft, 2000).

Work on the west coast of the U.S. as well as on the East Cape of New Zealand has highlighted wet storm sedimentation and how active margin continental shelves are often the repository of terrestrial materials and record event responses of rivers within their strata (e.g., Sommerfield and Nittrouer, 1999; Blair et al., 2004; Crockett and Nittrouer, 2004; Brackley, 2006; Nittrouer et al., 2007; Wadman and McNinch, 2008; Ma et al., 2008; Kniskern et al., 2010; Ma et al., 2010; Miller and Kuehl, 2010; Rose and Kuehl, 2010). Sediment texture in conjunction with geochemical properties is essential in identifying the presence of these events. They typically may present with higher percent clay fraction (Leithold and Hope, 1999; Wheatcroft and Borgeld, 2000; Wheatcroft and Drake, 2003), low ^{210}Pb activities (Kniskern et al., 2010), and low (depleted) δ^{13}C values (Leithold and Hope, 1999; Brackley et al., 2010), which together may help to identify them from background sedimentation. In addition, the emplacement of a sole fining upwards vs. a coarsening upwards sequence followed by a fining upwards sequence may distinguish between event triggers (Shanmugam, 2000; Goldfinger et al., 2003; Wheatcroft et al., 2007).

Recent work documents the importance of hyperpycnal flows generated at the mouths of small mountainous rivers in delivering a disproportionate amount of sediment to the continental shelf. These rivers, like the Waipaoa, are often high-yield, event-dominated, and collectively supply a significant amount of sediment to the world's oceans (Milliman and Syvitski, 1992; Foster and Carter, 1997; Wheatcroft, 2000). Hyperpycnal flows result when extreme rainfall and subsequent rapid erosion and denudation deliver suspended sediment to the river, increasing the density of the river water to the point where it exceeds that of the receiving body of water (Parsons et al., 2001). The threshold widely accepted as required for such a negatively buoyant flow is 40g L^{-1} (Mulder and Syvitski, 1995; Parsons et al., 2001; Hicks et al., 2004). Brackley (2006) points out that a key diagnostic indication of hyperpycnal flows in comparison to surface hypopycnal plume sedimentation is a strong terrestrial carbon signature. This has implications for the role of oceanic floods in the global carbon cycle, as resultant layers, if rapidly deposited and buried, would be important sinks for terrestrial carbon.

The influence of macrobenthos in reworking sedimentary strata can not be ignored, as bioturbation acts to erase emplaced physical sedimentary structures and can diffusively mix and homogenize physical and geochemical signatures (Guinasso and Schink, 1975; Nittrouer and Sternberg, 1981; Francois et al., 1997; Reed et al., 2006). Seasonal variations in physical hydrodynamic variables can also result in waxing and waning of the biological diffusivity of sediment (Lecroart et al., 2007). Diagenesis of organic material also has the potential to distort the originally (or event-instantaneously) emplaced $\delta^{13}C$ signature within strata. However in small river systems (like the Eel, Waiapu and Waipaoa) compared to large river systems, this is considered to be minor, especially because, as in the case of the Waipaoa, man-made levees keep material from entering an intermediate storage reservoir (Blair et al., 2004) and source material rapidly transits the entire land portion of the system. Indeed, it has been shown that the majority of sediment sourced in the Eel River catchment reaches the adjacent shelf quickly, especially during oceanic floods, where particulate organic carbon preserves a strong bimodal terrestrial signal (Leithold and Hope, 1999; Sommerfield and Nittrouer, 1999; Blair et al., 2004).

1.3 Poverty Margin Event Records

Interpretation of Poverty Margin stratigraphy throughout the Holocene reveals that low frequency, large magnitude signals related to volcanism, earthquakes, increased erosion, storminess, and intensification of El Niño-Southern Oscillation (ENSO) ca. 4ka were the major drivers of periods of increased frequency of event emplacement and preservation in lake, continental shelf, and slope records on the millennial timescale (Foster and Carter, 1997; Gomez et al., 2004; Pouderoux et al, 2010; Rose et al., In Prep). In contrast, recent relevant work on modern Poverty Shelf event-driven sedimentation has focused on the dramatic changes in sediment supply and accumulation patterns, including shelf seismic studies, facies classification, and modeling of the Waipaoa plume during fair weather vs. storm conditions (Foster and Carter, 1997; Wood, 2006; Brackley, 2006; Gerber et al., 2010; Miller and Kuehl, 2010; Rose and Kuehl, 2010; Bever, 2010). Modern (<100yr) facies are radially distributed from the Waipaoa mouth, ranging from physically laminated inner shelf sands, replaced by mixed layers and mottles on the mid-shelf, which grade into heavily bioturbated and mottled outer shelf muds (Figure 1C, Table 1; Rose and Kuehl, 2010). On the mid-shelf, in the location of mixed layers and mottles, ^{210}Pb records reveal areas of non-steady accumulation (Miller and Kuehl, 2010), indicating stratigraphy dominated by pulsed (storm) inputs (Figure 1C). This area, within both the Northern and Southern mid-shelf depocenters where accumulation rates are high, is a natural candidate for preservation of exceptional discharge events from the Waipaoa River.

Modern event-driven sedimentation on the Poverty Shelf has been investigated to a limited extent in sediments from the upper sea bed (Brackley, 2006; Brackley et al., 2010), and hyperpycnal plumes are yet to be definitively documented offshore of the Waipaoa River, although it is estimated that the Waipaoa generates hyperpycnal plumes with a 40-year periodicity (Hicks et al., 2004). Work on the nearby East Cape Waiapu River, which has one of the highest sediment yields in the world and where river-initiated hyperpycnal plumes are more frequent (est. 1 per year) has also shown that gravity driven transport, including hyperpycnal and wave-supported flows emplace event beds on the adjacent shelf with strong terrestrial components after river floods (Hicks et al., 2000, 2004; Ma et al., 2008; Kniskern et al., 2010; Ma et al., 2010). The potential for the modern WSS to produce a hyperpycnal flow during an oceanic flood is likely, given the dramatic modern 6-fold increase in Waipaoa sediment load due to the erosional processes and land use changes described above. In the absence of direct suspended sediment concentration measurements at the mouth of the Waipaoa during exceptional discharge events, the characteristics of storm sediment sequences preserved within marine deposits have the potential to clarify questions about frequency with which such events may be preserved (if at all) and the magnitude of specific events within the catchment as well as changes in frequency and/or intensity with time.

Cyclone Bola (1988), the most severe tropical storm on record impacting the East Cape of New Zealand, has served as a modern benchmark for investigators comparing other storm events recorded in cores. Cyclone Bola brought winds upwards of 100km h^{-1} and up to 900mm of rain in a 72-hour period, causing severe erosion and flooding within the WSS (Figure 2) and throughout the East Cape. During Cyclone Bola, Waipaoa River maximum discharge exceeded 4000m^3 s^{-1}, in comparison to an average 38m^3 s^{-1}; suspended sediment load was between 32 to 40 x 10^6t, over five times the mean annual suspended load, and winds reached 100km h^{-1} (Figure 2A, B, C; Foster and Carter, 1997; Hicks et al., 2004). The maximum sediment concentration recorded was 58g L^{-1}, well over the 40g L^{-1} threshold for hyperpycnal generation, making it likely that this 100-year recurrence interval storm produced a hyperpycnal plume at the Waipaoa River mouth (Foster and Carter, 1997; Page et al., 1999; Hicks et al., 2004; Figure 2A, B). A layer of fluid mud, consistent with this scenario, was also observed, up to 2m thick (Foster and Carter, 1997), which inundated the benthic fauna within Poverty Bay directly following the cyclone. Movement of this fluid mud layer, post-deposition could have occurred via wave-supported gravity flow, as shown by Ma et al., (2008, 2010) off the Waiapu River post-wet storms. This is not unlike observations of the fluid mud layer offshore of the Eel River after the 1995 flood (Leithold and Hope, 1999; Geyer et al., 2000; Traykovski et al., 2000). Brackley (2006) identified several event layers using grain size and stable isotopic analyses in three shelf cores. She interpreted the most recent event layer, a clay-rich, ^{13}C-depleted horizon 10cm thick on the inner-shelf and 1cm thick on the mid-shelf to have been emplaced by Cyclone Bola, but did not find evidence of this layer on the outer shelf (see Figure 1B for Brackley (2006) core locations). Catastrophic floods, such as generated by Cyclone Bola, are found to infrequently generate turbiditic hyperpycnites on Poverty Slope in the sedimentary record, and truncation of Poverty Slope cores preclude the identification of the Bola layer on the slope, where only one such record exists post maximum transgression (Pouderoux et al., 2012).

Lacustrine sediment cores from the East Coast of the North Island, including Lakes Tutira (black star, Figure 1A), Rotonuiaha, and Waikopiro, all within a few hundred kilometers of the WSS, have shown that stochastic inputs can also be distinguished from background lake sedimentation. These investigations of lake sequences near the WSS have yielded high resolution records reaching as far back as several thousand years (Eden and Page, 1998; Wilmshurst et al, 1997; Carter et al., 2004; Orpin et al., 2010). Lake records that have been interpreted to show a record of landscape erosion in response to climate and erosion regime changes may serve as an analogue for WSS perturbations and resultant shelf deposits. In Lake Tutira cores, for example, distinct volcanic, homogenite, and graded beds interpreted to be triggered by seismic and storm activity are distinguished from non-event based lake sedimentation using color, grain size and grading, diatom, palynological, and charcoal analyses. These beds have also been date-constrained by published tree ring and radiocarbon dates that correlate with tephra deposits (Orpin et al., 2010). Intra-lake vs. external storm sequences can be further determined by percent carbon and nitrogen (Orpin et al., 2010). Phases of increased storminess were identified and related to rain intensity, based on the historical record. In New Zealand, storm frequency and magnitude both increase during the positive phase of the Southern Oscillation Index (SOI), which is concomitant with increased rainfall and storm intensity in New Zealand (Eden and Page, 1998), however no correlation was discovered between event sedimentation in Lake Tutira and the entire 20th century record of ENSO (Orpin et al., 2010). A weak correlation was found between homogenite occurrence and proximity in time to seismic activity and these beds were found to decrease in thickness when earthquakes were more frequent (Orpin et al., 2010).

2. Methods

2.1 Core collection

In January 2005 aboard the R/V Kilo Moana (KM), a suite of eighty-seven box cores (max length 61cm) and paired Kasten cores (max length 270cm) were collected in a dense grid on the shelf between a water depth of ~26 to ~75m during low-flow Waipaoa River discharge and non-energetic wave conditions (Figure 2A). Box cores preserve the sediment-water interface, while Kasten cores may disrupt the first few centimeters but retrieve longer records. Eight of the box cores were subsequently chosen (Figure 1B), representing a diverse cross-section of shelf environments (from inner shelf to shelf break, depocenter to by-passing zone), for further study. Cores were selected based on shelf location and distribution of shelf facies, X-radiographs, and ^{210}Pb accumulation rates from Kasten core analyses (Figure 1C, Table 1). The goal was to have a representative sample of the spatial diversity on the shelf, but to make sure regions with high modern sedimentation rates or extremely non-steady state profiles were included in an attempt to target areas where storm sediment sequences were preserved (Miller and Kuehl, 2010; Rose and Kuehl, 2010).

Processing of box cores included sub-coring for Geotek® Multi-Sensor Core Logging (MSCL), used to log continuous down-core geophysical properties. Sub-were taken for digital X-radiography, collected within twenty-four hours of core retrieval. The sub-cores were then frozen for further sampling, including detailed textural and geochemical analyses. Sub-cores were also taken for radioisotopic analyses (Miller and Kuehl, 2010; Rose and Kuehl, 2010), which were sectioned in 1cm intervals (the top 5cm) and according to a geometric sampling plan, where sample spacing increases with depth into core. These samples were stored wet in plastic bags for immediate post-cruise analyses

2.2 Multi-Sensor Core Log and Bulk Density

A Geotek® Multi-Sensor Core Logger (MSCL) was used to record continuous down-core properties such as gamma attenuation, p-wave velocity, magnetic susceptibility (SI), and acoustic impedance at half centimeter increments. Sub-samples were taken every 20cm for laboratory bulk density ground-truthing measurements. Wet bulk density and fractional porosity were calculated using gamma ray attenuation and dry bulk density was then calculated assuming a grain density of 2.65g cm^{-3} (quartz) and seawater density of 1.025g cm^{-3}. All bulk density measurements reported herein are dry bulk density and profiles of bulk density reflect a correction of 1cm at the top of the core where a piece of foam was inserted to keep sediment from moving during horizontal MSCL measurements.

2.3 X-radiographs

Digital X-radiograph negative images were collected from 2.5cm thick rectangular sub-cores. Exposures are X-radiographic negatives; light values are the product of limited X-ray penetration indicating high bulk density sediments, while darker values indicate less dense sediment. X-radiography provides a nearly instantaneous reference for lithological changes such as grain size, sorting, and sediment layering within a core and can be used as a proxy for bulk density/water content. Using Varian Paxscan® Imaging software, each image was adjusted for optimal balance and contrast. X-radiographic sub-cores were kept frozen in storage for one year in New Zealand and then transported to the U.S. Before further sampling, they were X-rayed again to determine if any degradation of the sedimentary structures had occurred.

2.4 Post-Cruise Sampling

In August 2007, further subsampling of these X-radiographic sub-cores was undertaken, with a dual-objective sampling plan to target specific layers within the eight chosen box cores and to capture natural variability down core. After defrosting, rectangular stainless steel shim inserts, 5cm long by 2.3cm deep, tailored to excise sediment from the X-radiographic sub-cores, were inserted into the core for sample removal (Figure 3). Survey (S) samples were 1cm thick (~10g), taken every 5cm and designed to capture bulk changes down core. Target (T) samples were 0.5cm thick (~5g), guided by X-radiographs and MSCL to capture small-scale changes within specific layers of interest, thought to generally represent potential storm sediment pulses (Figure 3). Each S and T sample was split for grain size, ^{210}Pb geochronology, and carbon and nitrogen ($\delta^{13}C$ and $\delta^{15}N$) stable isotopic analyses.

2.5 Correction for Compaction and Expansion

Post-cruise X-radiographs, along with photographs taken of each box core being subsampled (with tape measure scale, Figure 3) compared with MSCL revealed that in each of the eight box cores, some degree of compaction or expansion had occurred during storage. A linear correction was applied to the midpoint of each textural/geochemical subsample removed from the X-radiographic plates in order to adjust the sample to the "true" (MSCL) depth. The equation applied to each sample followed:

Equation 1. $$z' = z - \frac{\Delta l}{l} z,$$

where z' represents the corrected depth, z represents the midpoint depth of the sample, Δl represents compaction or expansion in the X-radiographic plate and l represents the core thickness at time of extraction. This linear correction assumes all parts of the core expanded or contracted homogeneously and does not take into account differences in density of various layers. Depth corrections are listed in Table 1.

2.6 Grain Size Analyses

All samples were analyzed via wet sieve and pipette method. Samples were gently wet sieved with DI water through a 25μm mesh sieve to separate the sand fraction from silt and clay. The sand fraction was dried at 25°C and then weighed. The fine fraction (< 25μm) was then separated into silt and clay using standard pipette/graduated cylinder procedures and following the Stokes' settling law principle (Folk, 1980).

2.7 ^{210}Pb Geochronology

A member of the naturally-occurring ^{238}U decay series, ^{210}Pb is traditionally used to determine modern (< 100y) accumulation rates in marine and lacustrine environments (Appleby and Olefield, 1978). Particle reactive ^{210}Pb ($t_{1/2}$ = 22.3 years) is found associated with marine sediments above supported levels, supplied by natural decay of the parent ^{226}Ra in the water column, input from groundwater seepage, runoff, and atmospheric precipitation (Nittrouer et al., 1979). An optimal window for dating sediments using ^{210}Pb exists before it decays to supported levels, roughly about 5 half-lives, or 100 years. Assuming secular equilibrium, the ^{210}Po daughter was measured via alpha spectroscopy as a proxy for ^{210}Pb after Nittrouer et al. (1979).

^{210}Pb analyses were performed on S and T samples (Figure 4). To determine the activity profile type of each box core, total activity (dpm g^{-1}) of just S samples was considered, as T sampling biases towards non-steady state activity profiles. Only two cores (B52 and B85) showed probable steady-state activity but did not reach supported levels, and the remainder of the box cores had either non-steady or low, uniform activity profiles. Accumulation rates from longer Kasten cores retrieved during the same scientific cruise, many of which were in the same location as the box cores in this study, were used as proxies for accumulation rates (Figure 1C, Table 2). For B52 and B85, a supported value was derived from an average of the low, supported activities in corresponding Kasten cores (Miller and Kuehl, 2010), and accumulation rates were calculated using the slope of the box core profile that displayed logarithmic decay (Table 2; Figure 4).

2.8 Stable Isotopes

Stable carbon isotopes are used in this study to quantify the relative contribution of terrigenous, allochthonous organic carbon (OC) and marine sources of OC in S and T samples (Fry and Sherr, 1984; Hedges and Keil, 1995: Hedges et al., 1997). A group of samples was prepared and analyzed from samples that were dried directly after the cruise (February 2005) and corresponding samples that remained frozen in the X-radiographic plates (August 2007) to document whether contamination by bacterial decomposition or other sources during storage had occurred (Figure 6). All samples were dried, ground and acidified in muffled scintillation vials with 10% HCL in random order. Samples were then redried and weighed into tin capsules that had been rinsed with methanol. All samples were processed in the UC Davis Stable Isotope Facility using a continuous flow Isotope Ratio Mass Spectrometer (IRMS) for stable carbon ($\delta^{13}C$) and nitrogen ($\delta^{15}N$) analyses. Percent carbon was calculated by normalizing the amount of carbon reported for each sample to milligrams, dividing by the original sample mass and then multiplying by 100.

3. Results

3.1 Sedimentology of Modern (< 100yr) Sediments

Six of the eight box cores (B3, B6, B18, B24, B25, B61) show prominent layering and laminations of various thicknesses (Figure 6A, B). These cores are dominated by physical sedimentary structures with minor to moderate bioturbation and fall within the Inter-Laminated Muds and Sands (ILMS) and Mixed Layers and Mottles (MLM) facies defined by Rose and Kuehl (2010) (Figure 1C, Table 2). The other two cores, B52 and B85, are from locations situated farthest from the river mouth, within the two mid-shelf depocenters, and are completely bioturbated, homogeneous mud (Figure 6C).

3.1.1 Inner shelf and Midshelf Cores – B3, B6, B24, and B25, Figure 6A

These four cores are located closest to the mouth of Poverty Bay and were retrieved from the shallowest water depths (33 to 46m; Table 1). Each of these four cores fall within the ILMS facies classification designated by Rose and Kuehl (2010) (Figure 1C, Table 1). B3 is comprised of multiple high and low density layers, less than 2cm in thickness, in the lower 10cm of the core, with large burrows crosscutting these layers. Layering in the upper half of B3 is finely cross-bedded and more intensely bioturbated. B6 is dominated by two ~8cm thick, finely cross-bedded high density units, both of which increase in density down core. The topmost unit extends from the surface of the core to a distinct and wavy, undulating contact with a ~3cm thick low density unit. This low density unit, in turn, grades into the next high density unit, whose basal contact to a 1.5cm-thick low density layer is sharp and characterized by an even higher density lens just before the contact. A final, 2cm-thick high density unit caps a 5cm-thick low density unit extends to the end of the core. In B24, the upper 7cm is comprised of bioturbated homogenous mud with discontinuous higher-density basal lamina which sharply contacts a well defined 2cm-thick low density mud unit. This is followed by ~6cm of homogenous, bioturbated mud that grades into an 8cm-thick high density unit. The top ~3cm of this unit is well bioturbated and the lower 5cm is faintly laminated. This unit grades back into low density material with several faint, higher density lenses and laminae. The top ~5cm of B25 is comprised of a high density mud, the top 3cm of which is well bioturbated and the bottom 2cm of which is X-ray opaque and finely laminated with a scoured base. Below this, a lower density, highly bioturbated mud extends for ~10cm, the top of which is capped by a X-ray transparent mud. Several gastropod shells are seen in this unit and associated bioturbation obfuscates the transition from low to high density ~12cm into the core. However, the core does become more dense, grading into a roughly 8cm-thick, strongly laminated and cross-bedded high density sandy mud with a distinct smooth basal contact. This unit is underlain by several low and high density laminations, which have been slightly deformed (convex distortion at the sides) from the retrieval of the X-radiographic sub-core.

3.1.2 Depocenter Cores – B18 and B61, Figure 6B; B52 and B85, Figure 6C

The depocenter cores can be divided into two distinct categories - those that fall within the Mixed Layers and Mottles (MLM) facies, B18 and B61, and those that fall within the Mottled Muds (MM) facies, B52 and B85 (Table 1, Figures 1; Rose and Kuehl, 2010). One core from of each of these two categories is located within the Southern (B52, B61) and Northern (B18, B85) Depocenters. MLM depocenter cores, are also more centrally located within the depocenters described by modern ^{210}Pb-derived accumulation rates and have the highest ^{7}Be inventories of all the cores surveyed in this study. In contrast, those in the MM facies are situated on the outer flanks of depocenters, furthest from Poverty Bay mouth (Table 1; Rose and Kuehl, 2010; Miller and Kuehl, 2010).

In the Northern Depocenter, B18 is capped by a ~10cm low density, highly bioturbated sandy mud which grades into a ~5cm-thick high density silty unit (50-70% silt) which has fine internally bedded lamina and a sharp basal contact disrupted by bioturbation. Below this unit, multiple rhythmic units of 2-4cm-thick clay-rich low density units are inter-bedded with 0.5-1cm-thick higher density lenses. The deepest low density layer has a wavy contact to a massive high density unit (~7cm thick) which continues past the length of the core and is finely bedded at the base and slightly bioturbated. The most distinct feature of B61 in the Southern Depocenter is a stark 1.5cm-thick, high density layer that is internally laminated and has distinct upper and lower contacts, which bisects the core. Above this layer, massive mud is higher density and large single burrows crosscut the sediment. Below this layer, the mud is lower density and is dominated by a network of frequent burrows. The top

~10cm of B61 is homogeneous mottled mud. The bottom ~6cm of this core grades back into a more opaque unit with two distinct lamina <0.5cm thick – one high, and one low density.

B52 and B85, located within the Southern and Northern Depocenters, respectively, are comprised of homogenous mottled muds, evidence of intense bioturbation in these locations. A few shell fragments are found in the lower portion of B85. X-radiographs and bulk density measurements from MSCL logs show that both cores become more dense with depth, with minor internal bulk density fluctuations.

3.2 Core Profiles

3.2.1 ^{210}Pb

Survey profiles of total activity for the eight box cores reveal B3 and B6 clearly have low, uniform ^{210}Pb activity profiles (Figure 4). B18 and B61 are visibly non-steady-state. B52 and B85 have steady-state activity profiles but were not long enough to reach supported levels indicated by nearby Kasten cores (at 45 and between 65-92cm depth respectively; Table 2; Figure 4). Excess Activity profiles (with average Kasten core supported activity subtracted from total activity) are plotted in addition to Total Activity profiles, along with linear interpolation of accumulation rates for these cores (1.02 and 1.31cm yr^{-1}, respectively; Figure 4). Both B24 and B25 display some non-steady behavior, however activities are lower than the corresponding Kasten core's supported activity (1.39 and 1.04dmp g^{-1}, respectively; Table 2), making it more probable that they should be classified as "low, uniform."

Because accumulation rates could not be determined for the majority of box cores, ^{210}Pb accumulation rates from Kasten cores retrieved at the same location as, or nearby, each of the eight box cores were used as a proxies for accumulation rates and for confirmation of profile types (low and uniform, steady, non-steady; Figure 1B for Kasten core locations, Table 2). Of the eight box cores, 5 were in proximity of at least one Kasten core that displayed steady state profiles from which an accumulation rate could be calculated (Figure 1C, Table 2). For B24, B25, and B61, no nearby steady-state core Kasten core was available (and therefore no closely linked accumulation rate). Instead, approximate accumulation was calculated using the ^{210}Pb accumulation map showing interpolated accumulation contours (Table 2, Figure 1B, modified from Miller and Kuehl, 2010). According to locations associated only with steady-state Kasten and box cores for which ^{210}Pb accumulation rates could be calculated, the depth range of the Cyclone Bola (DCB) event layer was calculated (Equation 2). DCB depth ranges for box cores are reported in Table 2.

Equation 2. $DCB = \Delta t \cdot \omega$

where Δt is the time elapsed time between the Cyclone Bola event date to core collection and ω is the local accumulation rate. Two of the box cores exhibited a likely mixed layer at the surface, where activities were high and uniform, consistent with Miller and Kuehl (2010), who found 11 of 85 Kasten cores also displayed mixed layers (Figure 4, shaded gray boxes). The mixed layer depth, z_m, added to Equation 2 was modified for this case, as can be seen below:

Equation 3. $DCB = \Delta t \cdot \omega + z_m$

Grain-size corrections were not applied to total activity ^{210}Pb profiles of S and T samples. Instead ^{210}Pb profiles are used primarily in a non-traditional attempt to interpret whether a sample was within or outside of an event layer, based on the principle that rapidly settling wet storm sedimentation would produce "negative spikes" in activity as little time for particle scavenging exists (Kniskern et al., 2010). Depletions below average sedimentation can be used to pinpoint times of sediment injection beyond the ability for ^{210}Pb to be scavenged from the water column: i.e. a hyperpycnal or extreme suspended sediment concentration (Kniskern et al., 2010). Because sampling resolution is high, "low" peaks were actually "low regions", subtle depressions in ^{210}Pb that were flanked above and below by higher activities, as in B18, B24, B25, B61 and partially in B6 (Figures 6A and B). Two cores (B6 and B61) had large "high" ^{210}Pb activity peaks. In the inner shelf cores, B3 and B6, low uniform activities close to the supported activities of corresponding Kasten cores (Table 2) indicate sediments may have been deposited before the last century or, more likely, exposed to intense reworking, diluting the ^{210}Pb signal (Figure 6A).

3.2.2 Stable Isotopes and N:C Ratios

Abrupt $\delta^{13}C$ and N:C oscillations within box cores and event layers signify rapid changes in delivery mechanisms and sediment source pools (Figure 6). Stable carbon $\delta^{13}C$ and nitrogen to carbon ratios (Mass N:C) are plotted according to Leithold and Hope (1999), and indicate a mixed carbon source in all shelf cores, with a slight terrestrial leaning (Figure 7A). Delta ^{13}C samples range from -26.35 to -22.97‰, and mass N:C ratios range from 0.16 to 0.08 (Figure 7A). The range of $\delta^{13}C$ values and N:C ratios in each core and between cores is variable and overlap to varying degrees, with one notable exception. B52 (pink squares, Figure 8A), stands apart from the others isotopically with no overlap in $\delta^{13}C$ with other cores, except with the surface sample from its nearest neighbor, B61. B52 also has the smallest ranges in both $\delta^{13}C$ and N:C (Figure 8B). Most commonly, a weak positive correlation exists between $\delta^{13}C$ and N:C ratios (as N:C increases, $\delta^{13}C$ becomes more enriched), except for B61 and B3, which have weak negative correlations and B52 which has a stronger negative correlation (note: X-axis is oriented according to Leithold and Hope (1999), such that the value becomes more depleted to the right). There is a moderate positive correlation between $\delta^{13}C$ and ^{210}Pb – as values become more enriched (marine), they also tend to be higher in activity (Figure 8C). There are no discernable or significant correlations between texture and $\delta^{13}C$ (which was also the case in Waipaoa floodplain cores analyzed by Brackley, 2006). Even within T samples only, no trends are observed between texture and $\delta^{13}C$, likely because T samples represent both high and low density layers, and are an intrinsically heterogeneous subset of samples. According to core profiles (Figure 6) a sample shift towards the left (more depleted $\delta^{13}C$ and lower N:C ratios) represents an increase in terrestrially sourced sediments. All samples with a $\delta^{13}C$ more depleted than -23.92‰ had <10% sand. Significant fluctuations of more than 0.5‰ downcore occur in all cores, including the mottled muds observed in the two depocenter cores, B52 and B85 (Figure 6).

3.2.3 Grain Size and Bulk Density

Grain size varied with depth in each core (Figure 6). Average grain size amongst all samples and within S and T sample pools, individually, show that there is considerable variability between cores and core locations (Table 3). Interestingly, S sample variability was higher than T sample variability. Within the S sample pool, sand was the most variable in comparison to the widest range of values in percent clay found in the T sample pool, with silt being the least variable in both sample pools. Because the average S and T samples within the sand, silt, and clay fractions varied considerably, Student-T tests comparing S and T samples of each fraction were used to determine whether the sand silt and clay fractions of B3 and the sand fraction of B85 were significantly different (Table 3). Also, as T samples were chosen on the basis of standing out from clear suspension settling - and not biased towards sampling only low or high density layers - variability between high or low density layering was not differentiated. Bulk density profiles showed significant variability with depth in core profiles, which often correlate with density differences visible within X-radiographs and corroborate textural trends captured down core (Figure 6).

When considering both sample pools together (S and T), B24, B52 and B61, all located on the southern half of Poverty Shelf, have an average of less than 5% sand. B18, situated very close to the outer shelf, on the seaward flank of the Northern Depocenter, also has very low percent sand. In comparison, cores most proximal to the bypassing region, B3, B6 and B25, have much higher percent sand overall, and B85, within the Northern Depocenter, contains an average of almost 15% sand. Two cores within the ILMS facies, have the lowest and highest recorded percent silt of all the cores surveyed (B3 and B25, respectively). Highest percent clay is found in the Southern Depocenter cores, B52 and B61, while the lowest percent clay is found in the Northern Depocenter core, B85.

4. Discussion

4.1 Imagining the "Perfect Storm...*Event*"

Rarely are idealized sequences preserved in the stratigraphic record, especially on continental shelves where physical alteration by waves, currents, and biologic processes may disrupt, distort, modify, or rework primary strata (Guinasso and Schink, 1975; Nittrouer and Sternberg, 1981; Wheatcroft et al., 2003). However, there is utility in conceptualizing the "ideal" event-emplaced unit, under a variety of conditions, in order to be able to distinguish their remnants in the preserved record. Oceanic flood sedimentation, hyperpycnal flows and dry storms, all which may impact the WSS and Poverty Margin, have been hypothesized to be texturally, and in some cases geochemically ($\delta^{13}C$ and N:C), distinct, but in reality, the expected expression of such events is often subtle or convoluted (Mulder et al., 2003; Brackley, 2006). Conceptual diagrams representing 3 possible classes of event emplacement on the Poverty Shelf are highlighted, with idealized textural and stable isotopic profiles, along with expected ^{210}Pb signatures (Figure 8). Although these cartoons are not location-dependant, there are places on the shelf where each is more likely to be found.

At one end of the spectrum, a dry storm representing strong Southern Swell, the dominant and long-period wave direction (Pickrill and Mitchell, 1979), with no river input (i.e. no flood), as shown in Figure 8A, would be expected to rework the upper seabed by wave resuspension (Figure 8A). The resultant unit would have a distinct, probably scoured base with cross-bedding similar to that described as hummocky cross-stratification (Bougeois, 1980; Mount, 1982) and have higher density than surrounding sediment (light hues in Figure 8), perhaps with a subtle fining upwards signature. The $\delta^{13}C$ signature in a dry storm event layer would not be expected to change measurably, as fine sediment of marine and terrestrial sources would both be removed. Lead-210 activities would be expected to be higher than overlying sediment, since resuspension would allow additional scavenging of excess ^{210}Pb from the water column. On the Poverty Shelf, it may even be the case that some material could be shed from the emergent anticlines and reworked shoreward by southern swell. Shallow inner and outer Poverty Shelf locations would most likely be impacted by dry storms. While no location on the shelf is deep enough to escape some resuspension due to large waves (Wood, 2006), wave energy attenuates with depth, so if such a layer were to be emplaced within one of the deeper depocenter's, it would likely have a high preservation potential relative to deposition outside of the basin.

On the opposite end of the spectrum, sediment from a river flood, with no synchronous wave energy (i.e. not a high-energy cyclonic event), would likely enter Poverty Bay and Poverty Shelf via hypopycnal plume transport. This would emplace a finer layer overall, than in the previous scenario, with a fining upwards signature and gradational contact to underlying sediment (Figure 8B). Plant material might even be preserved in sediment deposited during this ideal flood event layer. Regardless, the entire layer would have low (terrestrial) $\delta^{13}C$ values, with the lowest values near the upper limit of the unit, though bioturbation may rework the upper contact, effectively diluting values to some degree. Owing to suspension settling of fines through the water column, high excess ^{210}Pb activities would be found within the layer, displayed as a steepening of the gradient of the decay profile in relation to overlying and underlying sediment. In this study region, depending on the suspended sediment concentration and constituent sediment size classes of the river flood plume, an event layer would become increasingly fine, overall, with distance from the Waipaoa mouth. Modeled Waipaoa floods show that initially, sand is largely retained in Poverty Bay, and sediment dispersal to the shelf is reliant on wave energy, either concurrent or non-synchronous with a flood event (Bever, 2010). If plume transport did allow for deposition on the shelf, it would likely not extend past the landward flanks of the depocenters, as emplacement would be dictated by plume steering by shelf currents, would be supply-limited, and also subjected to reworking and bioturbation once emplaced.

A hyperpycnal plume, in comparison, is theorized to emplace an event layer (hyperpycnite) that reflects the waxing and waning phases of a flood (Mulder et al., 2003). This deposit is thus comprised of a coarsening-upwards and then a fining-upwards unit, the transition between the two representing peak flood discharge (Figure 8C; Mulder et al., 2003). Sedimentary structures within a typical hyperpycnite may include cross-laminated climbing ripples and fine lamina, as well as a sharp or erosionally scoured bottom contact (Mulder et al., 2003). Stable carbon isotopic values would be expected to be lower (terrestrial) throughout, possibly with the lowest values in the finer portions of the bottom and upper contacts of the hyperpycnites due to grain size effects. Lead-210 activities would likely be lower, overall, than overlying and underlying sediment, owing to direct injection to the seabed and thus limited water column scavenging (Figure 8C).

4.2 Event Sedimentation on Poverty Shelf

In inner- and mid-shelf cores from this study, and from more densely spaced box and Kasten cores from other studies, it appears that event sedimentation is often preserved on Poverty Shelf (Miller and Kuehl, 2010; Rose and Kuehl, 2010). Detailed sampling of the eight box cores in this study provide high-resolution marine stratigraphic records of recent deposition on the shelf enabling investigation of whether or not event layer producing perturbations can be identified in modern Poverty Shelf sediments. X-radiographs and physical property data from MSCL, along with ^{210}Pb, textural, elemental and isotopic carbon and nitrogen analyses were used to characterize Poverty Shelf stratigraphy and allow us to test whether oceanic flood layers can be identified within a stratigraphic sequence and distinguished from resuspension and wind/wave events that are not accompanied by high flux of terrigenous sediment. In contrast to earlier characterizations of modern events on Poverty Shelf (Brackley, 2006; Brackley et al., 2010) which were limited in core coverage and used primarily texture and carbon isotopes to characterize an event signature, the holistic approach to sediment characterization in this study, using several different tools and greater extent of shelf coverage into the mid-shelf depocenters, allows for a more comprehensive characterization of the provenance of the layer, including the methods of transport.

Generally, X-ray transparent, low bulk density layers are comprised of fine sediments and have lower $\delta^{13}C$ values (terrestrial sources) than overlying and underlying sediment. In contrast, higher bulk density sediments are characterized by greater contributions of silt and sand, are often cross-bedded, and have more enriched $\delta^{13}C$ values. Regions of depressed ^{210}Pb activities are associated with areas where a paired high and low density layer make up a discrete unit. Spikes in ^{210}Pb activity are found coincident with return to underlying background sediments, regardless of sediment density (e.g. core B6 at 19cm and core B61 at 23cm; Figure 6A, C). Low density muddy units corresponding with $\delta^{13}C$ values representative of terrestrial carbon (e.g. core B24 at 8cm), support the idea that low density flood layers usually show an increase in land-derived carbon. In several cores, N:C ratio has small fluctuations, while in others, a large decrease in N:C is seen associated with low density units (ex. at 10-11 and 18-20cm in core B6 and 8cm in core B24). The signature decreased N:C values associated with event sedimentation may be intimately linked with grain size variations (Brackley, 2006), since organic matter may be protected from decomposition once sorbed to clay particles (Wakeham and Canuel, 2006). These distinct storm event layer characteristics have the potential to clarify questions about the magnitude of specific events within the catchment as well as regional changes in frequency and/or intensity over time with relation to natural and anthropogenic influences.

4.3 Textural and Geochemical Signature of the Cyclone Bola Event Layer

Cyclone Bola (1988, return period of >100yr), the most severe tropical storm on record in this region, tracked from east to west across the study area, brought intense rainfall and engendered mass failures in the erodible catchment lithologies and anthropogenically destabilized hillslopes (Figure 2D). During Cyclone Bola, concomitant high wind and wave energy on the shelf likely led to a mud-activating wave base which could have mobilized sediment in even the deepest portions of the two inner-shelf depocenters. Wood (2006) has shown that sediments as deep as ~80m can be mobilized during large wave events. The calculated Depth to Cyclone Bola (DCB; Table 2, Figure 6, black arrows) was used to estimate the depth within the cores at which an event layer produced by Cyclone Bola would be expected. Apparent Cyclone Bola event layers were visually identifiable in five cores (B18, B24, B25, B52, B61), at depths that were consistent with the calculated DCB (Figures 6A, B). With the DCB guiding the selection of the upper limit of the event layers, the layer thicknesses were determined based on the X-radiography plus the full suite of profile analyses (Figure 6, solid grey boxes). The physical and geochemical signatures of Cyclone Bola were found to be sedimentologically unique within shelf stratigraphy and can thus serve as a holotype modern storm event and benchmark comparison to other preserved events and prominent layers in downcore stratigraphy and in longer cores which may be examined in future studies.

The Cyclone Bola event layer has a characteristic internal fabric which is presumably tightly coupled with the hydrodynamics of the cyclone and associated oceanic flood. It is clearly distinct from physically laminated sediments indicative of strong inner-shelf wave reworking (Figure 8A), hypopycnal sedimentation (Figure 8B), and from homogeneous bioturbated muds, all seen in box and Kasten cores on Poverty Shelf. Scour surfaces at the base of the event layer are visible in X-radiographs and indicate initiation of energetic storm waves and currents, as higher energy promotes resuspension and removal of unconsolidated muds. Above the scoured basal contact, the Cyclone Bola event layer has a characteristic, coarse laminated and often cross-bedded lower unit followed by a fining-upwards top unit. Together, the two units presumably reflect the influence of hysteresis of the flood hydrograph. The basal unit is deposited during the waxing phase, when percent silt can be as great as 80% and percent clay decreases as it is resuspended and kept from settling to the seabed. Subsequent waning of the oceanic flood in response to storm energy decrease corresponds to the upper unit, which may be capped by a X-radiographically transparent horizon, when low density muds are deposited (silt returns to ~50%) and bioturbation signifies a recovering benthic community.

In the Cyclone Bola event layer within B6, B24 and B25, the cores located closest to Poverty Bay mouth, these two units are of roughly equal thickness. These cores, along with B3, are situated in the shallow inner zone of the bypassing region which is almost always above fair weather mud-activating wave base (30.2m, Wood 2006) and where net accumulation is low and physically laminated sands are observed in X-radiograph. Total thickness of the Cyclone Bola event layer in these cores is 9.00, 17.25 and 10.50cm, respectively (Table 2, Figure 6A, solid grey boxes). Lead-210 profiles have characteristically steep, sometimes vertical, low total activity profiles throughout the Cyclone Bola event layer in B6, B24 and B25, returning to higher activity below, and often above, the layer.

In core B61, in the Southern Depocenter, the thickness of the entire Cyclone Bola event layer is comparable (9.0cm), however the thickness of its constituent parts are quite different. A stark scour truncates underlying, heavily bioturbated mud followed by a thin, high density (with the highest percent silt recorded in this study), internally laminated basal unit (1.0cm), which grades into the upper, normally graded unit. The contact to overlying sediment is gradational and bioturbated, and both above and below the event layer, the textural signatures return to background homogenous muds. The thickness of the unit is based on a characteristically low ^{210}Pb activities, seen previously, and the area of variable $\delta^{13}C$ and N:C measurements, as the DCB lies within the event layer itself and the bulk density profile does not correspond to clear changes in texture, apparently indicating a MSCL issue.

The Cyclone Bola event layer identified in core B18 is dissimilar to all those previously discussed; basal scour is not seen, and a series of three, 1-2cm-thick, low density and two very thin high density couplets make up the 11cm-thick event layer (Figure 6B). The internally coarsest layers within the event layer are associated with mixed marine and terrestrial $\delta^{13}C$ signatures near -24‰, in comparison to the clay-rich low density fining upwards portions which have a more terrestrial $\delta^{13}C$ value of -25‰. The entire sequence is clearly defined by a lower bulk density profile and the signature, vertical depressed ^{210}Pb activity profile with a return to higher activities in overlying and underlying sediments.

Complete bioturbation in the MM depocenter cores B52 and B85, precludes any visual evidence for a Cyclone Bola event layer to be identified in X-radiographs, therefore the thickness and upper and lower limits of the event signature can only be hypothesized (Figure 6C, grey shaded boxes with question marks). Despite this, geochemical evidence of events exists. A 7cm thick layer having a dramatic swing of over 1‰ in $\delta^{13}C$ towards more depleted values is present just below one of the two DCBs calculated for B85, from a nearby Kasten core (7.77cm; Figure 6C). Concomitant increases in silt and clay provide evidence that, although highly bioturbated, mud from an oceanic flood, possibly Cyclone Bola, may still be traced to specific events. However, using the DCB calculated from B85 ^{210}Pb, a higher accumulation rate is found that places the DCB at ~27cm. In this case, the event previously described is much younger. At this depth, a bulk density profile change along with a small increase in sand is observed, but sample resolution is not fine enough to resolve other changes, if they are present. Four DCB calculations were made for core B52, located in the Southern Depocenter, and the upper limit is fairly well constrained by two of them along with distinct changes in profile characteristics, however the lower $\delta^{13}C$ values are not present (Table 2, Figure 6C). Instead, in the ~7cm layer, a slight uptick in silt content is recorded coincident with a small decrease in ^{210}Pb and a terrestrial N:C signature, however $\delta^{13}C$ values become slightly more positive (marine) at the same time.

The calculated DCB in B6 is likely unrealistic, given its low, uniform activities, signifying little net accumulation at this core site, where persistently energetic inner-shelf hydrodynamics are evidenced by physically dominated stratigraphy and no ^{7}Be activity (Rose and Kuehl, 2010; Table 2, Figure 5A). Possible event layers are present, identifiable X-radiographically and by geochemical profiles, but no date estimation can be made for them, including the Cyclone Bola event.

4.4 Delivery and Spatial Pattern of the Cyclone Bola Event Record

Characteristics of the Cyclone Bola event layer change with location on Poverty Shelf and may reveal differences in delivery to the variety of along-shelf environments represented by core locations. The Cyclone Bola event layer is similar in X-radiographic and geochemical profiles in inner shelf cores B6, B24, and B25, with equal thicknesses of high and low density material. The basal sandy wave-influenced portion, which comprises half of the unit in these cores, is one of the main differences between these layers and those seen in deeper cores. In the shallower areas, waves can more effectively resuspend and winnow fines during the waxing phase of the oceanic flood. Also, proximity to the Waipaoa River mouth enhances delivery of large additions (up to ~80%) of silty material. The overlying lower bulk density sediments are interpreted to correspond with the waning phase of the oceanic flood. The distinct textural signature, plus the characteristically low ^{210}Pb activities throughout the event layer (with a return to higher activities in older sediments) coupled with lower (terrestrial) $\delta^{13}C$ values, especially in the waning phase, make it likely that, at these locations, gravity driven emplacement of the Bola unit occurred, possibly via a hyperpycnal plume. A subsequent flood, later in 1988 (Figure 2A) may have helped to successfully bury the Cyclone Bola event layer in these regions. Other layers, similar to that of the Cyclone Bola event layer are seen in cores B6, B24, and B25, both above and below the Cyclone Bola event layer, as well as in core B3, making it likely that the inner and midshelf is where hyperpycnal plume sedimentation is most often captured.

With distance along-shelf in both directions, the character of the Cyclone Bola event deposit changes. In the MLM depocenter cores (B18 and B61), the Cyclone Bola event layer appears to be the *only* event recorded within core stratigraphy – above and below this layer, low density, heavily bioturbated mud and steady geochemical signatures indicate non-flood suspension settling (Figure 6B). It follows then that farther from the Waipaoa source, within the depocenters, only storms of equal or greater magnitude to Cyclone Bola have the potential to supply enough sediment to these areas to create a flood bed capable of transiting the mixed layer and being preserved within the modern stratigraphic record.

In B61, in the Southern Depocenter, the expression of the Cyclone Bola event layer is nearly as thick as on the inner-shelf but much less sandy overall, as this location is farther from the Waipaoa source and in deeper water. The signature of terrestrial carbon in $\delta^{13}C$ values is muted in comparison to the previously described cores, likely for the same reasons. However, texturally, this layer is similar in character to the inner- and midshelf cores. Strong hyperpycnal delivery to the inner flank of the Southern Depocenter (B61), downslope from the source near Poverty Bay, is consistent with Bever (2010) who found that flood sediment was steered to the south in modeling scenarios.

In contrast, in the Northern Depocenter, the event signature is quite different, composed of rhythmic low and high density units, as described above. It is clear that the stratigraphy within core B18 on the Northern Depocenter reflects multiple increases and decreases in storm intensity/shelf energetics, with clay rich sediments with low (depleted) $\delta^{13}C$ values emplaced as energy wanes and siltier sediments with higher (enriched) $\delta^{13}C$ values emplaced as energy intensifies. It is clear that these pulsed units were emplaced in succession and rapidly, as they are minimally bioturbated and the distribution of bioturbation does not favor the lower density units (Figure 6B). Hyperpycnal emplacement cannot be definitively confirmed, although the entire unit is ^{210}Pb depleted, and the shelf locations of both B61 and B18 fall with the zone of non-steady state Kasten cores (Miller and Kuehl, 2010; Figure 1C, dashed demarcation) and within the MLM facies (Rose and Kuehl, 2010), a veritable "sweet spot" for event sedimentation preservation. Alternatively, hypopycnal sinking from the river plume during reduced and re-intensified parts of the storm could have emplaced the event layer seen in B18, with high concentrations of clay and silt overwhelming the scavenging opportunities causing the low-activity ^{210}Pb signature.

If a hyperpycnal plume was able to travel downslope to the furthest shelf locations investigated, MM depocenter cores B52 and B85, no visual evidence is found in their records. Correlated geochemical signatures provide evidence that these locations did not escape the influence of the cyclonic storm but it is more likely that they are reflective of hypopycnal sedimentation or reworking of the extant seabed during the storm (Figure 6C). Higher accumulation rates at these locations plus a subsequent oceanic flood, less than a year after Cyclone Bola, likely aided in the preservation of the signature. Incidentally, the presumed Cyclone Bola event layer in cores B85 and B52 are thinner than all instances identified in these cores. The Southern Depocenter undoubtedly received a good deal of agitation due to exposure to southern swell during Cyclone Bola and thus the event recorded is interpreted to be more akin to a subtle resuspension signature, with the lowest $\delta^{13}C$ value recorded in this study (23.07‰), along with an uptick in silt presumably reflecting both removal of fines (and consequently sorbed terrestrial organic matter) via reworking and addition of autochthonous material (Figure 6C).

The interpreted hyperpycnal flow emplaced during Cyclone Bola clearly consumed the inner-to mid-shelf as evidenced by event layers at depths corresponding to the expected depth of Cyclone Bola in B6, B24 and B25, as well by clay-rich event layers of 10cm and 1cm thicknesses on the inner and mid-shelf, attributed to the cyclone (Figure 1B, "+" signs), petering out by the outer shelf (Brackley, 2006). The presumed hyperpycnal flow, traveling down slope, extended into both mid-shelf depocenters, evidenced by event layers in B18 and B61, but not to the further reaches of the depocenters in B85 and B52. If, indeed, all the cores in which the Cyclone Bola event layer was identified on the inner and mid-shelf were emplaced by a hyperpycnal plume, and the less proximal B85 and B52 depocenter cores did not experience such emplacement, a rough outline of hyperpycnal plume extent can be traced on the shelf. It is important to note that post-flood emplacement via wave-supported gravity flow, which is observed on the Waiapu shelf, can also result in emplacement of an event layer with a terrestrial signature (Ma et al., 2008 and 2010; Kniskern et al., 2010). However we examine the hyperpycnal method of delivery for Cyclone Bola on the Waipaoa shelf in detail given key geochemical and physical indications described below that are ubiquitous between cores.

Recalling the idealized diagrams of Figure 8 and given the observations of the Cyclone Bola event layer on the shelf, two diagrams are constructed which are slightly more complex in delivery and resultant event layer emplacement characteristics (than Figure 8) but are more realistic in representing Waipaoa River effluent and Poverty Shelf oceanographic conditions (Figure 9). Both are oceanic flood scenarios like that of Cyclone Bola, implying heavy rain and river flooding coincident with enhanced wave activity, as most deposition on Poverty Shelf has been shown to occur in the presence of increased wave/current action (Bever, 2010). The first scenario describes gravity driven event emplacement, while the second describes hypopycnal event emplacement (Figure 9A and B). These scenarios both emplace a fining-upwards sequence, but differences in ^{210}Pb, sorting and thickness may be distinguished. The events described in Figure 9 could be located on the inner to mid Poverty Shelf, as oceanic flood sediment dispersal has been shown to extend well out onto the shelf during flood situations (Foster and Carter, 1997; Brackley, 2006; Bever, 2010) and is preserved within the Cyclone Bola event layer, amongst other event layers, detailed in box cores from this study.

In the first diagram (Figure 9A), an event layer with material derived from a river flood plume is emplaced by gravity driven processes – either hyperpycnal, wave- or current-supported flows (Figure 9A). In this scenario the hypothetical lower coarsening upwards unit (Figure 8C) is not present due to high wave energies on the shelf either resuspending/removing/truncating it following deposition as the storm intensified (if a hyperpycnal flow as in Figure 8C) or indicating it was never deposited, for the same energetic reasons. Instead, a strongly scoured basal contact with underlying sediment is followed by a cross-bedded coarse unit that fines upwards. Lead-210 activities are lower than background sedimentation in this scenario, as seen in the Cyclone Bola event unit. This tell-tale ^{210}Pb low activity profile, which is essentially vertical, reflects gravity driven input, likely hyperpycnal, with no time for scavenging by suspension settling. If flood sediment is subsequently reworked via wave- or current-supported gravity flows, the tell-tale ^{210}Pb signature may remain, as seen within the flood deposits of the 1995 and 1997 Eel River (Sommerfield et al., 1999). The uptick in activity underlying the event layer signifies a return to pre-event sediment, similar to the Cyclone Bola event layers described. This event is expected to have a strong terrestrial signature. If emplaced by a hyperpycnal plume, climbing ripples might be found.

In the second scenario, the oceanic flood emplaces an event layer via a hypopycnal plume (Figure 9B). While this oceanic flood would also have a depleted δ^{13}C signature, enhanced scavenging via suspension settling would be expected to increase excess ^{210}Pb activity within the event layer. An alternate situation may occur, where although suspension settling is the mode of emplacement, suspended sediment concentration is sufficiently high such that ^{210}Pb is over-scavenged and becomes depleted within the water column, effectively causing depletion of ^{210}Pb activities (dashed ^{210}Pb profile, Figure 9B). In addition, in comparison to gravity driven emplacement of an oceanic flood, in the suspension settling scenario the event layer would have a likely weaker scour contact to underlying material, and, although not distinguished in Figure 9B, would likely be thinner and better sorted because of presumed supply differences and the nature of textural fractionation with increased distance from the source.

4.5 Event Layers in Response to Rainfall

Mass wasting in the Tutira Watershed due to Cyclone Bola via landsliding, channel incision, gully and sheet erosion produced a total volume of sediment of 1.35 x 10^6 m^3 (Page et al., 1994). In turn, the Cyclone Bola event layer recovered from cores in Lake Tutira has an average thickness of 36cm (Page et al., 1994). Much uncertainty lies in estimating rainfall based on event layer thickness, not only because event resistance can diminish the response/thickness from subsequent storms (Crozier and Preston, 1999; Page et al., 1994), but erosion type, magnitude and intensity is quite different between pre-historic, Maori and European land use regimes (Eden and Page, 1998; Orpin et al., 2010). However, a positive correlation exists between rainfall intensity and layer thickness in Lake Tutira sediments (Orpin et al., 2010), which likely holds true, to some extent, for wet storm sedimentation on the Poverty Shelf. On the Poverty Shelf, the Cyclone Bola event layer identified in our box cores is between 1.75cm and 17.75cm thick. Back-of-the-envelope budget calculations on the shelf, considering the maximum discharge of Cyclone Bola and assuming a grain density of 2.65g cm^{-3}, show that if the deposit extended only to the limits of the ILMS (Figure 1C; Rose and Kuehl, 2010), the average resultant unit would be 5.2cm in thickness, and if the area included both the ILMS and MLM, the resultant unit would be 4.17cm thick. This is consistent with the thicknesses actually observed, especially when considering primary hyperpycnal deposition would likely not include inner portions of the ILMS, and would also not be spread in equal thickness across the shelf. In addition, this calculation neglects the contribution of material resuspended from the seabed, which may be significant. Thus, the range of Cyclone Bola event layer thicknesses observed on the shelf, between 1.75-12.75cm, appear to be reasonable.

It should be noted that event layers on Poverty Shelf, resulting from more frequent, lower magnitude events than Cyclone Bola (<10 yr return period), may be quite different. Not only was Cyclone Bola a "100-yr event", but the main mechanism of erosion during Bola was landsliding, in comparison to the more ubiquitous contribution of gully erosion. Storms with a frequency <10 years produce the majority of the Waipaoa's sediment load (~86%; Trustrum et al., 1999; Brackley, 2006), however these storms may be less likely to be preserved, if at all, to the degree of the Cyclone Bola event layer. This may skew the resultant layer towards finer grain size, than might be expected for a storm of Cyclone Bola magnitude and intensity. However, in turn, such a layer may never make it into the stratigraphic record. In fact, despite the relatively quick transfer from mountainous source to shelf sink in the WSS and its proclivity for landsliding and high storm sediment yields, it may be that only high magnitude, low frequency events produce enough sediment to be preserved within shelf stratigraphy as event layers. This is in agreement with the commonly cited US analogue to the Poverty Shelf, the Eel River Shelf, where it is estimated that ~90% of modern shelf accumulation is presumed to result from high-frequency small storm events, which are completely obliterated by bioturbation, and where events of >100yr recurrence interval have potential to be preserved within shelf stratigraphy (Leithold and Blair, 2001; Bentley and Nittrouer, 2003; Blair et al., 2004). In addition, it is hypothesized here that storm event layers may prove to be of older ^{14}C ages, as the percentage of ^{14}C-dead (kerogen) carbon sourced from easily erodable (landsliding) sedimentary rocks within the Waipaoa catchment would increase and the contribution of modern aged carbon from marine sources would be expected to be overshadowed. This may be an avenue for future study. Regardless, Cyclone Bola represents a storm with a return frequency of >100 years, and it is clear that the importance of such high magnitude, low frequency events to shelf sedimentation should not be underestimated.

4.6 Depocenter Comparison

The discrete, tectonically created Poverty Shelf depocenters are landward of actively deforming anticlines, and separated by a bathymetric rise, characterized by low accumulation and high density sediments, the "bypassing zone". Although they are adjacent and share the Waipaoa source, differences seen in box core textural and carbon signature in the Northern and Southern Depocenters, especially within the MM facies cores, begets the question of how circulation on the shelf and/or delivery of oceanic flood events is differs between these two locations. Modern Waipaoa shelf currents experience a net northward flow, possibly the northern extension of the Wairarapa Coastal Current (WCC) which may intermittently reverse in direction (Chiswell, 2000; Stephens et al., 2001). Although, the stronger and more persistent East Cape Current (ECC) flows in a southerly direction, it is unlikely to influence shelf sedimentation, except in unusual eddy circumstances, as it lies seaward of the shelf break. Poverty Bay circulation is counterclockwise (Stephens et al, 2001; Bever et al., 2011), and this gyre moves the Waipaoa River plume to the southern portion of the bay, whereby it enters the shelf environment and is likely entrained by the WCC under fair-weather conditions.

Surprisingly, although both MM depocenter cores are characterized by homogenized mottled muds with little down-core density change, detailed stable isotopic and textural comparison of the two MM depocenter cores (B85 and B52) show there are striking differences in $\delta^{13}C$ values and percent sand content, which suggest dissimilar sediment delivery or mode of emplacement, timing, and/or circulation to the depocenters in general (not just event-instantaneous; Figure 6C). These differences are supported by the rapidly expanding understanding of shelf circulation and Waipaoa plume entrainment under storm and non-storm conditions (Bever 2010; Bever et al., 2011; J. Moriarty, Pers. Comm.).

The most striking difference between the two MM depocenter cores is the complete lack of overlap in $\delta^{13}C$ signature. The Southern Depocenter (B52) has more positive $\delta^{13}C$ values reflective of a marine signature, in comparison to the Northern Depocenter, which has lower $\delta^{13}C$ values consistent with mixed marine and terrestrial sources (Figure 7, pink [B52] and orange [B85] squares). As sediment transits Poverty Shelf, the terrestrial signature is attenuated as a result of distance from source (Brackley et al., 2010), and it appears that isotopic fractionation along-shelf occurs as well. The more positive values in the Southern Depocenter indicate an enhanced autochthonous (or diluted) carbon source or perhaps a more direct terrestrial input to the Northern Depocenter. The Southern Depocenter likely experiences disproportional reworking and removal of fines due to increased exposure to southern swell which could explain the differences in $\delta^{13}C$ values. An addition of more refractory material into the Southern Depocenter, transported from either (or a combination of) Hawke Bay or the rocky Mahia peninsula (as reported from satellite image analysis, Brackley, 2006; Wood, 2006; L. Carter, Pers. Comm.) and entrained into sediment-laden gyres into the WCC, would also dilute Waipaoa input and converge to create a more marine signature in the Southern Depocenter. In addition, increased transport of terrestrial/soil material from the East Cape, north of the study site, along with a greater quantity or more consistent delivery of fresh plume material during fair weather conditions from the Waipaoa to the Northern Depocenter could help explain the $\delta^{13}C$ discrepancy. The dominant northward WCC flow (augmented by the tidal cycle and infrequent strong southerly systems), supports this explanation (Chiswell, 2000; Stephens et al., 2006; Bever, 2010). Some amount of riverine sediment is dispersed to the Southern Depocenter, as the stable carbon isotopic signature still reflects a mixed terrestrial and marine source (Figure 6A). Using simple modeling scenarios, Wood (2006) showed that although little of the (generally deeper) Northern Depocenter is below the mud activating wave base, nearly the entire

Southern Depocenter experiences resuspension of non-cohesive deposits under storm conditions. Associated terrestrial organic carbon may be effectively trapped in the north, but removed in the south under these conditions.

Interestingly, percent sand sized fraction between the mid-shelf depocenters, including both the ILMS and MLM (B18 and B85 in the north and B61 and B52 in the south) is also different, the Northern Depocenter having a significantly higher percent sand content overall than the Southern Depocenter (Table 3, Figure 6B, C). This appears to be in direct disagreement with the above described $\delta^{13}C$ discrepancy as terrestrial material is often associated with more particle-reactive fine sediments. However, this textural finding is corroborated by Wood (2006) who found the top 1cm of Northern Depocenter mud (split from the from 85 box cores collected, 8 of which are the same used in this study) was generally coarser than the Southern Depocenter. It is possible that the promontory of the Mahia peninsula in the south could play a role in this textural observation, as it may shelter the Southern Depocenter, potentially retarding current movement over the shelf in its lee, resulting in more fines settling out of suspension in the south vs. the north. In addition, highest modern accumulation rates are measured using ^{7}Be and ^{210}Pb in the Southern Depocenter, and Gerber et al. (2010) have demonstrated with seismic reflection that the Northern Depocenter is overfilled. In addition, if during moderate, non-flood wave resuspension events, fines were removed from the Northern Depocenter and transported to the Southern Depocenter assisted by the presence of a net southeasterly flowing bottom current during reversal of the Wairarapa Coastal Current (Wood, 2006; L. Carter, Pers. Comm.), a finer, more marine $\delta^{13}C$ values would be emplaced in the Southern Depocenter.

5. Conclusions

Modern (<100yr) stratigraphy preserved offshore of the high-yield Waipaoa River, New Zealand on the Poverty Shelf is described using high resolution analyses of eight box cores located between and within two mid-shelf depocenters. This study provides a holistic approach to sediment characterization, using several different tools, allowing for a more comprehensive and detailed shelf-wide textural and geochemical identification of event sedimentation than has been previously been undertaken. The most catastrophic cyclone on record, which produced an oceanic flood, Cyclone Bola (1988) is identified texturally and geochemically within seven of the eight box cores. Specific findings from this study are as follows:

1. Eight box cores from the Poverty Shelf preserve prominent layering, laminations, and bioturbated muds in X-radiography, dependant on spatial location on the shelf and correlated to facies identified by Rose and Kuehl (2010).

2. Detailed profiles of box core bulk density, texture, ^{210}Pb and $\delta^{13}C$ values, provide high-resolution records of strata preserved on the Poverty Shelf, including preservation of stochastic inputs, such as event layers. Texture varies with shelf location and a range of $\delta^{13}C$ values consistent with a mixture of marine and terrestrial carbon is recorded in all cores.

3. Using previously published accumulation rates (Miller and Kuehl, 2010), the depth to an impact to the seabed from Cyclone Bola, the most severe modern storm on record in the study area, was estimated to be between ~8-20cm in the depocenters.

4. The Cyclone Bola event layer is distinguished from fair-weather background sedimentation by a texturally and geochemically unique signature. On the inner and mid-shelf, the event layer is composed of a coarse, internally laminated and cross-bedded unit followed by a fining upwards unit, interpreted to correspond to the oceanic flood and hyperpycnal flow emplacement. Carbon isotopes reflect a strong terrestrial source within the Cyclone Bola event layer. In completely bioturbated cores, located the farthest from the Waipaoa mouth, no physical signature is recorded. A resuspension event is recorded in the Southern Depocenter, coincident with the depth calculated to Cyclone Bola, and in the Northern Depocenter, a geochemical trace of terrestrial input is found, but it can not be definitively pinned to having been emplaced by Cyclone Bola.

5. Characteristic low, often vertical ^{210}Pb activities, with a return to higher activities in underlying and overlying sediments, are ubiquitous within the Cyclone Bola event layer on Poverty Shelf and are taken as the hallmark of gravity-driven emplacement of event layers here, interpreted to be emplaced by a hyperpycnal flow in all but the 2 most distal box core locations

6. There are dramatic differences in carbon stable isotopic and textural signature of the box core record between the two mid-shelf depocenters interpreted to be a function of additional sources in addition to the dominant Waipaoa source, as well as differences in circulation on the shelf and delivery of sediment to the depocenters.

Literature Cited

Appleby, P.G. and F. Oldfield. 1978. The calculation of Lead-210 dates assuming a constant rate of supply of unsupported ^{210}Pb to the sediment. *CATENA*, 5: 1-8.

Bever, A. 2010. Integrating Space-and-Time-Scales of Sediment Transport for Poverty Bay, New Zealand. Ph.D. Dissertation, College of William and Mary. 262 pp.

Bever, A., McNinch, J., Harris, C. 2011. Hydrodynamics and sediment-transport in the nearshore of Poverty Bay, New Zealand: Observations of nearshore sediment segregation and oceanic storms. *Continental Shelf Research*, 31: 507-526.

Bentley, S.J. and C.A. Nittrouer. 2003. Emplacement, modification, and preservation of event strata on a flood-dominated continental shelf: Eel shelf, Northern California. *Continental Shelf Research*, 23: 1465-1493.

Blair, N.E., Leithold, E.L., Aller, R.C. 2004. From bedrock to burial: the evolution of particulate organic carbon across coupled watershed-continental margin systems. *Marine Chemistry,* 92: 141-156.

Brackley, H.L. 2006. Land to ocean transfer of erosion-related carbon, Waipaoa sedimentary system, East Coast, New Zealand. PhD Dissertation, Victoria University of Wellington. 129 pp. plus appendices.

Brackley, H.L., Blair, N.E., Trustrum, N.A., Carter, L., Leithold, E.L., Canuel, E.A., Johnston, J.H., Tate, K.R. 2010. Dispersal and transformation of organic carbon across an episodic, high sediment discharge continental margin, Waipaoa Sedimentary System, New Zealand. *Marine Geology*, 270: 202-212.

Bouma, A. 1962. Sedimentology of some flysch deposits: A graphic approach to facies interpretation. Elsevier, Amsterdam. 167 pp.

Bourgeois, J. 1980. A transgressive shelf sequence exhibiting hummocky stratification: The Cape Sebastian sandstone (upper Cretaceous), southwestern Oregon. *Journal of Sedimentary Petrology*, 50: 681-702.

Carter, L. 2001. Currents of change: the ocean flow in a changing world. *NIWA Water and Atmosphere*, 4: 15-17.

Carter, L., Carter, R.M., McCave, I.N., Gamble, J. 1996. Regional sediment recycling in the abyssal Southwest Pacific Ocean. *Geology*, 24: 735-738.

Chiswell, S.M. 2000. The Wairarapa Coastal Current. *New Zealand Journal of Marine and Freshwater Research*, 40: 303-315.

Chiswell, S.M. 2005. Mean and Variability in the Wairarapa and Hikurangi Eddies, New Zealand. *New Zealand Journal of Marine and Freshwater Research*, 39: 121-134.

Crockett, J.S. and C.A. Nittrouer. 2004. The sandy inner-shelf as a repository for muddy sediment: an example from Northern California. *Continental Shelf Research*, 24: 55-73.

Crozier, M.J. and N.J. Preston. 1999. Modelling changes in terrain resistance as a component of landform evolution in unstable hillcountry. *In* Hergarten, S., Neugebauer, H.J., Eds., Process Modeling and Landform Evolution, Lecture Notes in Earth Sciences, 78. Springer Verlag, Berlin, 267-284.

Eden, D.N. and M.J. Page. 1998. Palaeoclimatic implications of a storm erosion record from late Holocene lake sediments, North Island, New Zealand, *Palaeogeography, Palaeoclimatology and Palaeoecology*, 139: 37-58.

Folk, R.L. 1980. Petrology of Sedimentary Rocks. Hemphill Publishing, Austin, TX, 184pp.

Foster, G. and L. Carter. 1997. Mud sedimentation on the continental shelf at an accretionary margin – Poverty Bay, New Zealand. *New Zealand Journal of Geology and Geophysics*, 40: 157-173.

Francois, F., Poggiale, J-C., Durbec, J-P., Stora, G. 1997. A new approach for the modeling of sediment reworking induced by a macrobenthic community. *Acta Biotheoretica*, 45: 295-319.

Fry, B. and E.B. Sherr. 1984. ^{13}C Measurements as indicators of carbon flow in marine and freshwater ecosystems. *Contributions In Marine Science*, 27: 13-47.

Gerber, T., Pratson., L., Kuehl, S., Walsh, J.P., Alexander, C., Palmer, A. 2010. The influence of post-glacial sea level rise and tectonics on sediment storage along the high-sediment supply Waipaoa continental shelf. *Marine Geology*, 270: 139-159.

Geyer, W.R., Hill, P., Kineke, G.C. 2004. The transport, transformation and dispersal of sediment by buoyant coastal flows. *Continental Shelf Research*, 24: 927-949.

Geyer, W.R., Traykovski, P., Hill, P., Milligan, T. 2000. The structure of the Eel river plume during floods. *Continental Shelf Research*, 28: 865-886.

Goldfinger, C., Grijalva, K., Burgmann, R., Morey, A.E., Johnson, J.E., Nelson, C.H., Gutierrez-Pastor, J., Ericsson, A., Karabanov, E., Chaytor, J.D., Patton, J., Gracia, E. 2008. Late Holocene rupture of the Northern San Andreas Fault and possible stress linkage to the Cascadia subduction zone. *Bulletin of the Seismological Society of America*, 98: 861-889.

Goldfinger, C., Morey, A.E., Nelson, C.H., Guitierrez-Patonr, J., Johnson, JE., Karabanov, E., Chaytor, J., Eriksson, A. 2007. Rupture lengths and temporal history of significant earthquakes on the offshore and north coast segments of the Northern San Andreas Fualt based on turbidite stratigraphy. *Earth and Planetary Science Letters*, 254: 9-27.

Goldfinger, C., Nelson, C.H., Johnson, J.E. 2003. Holocene earthquake records from the Cascadia subduction zone and Northern San Andreas Fault based on precise dating of offshore turbidites. *Annual Review of Earth and Planetary Sciences*, 31: 555-577.

Gomez, B., Carter, L., Trustrum, N.A. 2007. A 2400 yr record of natural events and anthropogenic impacts in intercorrelated terrestrial and marine sediment cores: Waipaoa sedimentary system, New Zealand. *Geological Society of America Bulletin,* 119: 1415-1432.

Gomez, B., Carter, L., Trustrum, N.A., Palmer, A.S., Roberts, A.P. 2004. El Nino – Southern Oscillation signal associated with middle Holocene climate change in intercorrelated terrestrial and marine sediment cores, North Island, New Zealand. *Geol*ogy, 32: 653-656.

Griffiths, G.A. 1982. Spatial and temporal variability in suspended sediment yields of North Island basins, New Zealand. *Water Resources Bulletin*, 8: 575-583.
Guinasso, N.L and D.R. Schink. 1975. Quantitative estimates of biological mixing rates in abyssal sediments. *Journal of Geophysical Research*, 80: 3032-3043.
Hedges, J.I. and R.G. Keil. 1995. Sedimentary organic matter preservation: an assessment and speculative synthesis. *Marine Chemistry*, 49: 81-115.
Hedges, J.I., Keil, R.G., Benner, R. 1997. What happens to terrestrial organic matter in the ocean? *Organic Geochemistry*, 27: 195-212.
Hicks, D.M., Gomez, B., Trustrum, N.A. 2000. Erosion thresholds and suspended sediment yields, Waipaoa River Basin, New Zealand. *Water Resources Research*, 36: 1129-1142.
Hicks, D.M., Gomez, B., Trustrum, N.A. 2004. Event suspended sediment characteristics and the generation of hyperpycnal plumes at river mouths: East Coast ContinentalMargin, North Island, New Zealand. *Journal of Geology*, 112: 471-485.
Kettner, A.J., Bomez, B., Syvitski, J.P.M. 2007. Modeling suspended sediment discharge from the Waipaoa river system, New Zealand: The last 3000 years. Water Resources Research, v.43: W07411, doi: 10.1029/2006WR005570.
Kniskern, T.A, Kuehl, S.A., Harris, C.K., Carter, L. 2010. Sediment accumulation patterns and fine-scale strata formation on the Waiapu River shelf, New Zealand. *Marine Geology*, 270: 188-201.
Kuehl, S.A., Pacioni, T.D., Rine, J.M. 1995. Seabed dynamics of the inner Amazon continental shelf: temporal and spatial variability of surficial strata. *Marine Geology,* 125: 283-302.
Kuehl, S., Alexander, C., Carter, L., Gerald, L., Gerber, T., Harris, C., McNinch, J., Orpin, A., Pratson, L., Syvitski, J., Walsh, J.P. 2006. Understanding sediment transfer from land to ocean. *EOS, Transactions*, 87: 281-286.
Lecroart, P., Schmidt, S., Anschutz, P, Jouanneau, J-M. 2007. Modeling sensitivity of biodiffusion coefficient to seasonal bioturbation. *Journal of Marine Research*, 65: 1-24.
Leithold, E.L. and R.S. Hope. 1999. Deposition and modification of a flood layer on the northern California shelf: lessons from and about the fate of terrestrial particulate organic carbon. *Marine Geology*, 154: 183-195.
Leithold, E.L. and N.E. Blair. 2001. Watershed control on the carbon loading of marine sedimentary particles. *Gecochemica et Cosmochimica Acta*, 65: 2231-2240.
Leithold, E.L., Blair, N.E., Perkey, D.W. 2006. Geomorphologic controls on the age of particulate organic carbon from small mountainous and upland rivers. *Global Biogeochemical Cycles*, 20: 3022-3033.
Lewis, K.B. 1973. Erosion and deposition on a tilting continental shelf during Quaternary oscillations of sea level. *New Zealand Journal of Geology and Geophysics*, 16: 281-301.
Ma, Y., Friedrichs, C.T., Harris, C.K., Wright, L.D. 2010. Deposition by seasonal wave-and current-supported sediment gravity flows interacting with spatially varying bathymetry: Waiapu shelf, New Zealand. *Marine Geology*, 275; 199-211.

Ma, Y., Wright, L.D., Friedrichs, C.T. 2008. Observations of sediment transport on the continental shelf off the mouth of the Waiapu River, New Zealand: Evidence for current-supported gravity flows. *Continental Shelf Research*, 28; 516-532.

Margins Science Plans. 2003. Source-to-Sink NSF MARGINS Program Science Plans. Lamont-Doherty Earth Observatory of Columbia University, New York.

Miller, A.J, and S.A. Kuehl. 2010. Shelf sedimentation on a tectonically active margin: A modern sediment budget for Poverty continental shelf, New Zealand. *Marine Geology*, 270: 175-187.

Milliman, J., and J.P.M. Syvitski. 1992. Geomorphic/tectonic control of sediment discharge to the ocean: the importance of small mountainous rivers. *Journal of Geology*, 100: 525-544.

Mount, J.F. 1982. Storm-surge-ebb origin of hummocky cross-stratified units of the Andrews Mountain Member, Campito Formation (lower Cambrian), White-Inyon Mountains, eastern California. *Journal of Sedimentary Petrology*, 52: 941-958.

Mulder, T. and J.P.M. Syvitski. 1995. Turbidity currents generated at river mouths during exceptional discharges to the world oceans. *Journal of Geology*, 103: 285-299.

Mulder, T., Syvitski, J.P.M., Migeon, S., Faugeres, J.C., Savoye, B. 2003. Marine hyperpycnal flows: initiation, behavior and related deposits. A review. *Marine and Petroleum Geology*, 20: 861-882.

Nittrouer, C.A., Austin, J.A., Field, M.E., Kravitz, J.H., Syvitski, J.P.M., Wiberg, P.L. 2007. Writing a Rosetta stone: insights into continental-margin sedimentary processes and strata. C. Nittrouer, J. Austin, M. Field, J. Kravitz, J. Syvitski and P. Wiberg (Eds.), *In* Continental Margin Sedimentation, Wiley-Blackwell, Hoboken, N.J., pp 1-48.

Nittrouer, C.A. and R.W. Sternberg. 1981. The formation of sedimentary strata in an allochthonous shelf environment: The Washington continental shelf. *Marine Geology*, 42: 201-232.

Nittrouer, C.A., Sternberg, R.W., Carpenter, R., Bennett, J.T. 1979. The use of Pb-210 geochronology as a sedimentological tool: application to the Washington continental shelf. *Marine Geology*, 31: 297-316.

Orpin, A.R., Alexander, C., Carter, L., Kuehl, S., Walsh, J.P. 2006. Temporal and spatial complexity in post-glacial sedimentation on the tectonically active, Poverty Bay continental margin of New Zealand. *Continental Shelf Research*, 26: 2205-2224.

Orpin, A.R., Carter, L., Page, M.J., Chochran, U.A., Trustrum, N.A., Gomez, B., Palmer, A.S., Mildenhall, D.C., Rogers, K.M., Brackley, H.L., Northcote, L. 2010. Holocene sedimentary record from Lake Tutira: A template for upland watershed erosion proximal to the Waipaoa Sedimentary Systerm, northeastern New Zealand. *Marine Geology*, 270: 11-29.

Page, M.J., Reid, L.M., Lynn, I.H. 1999. Sediment production form Cyclone bola landslides, Waipaoa catchment. *New Zealand Journal of Hydrology*, 38: 289-308.

Page, M.J., Trustrum, N.A., Brackley, H.L., Gomez, B., Kasai, M., Marutani, T. 2001. Waipaoa River (North Island, New Zealand). Marutani T., Brierley, G.J., Trustrum, N.A., Page, M.J., (Eds.), *In* Source-to-Sink Sedimentary Cascades in Pacific Rim Geo-Systems, Matsumoto Sabo Work Office, Ministry of Land, Infrastructure and Transport, Japan, pp. 86-101.

Page, M.J., Trustrum, N.A., Dymond, J.R. 1994. Sediment budget to assess the geomorphic effect of a cyclonic storm, New Zealand. *Geomorphology*, 9: 169-188.

Parsons, J.D., Bush, J.W.M., Syvitski, J.P.M. 2001. Hyperpycnal plume formation from riverine inflows with small sediment concentrations. *Sedimentology*, 48: 465-478.

Pickrill, R.A. and J.S. Mitchell. 1979. Ocean wave characteristics around New Zealand. *New Zealand Journal of Marine and Freshwater Research*, 13: 501-520.

Pouderoux, H., Prouste, J-N., Lamarche, G., Orpin, A., Neil, H. 2012. Postglacial (after 18 ka) deep-sea sedimentation along the Hikurangi subduction margin (New Zealand): Characterization, timing and origin of turbidites. *Marine Geology*, 295-298: 51-76.

Reed, D., Huang, K., Boudreau, B.P., Meysmann, F.J.R. 2006. Steady-state tracer dynamics in a lattice-automaton model of bioturbation. *Geochemica et Cosmochimica Acta*, 70: 5855-5867.

Rose, L.E. and S.A. Kuehl. 2010. Recent sedimentation patterns and facies distribution on the Poverty Shelf, New Zealand. *Marine Geology*, 270: 160-174.

Rose, L.E., Kuehl, S.A., Orpin, A.R., Alexander, C. R., Palmer, A.S. In Prep. Complete, High-Resolution Shelf Record of Changes in Sediment Supply, Eustacy, Tectonics and Climate from LGM-Present, Poverty Shelf, N.Z. 31pp.

Sadler, P.M. 1981. Sediment accumulation rates and the completeness of stratigraphic sections. *Journal of Geology*, 89: 569-584.

Shanmugam, G. 2000. 50 years of the turbidite paradigm (1950s-1990s): deep-water processes and facies models – a critical perspective. *Marine and Petroleum Geology*, 17: 285-342.

Sommerfield, C.K. and C.A. Nittrouer. 1999. Modern accumulation rates and a sediment budget for the Eel shelf: a flood-dominated depositional environment. *Marine Geology*, 154: 227-241.

Sommerfield, C.K., Nittrouer, C.A., Alexander, C.R. 1999. ^{7}Be as a tracer of flood sedimentation on the northern California continental margin. *Continental Shelf Research*, 19: 335-361.

Stephens, S.A. Bell, R.G., Black, K.P. 2001. Complex circulation in a coastal embayment: shelf current, wind and density - driven circulation in Poverty Bay, New Zealand. *Journal of Coastal Research Special Issue*, 34: 45-59.

Traykovski, P., Geyer, W.R., Irish, J.D., Lynch, J.F. 2000. The role of wave-induced density-driven fluid mud flows for cross-shelf transport on the Eel River continental shelf. *Continental Shelf Research*, 20: 2113-2140.

Trustrum, N.A., Gomez, B., Page, M.J., Reid, L.M., Hicks, D.M. 1999. Sediment production, storage and output: The relative role of large magnitude events in steepland catchments. *Zeitshrift fur Geomorphologie Supplement*, 115: 71-86.

Wadman, H.M. and J.E. McNinch. 2008. Stratigraphic spatial variation on the inner-shelf of a high-yield river, Waiapu River, New Zealand: Implications for fine-sediment dispersal and preservation. *Continental Shelf Research*, 28: 865-886.

Wakeham, S.G. and E.A. Canuel. 2006. Degradation and preservation of organic matter in marine sediments. *Handbook of Environmental Chemistry*, 2: 1-27.

Walling, D.E. and B.W. Webb. 1996. Erosion and sediment yield: a global overview. *International Association of Hydrological Sciences Publications*, 236: 3-19.

Wheatcroft, R.A. 2000. Oceanic flood sedimentation: a new perspective. *Continental Shelf Research*, 20: 2059-2066.

Wheatcroft, R.A. and J.C. Borgeld. 2000. Oceanic flood deposits on the northern California shelf: large-scale distribution and small-scale physical properties. *Continental Shelf Research*, 20: 2163-2190.

Wheatcroft, R.A. and D.E. Drake. 2003. Post-depositional alteration and preservation of sedimentary event layers on continental margins. *Marine Geology*, 199: 123-137.

Wheatcroft, R.A., Wiberg, P. L., Alexander, C.R., Bentley, S.J., Drake, D.E., Harris, C.K., Ogston A.S. 2007. Post-depositional alteration and preservation of sedimentary strata. *In* C. Nittrouer, J. Austin, M. Field, J. Kravitz, J. Syvitski and P. Wiberg (Eds.), *Continental Margin Sedimentation,* Wiley-Blackwell, Hoboken, N.J., pp 101-155.

Wilmshurst, J.M., McGlone, M.S., Partridge, T.R. 1997. A late Holocene history of natural disturbance in lowland podocarp/hardwood forest, Hawke's Bay, New Zealand. *New Zealand Journal of Botany*, 35: 79-96.

Wood, M.P. 2006. Sedimentation on a high input continental shelf at the active Hikurangi margin, Poverty Bay, New Zealand. Unpublished M.S. thesis, Victoria University of Wellington. 141 pp. plus appendices.

Table 1. Box core location, facies, ^{7}Be and length correction information. Facies classifications include Interlaminated Muds and Sands (ILMS), Mixed Layers and Mottles (MLM) and Mottled Muds (MM).

Box Core	Lat (S)	Long (E)	Length (cm)	Water Depth (m)	Facies Classification*	^{7}Be Inventory (dpm cm^{-2})*	Length Correction (cm)**
B3	38.7698	178.1176	20	38	ILMS	0.000	-1.3
B6	38.7352	178.1485	25	33	ILMS	0.972	-1.3
B18	38.7623	178.1905	36	53	MLM	0.566	-3
B24	38.8248	178.0729	35	46	ILMS	1.015	+1
B25	38.7827	178.0831	26	38	ILMS	0.040	-7
B52	38.9255	178.004	38	50	MM	1.299	+2
B61	38.8763	178.0491	43	49	MLM	1.013	-8
B85	38.6838	178.1911	39	46	MM	2.884	+4

*Rose and Kuehl, 2010
**See section 2.5, "Correction for Compaction and Expansion"

Table 2. Box core and corresponding Kasten cores ^{210}Pb information, accumulation rates and calculated depth to Cyclone Bola (DCB).

Box Core	Box Core or Corresponding Kasten Core	^{210}Pb Accumulation Rate (cm yr^{-1})† or Profile type	Penetration Depth of Excess ^{210}Pb Activity (cm)†	^{210}Pb supported Activity (dpm g^{-1})†	Mixed Layer Depth (cm)†	Depth to Bola (DCB, cm; see Figure 6)**	Interpreted Thickness of Bola Event Layer (cm; see Figure 6)
B3	**B3**	**Low, uniform**					**-**
	K10	Low, uniform		0.93		-	
	K18	0.16	12	0.87		2.70**	
	K73	Non-steady				-	
	K90	Low, uniform				-	
	K72	Low, uniform		1.04***		-	
	K24	Low, uniform				-	
B6	**B6**	**Low, uniform**					**9.00**
	K10	Low, uniform				-	
	K87	0.48	21	0.90		8.11**	
B18	**B18**	**Non-steady**					**11.00**
	K17	1.12	105	0.71		18.90**	
	K16	0.83	73	0.45		14.00**	
B24	**B24**	**Non-steady; 0.25***				**4.22**	**17.75**
	K25	Low, uniform				-	
	K26	0.22	29	1.39		3.71**	
	K69	Non-steady				-	
B25	**B25**	**Low, uniform; 0.50***				**8.44**	**10.50**
	K24	Low, uniform		1.04***		-	
	K72	Low, uniform		1.04***		-	
B52	**B52**	**Steady-state; 1.02**	**Not reached**	**0.80**	**5.5**	**22.73**	**7.00 - ?**
	K45	0.85	92	0.77		14.35**	
	K46	0.59	65	0.75		9.96**	
	K49	0.87	75	0.89		14.69**	
B61	**B61**	**Non-steady; 1.00***				**16.88**	**8.25**
	K66	Non-steady				-	
	K35	Non-steady				-	
B85	**B85**	**Steady-state; 1.31**	**Not reached**	**0.58**	**5.5**	**27.63**	**7.75-1.75 - ?**
	K79	0.46	45	0.58		7.77**	

†Kasten core ^{210}Pb profiles from Miller and Kuehl, 2010; box core ^{210}Pb profiles from this study, see Figure 4.
*Estimated from Accumulation Map (Miller and Kuehl, 2010), see Figure 1B.
**Kasten core information did not included mixed layer depth, therefore Kasten core DCB calculation does not reflect a possible mixed layer
***Averaged from low, uniform activity profiles from Miller and Kuehl, 2010. Note that these activities are similar to those found in corresponding box core profiles.

Table 3. Mean and standard deviations for KM box core textural data. Numbers in parentheses next to box core IDs indicate the number of samples corresponding to each average.

	All Samples (S and T)		
Box Core	% Sand	% Silt	% Clay
B3 (13)	30.33 ± 17.57	37.74 ± 8.32	31.93 ± 11.84
B6 (18)	18.25 ± 15.84	50.38 ± 19.43	31.36 ± 16.03
B18 (17)	4.73 ± 4.99	56.45 ± 8.95	38.82 ± 9.91
B24 (19)	3.04 ± 3.25	59.07 ± 12.07	37.88 ± 12.98
B25 (14)	10.88 ± 6.52	60.45 ± 5.64	28.66 ± 11.32
B52 (10)	3.32 ± 1.31	57.59 ± 4.47	39.09 ± 5.01
B61 (15)	1.34 ± 2.32	44.25 ± 9.89	54.41 ± 11.22
B85 (14)	14.94 ± 5.19	55.54 ± 5.40	29.52 ± 3.64

	Survey Samples		
Box Core	% Sand	% Silt	% Clay
B3 (5)	45.00 ± 15.57	31.77 ± 10.92	23.24 ± 5.68
B6 (6)	17.21 ± 15.77	60.67 ± 14.52	22.12 ± 14.83
B18 (8)	7.13 ± 6.18	58.15 ± 10.47	34.72 ± 10.24
B24 (8)	2.80 ± 3.58	57.32 ± 13.20	39.88 ± 14.61
B25 (7)	13.33 ± 7.87	62.80 ± 4.46	23.87 ± 10.23
B52 (8)	3.53 ± 1.41	58.81 ± 4.17	37.66 ± 4.55
B61 (8)	1.79 ± 3.14	41.61 ± 10.19	56.60 ± 12.58
B85 (8)	17.51 ± 5.28	53.42 ± 5.73	29.06 ± 2.94

	Target Samples		
Box Core	% Sand	% Silt	% Clay
B3 (8)	21.17 ± 11.88*	41.47 ± 3.02*	37.36 ± 11.59*
B6 (12)	17.51 ± 15.58	45.30 ± 16.75	37.19 ± 16.33
B18 (9)	2.59 ± 2.33	54.94 ± 7.68	42.47 ± 9.12
B24 (11)	3.22 ± 3.15	60.35 ± 11.67	36.43 ± 12.17
B25 (7)	8.44 ± 4.86	58.11 ± 6.03	33.45 ± 10.93
B52 (2)	2.59 ± 0.61	53.33 ± 2.98	44.07 ± 3.59
B61 (7)	0.83 ± 0.68	47.27 ± 9.34	51.90 ± 9.77
B85 (6)	11.50 ± 2.47*	58.36 ± 3.65	30.13 ± 4.65

* Statistically significant ($P < 0.05$) difference from corresponding Survey sample fraction.

Chapter 2 Figure Legend

Figure 1.
A. North Island, New Zealand with study area indicated by red box. WC = Waipaoa River Catchment. TVZ = Taupo Volcanic Zone. RP = Raukumara Peninsula. EC = East Cape. LT (star) = Lake Tutira. **B.** Poverty Margin location map with R/V Kiloa Moana (KM) box cores. Spatial distribution of ^{210}Pb accumulation rates (cm yr^{-1}) underlain from Miller and Kuehl (2010). W = Waipaoa River Mouth. **C.** R/V Kiloa Moana box cores and accompanying Kasten cores overlain on facies distribution according to Rose and Kuehl, 2010. Kasten cores were used to find accumulation at the box core locations. Cores are overlain on facies distribution (Rose and Kuehl, 2010). X-radiographic examples of facies observed in three representative box cores from this study.

Figure 2.
A. Record of Waipaoa River discharge and sediment concentration at Kanakania gauging station from 1970-2010. Dashed line indicates threshold above which it is hypothesized that a hyperpycnal flow may be initiated (40g L^{-1}). Data are from the Gisborne District Council courtesy of Greg Hall and Dave Peacock. Figure modified from Julia Moriarty, personal communication. **B.** Record of Waipaoa River discharge and sediment concentration at Kankania gauging station during Cyclone Bola (March 1988). The threshold for hyperpycnal flow initiation was exceeded. Figure modified from Julia Moriarty, personal communication. **C.** Photograph of bridge over the swollen Waipaoa River at Kankania gauging station during Cyclone Bola, courtesy of Dave Peacock. **D.** Photograph of widespread landsliding post-Cyclone Bola in the nearby Waimata catchment, courtesy of Neal Trustrum.

Figure 3.
Example of X-radiograph guiding KM box core sampling - Survey (S; 1cm thickness, every 5cm) and Target (T; 0.5cm thickness) samples shown.

Figure 4.
^{210}Pb total activity profiles for the eight box cores are shown in the first two columns. In the second column, excess activity profiles and calculated accumulation rates are shown for steady-state cores that extended beyond the penetration depth of ^{210}Pb (B24, B61).

Figure 5.
Comparison of δ^{13}C from KM samples from the same depth interval within cores to ensure no degradation. One set was dried immediately post cruise (February 2005) and analyzed and the other set was kept frozen in X-radiographic subsamples, thawed and then processed (August 2007).

Figure 6.
KM box core depth profiles. **A.** Inner shelf and midshelf cores: B3, B6, B18, B24 **B.** MLM depocenter cores: B25, B52 **C.** MM depocenter cores: B61, B85. Parameters

included for each core are: dry bulk density (g cc^{-3}), percent clay silt and sand, ^{210}Pb total activity (dpm g^{-1}, grain size corrected), $\delta^{13}C$ and mass N:C ratios, along with corresponding X-radiograph. X-axes are the same for each core except for those in gray, which note changes in the X-axis range. Arrows signify calculated DCB.

Figure 7.
A. KM box core $\delta^{13}C$ vs. N:C plotted according to Leithold and Hope, 1999, with regression lines shown. **B.** KM box cores plotted by the range of $\delta^{13}C$ and N:C values found in each core. **C.** KM box core ^{210}Pb and $\delta^{13}C$.

Figure 8.
Conceptual diagrams of idealized units emplaced by a variety of end-member riverine and oceanographic conditions. **A.** "Dry Storm" – southern swell (waves), no flood. **B.** River flood, suspension settling, no waves. **C.** Hyperpycnal flow.

Figure 9.
Conceptual diagrams of units emplaced during Cyclone Bola. **A.** Oceanic flood with gravity driven event emplacement. **B.** Oceanic flood with suspension settling event emplacement.

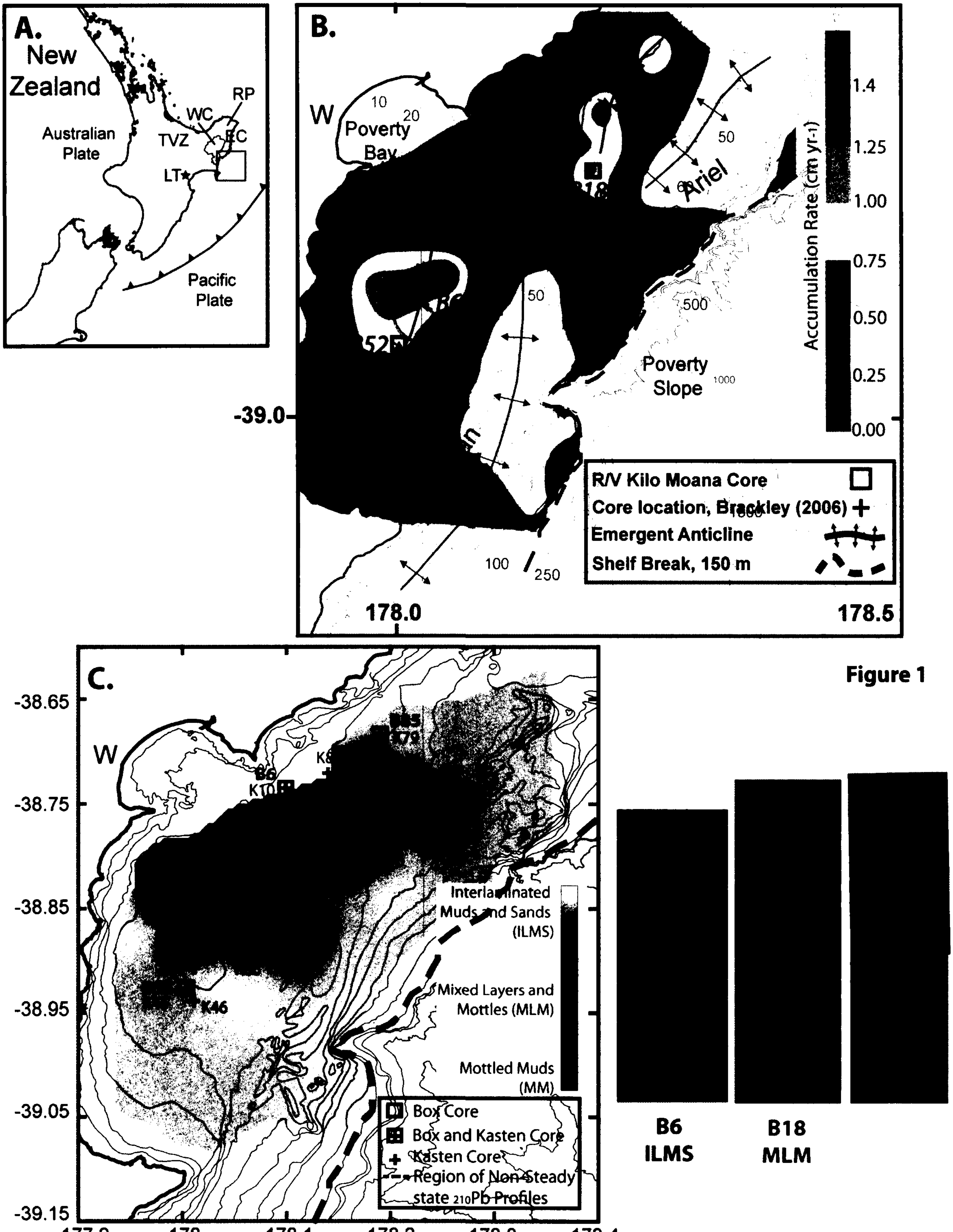

A.
New Zealand
Australian Plate
TVZ
WC
RP
EC
LT
Pacific Plate
B.
W
10
20
Poverty Bay
50
Ariel
500
Poverty Slope
1000
-39.0
50
100
250
178.0
178.5
Accumulation Rate (cm yr-1)
1.4
1.25
1.00
0.75
0.50
0.25
0.00
R/V Kilo Moana Core
Core location, Brackley (2006)
Emergent Anticline
Shelf Break, 150 m
C.
-38.65
-38.75
-38.85
-38.95
-39.05
-39.15
177.9
178
178.1
178.2
178.3
178.4
W
B6
K10
K46
Interlaminated Muds and Sands (ILMS)
Mixed Layers and Mottles (MLM)
Mottled Muds (MM)
Box Core
Box and Kasten Core
Kasten Core
Region of Non-Steady state 210Pb Profiles
B6 ILMS
B18 MLM

Figure 1

Figure 2

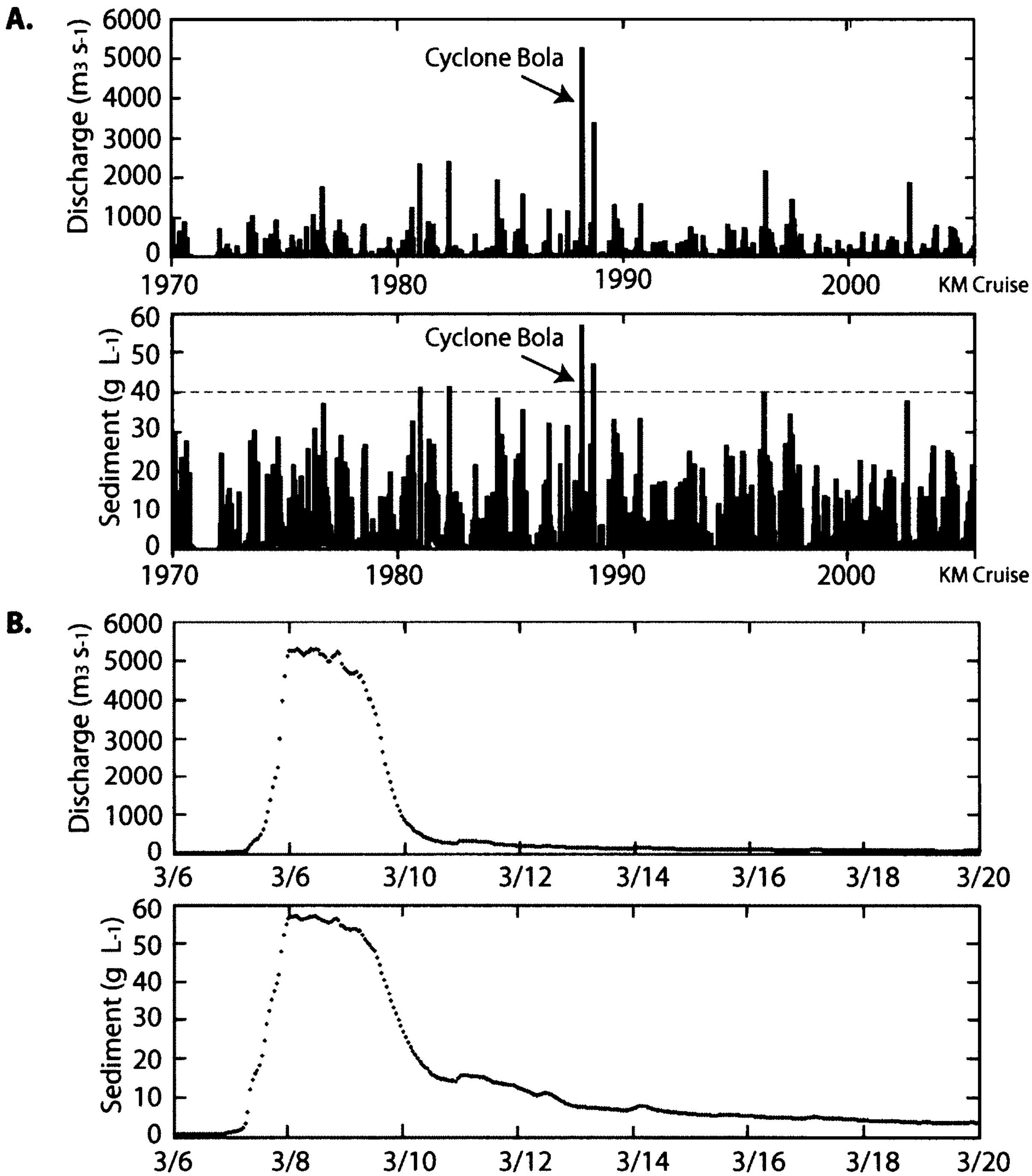
A.
Discharge (m3 s-1)
Cyclone Bola
1970
1980
1990
2000
KM Cruise
Sediment (g L-1)
Cyclone Bola
B.
Discharge (m3 s-1)
Sediment (g L-1)
3/6
3/8
3/10
3/12
3/14
3/16
3/18
3/20

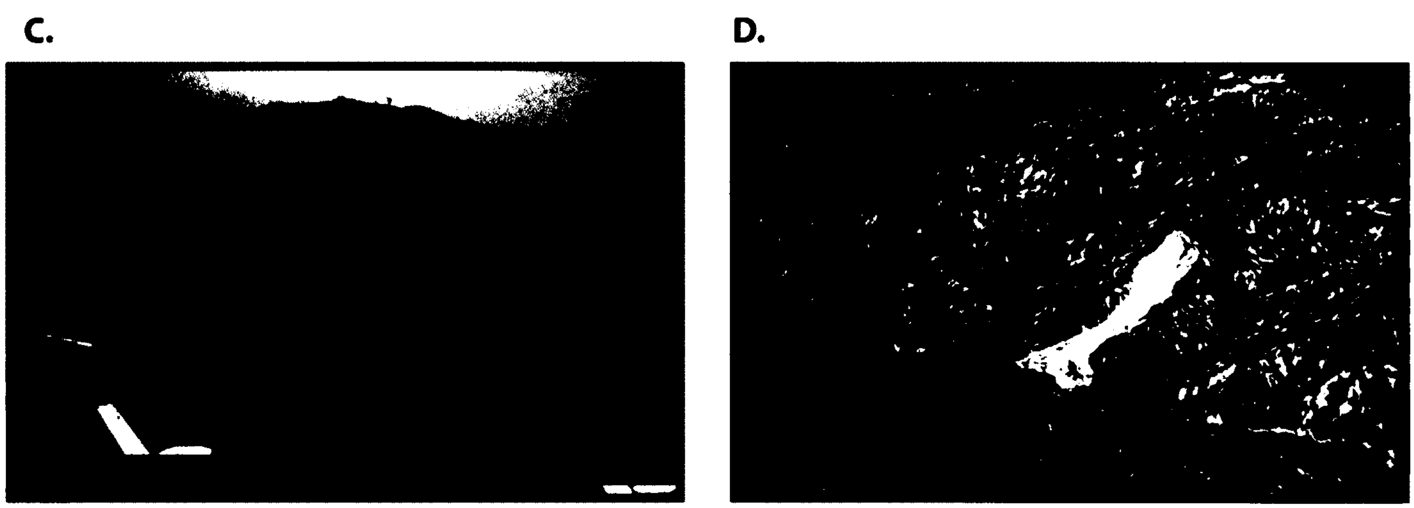
C.
D.

Figure 3

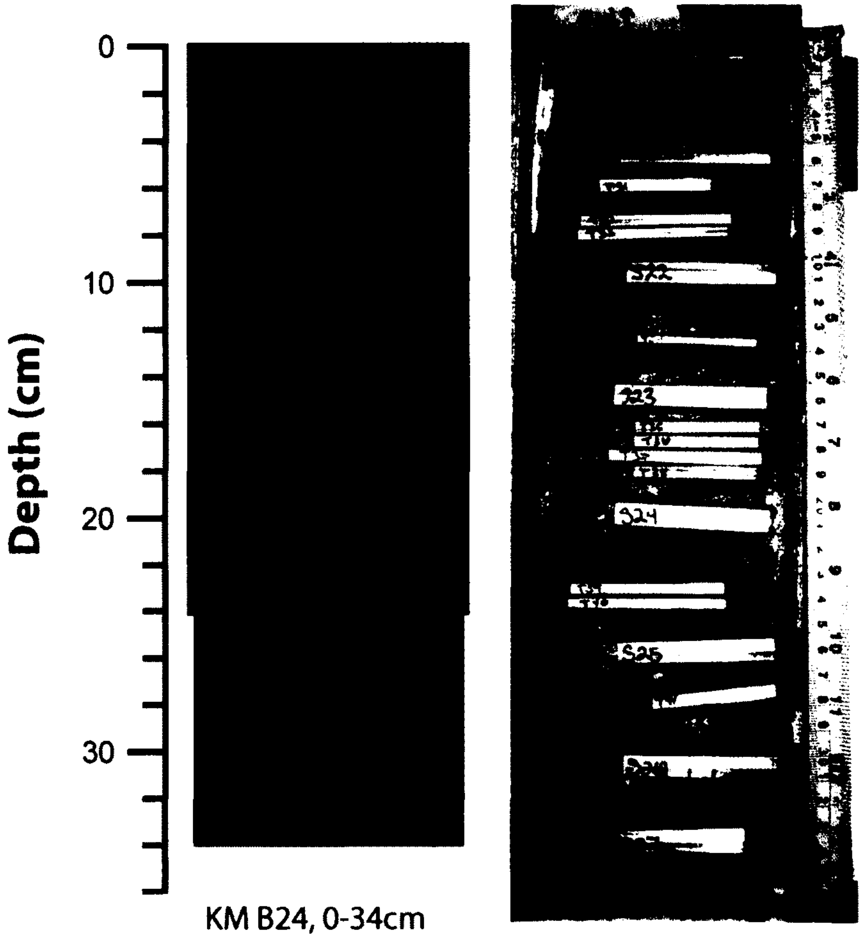

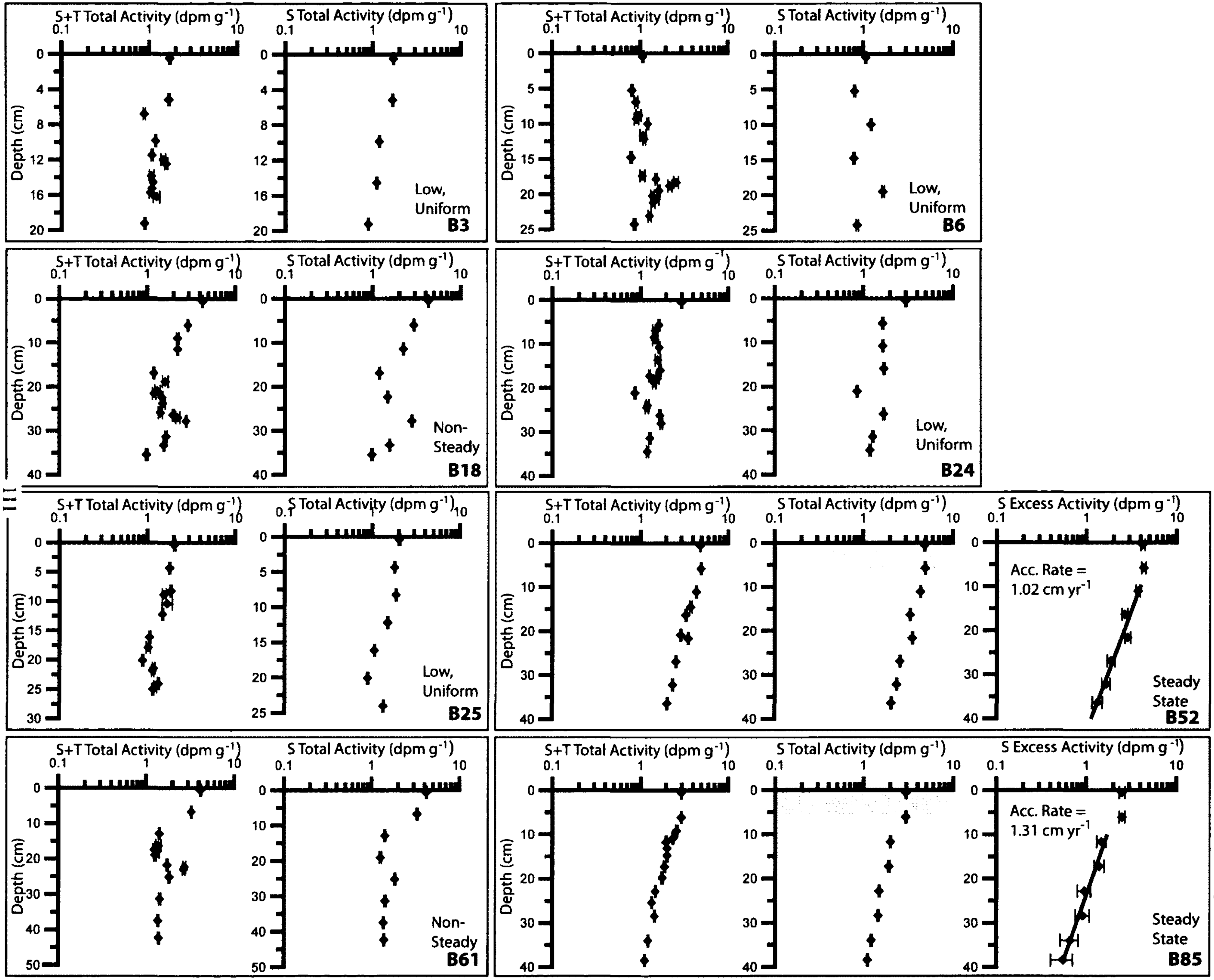
S+T Total Activity (dpm g⁻¹)
S Total Activity (dpm g⁻¹)
S Excess Activity (dpm g⁻¹)
Depth (cm)
Low, Uniform
B3
Low, Uniform
B6
Non-Steady
B18
Low, Uniform
B24
Low, Uniform
B25
Acc. Rate = 1.02 cm yr⁻¹
Steady State
B52
Non-Steady
B61
Acc. Rate = 1.31 cm yr⁻¹
Steady State
B85

Figure 4

Figure 5

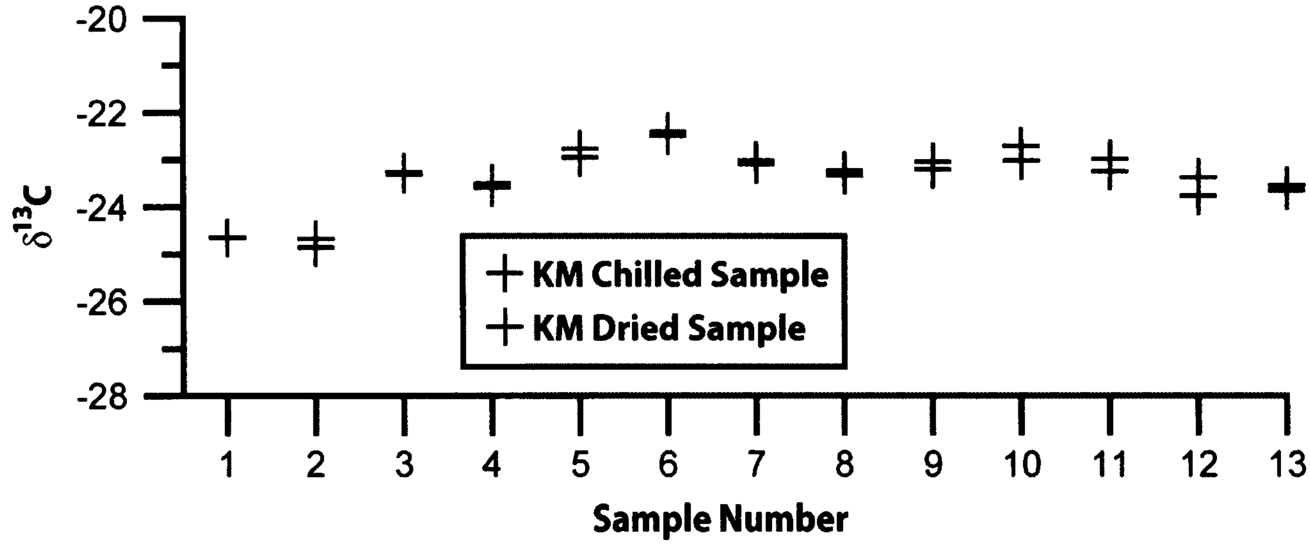

-20
-22
-24
-26
-28
$\delta^{13}C$
KM Chilled Sample
KM Dried Sample
1
2
3
4
5
6
7
8
9
10
11
12
13
Sample Number

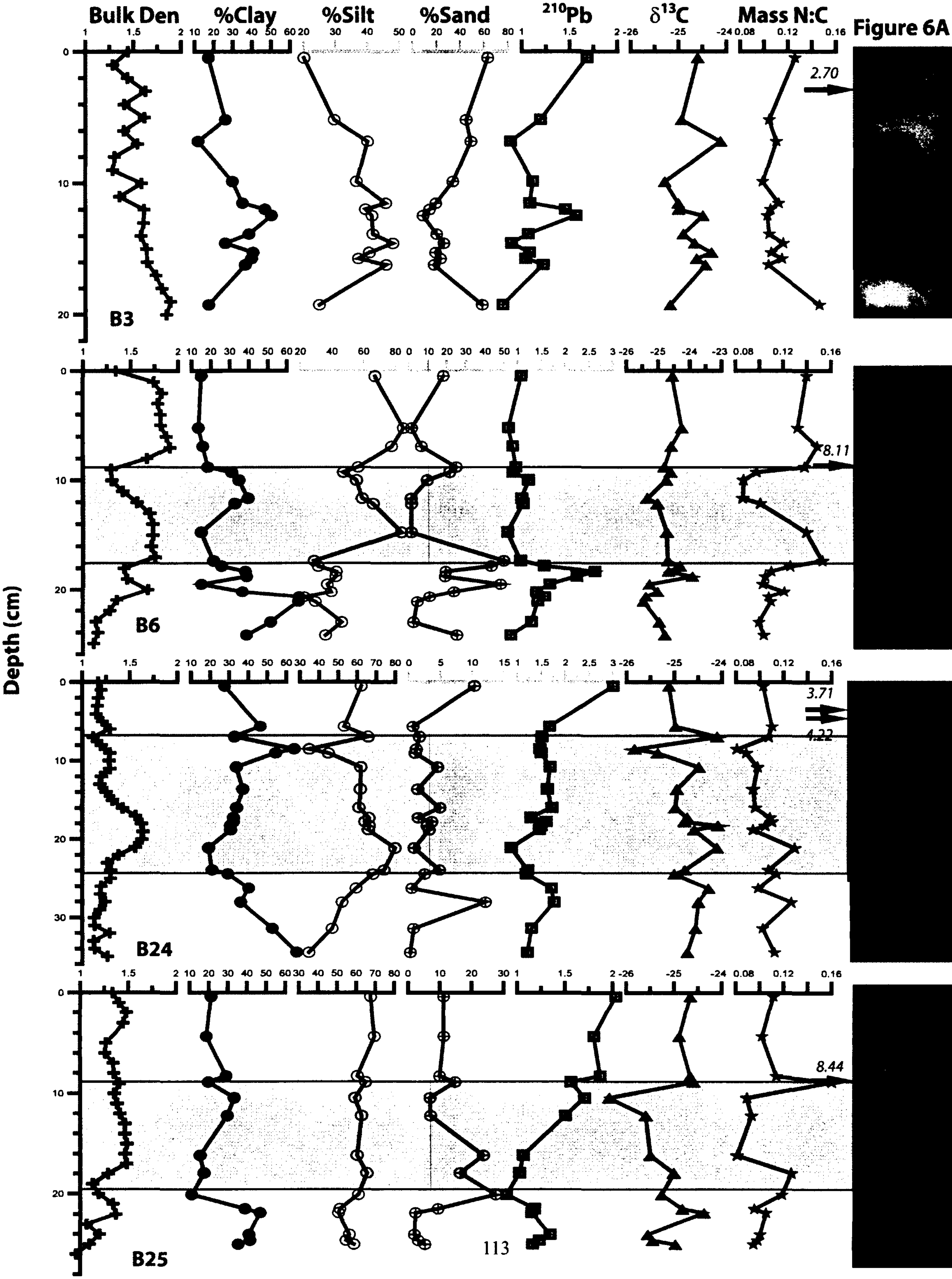
Bulk Den
%Clay
%Silt
%Sand
^{210}Pb
δ^{13}C
Mass N:C
Depth (cm)
B3
B6
B24
B25
2.70
8.11
3.71
4.22
8.44

Figure 6A

Figure 6B

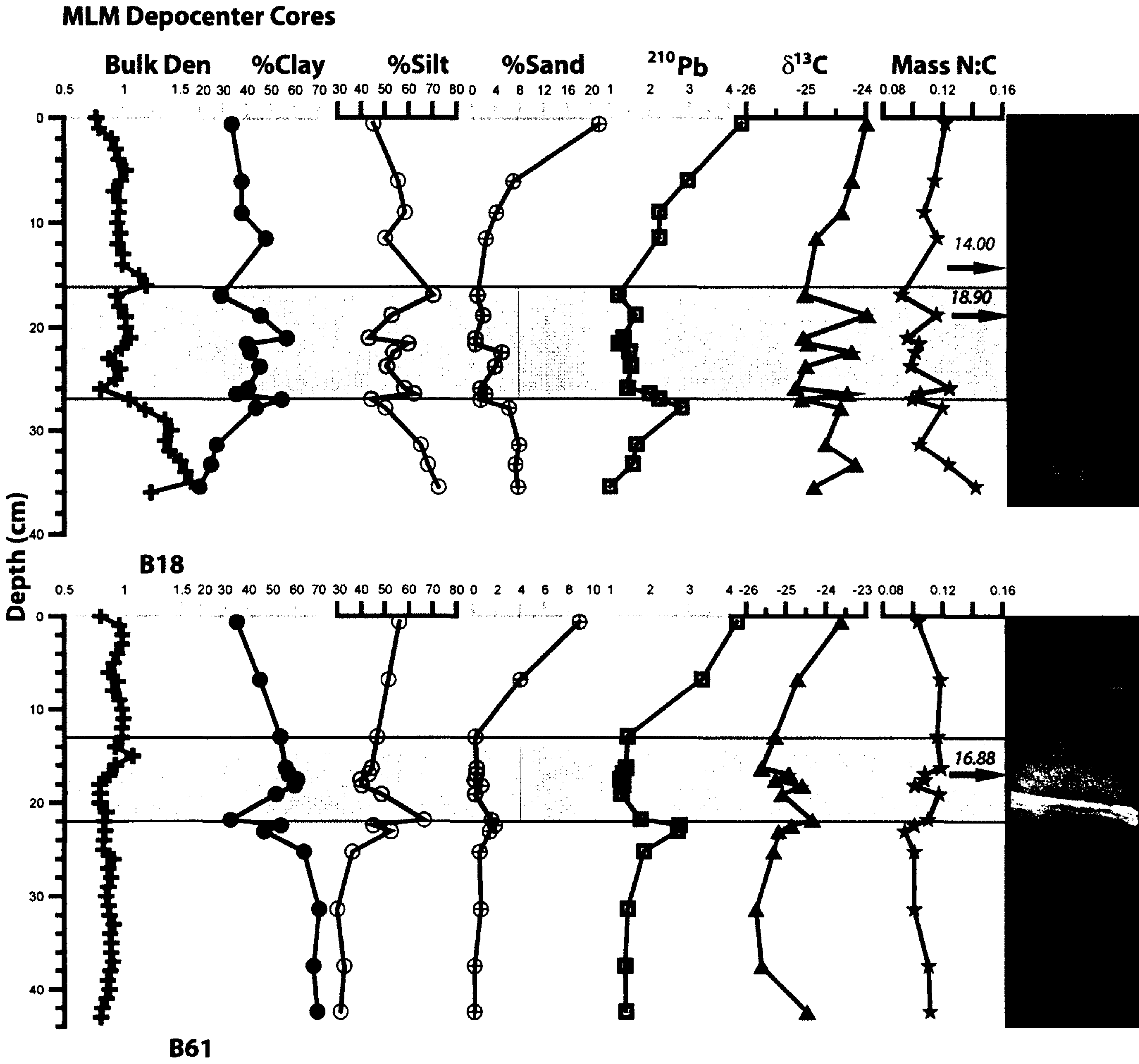
MLM Depocenter Cores
Bulk Den
%Clay
%Silt
%Sand
^{210}Pb
δ^{13}C
Mass N:C
Depth (cm)
14.00
18.90
16.88
B18
B61

MM Depocenter Cores **Figure 6C**

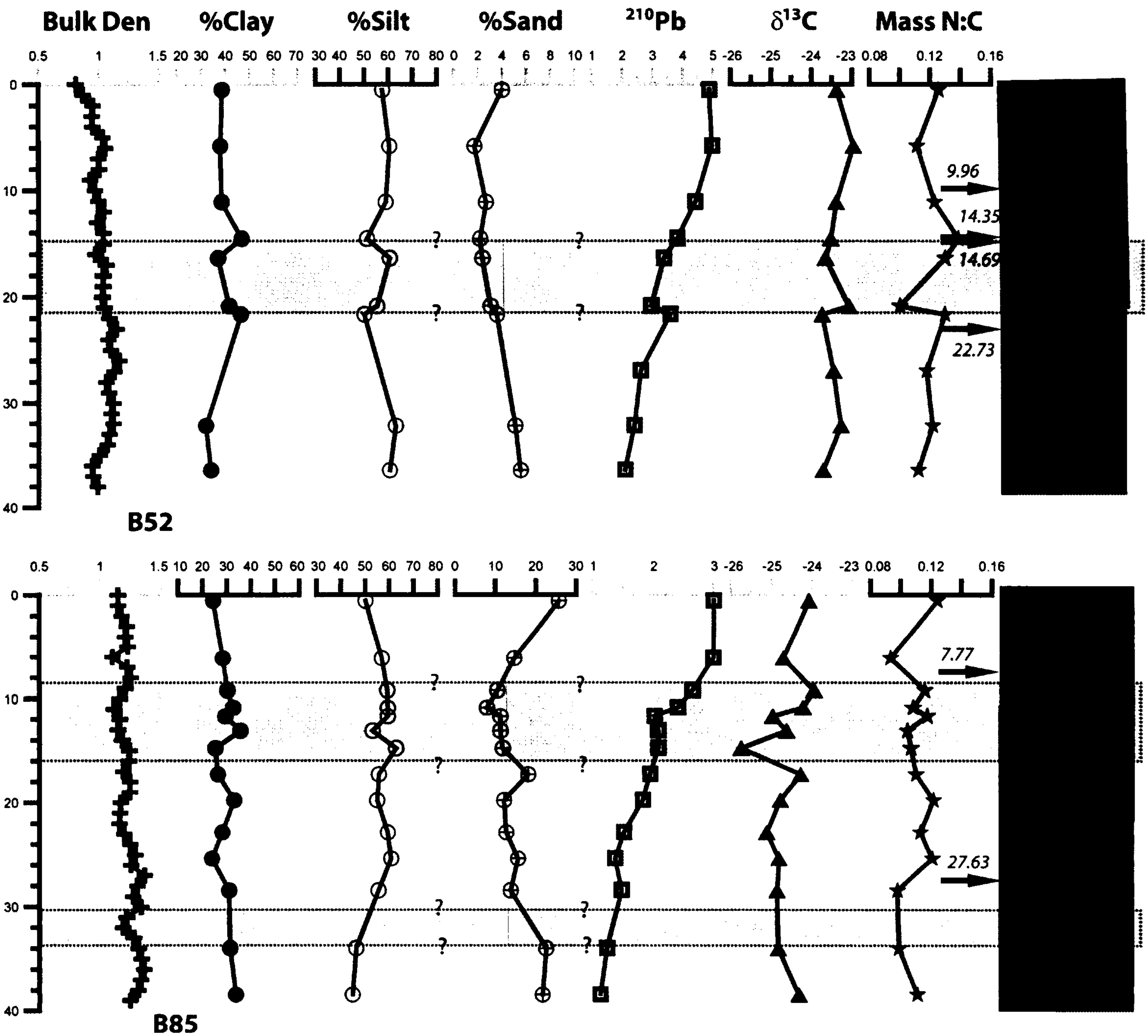

Figure 7

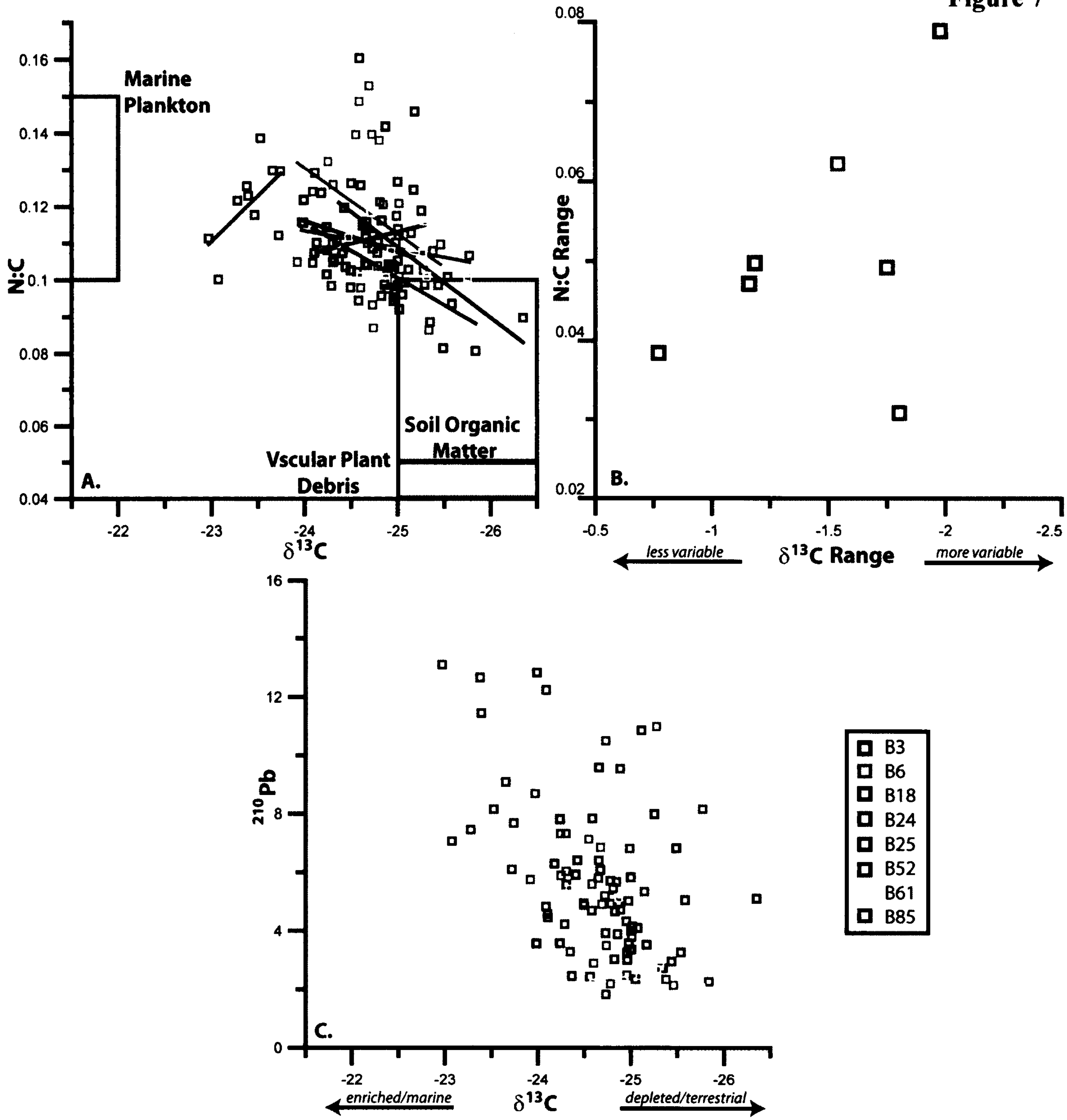
A.
Marine Plankton
Soil Organic Matter
Vscular Plant Debris
N:C
δ13C
B.
N:C Range
δ13C Range
less variable
more variable
C.
210Pb
δ13C
enriched/marine
depleted/terrestrial
B3
B6
B18
B24
B25
B52
B61
B85

Figure 8

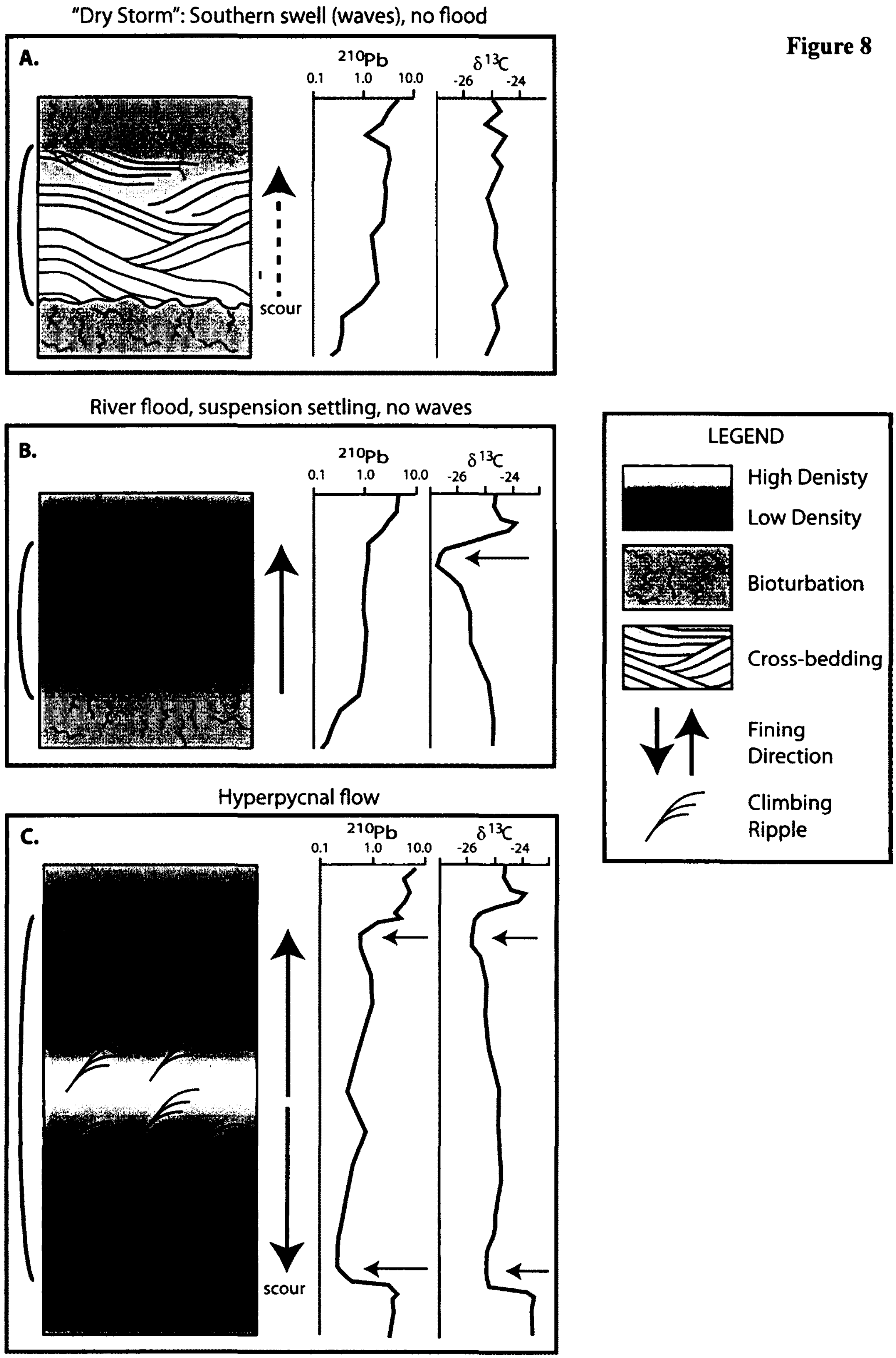
"Dry Storm": Southern swell (waves), no flood
A.
210Pb
0.1
1.0
10.0
δ13C
-26
-24
scour
River flood, suspension settling, no waves
B.
Hyperpycnal flow
C.
LEGEND
High Denisty
Low Density
Bioturbation
Cross-bedding
Fining Direction
Climbing Ripple

Figure 9

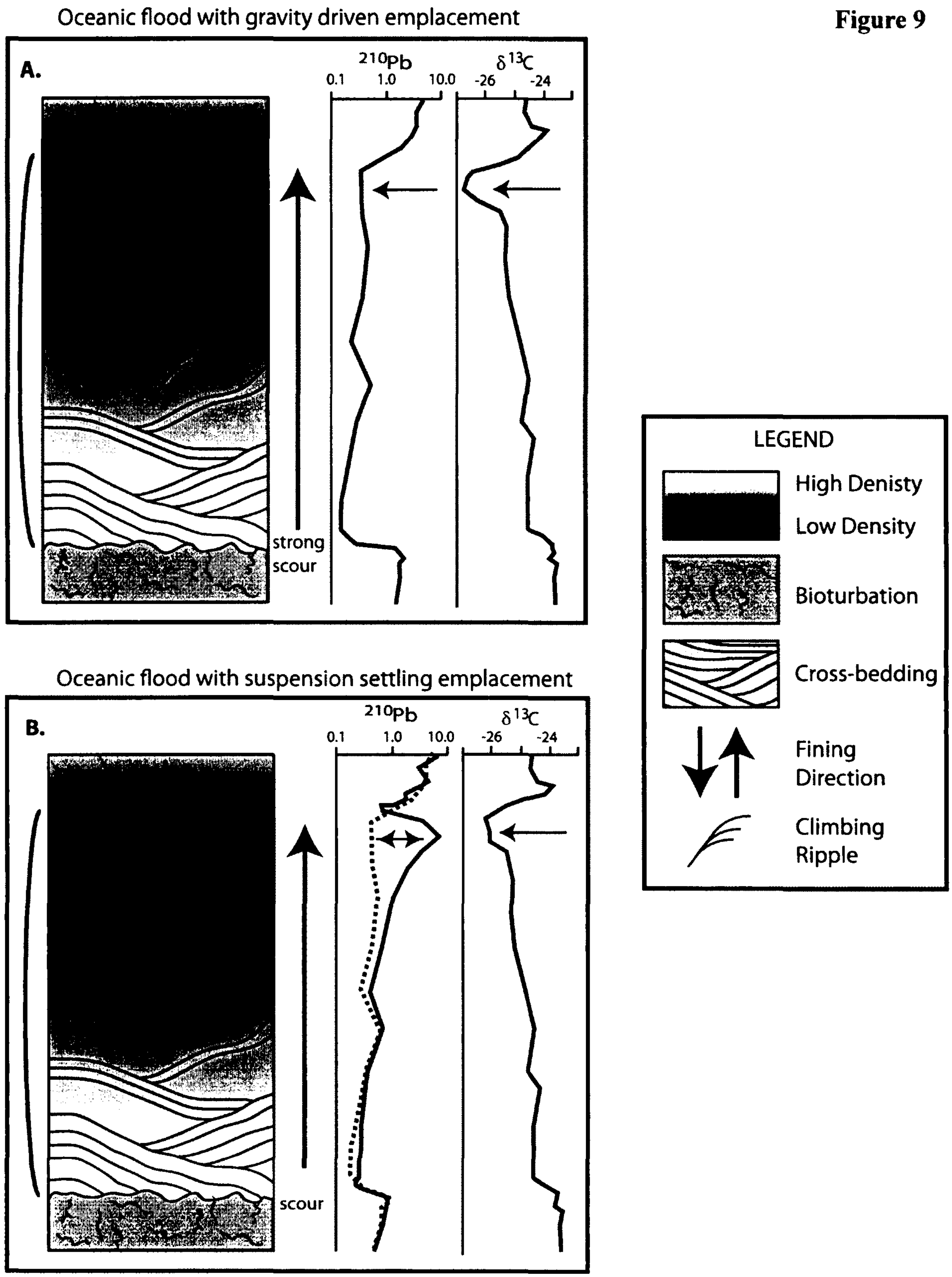
Oceanic flood with gravity driven emplacement
A.
210Pb
0.1
1.0
10.0
δ13C
-26
-24
strong
scour
Oceanic flood with suspension settling emplacement
B.
210Pb
0.1
1.0
10.0
δ13C
-26
-24
scour
LEGEND
High Denisty
Low Density
Bioturbation
Cross-bedding
Fining
Direction
Climbing
Ripple

CHAPTER 3

Event Layer Frequency, Characteristics, and Preservation on the Waipaoa Continental Shelf Throughout the Holocene

1. Introduction

Over millennial timescales, the stratigraphic record on continental shelves can preserve proxies of changing climate, landscape, and oceanographic conditions (e.g., Hedges and Keil, 1995; Meyers, 1997; de Haas et al., 2002). Glacio-eustatic sea level oscillations, constructed from deep ocean sediments and numerous paleaoenvironmental proxies (Vail et al., 1977; Haq et al., 1988) create and destroy accommodation space on continental margins and are a first order determinant of shelf sediment storage (Prothero and Schwab, 1996). As a result of rapid sea level rise since the Last Glacial Maximum (LGM), passive margins dominated by river sediment inputs developed ravinements, thus complete post-LGM passive shelf records are rare and are more often punctuated by disconformities which preclude reconstruction of rapidly changing earth and environmental conditions at the land-ocean interface.

Active margins with high-yield rivers play a disproportionate role relative to passive margins, in supplying sediment globally to the coastal ocean and continental shelf (Milliman and Syvitski, 1992; Mulder and Syvitski, 1995; Lyons et al., 2002). Therefore, on active margins with tectonically-driven accommodation and where sediment supply is large, such as those of the Western Pacific, expanded sedimentary sections can be found. Transgressive sequences from these margins may contain near continuous records of mixed terrestrial and marine signals. Within this strata, event layer producing perturbations, such as extreme rainfall and wave resuspension events, earthquakes, and mass flows may be captured, which punctuate normal marine water column sedimentation with large additions of terrestrial sediment with unique textural and geochemical characteristics. Thus, the high-resolution stratigraphic record of active margin shelves can be used to reconstruct periods of changing storm frequency and intensity in relation to glaceo-eustatic and climate fluctuations and can be linked with land and slope records.

One of the goals of the MARGINS Source-to-Sink (S2S) program is to investigate continental shelf strata in order to better understand how landscape evolution impacts the formation and preservation of events (Margins Science Plans, 2003). Several giant piston cores (12.83-25.34m) were retrieved aboard the R/V Marion DuFresne (MD) in February 2006 on the continental shelf adjacent to the high-yield Waipaoa River, a MARGINS S2S study site. Using these cores, this study explores the continuous record of environmental change from the late Pleistocene to present. Imprinted upon the record of competing eustatic and tectonic controls on sedimentation (Rose and Kuehl, In Prep.), evidence for temporal and spatial changes in event layer frequency and type are documented by examination of lithostratigraphic, textural and stable isotopic variability. Using this information, we can address to what degree high and low frequency and magnitude perturbations are preserved in records on the continental shelf. In lieu of the S2S goals, it is important to explore the impact of exceptional stochastic storm and flood events on the continental shelf because such events can indicate changes in supply, transport, accumulation and preservation of material in the short term (individual events) and on longer timescales (regime shifts).

1.1 Regional Setting: Poverty Margin and the Waipaoa River

Poverty Margin lies at the active boundary between the Pacific and Australian plates off the northeastern coast of New Zealand (Figure 1A), where oblique subduction and mountain building combine with a vigorous temperate maritime climate to produce some of the highest sediment yields in the world (Griffiths, 1982; Walling and Webb, 1996; Hicks et al., 2000, 2004). Although it has a relatively small catchment of $2205 km^2$, the modern Waipaoa River has a yield of $6800 t\ km^2\ yr^{-1}$ and discharges approximately $15 Mt\ yr^{-1}$ of suspended sediment to the adjacent Poverty Shelf and Slope (Figure 1B). The Waipaoa River has a comparatively short sediment transfer time from steepland source to continental sink (Blair et al., 2004) and as such, is characterized as roughly "bypassing," since lengthy storage of catchment sediment in successive reservoirs is not significant (Brackley, 2006). Modern, rapid sediment supply is apparent from the presence of ^{7}Be in surface sediments shelf-wide and accumulation rates of up to $0.59 cm\ y^{-1}$ on the outer shelf (Miller and Kuehl, 2010; Rose and Kuehl, 2010). During normal fair-weather conditions, Waipaoa sediment enters Poverty Bay and becomes entrained in an anticlockwise gyre before reaching Poverty Shelf (Stephens et al., 2001; Brackley, 2006; Bever, 2010). The predominant shelf current is the Wairapara Coastal Current (WCC), a weak bottom current with mean ambient northeastward flow which can be intensified by southern swell and is hypothesized to experience intermittent reversals (Chiswell, 2000; Stephens et al., 2001). Seaward of the shelf break (at 150 meters below sea level [mbsl]) on Poverty Slope, warm water from the Tasman Front and subtropical gyre flows to the south, forming the saline East Cape Current (ECC, Figure 1A; Carter et al., 1996; Carter, 2001; Chiswell, 2005). The ECC meets cold, subantarctic water moving north at the Chatham rise, where both flows are deflected 90° and converge as the Subtropical Convergence (STC, Figure 1A; Carter, 2001).

Active deformation from subduction-related underplating drives uplift in the Waipaoa catchment's axial mountain range at an estimated rate of 4mm y^{-1}, (with a maximum of 10mm y^{-1}), subsidence on the continental shelf up to 4mm y^{-1}, and coseismic deformation generated by large earthquakes (Lewis, 1980; Lewis and Pettinga, 1993; Reyners and McGinty, 1999). This tectonic underpinning causes crushing and fracturing of catchment lithologies including Jurassic through Pliocene sedimentary rocks, encouraging continued erosion (Hicks et al., 2004; Page et al., 2001). In the Holocene, over 15 large magnitude earthquakes (M_w = >7.3) have been identified that impacted the region. These were interpreted from post-maximum transgression (~7ka) uplifted terraces as well as a variety of paleoenvironmental indicators (Table 1; Ota et al., 1988; Berryman et al., 1989; Berryman, 1993; Brown, 1995; Berryman et al., 2000; Cochran et al., 2006; Hayward et al., 2006; Litchfield et al., 2010). Several of these earthquakes have been correlated with catastrophic turbidite sequences on Poverty Slope (Table 1; Pouderoux et al., 2012). Eruptions from the Taupo Volcanic Zone (Figure 1A, Table 1), located 120km to the northwest of the Waipaoa catchment, distributed ashfall throughout the East Cape and form strong, laterally continuous seismic reflections on Poverty Shelf and Slope, providing excellent markers to chronostratigraphically link catchment, shelf, and slope stratigraphy (Gerber et al, 2010; Carter et al, 2002; Orpin, 2004; Lowe et al., 2008; Pouderoux et al., 2012). Glass shard analysis of several Poverty Shelf cores (3 of which are discussed at length in this study) have positively identified the Taupo, Waimihia and Whakatane tephras (Gerber et al., 2010; Rose et al., In Prep.). Published data for marine cores ODP 181-1124 (Carter et al., 1999) and MD97-2121, an earlier shorter core taken from the Poverty mid-shelf (Figure 1B; Carter et al., 2002; Alloway et al., 2007) from northeastern New Zealand report a robust, linear correlation between AMS-radiocarbon and tephra dates to core depth.

Since the LGM at 24ka, global sea level has risen from a low of 125±5mbsl to present highstand due to ice volume reduction (Figure 1D; Fleming et al., 1998; Cochran et al., 2006; Lui et al., 2004). Indo-Pacific sea level rise and fall have been nearly synchronous with global observations (Suggate, 1990; Lui et al., 2004). During the LGM, Waipaoa sediments presumably bypassed the modern shelf, as low stand was near the present depth of the modern shelf break (150mbsl), and were deposited on the modern slope (Orpin et al., 2006; Alexander et al., 2010; Rose et al., In Prep.). Rates of post-glacial sea level rise for the Western Pacific show marked "stair-stepped" variability through time. The "risers" are linked with warming and rapid sea level rise linked to melt water pulses (mwp), the most intense of which occurs at 14ka (mwp-1a, Figure 1D; Suggate, 1990; Liu et al., 2004). Periods of little change in sea level include the Younger Dryas at 12.8-11.6ka (Figure 1D). In response to sea level fluctuations, Poverty Bay has experienced large changes in geometry (Figure 1C). Maximum transgression culminates between 8.7 and 5.5ka, during which the bay was three times the present surface area and stretched 20km inland, with the Waipaoa River mouth roughly 12km inland of its present location (Brown, 1995; Wolinsky et al., 2010; Bever, 2010). As the rate of sea level rise became more subdued with essentially stable sea level for the last 4ka (Figure 1D, inset; Ota et al., 1988; Brown, 1995, Alloway et al., 2007), progradation of the Waipaoa substantially infilled the proto-Poverty Bay causing seaward advancement of the coastline (Wolinsky et al., 2010; Rose et al, In Prep.). Globally, over the past 7ka years, sea level has had a continuous and uniform rise of 3-5m (Fleming et al., 1998).

Poverty Shelf is thus mantled with a post-glacial sedimentary sequence in excess of 45m thickness which reflects the dynamics of rapidly changing sea level as well as accommodation within two prominent mid-shelf basins and a shelf break depocenter (Lewis, 1973; Foster and Carter, 1997; Gerber et al., 2010; Rose et al., In Prep.). These Northern and Southern Depocenters are constrained at their seaward edges by the emergent, coastline-parallel Lachlan and Ariel anticlinal ridges and bisected by a sandier zone of little net modern accumulation (Figure 1B; Foster and Carter, 1997; Orpin et al., 2006; Miller and Kuehl, 2010). High-resolution Holocene age models constructed for mid-shelf, outer-shelf and slope cores (based on a suite of 94 radiocarbon ages), including the cores in this study, allowed for examination of accumulation rates on the Poverty Shelf and Slope over the Late Quaternary (Figure 1B and Table 2 for core locations; Figure 2 for accumulation rates; Rose et al., In Prep.). Distinct changes in accumulation rates interpreted from trendline analysis (Figure 2; Table 3) were used to analyze major shifts and variations in sediment supply and accommodation on Poverty Margin which are interpreted with respect to facies distribution, tectonics, and climate forcing (Figure 2; Rose et al., In Prep.). Shelf break accumulation is low before 7ka, followed by a four-fold increase in accumulation (Figure 2; Table 3). The Southern Depocenter is characterized by a relatively steady accumulation rate overall, with the exception of a spike in accumulation rate between ~7-6ka (Figure 2; Table 3). Accumulation rates are elevated in the Northern Depocenter from 10ka through ~4ka, after which they decrease by a factor of two. In supplement to age models, point-to-point calculations provided an instantaneous record of sedimentation rate between adjacent radiocarbon ages allowing the authors to distinguish periods of relatively high or low variability (Figure 5B). Dramatic swings in point-to-point accumulation rates between 9ka and 5ka for mid-shelf depocenter cores indicated periods of high sediment supply variability. After 5ka, accumulation rates in mid-shelf depocenter cores dropped off and became less variable until ~1ka when accumulation rates increased again. Point-to-point accumulation on the shelf break was low until trending upward between 7ka and 4ka, after which the accumulation rate fell until just after 1ka, when a dramatic increase was recorded.

In addition to accumulation rate observations, we identified four dominant facies (1-4, in descending order, with youngest first and oldest last) on Poverty Shelf using observations of primary structure preservation and degree of bioturbation in X-radiographs (Rose et al., In Prep.). Textural and carbon isotopic values within these facies revealed sympathetic temporal shifts coincident with landward movement of the Waipaoa River, maximum transgression, and regression of Poverty Bay shoreline as sea level stabilized (Rose et al., In Prep.). Facies 1, found in the mid-shelf depocenters, extended to ~3.5ka, was characterized by a high degree of bioturbation and was the most texturally coarse of facies on the mid-shelf. It roughly coincided with the observed decrease in accumulation (Figure 2A) in the Northern Depocenter and the onset of El-Niño-Southern Oscillation (ENSO) in the Indo-Pacific. Facies 2 underlies Facies 1 and was much finer, had a higher degree of primary sedimentary structure preservation and extended to ~6.5ka, corresponding with the timing of maximum transgression and interpreted as representative of a transitional period towards enhanced trapping, basin-fill progression, and the advancement of Poverty Bay shoreline. High and variable point-to-point accumulation rates were observed throughout this time period, possibly influenced by shifting loci of deposition that would have also encouraged structure preservation (Figure 2B). Facies 3, the first encountered in the Shelf Break Depocenter and the oldest facies retrieved from mid-shelf depocenters (except for the very end of MD3007), had the highest proportion of fine sediment of all facies. It was comprised of mainly homogeneous, bioturbated, mottled muds emplaced when accumulation was high and steady, with the highest (enriched) $\delta^{13}C$ values of all facies, revealing a more marine-dominated carbon input, when the margin was clearly starved of coarse material as the proto-Poverty Bay shoreline retreated and course material was trapped within the growing Waipaoa embayment (Figure 1C, D). Finally, Facies 4 was found at the deepest portion on the shelf break and in one of the Northern Depocenter cores (MD3007), below 11.8ka and 9.5ka, respectively. It was characterized by bioturbated muds interspersed with remnant layers of varied densities, was significantly coarser than Facies 3, and contained concentrated deposits of shelly material indicative of a shallow water environment. This facies was interpreted to represent rapid sedimentation from a source position that must be changing in response to eustacy.

Imprinted upon the stratigraphic record is evidence of the micro-tectonic complexity of Poverty Shelf, which resulted in differences in basin fill stratigraphy within these depocenters over the Holocene (Ota et. al., 1988; Brown, 1995). A "pivotal zone", created by a tectonic transition that runs shore-perpendicular through Poverty Bay and presumably across the Poverty Shelf at the boundary of two rupture segments, delineates an eastern uplifting region and a western area of subsidence (Figure 1B; Ota et. al., 1988; Brown, 1995; Wallace et al., 2009). This local tectonic complexity is reflected in the nature of strata formation during the Holocene. Seismic profiles show Northern Depocenter progradational, seaward-dipping geometries (Gerber et al., 2010) that indicate accommodation space quickly filled, in contrast to those from the Southern Depocenter which are concave-up, lapping onto the emergent Lachlan anticlinal ridge, suggesting that subsidence has kept pace with or exceeded supply. At the Shelf Break Depocenter, sediment accumulation increased dramatically post-maximum transgression, as evidenced by age-model and grain-size records (Rose and Kuehl, In Prep.). Thus, these depocenters are natural candidates for preservation of exceptional discharge events from the Waipaoa within the stratigraphic record.

Onset of ENSO in Polynesia commenced ~4 ka and speleothems and peat-bogs in New Zealand record increasing wetness at this time, associated with increased storminess (Hellstrom et al., 1998; McGlone and Wilmshurst, 1999). Associated large magnitude rainstorms engendered the transition to landsliding as the dominant modern form of hillslope erosion, followed by gully and sheet erosion (Page et al. 1994a, b; Griffiths, 1982; Foster and Carter, 1997; Hicks et al., 2004; Gomez et al., 2004). Prior long core investigations of Poverty Shelf reveal large magnitude textural and isotopic signals presumed to reflect increasingly energetic shelf oceanographic conditions related to the intensification of ENSO, in addition to continued infilling and shoaling of the shelf ca. 4ka (Foster and Carter, 1997; Gomez et al., 2004).

Anthropogenic disturbance to the Waipaoa catchment has been dramatic, increasing the susceptibility of the landscape to mass failures and accelerating rates of erosion (Wilmshurst, 1997; Page et al., 2000). This is recorded on Poverty Margin as a shelf-wide fining-upwards signature after the first occurrence of indigenous peoples ca. 0.9 ka (Foster and Carter, 1997; Wilmshurst, 1997; Gomez et al., 2004, 2007; Rose et al., In Prep.). Polynesian (Maori) settlers burned vast swaths of native forest and Europeans aggressively converted scrubland to pasture at the beginning of the 19^{th} century (Wilmshurst, 1997; Wilmshurst et al., 1997; Eden and Page, 1998; Page et al., 2001). Currently, only 3% of the Waipaoa catchment retains its original native forest (Page et al., 2001), which influences the quality and quantity of sediment available to be eroded and transported via the Waipaoa to the marine environment. Sedimentation rates are 6-8 times higher than pre-industrial rates, from an estimated pre-human 2.3Mt yr^{-1} to today's 15Mt yr^{-1} (Kettner et al., 2007; Wilmshurst, 1997; Miller and Kuehl, 2010). In New Zealand, annual soil carbon loss to the coastal ocean is estimated to be between 3-11Mt yr^{-1} (Tate et al., 2000), and although the contribution of the Waipaoa River is unknown, it likely plays a large role in export to the coastal ocean.

1.2 Event Sedimentation and the Poverty Margin Record

Event layer producing perturbations, such as extreme rainfall and wave resuspension events, earthquakes, mass flows and volcanoes can punctuate background marine water column sedimentation with large additions of terrestrial sediment or can produce secondary structures due to reworking. These signals may impart unique textural and geochemical characteristics that can be preserved in the stratigraphic record and traced back to their mode of initiation. Observations of such events actively emplacing strata on the seabed are rare, complicated by the logistics and danger associated with event response. Anecdotal accounts may provide information on modern event sedimentation, however these do not inform beyond modern occurrences. Using the lithostratigraphic, textural, and geochemical record, one can identify and differentiate between event sedimentation and fair-weather suspension settling, and can reconstruct possible modes of initiation and emplacement.

Numerous hydrodynamic, physical, biological and environmental factors operating over time and space influence the probability that sediment layers will be preserved below the zone of sediment mixing in the zone of preservation, a horizon unalterable by physical and biological processes (Guinasso and Schink, 1975; Nittrouer and Sternberg, 1981; Kuehl et al., 1995; Wheatcroft and Drake, 2003). Diagenesis of organic matter can potentially distort the originally (or event-instantaneously) emplaced $\delta^{13}C$ signature within strata. However in small river systems (like the Eel, Waiapu and Waipaoa) compared to large river systems, this is considered to be minor, especially because, as in the case of the Waipaoa, man-made levees keep modern material from entering an intermediate storage reservoir (Blair et al., 2004). Over longer time scales, under forest cover, source material rapidly transited the entire land portion of the system (Phillips and Gomez, 2007). Indeed, it has been shown that the majority of sediment sourced in the Eel River catchment reaches the adjacent shelf quickly, especially during oceanic floods, where particulate organic carbon preserves a strong bimodal terrestrial signal (Leithold and Hope, 1999; Sommerfield and Nittrouer, 1999; Blair et al., 2004). Conditions will favor preservation of stochastic sediment pulses if accumulation rates are high and/or subsequent events follow (effectively increasing the short term accumulation rate by burying the event and removing it from biological and physical reworking), event layers are thick, and physical and biological mixing is minimal (Guinasso and Schink, 1975; Nittrouer and Sternberg, 1981; Kuehl et al., 1995; Wheatcroft and Drake, 2003; Wheatcroft et al., 2007). On longer timescales, beyond the scope of this investigation, the cumulative effects of time (i.e. hiatus in deposition, compaction, erosion, etc.) may render a sedimentary sequence incomplete (Sadler, 1981). However, if preserved, the geochemical, textural, and radioisotopic properties of event strata may provide a wealth of information on changes over time in trigger mechanisms, event magnitude/frequency relationships, climate, and anthropogenic influences.

Several texturally distinguishable event sediment deposits have been recognized theoretically, in the geologic record and in sediment core stratigraphy, including the Bouma sequence (turbidites) and hyperpycnites (Mulder et al., 2003; Eden and Page, 1998; Kuehl et al., 1995; Shanmugam, 2000; Leithold and Hope, 1999; Wheatcroft and Borgeld, 2000; Wheatcroft and Drake, 2003; Geyer et al., 2000, 2004; Goldfinger et al., 2008). The Bouma sequence is a classic idealized stratigraphic set of beds that result from a turbidity current which deposits a characteristically fining upwards unit with a scoured base (Bouma, 1962; Shanmugam, 2000). Hyperpycnal flows result when extreme rainfall and subsequent rapid erosion and denudation cause the density of the river/suspended sediment slurry to increase relative to the receiving body of water and can deliver a disproportionate amount of sediment to the continental shelf (Parsons et al., 2001; Mulder et al., 2003). The threshold widely recognized as required for such a negatively buoyant flow is 40g L^{-1} (Mulder and Syvitski, 1995; Parsons et al., 2001; Hicks et al., 2004). The resultant deposit, termed a hyperpycnite, is composed of a coarsening upwards sequence, followed by a fining upwards set of units, representing the waxing and then waning legs of the causal hyperpycnal flood. Thus, the emplacement of a sole fining upwards vs. a coarsening upwards followed by a fining upwards sequence may distinguish between event triggers (Shanmugam, 2000; Goldfinger et al., 2003; Wheatcroft et al., 2007). Wheatcroft (2000) showed that oceanic floods, caused by extreme rainfall events that produce atypical discharge from small rivers, may also generate characteristic textural fingerprints which can be used to interpret the stratigraphic record. Oceanic flood sedimentation has been documented on the active continental margins off the Eel River on the West Coast of the U.S. and the East Cape of New Zealand. Clearly events with concomitant rain on land and elevated shelf wave action can be preserved in active margin shelf stratigraphy, providing high-fidelity records of event responses of rivers (e.g., Sommerfield and Nittrouer, 1999;

Wheatcroft, 2000; Blair et al., 2004; Crockett and Nittrouer, 2004; Brackley, 2006; Nittrouer et al., 2007; Wadman and McNinch, 2008; Miller and Kuehl, 2010; Rose and Kuehl, 2010). Sediment texture is essential in identifying the presence of oceanic flood event layers, as the percent clay fraction is higher than during normal deposition (Leithold and Hope, 1999; Wheatcroft and Borgeld, 2000; Wheatcroft and Drake, 2003). It follows that geochemical signatures, including those of stable carbon and nitrogen isotopes, and other proxies for terrestrial vs. marine sedimentation (e.g. magnetic susceptibility, palynology, foraminiferal assemblages) within the stratigraphic record may help to strengthen textural interpretations of event and non-event sedimentation. Brackley (2006) points out that a key potential signature in the organic carbon content of hyperpycnal flows is their possibility of recording a strong terrestrial signature in comparison to hypopycnal plume sedimentation. This has implications for the role of oceanic floods in the global carbon cycle, as resultant layers, if rapidly deposited and buried, would be important sinks for terrestrial carbon.

Lake sediments from Lakes Tutira (black star, Figure 1A), Rotonuiaha and Waikopiro, all within a few hundred kilometers of this study's research site, have yielded high resolution environmental records reaching as far back as several thousand years (Eden and Page, 1998; Wilmshurst, 1997; Wilmshurst and McGlone, 1997; Carter et al., 2004). In Lake Tutira cores, distinct volcanic, homogenite, and graded beds, interpreted to be triggered by seismic and storm activity, are distinguished from non-event based lake sedimentation using color, grain size and grading, palynological, and charcoal analyses, and are date-constrained by published tree ring and radiocarbon dates correlated with tephra deposits (Orpin et al., 2010). Phases of increased storminess were identified (Table 1) and related to rain intensity, based on the historical record. In New Zealand, storm frequency and magnitude both increase during the positive phase of the Southern Oscillation Index (SOI), which is concomitant with increased rainfall and storm intensity there (Eden and Page, 1998), however no correlation was discovered between event sedimentation in Lake Tutira and the entire 20th century record of ENSO (Orpin et al., 2010). A weak correlation was found between homogenite occurrence and proximity in time to seismic activity and these beds were found to decrease in thickness when earthquakes were more frequent (Orpin et al., 2010). It is possible that storm sequences documented in these cores may be correlated to Poverty Shelf strata.

Analyses of modern (< 100yr BP) Poverty Shelf sediments have shown that event sequences are regularly preserved within the stratigraphic record (Brackley, 2006; Rose and Kuehl, In Prep.). Because of increased sediment availability due to the increased erosion within the Waipaoa catchment, modern hyperpycnal flows generated by the Waipaoa are estimated to have a 40-year recurrence interval (Hicks et al., 2004). The modern spatial distribution of resultant layers, their textural and geochemical characteristics and thickness appear to be dependant first and foremost on the size of the causal event, but also on shelf location. On the inner-shelf, where physical mixing is intense and little net accumulation is found (Miller and Kuehl, 2010; Rose and Kuehl, 2010; Rose and Kuehl, In Prep.), physically reworked and cross-bedded lamina abound. Advancing across shelf, facies grade from mixed layers and mottles on the mid-shelf to mottled muds, where only faint geochemical signatures of events are preserved (Rose and Kuehl, 2010; Rose and Kuehl, In Prep.). Event preservation is shown to be optimal on the landward flanks of the Northern and Southern Depocenters, within an area of non-steady state accumulation and where mixed layers and mottles are preserved (Miller and Kuehl, 2010; Rose and Kuehl., In Prep.). Here, the most intense storm on record, 100-year recurrence interval Cyclone Bola (1988), presumed to have caused a hyperpycnal plume, is recorded primarily as a scoured basal unit with cross-bedded sand fining upward into a low density upper unit, with an average thickness of ~14cm (Rose and Kuehl., In Prep.). In the absence of direct suspended sediment concentration measurements at the mouth of the Waipaoa during exceptional discharge events, the characteristics of storm sediment sequences preserved within Poverty Shelf deposits have the potential to clarify questions about the magnitude of specific events within the catchment as well as changes in frequency and/or intensity with time. This Cyclone Bola event layer may be used as a modern analogue to other preserved events in the stratigraphic record.

Postglacial sediments on Poverty Slope show that the hemipelagite record is frequently disrupted by turbidites (Pouderoux et al., 2012). Glacio-eustatic and climate changes are found to control characteristic turbidite facies and sediment routing throughout the last 18ka. For instance, during late lowstand (18.5-17ka, Figure 1D) very high slope sedimentation rates are measured along with high turbidite frequency in Poverty Canyon and low frequency in bypassed slope basin systems. Turbidite frequency in these slope basins increased and texture fined between 17-7ka as sea level rose and the proto-Waipaoa disconnected from the modern shelf break, reorganizing turbidite routing to basins. Earthquakes are recognized as the predominant triggering mechanism for turbiditic sequences on Poverty Slope, with a return time of 270 years, which is more frequent than other Hikurangi Margin slope earthquake-induced turbidites, attributed to the Poverty Slope's proximity to deep seated seismic activity (Ota et al., 1988; Brown et al., 1995; Pouderoux et al, 2012). Catastrophic floods, such as that generated by Cyclone Bola, are found to infrequently generate turbiditic hyperpycnites on Poverty Slope, with only one such record existing post maximum transgression (Pouderoux et al., 2012).

2. Methods

2.1 Core Collection and On-Board Processing

In February 2006 aboard the R/V Marion DuFresne (MD), 7 giant piston "Calypso" cores (12.83-25.34m; Proust et al., 2006) were collected from Poverty Margin from a cross section of shelf environments including two mid-shelf basins, a shelf break depocenter and two slope basins. Locations were informed by a previous Chirp seismic study (Gerber et al., 2010) in an attempt to target sequences with the greatest likelihood of preserving a complete Holocene record of shelf inundation (Table 1, Figure 1B). Three of these cores are discussed in detail in this study (MD3001, MD3004, and MD3006, from the Northern, Southern, and Shelf Break Depocenters, respectively), along with a fourth companion core to MD3001, MD3007 (Table 1, Figure 1B). Onboard processing of cores included splitting and subsampling and visual/digital logging of core properties (grain size, color, layering, contact types, incidence of wood/shells, etc.). A Geotek® Multi-Sensor Core Logger

(MSCL) was used to record continuous downcore properties such as gamma attenuation, p-wave velocity, magnetic susceptibility (SI), and acoustic impedance in half centimeter increments. Bulk density records were processed, post-cruise, to remove any core gaps. Cores were subsampled for textural, elemental and isotopic carbon and nitrogen analyses. Samples were removed at 1.5m intervals and immediately frozen for bulk organic carbon analysis. Macro- and microscopic tephra layers were detected with visual inspection of core halves and magnetic susceptibility profiles from MSCL.

Further core sampling was undertaken at NIWA in August 2007, where split and archived sections of each core had been stored in refrigerated containers. Samples were removed as described below.

2.2 X-radiographs

Digital X-radiograph negative images were collected from 2.5cm-thick rectangular sub-cores post-cruise. Exposures are X-radiographic negatives; light values are the product of limited X-ray penetration indicating high bulk density sediments, while darker values indicate less dense sediment. X-radiography provides a nearly instantaneous reference for lithological changes such as grain size, sorting, and sediment layering within a core and can be used as a proxy for bulk density/water content. Using Varian Paxscan® Imaging software, each image was adjusted for optimal balance and contrast. X-radiographs were used to identify whole shells for removal for ^{14}C analyses and, along with MSCL as an additional guide, to target potential event layer sedimentation for further sampling (Figure 3).

2.3 Radiocarbon

Seventy-five radiocarbon dates were determined from whole or partially intact gastropod and scaphopod shells (71) and wood samples (4). Samples were kept frozen until sonified and washed prior to shipment to the Woods Hole NOSAMS facility and GNS Science Rafter Laboratory (New Zealand) for AMS analysis. All ages herein are in calibrated years before present (cal. y BP), using the MARINE09.14 calibration curve (Reimer et al., 2009) in CALIB Rev 6.0 (Stuiver et al., 1998), with a delta-R (-5) and delta-R standard deviation (57). Raw plots of age versus depth revealed 10 age reversals amongst the 4 cores in this study. Reversals were removed that could be attributed to the following: (1) two samples that were extremely close in age within the core (within the error of the ^{14}C) [3]; (2) a date found for wood surrounded by only whole shells [2]; (3) two samples that were extremely close in depth [1]; and (4) an end of the core disturbance due to retrieval [1]. One sample fit both criteria 1 and 3. This leaves two reversals that can not be removed using the above criteria which were averaged for the sake of age model integrity.

2.4 Stable Isotopes

Stable carbon isotopes are used to quantify the relative contribution of terrigenous and marine source pools in continental shelf sediments (Fry and Sherr, 1984; Hedges and Keil, 1995: Hedges et al., 1997). Splits of bulk sediment samples from each of the cores (immediately frozen onboard and then processed post cruise in March 2006 vs. dried after removal in August 2007 and processed in 2011) were used to ensure no bacterial degradation or contamination had occurred between analyses (Figure 4). Initially analyses were performed every 1.5m. A further effort was then made to fill in the large gaps (1.5m) of the original $\delta^{13}C$ survey with Survey (S) samples removed at 20cm intervals, and in addition, Target (T) samples, at up to 0.5cm resolution, allowing for vertical sampling within an event unit (Figure 3). This increased coverage of MD3001 by 213 samples, MD3004 by 50 samples, MD3007 by 24 samples, and MD3006 by 6 samples.

All S and T samples were dried, ground and acidified in muffled scintillation vials with 10% HCL in random order. Samples were then redried and weighed into tin capsules that had been rinsed with methanol. All samples were analyzed by the UC Davis Stable Isotope Facility using a continuous flow Isotope Ratio Mass Spectrometer (IRMS) for stable carbon and nitrogen analyses. Percent carbon was calculated by normalizing the amount of carbon reported for each sample to milligrams, dividing by the original sample mass (mg) and then normalizing to 100%.

2.5 Grain Size Analyses

Combined wet sieve and pipette and Sedigraph® techniques were used to measure grain size. Bulk grain size measurements were initially performed at 25cm intervals at the Skidaway Institute of Oceanography. The silt and clay fraction was determined using a Sedigraph® 5100, which relates X-ray bean attenuation in a settling cell to grouped size classification. Further sieve and pipette work was performed on selected T samples at half to one-cm intervals and a few S samples in 2011 at the Virginia Institute of Marine Science, adding 73 samples to MD3001 and

27 samples to MD3004. These additional samples were analyzed by wet sieving with DI water through a 25µm-mesh sieve to separate the sand fraction from silt and clay. The sand fraction was dried at 25°C and then weighed. The fine fraction (< 25µm) was then separated into silt and clay using standard pipette/graduated cylinder procedures and following the Stokes' settling law principle (Folk, 1980). Textural profiles are the combined sedigraph and sieve and pipette samples.

3. Results

3.1 Lithostratigraphy of the Holocene Record – Event and Non-Event Deposition

Marion DuFresne core stratigraphy is composed of heavily bioturbated marine muds punctuated by numerous events. Using a combination of detailed X-radiographic analyses, archived descriptive logs of cores (Proust et al., 2006) as well as magnetic susceptibility profiles in some instances, 6 basic lithotypes, including event and non-event sedimentation, were distinguished within the core records, which aided in the interpretation of shelf stratigraphy since the Late Quaternary. Figure 5 shows X-radiographic examples of each lithotype and Table 4 details each lithotype's frequency of occurrence, thickness in length and years (using age model chronology), textural, and geochemical characteristics within the Northern (MD3001), Southern (MD3004) and Shelf Break (MD3006) Depocenters. These lithotypes are as follows: (1) tephras, (2) bioturbated mud, (3) low density layers, (4) graded layers, (5) high density layers and, (6) remnant layer(s). This approach assumes each lithotype is mutually exclusive; in order to eliminate descriptive overlap (rendering ambiguous interpretation), several lithotype subtypes are recognized. These subtypes, described below, accommodate heterogeneity within lithotypes and help distinguish key differences that might affect interpretation of how the layer was emplaced. It should be noted that geochemical trends reported in Table 4 are often ambiguous when considered independently. For example, graded layers may contain sandy muds with depleted $\delta^{13}C$ values followed by low density material with enriched $\delta^{13}C$ values; averaging through the entirety of the layer will mask this important intra-layer variability.

Lithotype 1 is comprised of macroscopic tephras, which are found uncommonly throughout each core (3.06% and 1.67% and 0.54% of thickness in MD3001, MD3004, and MD3006 respectively; Table 4). Type 1A is reserved for pure, ashfall tephra, usually normally graded, sandy (sugary) in texture and light grey to pink and often have coincident very high magnetic susceptibility (Figure 5A). Type 1B describes units with mixed components of mud and tephra, either highly bioturbated smaller ashfall occurrences or tephric sand within a muddy matrix (Figure 5A and 5B [in MD3004]).

Lithotype 2 (Figure 5B) describes non-event, homogeneous, highly bioturbated olive mud units that make up the majority of thickness in all cores (82.38%, 86.68%, 95.83% of thicknesses, Table 4). Plant fragments, organic-rich pockets, and dark streaks are common. Lithotype 2 is further divided into three textural subtypes that have progressively increasing sand contents and decreasing clay content: 2A, mud; 2B, sandy mud to sandy silt; 2C, muddy sand. These subtypes often grade into one another, but density changes are distinct enough to be obvious via the naked eye and confirmed by X-radiography. Lithotype 2B is not found within the Shelf Break Core (MD3006) and 2C is not found within the Northern Depocenter Core (MD3001; Figure 6).

Lithotypes 3 and 4 are exclusive to the Northern and Southern Depocenter cores (Figure 6). Lithotype 3A units are singular, thin (avg. thickness 1.62cm and 2.33cm in MD3001 and MD3004, respectively), low density (X-radiographically transparent) units, found frequently throughout, and unassociated with higher density or graded layers (Figure 5C). One low density layer in MD3001 is has an extremely wood rich composition, necessitating the distinction of Lithotype 3B. Lithotype 4, is comprised of graded units (Figure 5D) and is the most common layering type (27 and 22 occurrences, within the Northern and Southern Depocenters cores, respectively). Most often within the cores, normally graded units are singular occurrences comprised of a high density, sometimes cross-bedded, basal unit that grades into lower density mud. Less frequently, stacked, rhythmic graded units are observed.

High density singular units, Lithotype 5, are found in all depocenter cores (Figure 5E). This lithotype occurred three times more frequently in the Northern than in the Southern Depocenter, and was uncommon at the Shelf Break Depocenter (Table 4). These units are comprised of X-ray opaque, sometimes finely laminated and cross-bedded silts and sands. Only once, in the Northern Depocenter, are multiple stacked X-ray opaque layers found, in the very top of the core.

Finally, Lithotype 6, is found infrequently on the mid-shelf, but is the most common lithotype in the Shelf Break Depocenter (Figure 5F). This lithotype describes a highly bioturbated remnant layer or groups of layers that are not completely destroyed, but degraded to the point of being unable to classify the unit confidently as falling under Lithotypes 3-5.

3.2 Physical Properties and Geochemical Profiles

Marion DuFresne depocenter cores, MD3001, MD3004 and MD3006 are plotted showing textural, magnetic susceptibility (SI), and $\delta^{13}C$ profiles, all vs. age determined using MD age models (Figures 7, 8, and 9). Textural and stable isotopic sample resolution is highest in MD3001, which enables high variability over time to be examined, compared with MD3004 and MD3006. Because of the enhanced resolution of carbon measurements in MD3001, percent carbon is also plotted, with additional magnetic susceptibility and some $\delta^{13}C$ information from a nearby core, MD3007 (Figure 8).

3.2.1 Texture

Several gross textural shifts occur in the Poverty Shelf record in the Holocene, as well as changing degrees of variability (Figures 7, 8 and 9). Four distinct textural modes are identified in the Northern (MD3001) and Southern (MD3004) Depocenters, that are very nearly sympathetic (Figures 7 and 8). In these cores, mode 1 (shaded light gray box, Figures 7-9) describes a generally fining upwards section, from the base of each core to ~5.8ka in MD3001 and ~6.0ka in MD3004. Mode 2 begins stratigraphically above Mode 1, is characterized by a coarsening upwards signature and ends at 3.2ka in the Northern and 3.5ka in Southern Depocenters. A dramatic coarsening at this point identifies the transition to Mode 3 (shaded dark gray box), which continues to coarsen upwards and ends at ~0.55ka in the north and ~.20ka in the south, with an equally dramatic textural reversal to much finer sediments, Mode 4, through to the present.

Within the Northern Depocenter (MD3001), Mode 1 is characterized by extremely pronounced percent silt and clay variability, with silt content rarely dipping below 45%. Mode 1 is further split into three subsections, A, B, and C, to highlight three intra-mode changes. Mode 1A is characterized by high variability in clay, silt *and* sand, and a fining upwards (lowermost black arrow, Figure 7). Nine excursions where percent silt exceeds 60% occur within the ~1ka represented by Mode 1A, and another 10, over 50%, all of which have concomitant decreases in percent clay, and many of which co-occur with increases in sand, even though a decrease in sand percent is the general trend in Mode 1. Mode 1B in the Northern Depocenter remains variable but to a lesser degree, with only 3 excursions beyond 60% clay, with no correlation to sand. Percent sand is extremely unchanging at an average of 2.6% (black arrow). Percent clay increases steadily through Mode 1A, stabilizes in 1B, but changes at the transition to 1C, dropping off, while percent silt increases subtly. Percent sand increases in Mode 1C, and becomes more variable again. Again, several silt excursions beyond 60% are recorded, with a few clay excursions that also reach 60%.

In the Southern Depocenter (MD3004), Mode 1 is split into two subtypes, A and B (Figure 8). In Mode 1A in the Southern Depocenter, as in the Northern Depocenter, a fining upwards signature is recorded (lowermost black arrow, Figure 9). Percent sand decreases linearly from ~25% to ~ 7% between ~11ka and ~9.5ka and clay percent jumps more than 10%. In Mode 1B, continuing to ~6.0ka, the sand fraction remains extremely low and clay content continues to increase, as in the Northern Depocenter's Mode 1C. Percent silt remains fairly constant at 50% throughout Modes 1. The Southern Depocenter record is not nearly as variable as the Northern Depocenter, but this may be due to slightly lower overall sample resolution.

Mode 2 describes a clear coarsening (black arrows, Figure 7 and 8), with increased percent sand from an average 2.6% in Mode 1A to 9%, with a high of ~20% in the Northern Depocenter and from an average 7% to 13% in the Southern Depocenter. In Mode 2, a slight concomitant decrease in the clay and silt fractions (grey arrow, Figure 7) are observed in the Northern Depocenter, while percent silt and clay remain relatively unchanged in the Southern Depocenter. Variability wanes in the Northern Depocenter, although sample resolution also becomes coarser. However, lithostratigraphy shows far fewer events after the middle portion of Mode 2 (see Discussion below), providing an independent check on the trends in variability.

A major coarsening shift in both mid-shelf depocenter cores marks the sharp transition into Mode 3 at ~3.2ka in the north and 3.5ka in the south (dark gray shaded box), also coincident with the occurrence of the Waimihia ashfall tephra, which is identified in the Shelf Break Depocenter at ~3.25ka as well (MD3006; Figures 5A, 7, 8, and 9). Within Mode 3, average percent sand jumps to 30% in the Northern and 41% in Southern Depocenters (black arrows, Figures 7 and 8). Percent silt decreases in both mid-shelf cores from an average of 55% within Mode 2 to 40% in Mode 3 (grey arrows, Figures 7 and 8). Finally, Mode 1 commences with an equally as dramatic fining signature, at 0.5ka in the north and 0.2ka in the south. Percent sand drops to an average ~5% in the north and to an average 40% from a high of 60% (at the very top of Mode 3) in the south.

In the Shelf Break Depocenter (MD3006; Figure 9), as seen on the mid-shelf, the oldest portion of the record is characterized by a dramatic fining signature, from ~14.75ka to 11.25ka, Mode1. The degree of this change is even more pronounced than on the shelf, where sediments fined from a maximum 70% (average 53%) sand to ~15% over 3ka. From 11.25ka through 5ka, in contrast to mid-shelf cores, the shelf break record continues to fine with an average of 9% sand, and then appears to level out to constant 4.6% sand, with a subtle increase in percent silt to 1.75ka. Between 1.75-0.5ka, a brief coarsening trend is recorded, as the clay fraction drops and sand increases to 8%. From 0.5ka to the top of the core, percent sand drops to nearly zero, as clay increases to over 60%, just as within the mid-shelf's Mode 4.

3.2.2 Magnetic Susceptibility

Magnetic susceptibility shows multiple small excursions throughout the Holocene in all shelf cores. At 3.1ka (MD3001), ~3.2ka (MD3007), 3.5ka (MD3004), and 3.25ka (MD3006) the Waimihia ashfall is identified, the largest coincident magnetic susceptibility spike (labeled on Figure 7, 8, and 9). Several other major excursions are evident, especially in the most recent 3ka of each core. The body of each core contains numerous minor fluctuations below 3.5ka and prior to 9ka. In the Northern Depocenter core MD3007 (just beyond the extent of MD3001) at ~9.5ka and also at ~9.6ka in MD3004, another large spike is recorded (Figure 8). In the first 1ka of the Southern Depocenter (MD3004) and the first 3ka in the Shelf

Break Depocenter (MD3006), a shift from high to low magnetic susceptibility is recorded, coincident with Mode 1A and Mode 1, respectively within the two cores.

3.2.3 Stable Carbon Isotopes

Initial surveys of $\delta^{13}C$ and N:C ratios from MD cores taken every 1.5m indicate a mixed assemblage of marine and terrestrial carbon in all shelf cores (Figure 10). A sample shift towards the right (more depleted $\delta^{13}C$) represents an increase in terrestrially sourced sediments, as with core profiles (Figures 7-9). In the Northern Depocenter, sampling resolution allows us to see that $\delta^{13}C$ was extremely variable in the lower half of the core, with 10 excursions more depleted than -26.20‰, that span almost 3‰, up to ~5.2ka (Figure 7). The majority of these excursions are coincident with positive spikes in percent carbon, while a few are correlated with negative spikes. Target (T) samples (chosen by X-radiographic guide) nearly always capture large variabilities in $\delta^{13}C$, however several excursions were not clearly identified X-radiographically, but were captured in Survey (S) sampling. After ~5.2ka, in the upper half of the Northern Depocenter core, excursions are much less frequent and $\delta^{13}C$ values never exceed -26.20‰. Not considering excursions, subtle variations in background $\delta^{13}C$ are apparent. From the bottom of the core to ~7.3ka (coincident with the upper boundary of textural Mode 1B), $\delta^{13}C$ is slightly more enriched, often beyond -25‰. After ~7.3ka and through to ~3.2ka (coincident with the upper boundary of textural Mode 2), $\delta^{13}C$ becomes more depleted, and then, after ~3.2ka, again has a more enriched signature. Percent carbon (shown for MD3001 only) is also highly variable, especially prior ~5.2ka, with no sample exceeding 3%.

In the Southern Depocenter (MD3004) and Shelf Break Depocenter (MD3006), variability in $\delta^{13}C$ is not as prominent because sample resolution is coarser than in the Northern Depocenter (Figures 8 and 9). $\delta^{13}C$ values show a general trend of increasing terrestrial influence (lower $\delta^{13}C$ values) with depth on the shelf break (Figure 9).

4. Discussion

4.1 Lithotype Interpretations

The lithotypes identified on Poverty Shelf offer a comprehensive way to contextualize and examine geochemical and textural variations that independently might be less informative but together can help identify event layers. X-radiographically and visually identified lithotypes help to discriminate between non-event suspension settling and a variety of event lithologies. This differentiation, in turn, allows for type and frequency analysis as well as investigation into driving mechanisms.

Distinct X-radioghraphs, texture, MSCL, and $\delta^{13}C$ profiles distinguish Lithotype 1A, ashfall tephras (Figure 5A, Table 4). An example of this is seen in the Southern Depocenter (Figure 5A). Without a split-core visual or glass shard identification, spikes in magnetic susceptibility along with textural and $\delta^{13}C$ analyses can confirm a tephra. Within this tephra unit, sand content increases to almost 70% and percent carbon and $\delta^{13}C$ drop from higher background levels. Several unidentified tephras in the last 3ka are found via X-radiograph and/or magnetic susceptibility spike, presumably reflecting volcanic eruptions, potentially including the Mapara, Taupo and Kaharoa tephras (Figures 6-9).

In contrast, within Lithotype 1B, the largely discontinuous and dispersed nature of tephric material means these layers may either represent a poorly preserved ashfall or a tephric-rich mud that is the result of increased erosion of the Waipaoa catchment soil mantle and associated tephric material and subsequent delivery via storm activity to the shelf. A good example of using lithotype analysis plus textural and geochemical evidence to identify a tephra is seen at ~1.85ka in the Southern Depocenter (MD3004; Figure 5B). Here, a visual identification was not recorded in the core log, but the X-radiograph shows discontinuous/interrupted laminations and this, coupled with a MSCL spike, positively identifies the unit as a tephra, reworked at its upper and lower boundaries. In another instance, at ~9.7ka in the Southern Depocenter, Lithotype 1B is identified by photographs and X-radiography, as a thin unit near the bottom of the record (Figure 6). Although glass shard analysis and detailed $\delta^{13}C$ analyses were not done, when combining lithostratigraphic observations with textural and magnetic susceptibility records (Figure 8), it is clear that the unit is the result of tephra emplaced by volcanic activity. In contrast, some tephric material was identified when logging the split Northern Depocenter core (MD3001) visually, located just above a wood-rich low density layer (Figure 5C, Lithotype 3B), and relatively high sand content sand was found here (19%). However, geochemical evidence points to flood origin as percent carbon within the sample is the highest recorded in any core within this study (~3%) and $\delta^{13}C$ is extremely depleted (>-29‰; Figure 8). Subsequent analysis of the samples within several centimeters of this unit shows sand content falls to between 7-9%, which is not what would be expected with a typical tephra Lithotype (1A or 1B) sand percent.

Lithotype 2 comprises more than 80% of the record within both mid-shelf depocenters and over 95% on the shelf break, and is the product of suspension settling and bioturbation. The overwhelming dominance of this lithotype within the Shelf Break Depocenter reveals that events very rarely are preserved at this farthest location from the Waipaoa source (Figure 6). Examples of the (sometimes subtle) differences between Lithotype 2 subtypes are seen in Figure 5B. Lithotype 2C is only found within the Southern Depocenter (MD3004) in the first 1ka of the stratigraphic record and in the Shelf Break Depocenter (MD3006).

The occurrence of Lithotypes 3-6 in the Northern and Southern Depocenters (MD3001 and MD3004; Figures 5C-F, 6-8) are clear evidence that event signals are propagated from catchment to shelf and preserved in the Holocene Poverty Shelf record. Lithotype 3, low density single units, typically are comprised of nearly 90% silt and clay (Table 4) and are interpreted to be deposited during periods of rapid sedimentation, perhaps hyperpycnal in nature, with no evidence of reworking by wave action. The one occurrence of Lithotype 3B at the bottom of the Northern Depocenter record is extremely wood-rich, and probably indicative of an atypical flood event layer (Figure 5C). At this point in time, the proto-Waipaoa river mouth was several kilometers inland from its current position (Figure 1C), making it unlikely that this represents a hyperpycnal input by virtue of the core's shelf location in relation to the river mouth. One possibility is that a forest fire, perhaps volcanic in origin, freed a preponderance of wood that was transported via subsequent floods.

This light woody debris may have rafted across the shallow shelf and been deposited in the Northern Depocenter. A slightly younger remnant layer is also found on the shelf break, within 100 years of this woody event layer on the Northern Depocenter, perhaps signaling a large enough flood that riverine material transited the entire shelf.

Lithotype 4 is interpreted to be the product of an oceanic flood emplacing a unit that reflects both increased sediment supply and strong oceanographic conditions that wane as the flood and wave energy ease (e.g. recalling the characteristics of a Bouma sequence; Bouma 1962). This lithotype normally has a strong, high density, sandy basal contact, with frequent crossbedding, evidence of deposition under energetic flow conditions (Figure 5D). The basal unit grades into a lower density, usually bioturbated, upper unit, providing evidence that deposition occured as flow decelerated and often has a wavy or diffuse contact with Lithotype 2. This lithotype is the most common event unit recognized in both mid-shelf depocenters accounting for 42% and 62% of the record in the Northern and Southern Depocenters, respectively and are also, on average, the thickest of event units emplaced (Table 4). In a few instances closely stacked or repeated Lithotype 4s of variable thickness (several centimeters to less than 1cm) are observed, which may point to repeated oceanic flood deposits or subsequent pulses of the same flood material (Figure 5D).

In contrast, Lithotype 5, high density layers, which often display cross-bedding and well-defined, straight basal contacts (Figure 5E) are interpreted to be the result of strong oceanographic forcing conditions likely with no, or at least uncoupled from, attendant rain/flood. Lithotype 5 occurs nearly three times as commonly in the Northern than Southern Depocenter and in both depocenters, has the lowest percent carbon of any lithotype (0.37% and 0.16% in the Northern and Southern Depocenters, respectively; Table 4), presumably reflecting minimal terrestrial carbon sorption to clays. In the Northern Depocenter, Lithotype 5 has a combined average of over 50% sand and silt and in the Southern Depocenter over 95% sand and silt (Table 4), indicating intense reworking and winnowing of fines. The majority of export of stored sediment from Poverty Bay has been shown to occur during high wave events (which may or may not be coupled with oceanic floods; Bever, 2010), and would obviously resuspend sandier material to be transported shelf-ward as well as fines to be transported off-shelf. It is likely that Lithotype 5 beds in mid-shelf depocenters are a result of this oceanographic coupling. Further, during oceanic floods, preliminary model simulations show plumes are steered towards the south (J. Moriarty, Pers. Comm.), which is consistent with the higher sand and silt, overall, seen in Southern Depocenter Lithotype 5 units throughout the Holocene, and may, also implicate hyperpycnal inputs that are truncated or subsequently reworked. Lithotype 5 is the only type of intact event recorded at the Shelf Break Depocenter, and only twice observed within textural Mode 1, when the Waipaoa source is presumed to be much closer to the shelf break. As sea level rose and proximity of the riverine source decreased, even during strong oceanic flood, events likely simply did not have the energy to propagate to and make a significant impact on the deepening and fining Shelf Break Depocenter location. It is probable that many of the event remnants (Lithotype 6, Figure 5F) recorded at the Shelf Break Depocenter are the result of strong wave events, and not oceanic flood sedimentation, thus representing remnants of Lithotype 5. This would be especially likely for those emplaced after the

Waipaoa River mouth became more distal to that location, after textural Mode 1, between ~12.5 and 11ka.

4.2 Significance of Temporal Distribution of Lithotypes

The Northern Depocenter has the most frequently preserved event layers (counting all Lithotypes 1, 3-6) overall, amongst the shelf environments represented in this study - 59 compared to the Southern Depocenter's 43 and the Shelf Break's at 17, most of which are event remnants (Table 4). Regions of notable non-event deposition are found in the upper and lower portions of the stratigraphic record, with a marked increase in event preservation incidence observed in the mid-Holocene in both mid-shelf depocenters (brackets, Figure 6).

In the Northern Depocenter, this period of increased preservation demonstrated by lithotype stratigraphy is between ~7.4 and ~4.6ka with one event preserved every 70 years (or every 21.23cm). This time period overlaps with the period of rapid fluctuations within point-to-point accumulation rates (pink and dark blue lines, Figure 2B; Rose et al., In Prep.) and is synchronous with textural Mode 1, where increased grain size and isotopic variability characterizes the record, extending from ~5ka to ~7.3ka (Figure 6 and 7). In addition, in facies analysis from Rose et al. (In Prep.), Facies 2, was identified (in the same core) to extend from 6.9 to 3.4ka and attributed to increased event preservation. At ~4.6ka, the incidence of event preservation diminishes, as well as the variability in point-to-point accumulation rates (Figure 2B).

A similar clustering of lithostratigraphic event frequency is recorded in the Southern Depocenter in a smaller spatial window, between ~4.8ka and ~6.8ka, at one every 95 years (or every 21.24cm; Figure 6). The period of enhanced preservation in the Southern Depocenter is clearly shorter than in the Northern Depocenter, either reflecting more frequent steering of events towards the north, more relative frequent reworking and destruction of layers in the south via bioturbation, or a combination of the two. This enhanced preservation is synchronous with the increased variability in point-to-point accumulation (Figure 2B, also shorter than in the Northern Depocenter) and nearly synchronous with the almost three fold (compared to underlying and overlying accumulation) uptick in accumulation recorded between 5.5 and 7.0ka (0.41cm yr^{-1}, Table 2). Again, Facies 2, extending from 6.4 to 3.5ka in the Southern Depocenter overlaps with the increased incidence of preserved events in this location (Rose et al., In Prep.).

Clearly, the onset of increased preservation of events shown by lithostratigraphic and facies analysis is in sync with the timing of maximum transgression (~7ka). After 7ka, subsequent rapid progradation of the Waipaoa River Mouth, engendered enhanced capture of event sedimentation in the mid-shelf depocenters. Both mid-shelf depocenters also record a coarsening (textural Mode 2 and seen in a transition from Lithotype 2A to 2B in the upper half of MD3001, Figures 6-8), showing increased bypassing of river sediment to the shelf, from Poverty Bay as the river mouth and shoreline advance. The high variability in point-to-point accumulation reflects the stochastic and episodic nature of large storm and flood events (Figure 2B). We suspect this "sweet spot", the period of increased fidelity of the stratigraphic record on the mid-shelf in the mid-Holocene, is produced as a result of higher accommodation and lower amounts of physical and biological reworking when sediment supply was increasing and the mid-shelf basins were underfilled.

Throughout the Holocene, more event layers were preserved within the Northern Depocenter core as compared to the Southern Depocenter core , and prior to the period of enhanced event preservation, the incidence of events was far fewer in both locations. In the early Holocene, despite no change in accumulation rate recorded in the Northern Depocenter in comparison with the later "sweet spot" (Figure 2A; Rose et al., In Prep.), preservation of Lithotypes 1 and 3-6 is one every 156 years. In the Southern Depocenter, events are even less frequently preserved at one every 326 years. In fact, most of the events in the early Holocene in both depocenters appear to be prior to ~8.5ka (coincident with textural Mode 1A in the north, Figure 6). In the Northern Depocenter record at its inception, immediate and much more frequent occurrence of silty excursions (even with relatively little lithotype evidence of events) show that rapid changes were experienced on the shelf in the time between the Southern Depocenter's Mode 1A and the Northern Depocenter's as the locus of Waipaoa River deposition rapidly transgressed and was rearranged (Figure 7). After ~8.5ka in both mid-shelf depocenters, nearly 1ka goes by uninterrupted and this event hiatus is coincident with Facies 3, comprised of mottled and homogeneous muds, interpreted to reflect a filtered riverine input (Rose et al., In Prep.). The event preservation hiatus also corresponds with the time period when the proto-Poverty Bay coastline was rapidly shifting inland creating accommodation space in the bay, and consequently, trapping of events within the bay was highly likely. Also, because of the geometry of the bay, large wave events which are shown to help export material from the Bay in modern modeling scenarios (Bever, 2010), may not have as efficiently resuspended and subsequently exported coarser material to the shelf depocenters during this time. Additionally, prior to ~7.4ka, incidences of major isotopic excursions captured in Survey (S) samples show that, although some events are not visible with the naked eye or by X-radiography, therefore not captured in lithotype analysis, many are recorded isotopically within shelf stratigraphy – an example of which is seen in the correspondence of an excursion within the example Lithotype 2A in Figure 5B. These excursions, with extremely depleted $\delta^{13}C$ values and high percent carbon with associated increases in silt content clearly point to a river flood origin, perhaps without attendant high wave action or oceanic floods reworked by bioturbation (and therefore no record observed in lithostratigraphy).

After ~4.6ka in the Northern Depocenter and ~4.8 in the Southern Depocenter, event layer preservation decreases and event layers are less frequent than any previous time period preserved, at one every 244 and 340 years, respectively. This is likely linked with rapidly diminishing accommodation within the depocenters. Effective depocenter shoaling increases the chance of layer destruction due to wind and wave driven resuspension. Increases in sand content are recorded (textural Mode 3), with the Southern Depocenter observed to be slightly coarser than the Northern Depocenter, corroborated by facies analysis (Rose et al., In Prep.). Events are more regularly spaced in the Southern Depocenter in this time period than in the Northern

Depocenter, reflective of both a relatively unchanged accumulation rate in comparison with the recorded decrease in accumulation in the Northern Depocenter (Figure 2A). This is in agreement with sequence stratigraphic interpretations from seismic reflection that show the basins are infilling in fundamentally different ways – i.e. over-filled progradational geometries in the Northern Depocenter and underfilled, concave-up reflectors in the Southern Depocenter (Gerber et al., 2010).

In the most recent 500 years of the record, the Northern Depocenter preserves more incidences of event sedimentation, with one every 68 years (up until core truncation at 200yr BP) – namely high density lithotypes, further evidence of decreasing ability to preserve low density, easily resuspendable layers, if they were emplaced. In contrast, along with the noted regularity in Southern Depocenter event layer spacing, more low density Lithotype 3 units are found than in the north, and almost all events within the last ~1.5ka here are lithotypically low density layers, invoking the hypothesized continued accommodation as well as indicating more efficient capture of low density producing events in this time period.

4.3 Coherence Between Depocenters

Although there is a good degree of general temporal coherence between the Northern and Southern Depocenters texturally and with regard to the event preservation "sweet spot" and hiatuses, only a dozen or so individual events appear to be correlated between them, and even fewer between the mid-shelf depocenters and the Shelf Break Depocenter (Figure 6). Those of the same lithotype that occur within a ca. 100 years of each other are identified with grey arrows (double ended arrows,

Figure 6), one exception being the dated Waimihia tephra. Another possible exception is a distinct series of stacked, normally graded Lithotype 4 units (grey question mark, Figure 6) at ~8.6ka in the north and 8.9ka in the south, coincident with a remnant layer on the Shelf Break Depocenter at ~8.9ka, which could possibly indicate an event or series of events that were widespread enough to impact the entire shelf. Other events may be coherent between depocenters, but may be emplaced as non-corresponding lithotypes as smaller scale patchiness may affect preservation. In addition, stochastic sedimentation may be steered to different shelf locations depending on oceanographic conditions, greatly influencing the character of event deposition between depocenter cores, and perhaps even within each depocenter (Bever, 2011; Rose and Kuehl, In Prep.). Uncertainty within the age models (instrumental error avg. amongst cores is 87 years) may explain some of the offsetting of event lithotypes between the depocenters, but more likely, different events are recorded between the depocenters. If indeed some event layers are coherent between depocenters but emplaced as different lithotypes, they could not be identified as such without further refinement of the core age model.

Although determining between-depocenter coherence of events proved challenging, textural transitions (modes) on the shelf are well defined in core profiles (black horizontal arrows at transitions between gray shaded boxes, Figures 7-9). In the Northern and Southern Depocenters these transitions are nearly synchronous providing evidence that the changes in sediment supply and sea level rise impacted the depocenters in similar ways. In the Northern Depocenter core, these transitions are enhanced by gross changes in variability of $\delta^{13}C$ and even percent carbon trends within the core. On the shelf break, textural transitions correspond with facies changes (Rose et al., In Prep.) and are clearly reflected in the non-event dominated lithostratigraphic column (Figure 9). The decrease in magnetic susceptibility in textural Mode 1 at the Shelf Break Depocenter likely reflects a waning nearby source of freshly eroded sedimentary rocks with more coercive minerals. In this section, not only are sediments texturally more coarse than those above, but they also have a more depleted $\delta^{13}C$ signature. Following this reduction, the bottom of both mid-shelf depocenters also experience a magnetic susceptibility excursion that is presumably reflective of the transgressive ravinement surface (Figures 7 and 8).

Textural Mode 1 terminates at ~5.8 and ~6.0ka in the Northern and Southern Depocenters, respectively, in good agreement with the terminus of the mid-Holocene phase of Waipaoa River downcutting recorded by other investigators (Carter et al., 2002; Gomez et al., 2000b; Phillips and Gomez, 2007), and slightly prior to the end of the preservation "sweet spot" of event preservation. After this textural transition, the coarsening trend on the shelf commences, indicative of intensifying shelf circulation and reworking, along with capture of coarser material from enhanced source-to-shelf flux as the Waipaoa prograded (Rose et al., In Prep.) and as the river mouth was exposed to coastal energy (Bever, 2010). Waipaoa flux has been interpreted to have decreased after this time, modeled and inferred from a single location on the mid-shelf, whose record does not extend beyond 6ka (Figure 1B, MD2122; Gomez et al., 2004; Phillips et al., 2007). This trend is captured within both the Northern and Southern Depocenters in point-to-point accumulation (Figure 5B), and after ~4ka in shelf age models. But, a concomitant and continued increase in accumulation recorded in the Shelf Break Depocenter suggests that instead of reduced terrigenous flux creating the decrease in accumulation on the shelf, increased bypassing due to continued infilling-to-overfilling regime may be the reason. In addition, $\delta^{13}C$ and percent carbon records do not record a sympathetic enrichment, which would be expected if terrigenous material was reduced by half, as suggested by these authors.

4.4 Earthquakes in the Holocene Poverty Shelf Record

Over the last 7ka, almost 20 large magnitude earthquakes (M_w = >7.3) have been dated on the East Cape compiled from post-maximum transgression (~7ka) uplifted terraces as well as a variety of paleoenvironmental indicators (Table 1; Ota et al., 1988; Berryman et al., 1989; Berryman, 1993; Brown, 1995; Berryman et al., 2000; Hayward et al., 2006; Cochran et al., 2006; Litchfield et al., 2010). Several of these earthquakes have been correlated with catastrophic turbidite sequences on the Poverty Slope (Pouderoux et al., 2012). On the Poverty Shelf, prior to 3ka, nearly every seismic event can be correlated with an event layer in the Northern Depocenter, falling directly in or within 100yrs of an event layer, while only about half of all earthquakes are correlated with event sedimentation in the Southern Depocenter (yellow stars on y-axes, Figure 6). However, it is impossible to tell if the occurrence of earthquakes is actually the causal mechanism for events recorded within the lithostratigraphic record. Even if causation was possible, given uncertainty in the age model as well as with published dates of earthquakes, it is impossible to tell if an event layer above or below yet temporally proximal to an earthquake is the resultant unit. Additionally, there does not appear to be a specific lithotype which is more commonly associated than any other with an earthquake. This likely means that the mode of emplacement of any individual event layer by a subsequent storm, although potentially enhanced by landscape response to prior seismic activity, is the main determinant of the physical and geochemical character of the event layer, instead of a direct *in situ* earthquake-layer link (i.e. soft sediment deformation). A resultant unit would then still be dependant on catchment, flood, and oceanographic specific conditions; the earthquake itself would simply act as a landscape primer.

Several radiocarbon age reversals were removed as described in the results above, to keep age model integrity, however two are worthy of mention due to their near co-occurrence with known earthquake activity and because they are the largest of any of the excursions documented. Both reversals occur in the Northern Depocenter, in the top portions of the cores, and show older material emplaced on younger material, the reversal spanning over 1.0ka. The first reversal, in MD3001, encompasses two samples (one wood, one whole shell) and the other, three samples in MD3007 (whole shells). In MD3001, the reversal begins after 2.9ka (the last date within the age model prior to the reversal), less than 30 years post a major known earthquake (Table 1) and also just after the Waimihia tephra occurrence (Figure 5A). The presumed correlated unit, one of the thickest Lithotype 5 occurrences, is high density, massive, with pieces of wood lodged in the very top. However, textural and geochemical profile sampling was too coarse to capture the event. This reversal is correlated with a silty turbidite on the Poverty Slope (MD3003, location on Figure 1B; red bar on age axes, Figure 6) with an erosive basal contact, interpreted to be the only hyperpycnite recorded on Poverty Slope since maximum transgression. The timing of the Northern Depocenter event layer and the Poverty Slope hyperpycnite is also correlated to a very large storm bed recorded in a Lake Tutira sediment core (Orpin et al., 2010; Pouderoux et al., 2012).

The other major reversal is younger and occurs in the Northern Depocenter Core (MD3007, which has not been analyzed lithostratigraphically or geochemically in this study), after 1.5ka, also within 100yrs post a known large magnitude earthquake. This reversal is also correlated to a basally erosive, silty, but non-hyperpycnite, turbidite on Poverty Slope, interpreted to have formed due to earthquake activity (Pouderoux et al., 2012). Interestingly, lithostratigraphy in the two main mid-shelf cores analyzed shows a correlated singular low density unit preserved within both the Northern and Southern Depocenters at this time. The absence of such reversals in the Southern Depocenter may have a geophysical explanation or be related to differences in geotechnical properties of mid-shelf depocenter sediments rendering the Northern Depocenter seabed more prone to reorganization at the advent of a large southern swell event.

Within the Lake Tutira record, a relationship between the thickest homogenite deposits, interpreted as remobilized lake sediments emplaced by gravity flows, are found to be preceded by a large magnitude earthquake. In addition, distinct time periods when homogenites are thin and occur frequently (<25 years between events) are found to be related to clusters of earthquake events, interspersed with periods of infrequent reoccurrence (>50 years, Table 1) but thicker individual homogenite beds (Orpin et al., 2010). These authors suggest such trends are related to landscape response and recovery, as initially, earthquake shaking causes landscape destabilization and large sediment yields to be readily available to enter into the lake record, but, as earthquake frequency is increased, homogenite thickness decreases due to a deficit of freed regolith and sediment to enter the lake. This type of tightly coupled coherence between lake sedimentation and coseismic frequency does not appear to hold up on Poverty Shelf, where, although individual large magnitude earthquakes have been found to be temporally associated with event deposits in some cases, hiatuses and changes in thickness of event beds are not correlated with the absence or frequency of earthquake occurrence clustering. One reason this may be the case is simply that fewer event deposits are preserved in shelf stratigraphy as a result of exposure to destruction by physical and biological agents, masking any possible relationship that may have been initially emplaced. Over 1000 storm event beds are recorded in the 7ka-long Tutira record (Orpin et al., 2010), as compared to the Poverty Shelf's maximum 59 events over the last ~10ka in the Northern Depocenter.

4.5 Linking Poverty Margin Records: Poverty Shelf in the Source-to-Sink Context

Reid and Page (2003) and Page et al. (1994a, b) show that for regions surrounding Lake Tutira, during Cyclone Bola, as rainfall increases, landslide density and sediment generation also increase. Subsequently, Orpin et al., (2010), found a positive correlation between recorded storm rainfall intensity and event layer thickness in the Lake Tutira record. It follows that a similar relationship may exist between rainfall intensity and Poverty Shelf event layer thickness. In the modern record under current landscape/erosion conditions, Cyclone Bola (100yr recurrence interval) emplaced an event layer on the shelf with an average thickness of 10.6cm after >300mm day^{-1} of rain (Page et al., 1994b; Rose and Kuehl, In Prep.). Orpin et al. (2010), for example, estimated that a modern Bola-sized event would generate a layer ~17cm in thickness in Lake Tutira, while a prehistoric Bola-sized event might generate a layer ~3cm thick. On Poverty Shelf, average layer thickness for Lithotype 4, the most common found in the Holocene record, are 7.1cm and 5.9cm in the Northern and Southern Depocenters, respectively. Factoring out the 6-fold increase in sediment load of the Waipaoa between modern non-forested catchment cover and pre-human forested cover (Reid and Page, 2003; Kettner et al., 2007), and using the relationship between Bola daily rainfall (~300mm) and its resultant average shelf event layer thickness (Rose and Kuehl, In Prep.), the average Lithotype 4 oceanic flood layers would have been produced by approximate rainfalls of 885 and 1100mm day^{-1}. This is quite high, however rainfall events larger than Bola have been recognized in the stratigraphic record (Eden and Page, 1998; Orpin et al., 2010) and these values do not exceed modern mean annual Waipaoa catchment rainfall. The calculation also does not take into account stacked instances of Lithotype 4, which, if removed would lower the average thickness of this lithotype in the Holocene record. The calculation also assumes the processes that emplace the Cyclone Bola oceanic flood event layer on the shelf were those operating at the time of event lithotypes emplaced in the Holocene stratigraphic record, for instance changes in water depth and source location due to rising sea level and relative level of infilling of the mid-shelf depocenters. It is notable, however, that the Holocene record of event layer thicknesses (Lithotypes 3-6) are quite comparable in thickness to modern event layers – many even larger (Table 4; Brackley, 2006; Rose et al., In Prep.). It follows that such layers may actually be records of storms with intensities greater than any on record in the last century. Many caveats exist in this type of inquiry however, including changes in climate and landscape conditions including vegetative cover, erosion regime, storage, event resistance and variability under modern vs. Holocene timescales within the Waipaoa catchment (Philips and Gomez, 1997; Eden and Page, 1998; Crozier et al., 2010). In addition, complexities, not present in a lake system, may diminish the power of such a relationship between rainfall and correlated event sedimentation on the continental shelf including temporal decoupling of the event with the emplaced layer, and changes in preservation potential (compared to the likelihood that *every* rainfall/erosion event will be captured, to some extent in the Tutira lake record). A first approximation suggests that, at the very least, pre-modern oceanic flood layers, with averages of the same thickness, would have likely resulted from storms of greater intensity than those that produce comparable thicknesses in the modern record.

Unlike on Poverty Slope, there appears to be no correlation between event frequency and several eustatic still-stand periods recognized in the Western Pacific (Figure 1D; Lui et al., 2004; Carter et al., 2002). On the slope, nearly all hyperpycnites were dated within these periods, suggesting that subdued sea level rise engendered better connectivity between source to slope sink (Pouderoux et al., 2012). Whether or not event signatures were emplaced and then reworked/removed, therefore never being preserved during this time, cannot be known. Evidence of event emplacement and subsequent removal are suggested by the four events captured only texturally and geochemically (not evident in X-radiographically and therefore included in the lithostratigraphic interpretation). These events occur between 8-9ka, during a relative still-stand (Figure 1D) and although strong textural and geochemical remnants of their existence are evident, can not be identified structurally. Elsewhere throughout the Holocene, as explored above, event preservation on the shelf appears to be driven by a combination of rapid sea level rise and consequent enhanced Waipaoa flux to the shelf.

Clearly, Poverty Margin lake, shelf, and slope records contain a wealth of information about event magnitudes and frequencies throughout the Holocene and provide dramatically different records of signal preservation. Along the continuum of reservoirs from land to sea, the Poverty Shelf record offers a spatial intermediary between the lake and slope records. Over-sensitivity to landscape response and non-attachment to oceanographic conditions of lake records mean that limited conclusions can be drawn about long-term climate regime shifts impacting sea level eustacy, and the slope record is limited in scope because its deeper location renders it dependant on sedimentary source, ensuring only the signals of the most catastrophic events are preserved in the record. The Poverty Shelf record provides an intermediate filter in space and time along the continuum. The shelf record captures the influence of tectonics, climate change, and sea level rise on strata formation via changes in event and non-event periods of preservation as well as textural and isotopic shifts. However, it also clearly preserves a response to extreme and episodic events, such as oceanic flooding (seen in Lithotypes 3-6). Ensemble, the linked land, shelf, and slope records enable us to find important continuities and discontinuities in the concurrent records, showing that some events – including storms and associated oceanic floods and large earthquakes can be captured in the record of all three, while the majority of may be preserved in one location, but not (or not recorded) in another.

5. Conclusions

1. X-radiographic, textural, magnetic susceptibility and stable carbon isotopic profiles reveal that the Poverty Shelf stratigraphic record preserves both evidence of exceptional stochastic event sedimentation as well as regime shifts in supply, transport, and accumulation of sediments due to longer-time scale perturbations related to climate, sea level, and tectonics. Lithotypes analyses reveals event beds include ashfall tephras, low and high density singular units and graded beds. Periods of non-event deposition are characterized by homogeneous mottled muds, which make up the majority of the shelf records.
2. A period of increased event preservation, corresponding with higher and variable point-to-point accumulation rates in the Northern (~5-7.3ka) and Southern (~4.8-6.8ka) Depocenters in the mid-Holocene directly post maximum transgression. This "sweet spot" is interpreted to be a function of increased fidelity of the stratigraphic record resulting from under filled basins due to ample accommodation as well as lower amounts of physical and

biological reworking. Event coherence between depocenter cores is not confirmed.

3. Prior to and after this "sweet spot", the event record is sparser, and periods of non-event bed preservation characterize the shelf records. Before ~7ka, non-deposition is interpreted to be caused by shifting of the Waipaoa River mouth inland, rapid sea level rise sediment trapping within Poverty Bay, effectively filtering the ability of events to be preserved in the mid-shelf. After ~4.6ka, continued infilling of the basins and shoaling of the shelf along with increased reworking and removal due to physical oceanographic conditions and onset of ENSO are determined to be likely causes for the reduction in event layer preservation.
4. Shifts in textural modes, enhanced by magnetic susceptibility logs and stable carbon measurements highlight changes in sediment supply, sea level rise and Waipaoa River source. These shifts are correlated with facies previously identified on Poverty Shelf (Rose et al., In Prep.).
5. Several known dated earthquakes impacting the Poverty Margin can be correlated with but are not presumed to be the cause of event lithotypes in the stratigraphic record. No relationship exists between event character, frequency or thickness and seismic activity. Two large age model reversals within the Northern Depocenter are linked with earthquake occurrence.
6. The Poverty Shelf stratigraphic record may be viewed as an intermediary filter along the continuum of reservoirs where event signals can be preserved from land to sea. High frequency, low magnitude rainfall events, recorded in lake

records (Eden and Page, 1998; Orpin et al., 2010), are not preserved on the shelf, while lower frequency, high-magnitude oceanic flood (possibly enhanced by sediment supply directly linked with seismic activity on land) and wave reworking events are interpreted to be the mechanism of emplacement of the event layers preserved. In comparison, only the most catastrophic oceanic floods are interpreted to be recorded on Poverty Slope, along with turbidites emplaced due to seismic destabilization (Pouderoux et al., 2011).

Literature Cited

Alexander, C.R., Walsh, J.P., Orpin, A.R. 2010. Modern sediment dispersal and accumulation on the outer Poverty continental margin. *Marine Geology*, 270: 213-226.

Alloway, B.V., Lowe, D.J., Barrell, D.J.A., Newnham, R.M., Almond, P.C., Augustinus, P.C., Bertler, N.A.N., Carter, L., Litchfield, N.J., McGlone, M.S., Shulmeister, J., Vandergoes, M.J., Williams, P.W., NZ-INTIMATE members. 2007. Towards a climate event stratigraphy for New Zealand over the past 30,000 years. *Journal of Quaternary Science*, 22: 9-35.

Berryman, K. 1993. Age, height, and deformation of Holocene marine terraces at Mahia Peninsula, Hikurangi Subduction Margin, New Zealand. *Tectonics*, 12: 1347-1364.

Berryman, K.B, Marden, M., Eden, D., Mazengarb, C., Ota, Y., Moriya, I. 2000. Tectonic and paleoclimatic significance of Quaternary river terraces of the Waipaoa River, east coast, North Island, New Zealand. *New Zealand Journal of Geology and Geophysics*, 43: 229-245.

Berryman, K.B., Ota, Y., Hull, A.G. 1989. Holocene paleoseismicity in the fold and thrust belt of the Hikurangi subduction zone, eastern North Island, New Zealand. *Tectonophysics*, 163: 185-195.

Bever, A. 2010. Integrating Space-and-Time-Scales of Sediment Transport for Poverty Bay, New Zealand. Ph.D. Dissertation, College of William and Mary. 262 pp.

Bever, A., McNinch, J., Harris, C. 2011. Hydrodynamics and sediment-transport in the nearshore of Poverty Bay, New Zealand: Observations of nearshore sediment segregation and oceanic storms. *Continental Shelf Research*, 31: 507-526.

Blair, N.E., Leithold, E.L., Aller, R.C. 2004. From bedrock to burial: the evolution of particulate organic carbon across coupled watershed-continental margin systems. *Marine Chemistry* 92, 141-156.

Bouma, A. 1962. Sedimentology of some flysch deposits: A graphic approach to facies interpretation. Elsevier, Amsterdam. 167 pp.

Brackley, H.L. 2006. Land to ocean transfer of erosion-related carbon, Waipaoa sedimentary system, East Coast, New Zealand. PhD Dissertation, Victoria University of Wellington. 129 pp. plus appendices..

Brown, L.J. 1995. Holocene shoreline depositional processes at Poverty Bay, a tectonically active area, Northeastern North Island, New Zealand. *Quaternary International*, 26: 21-33.

Carter, L. 2001. Currents of change: the ocean flow in a changing world. *NIWA Water and Atmosphere*, 4: 15-17.

Carter, L., Carter, R.M., McCave, I.N., Gamble, J. 1996. Regional sediment recycling in the abyssal Southwest Pacific Ocean. *Geology*, 24: 735-738.

Carter, R.M., McCave, I.N., Richter, C., Carter, L., shipboard party. 1999. Leg 181 Summary: southwest Pacific paleoceanography: Proceedings of the Ocean Drilling Program, Initial Reports Vol. 181. Including original data from ODP Janus Web Database: www-odp.tamu.edu/publications/181_IR/181ir.htm.

Carter, L., Northcote, L., Page, M., Brackley, H., Trustrum, N., Gomez, B., Palmer, A. 2004. Drilling Lake Tutira for evidence of climate change. *NIWA Water and Atmosphere*, 12: 12-13.

Carter, L., Manighetti, B., Elliot, M., Trustrum, N., Gomez, B. 2002. Source, sea level and circulation effects on the sediment flux to the deep ocean over the past 15 ka off eastern New Zealand. *Global and Planetary Change*, 33: 339-355.

Chiswell, S.M. 2000. The Wairarapa Coastal Current. *New Zealand Journal of Marine and Freshwater Research*, 40: 303-315.

Chiswell, S.M. 2005. Mean and Variability in the Wairarapa and Hikurangi Eddies, New Zealand. *New Zealand Journal of Marine and Freshwater Research*, 39: 121-134.

Cochran, U., Berryman, K., Zachariasen, J., Mildenhall, D., Hayward, B., Southall, K., Hollis, C., Barker, P., Wallace, L., Alloway, B. 2006. Paleoecological insights into subduction zone earthquake occurrence, eastern North Island, New Zealand. *Geological Society of America Bulletin*, 118: 1051-1074.

Crockett , J.S. and C.A. Nittrouer. 2004. The sandy inner shelf as a repository for muddy sediment: an example from Northern California. *Continental Shelf Research*, 24: 55-73.

Crozier, M.J. and N.J. Preston. 1999. Modelling changes in terrain resistance as a component of landform evolution in unstable hillcountry. *In* Hergarten, S., Neugebauer, H.J., Eds., Process Modeling and Landform Evolution, Lecture Notes in Earth Sciences, 78. Springer Verlag, Berlin, 267-284.

Eden, D.N. and Page, M.J. 1998. Palaeoclimatic implications of a storm erosion record from late Holocene lake sediments, North Island, New Zealand, *Palaeogeography, Palaeoclimatology and Palaeoecology*, 139: 37-58.

Fleming, K., Johnston, P., Zwartz, D., Yokoyama, Y., Lambeck, K., Chappel, J. 1998. Refining the eustatic sea-level curve since the Last Glacial Maximum using far- and intermediate-field sites. *Earth and Planetary Science Letters*, 163: 327-342.

Folk, R.L. 1980. Petrology of Sedimentary Rocks. Hemphill Publishing, Austin, TX, 184pp.

Foster, G. and L. Carter. 1997. Mud sedimentation on the continental shelf at an accretionary margin – Poverty Bay, New Zealand. *New Zealand Journal of Geology and Geophysics*, 40: 157-173.

Fry, B. and E.B. Sherr. 1984. ^{13}C Measurements as indicators of carbon flow in marine and freshwater ecosystems. *Contributions In Marine Science*, 27: 13-47.

Gerber, T., Pratson., L., Kuehl, S., Walsh, J.P., Alexander, C., Palmer, A. 2010. The influence of post-glacial sea level rise and tectonics on sediment storage along the high-sediment supply Waipaoa continental shelf. *Marine Geology*, 270: 139-159.

Geyer, W.R., Hill, P., Kineke, G.C. 2004. The transport, transformation and dispersal of sediment by buoyant coastal flows. *Continental Shelf Research*, 24: 927-949.

Geyer, W.R., Traykovski, P., Hill, P., Milligan, T. 2000. The structure of the Eel river plume during floods. *Continental Shelf Research*, 28: 865-886.
Goldfinger, C., Grijalva, K., Burgmann, R., Morey, A.E., Johnson, J.E., Nelson, C.H., Gutierrez-Pastor, J., Ericsson, A., Karabanov, E., Chaytor, J.D., Patton, J., Gracia, E. 2008. Late Holocene rupture of the Northern San Andreas Fault and possible stress linkage to the Cascadia subduction zone. *Bulletin of the Seismological Society of America*, 98: 861-889.
Goldfinger, C., Nelson, C.H., Johnson, J.E. 2003. Holocene earthquake records from the Cascadia subduction zone and Northern San Andreas Fault based on precise dating of offshore turbidites. *Annual Review of Earth and Planetary Sciences*, 31: 555-577.
Gomez, B., Carter, L., Trustrum, N.A. 2007. A 2400 yr record of natural events and anthropogenic impacts in intercorrelated terrestrial and marine sediment cores: Waipaoa sedimentary system, New Zealand. *Geological Society of America Bulletin*, 119: 1415-1432.
Gomez, B., Carter, L., Trustrum, N.A., Palmer, A.S., Roberts, A.P. 2004. El Nino – Southern Oscillation signal associated with middle Holocene climate change in intercorrelated terrestrial and marine sediment cores, North Island, New Zealand. *Geology*, 32: 653-656.
Griffiths, G.A. 1982. Spatial and temporal variability in suspended sediment yields of North Island basins, New Zealand. *Water Resources Bulletin*, 8: 575-583.
Guinasso, N.L and D.R. Schink. 1975. Quantitative estimates of biological mixing rates in abyssal sediments. *Journal of Geophysical Research*, 80: 3032-3043.
Haq, B.U., Hardenbol, J., Vail, P.R. 1988. Mesozoic and Cenozoic chronostratigraphy and cycles of sea-level change. *Sea-Level Changes – An Integrated Approach*, SEPM Special Publication, 42: 71-108.
de Haas, H., van Weering, T.C.E., de Stigter, H. 2002. Organic carbon in shelf seas: sinks or sources, processes and products. *Continental Shelf Research*, 22: 691-717.
Hayward, B.W., Grenfell, H.R., Sabaa, A.T., Carter, R., Chochran, U., Lipps, J.H., Shane, P.R., Morley, M.S. 2006. Micropaleontological evidence of large earthquakes in the past 7200 years in southern Hawke's Bay, New Zealand. *Quaternary Science Reviews*, 25: 1186-1207.
Hedges, J.I. and R.G. Keil. 1995. Sedimentary organic matter preservation: an assessment and speculative synthesis. *Marine Chemistry*, 49: 81-115.
Hedges, J.I., Keil, R.G., Benner, R. 1997. What happens to terrestrial organic matter in the ocean? *Organic Geochemistry*, 27: 195-212.
Hellstrom, J., McCulloch, M., Stone, J. 1998. A detailed 31,000-year record of climate and vegetation change from the isotope geochemistry of two New Zealand speleothems. *Quaternary Research*, 50: 167-178.
Hicks, D.M., Gomez, B., Trustrum, N.A. 2000. Erosion thresholds and suspended sediment yields, Waipaoa River Basin, New Zealand. *Water Resources Research*, 36: 1129-1142.
Hicks, D.M., Gomez, B., Trustrum, N.A. 2004. Event suspended sediment characteristics and the generation of hyperpycnal plumes at river mouths: East

Coast Continental Margin, North Island, New Zealand. *Journal of Geology*, 112: 471-485.
Kettner, A.J., Gomez, B. and Syvitski, J.P.M. 2007. Modeling suspended sediment discharge from the Waipaoa river system, New Zealand: The last 3000 years. Water Resources Research, v.43, W07411, doi: 10.1029/2006WR005570.
Kuehl, S.A., Pacioni, T.D., Rine, J.M. 1995. Seabed dynamics of the inner Amazon continental shelf: temporal and spatial variability of surficial strata. *Marine Geology*, 125: 283-302.
Leithold, E.L. and R.S. Hope. 1999. Deposition and modification of a flood layer on the northern California shelf: lessons from and about the fate of terrestrial particulate organic carbon. *Marine Geology*, 154: 183-195.
Lewis, K.B. 1973. Erosion and deposition on a tilting continental shelf during Quaternary oscillations of sea level. *New Zealand Journal of Geology and Geophysics*, 16: 281-301.
Lewis, K.B. 1980. Quaternary sedimentation on the Hikurangi oblique-subduction and transform margin: *In* Sedimentation in a Oblique-Slip Mobile Zones Vol. 4., P.F. Balance and H.G. Reading Eds., International Association of Sedimentologists, Special Publication. pp. 171-189.
Lewis, K.B. and J.R.Pettinga. 1993. The emerging, imbricate frontal wedge of the Hikurangi margin: *In*, South Pacific Sedimentary Basins. Sedimentary Basins of the World vol. 2, P.F. Balance Ed., Elsevier Science Publishers, Amsterdam. pp. 225-250.
Litchfield, N., Wilson, K., Berryman, K., Wallace, L. 2010. Coastal uplift mechanisms at Pakarae River mouth: Constraints from a combined Holocene fluvial and marine terrace dataset. *Marine Geology*, 270: 72-83.
Lowe, D.J., Shane, P.A.R., Alloway, B.V., Newnham, R.M. 2008. Fingerprints and age models for widespread New Zealand tephra marker beds erupted since 30,000 years ago: a framework for NZ-INTIMATE. *Quaternary Science Reviews*, 27: 95-126.
Lui, J.P., Milliman, J.D., Gao, S., Cheng, P. 2004. Development of the Yellow River's subaqueous delta, North Yellow Sea. *Marine Geology*, 209: 45-67.
Lyons, W.B., Nezt, C.A., Carey, A.E., Hicks, D.M. 2002. Organic carbon fluxes to the ocean from high-standing islands. *Geology*, 30: 443-446.
Margins Science Plans. 2003. Source-to-Sink NSF MARGINS Program Science Plans. 2004. Lamont-Doherty Earth Observatory of Columbia University, New York.
McGlone, M.S. and J.M. Wilmshurst. 1999. A Holocene record of climate, vegetation change and peat bog development, east Otago, South Island, New Zealand. *Journal of Quaternary Science*, 14: 239-254.
Miller, A.J. and S.A. Kuehl. 2010. Shelf sedimentation on a tectonically active margin: A modern sediment budget for Poverty continental shelf, New Zealand. *Marine Geology*, 270: 175-187.
Milliman, J. and J.P.M. Syvitski. 1992. Geomorphic/tectonic control of sediment discharge to the ocean: the importance of small mountainous rivers. *Journal of Geology*, 100: 525-544.

Mulder, T. and J.P.M. Syvitski. 1995. Turbidity currents generated at river mouths during exceptional discharges to the world oceans. *Journal of Geology,* 103: 285-299.

Mulder, T., Syvitski, J.P.M., Migeon, S., Faugeres, J.C., Savoye, B. 2003. Marine hyperpycnal flows: initiation, behavior and related deposits. A review. *Marine and Petroleum Geology*, 20: 861-882.

Meyers, P.A. 1997. Organic geochemical proxies of paleoceanographic, paleolimnologic, and paleoclimatic processes. *Organic Geochemistry*, 27: 213-250.

Nittrouer, C.A., Austin, J.A., Field, M.E., Kravitz, J.H., Syvitski, J.P.M., Wiberg, P.L. 2007. Writing a Rosetta stone: insights into continental-margin sedimentary processes and strata. In: C. Nittrouer, J. Austin, M. Field, J. Kravitz, J. Syvitski and P. Wiberg (Eds.), *Continental Margin Sedimentation*, Wiley-Blackwell, Hoboken, N.J., pp 1-48.

Nittrouer, C.A. and R.W. Sternberg. 1981. The formation of sedimentary strata in an allochthonous shelf environment: The Washington continental shelf. *Marine Geology*, 42: 201-232.

Orpin, A.R. 2004. Holocene sediment deposition on the Poverty-slope margin by the muddy Waipaoa River, East Coast New Zealand. *Marine Geology*, 209: 69-90.

Orpin, A.R., Alexander, C., Carter, L., Kuehl, S., Walsh, J.P. 2006. Temporal and spatial complexity in post-glacial sedimentation on the tectonically active, Poverty Bay continental margin of New Zealand. *Continental Shelf Research*, 26: 2205-2224.

Ota, Y., Berryman, K.B, Hull, A.G., Miyauchi, T., Iso, N. 1988. Age and height distribution of Holocene transgressive deposits in eastern North Island, New Zealand. *Palaeogeography, Palaeoclimatology, Palaeoecology*, 68: 135-151.

Page, M.J., Trustrum, N.A., Brackley, H.L., Gomez, B., Kasai, M., Marutani, T. 2001. Waipaoa River (North Island, New Zealand). *In* Marutani T., Brierley, G.J., Trustrum, N.A., Page, M.J., (Eds.), *Source-to-Sink Sedimentary Cascades in Pacific Rim Geo-Systems*, Matsumoto Sabo Work Office, Ministry of Land, Infrastructure and Transport, Japan, pp. 86-101.

Page, M.J., Trustrum, N.A., DeRose, R.C. 1994a. A high resolution record of storm induced erosion from lake sediments, New Zealand. *Journal of Paleolimnology*, 11: 333-348.

Page, M.J., Trustrum, N.A., Dymond, J.R. 1994b. Sediment budget to assess the geomorphic effect of a cyclonic storm, New Zealand. *Geomorphol*ogy, 9: 169-188.

Page, M.J., Trustrum, N.A., Gomez, B. 2000. Implications of a century of anthropogenic erosion for future land use in the Gisborne-East Coast region of New Zealand. *New Zealand Journal of Geography,* 56, 13-24.

Parsons, J.D., Bush, J.W.M., Syvitski, J.P.M. 2001. Hyperpycnal plume formation from riverine inflows with small sediment concentrations. *Sedimentology*, 48: 465-478.

Phillips, J.D. and B. Gomez. 2007. Controls on sediment export from the Waipaoa River basin, New Zealand. *Basin Research*, 19: 241-252.

Pouderoux, H., Prouste, J-N., Lamarche, G., Orpin, A., Neil, H. 2012. Postglacial (after 18 ka) deep-sea sedimentation along the Hikurangi subduction margin (New Zealand): Characterization, timing and origin of turbidites. *Marine Geology*, 295-298: 51-76.
Prothero, D.R. and F. Schwab, eds. Sedimentary Geology. New York: W. H. Freeman and Company, 1996. 600 pp.
Proust, J.N., Lamarche, G., Migeon, S., Neil, H., shipboard scientific party. 2006. Les Rapport de campagnes a la mer, MD152/MATACORE, Institute Polaire Francais, Plouzane, France, 107 pp.
Reid, L.M. and M.J. Page. 2003. Magnitude and frequency of landsliding in a large New Zealand catchment. *Geomorphology*, 49: 71-88.
Reimer, P.J., Baillie, M.G.L., Bard, E., Bayliss, A., Beck, J.W., Blackwell, P.G., Ramsey, C.B., Buck, C.E., Burr, G.S., Edwards, R.L., Friedrich, M., Grootes, P.M., Guilderson, T.P., Hajdas, I., Heaton, T.J., Hogg, A.G., Hughen, K.A., Kaiser, K.F., Kromer, B., McCormac, F.G., Manning, S.W., Reimer, R.W., Richards, D.A., Southon, J.R., Talamo, S., Turney, C.S.M., van der Plicht, J., Weyhenmeye, C.E. 2009. INTCAL09 and MARINE09 radiocarbon age calibration curves, 0–50,000 years cal. BP. *Radiocarbon*, 51: 1111-1150.
Reyners, M. and P. McGinty. 1999. Shallow subduction tectonics in the Raukumara Peninsula, New Zealand, as illuminated by earthquake focal mechanisms. *Journal of Geophysical Research,* 104: 3025-3034.
Rose, L.E. and S.A. Kuehl. 2010. Recent sedimentation patterns and facies distribution on the Poverty Shelf, New Zealand. *Marine Geology*, 270: 160-174.
Rose, L.E. and S.A. Kuehl. In Prep. Modern Event Layers on the Waipaoa Continental Shelf: Characteristics, Preservation and Possible Modes of Initiation. 51pp.
Rose, L.E., Kuehl, S.A., Orpin, A., Alexander, C., Palmer, A. In Prep. Complete, high-resolution shelf record of changes in sediment supply, eustacy, tectonics and climate from the LGM-present, Poverty Shelf, N.Z. 31pp.
Sadler, P.M. 1981. Sediment accumulation rates and the completeness of stratigraphic sections. *Journal of Geology*, 89: 569-584.
Shanmugam, G. 2000. 50 years of the turbidite paradigm (1950s-1990s): deep-water processes and facies models – a critical perspective. *Marine and Petroleum Geology*, 17: 285-342.
Sommerfield, C.K. and C.A. Nittrouer. 1999. Modern accumulation rates and a sediment budget for the Eel shelf: a flood-dominated depositional environment. *Marine Geology*, 154: 227-241.
Stephens, S.A. Bell, R.G., Black, K.P. 2001. Complex circulation in a coastal embayment: shelf current, wind and density - driven circulation in Poverty Bay, New Zealand. *Journal of Coastal Research Special Issue*, 34: 45-59.
Stuiver, M., Reimer, P.J., Bard, E., Beck, J.W., Burr, G.S., Hughen, K.A., Kromer. B., McCormac, F.G., v.d. Plicht, J., and Spurk, M. 1998. INTCAL 98 radiocarbon age calibration 24,000–0 cal BP. *Radiocarbon*, 40: 1041-1083.

Suggate, R.P. 1990. Late Pliocene and Quaternary Glaciations of New Zealand. *Quaternary Science Reviews,* 9: 175-197.

Tate, K.R., Scott, N.A., Parshotam, A., Brown, L., Wilde, R.H., Giltrap, D.J., Trustrum, N.A., Gomez, B. and Ross, D.J. 2000. A multi-scale analysis of a terrestrial carbon budget: Is New Zealand a source or sink of carbon? *Agriculture, Ecosystems and Environment,* 82: 229-246.

Vail, P.R., Mitchum, R.M., Thompson, S. 1977. Global cycles of relative changes in sea level. *American Association of Petroleum Geologists Memoirs,* 26: 83-98.

Wadman, H.M. and J.E. McNinch. 2008. Stratigraphic spatial variation on the inner shelf of a high-yield river, Waiapu River, New Zealand: Implications for fine-sediment dispersal and preservation. *Continental Shelf Research,* 28, 865-886.

Wallace, L.M., Reyners, M., Cochran, U., Bannister, S., Barnes, P.M., Berryman, K., Downes, G., Eberhart-Phillips, D., Fagereng, A., Ellis, S., Nicol, A., McCaffrey, R., Beavan, R.J., Henrys, S., Sutherland, R., Barker, D.H.N., Litchfield, N., Townend, J., Robinson, R., Bell, R., Wilson, K., Power, W. 2009. Characterizing the seismogenic zone of a major plate boundary subduction thrust: Hikurangi Margin, New Zealand. *Geochemistry, Geophysics, Geosystems,* 10: 32pp.

Walling, D.E. and B.W. Webb. 1996. Erosion and sediment yield: a global overview. *International Association of Hydrological Sciences Publications,* 236: 3-19.

Wheatcroft, R.A. and J.C. Borgeld. 2000. Oceanic flood deposits on the northern California shelf: large-scale distribution and small-scale physical properties. *Continental Shelf Research,* 20: 2163-2190.

Wheatcroft, R.A. and D.E. Drake. 2003. Post-depositional alteration and preservation of Sedimentary event layers on continental margins, I. The role of episodic sedimentation. *Marine Geology,* 199: 123-137.

Wheatcroft, R.A., Wiberg, P. L., Alexander, C.R., Bentley, S.J., Drake, D.E., Harris, C.K., Ogston A.S. 2007. Post-depositional alteration and preservation of sedimentary strata. *In* C. Nittrouer, J. Austin, M. Field, J. Kravitz, J. Syvitski and P. Wiberg (Eds.), *Continental Margin Sedimentation,* Wiley-Blackwell, Hoboken, N.J., pp 101-155.

Wilmshurst, J.M. 1997. The impact of human settlement on vegetation and soil stability in Hawke's Bay New Zealand. *New Zealand Journal of Botany,* 35: 97-111.

Wilmshurst, J.M., McGlone, M.S., Partridge, T.R. 1997. A late Holocene history of natural disturbance in lowland podocarp/hardwood forest, Hawke's Bay, New Zealand. *New Zealand Journal of Botany,* 35: 79-96.

Wolinsky, M.A., Swenson, J.B., Litchfield, N., and McNinch, J.E. 2010. Coastal progradation and sediment partitioning in the Holocene Waipaoa Sedimentary System, New Zealand. *Marine Geology,* 270: 94-107.

Table 1.

Compilation of events (earthquakes, tephras, hyperpycnites, etc) that impacted the Waipaoa catchment and Poverty Margin since the LGM. Tephras in bold have been positively identified by glass shard analysis in one or more cores in this study. Literature sources cited include: 1. Cochran et al., 2006. 2. Berryman et al. (1993a). 3. Hayward et al. (2006). 4. Orpin et al. (2010). 5. Brown et al. (1995). 6. Berryman et al. (1989). 7. Pondereaux et al. (2011).

Event	Year/Time Period (ka)	Reference
>M_W = 7.3 Earthquake	7.0	3
	5.8	3
	5.5	5
	5.1	1
	4.5	2
	4.2	3
	3.9	5
	3.5	2
	3.2	1
	3.0	3
	2.3	1, 6
	2.1	3,
	1.9	2
	1.6	2, 3, 5
	1.0	1, 5, 6
	0.6	3, 5, 6
	0.3	6
	0.250	2
	1855 AD	1
Dated Tephras		
Kaharoa	0.636	
Taupo	1.717	
Mapara	2.075	
Waimihia	3.410	
Whakatane	5.530	
Tuhua	7.005	
Increased Storminess from Lake Tutira Record	0.6-1	4
"	1.5-1.8	4
"	2.1-2.5	4
"	4.3-5.0	4
"	5.6-5.7	4
Earthquake Hiatus	0.6-1.6	4
"	1.9-3.0	4
"	4.5-5.4	4
Hyperpycnite Turbidites	2930 ± 190	
	7657 ± 137	
	11544 ± 184	
	12863 ±288	
	14011 ± 347	

Table 2.

Marion DuFresne (MD) core locations and information.

Core	Location	Latitude	Longitude	Length (m)	Water Depth (mbsl)	Oldest ^{14}C Age
MD3001	N. Depocenter	38 44.31 S	178 13.08 E	22.57	59	9577 ±85
MD3007	N. Depocenter	38 43.58 S	178 13.99 E	23.47	61	10179 ±71
MD3004	S. Depocenter	38 51.49 S	178 04.90 E	16.36	52	10035 ±107
MD3006	Shelf Break Depocenter	38 57.60 S	178 10.92 E	25.34	122	14354.5 ±216

Table 3.

Marion DuFresne age model accumulation rates showing rates and associated 95% confidence interval within designated time periods.

Core	**Age Range (ka)**	**Accumulation Rate (cm yr^{-1})**
MD3001	0-4	0.09 ± 0.00
	4-10	0.33 ± 0.04
MD3007	0-4	0.07 ± 0.31
	4-10	0.28 ± 0.02
MD3004	0-5.5	0.12 ± 0.01
	5.5-7	0.41 ± 0.67
	7-10	0.16 ± 0.32
MD3006	0-7	0.28 ± 0.03
	7-14	0.06 ± 0.02

Table 4.

Summary of lithotypes identified, which are used as a template for determining depositional environment. Information on bed types, frequency of occurrence, textures, and thicknesses accompany average magnetic susceptibility. $\delta^{13}C$ and % carbon for each lithotype. A. MD3001, Northern Depocenter. B. MD3004, Southern Depocenter. C. MD3006, Shelf Break Depocenter.

Table 4A - MD3001 – Northern Depocenter

Lithotype	Quick Reference Name	# of Beds	Total Thickness of Units (cm)	Total Thickness of Units (yr)	Thickness Avg., Range (cm)	Thickness Avg. (yr)	Mag. Sus. Avg. (SI)	Mag Sus. Range (SI)	% Sand	% Silt	% Clay	$\delta^{13}C$ Avg.	% Carbon
1A	Ashfall Tephra	4	23.92	134.78	5.98, 4.84-7.11	33.69	29.8	12-77	4.64	48.95	46.41	-25.12	0.42
1B	Mixed Mud & Tephra	8	43.76	283.11	5.47, 1.44-13.33	35.39	34.5	11-75	20.58	47.52	31.88	-24.95	0.39
2A	Bioturbated Olive Mud	39	1197.71	4110.84	31.52, 1.92-167.83	108.18	19.9	8-56	6.71	52.54	40.76	-25.06	0.50
2B	Bioturbated Olive Sandy Mud	22	624.65	3545.36	28.39, 2.76-97.56	161.15	24.9	7-70	11.15	52.65	36.20	-25.37	0.47
2C	Bioturbated Olive Muddy Sand	-											
3A	Low Density, Single Layer	13	16.24	72.4	1.62, 0.7-3.85	7.24	20.4	13-46	10.19	47.64	42.13	-25.20	0.47
3B	Wood-rich, Single Layer	1	3.7	9	3.7	9	7.5	No data	No data	No data	No data	No data	No data
4	Normally Graded Layer	27	192.18	703.76	7.12, 2.12-30.57	26.07	18.1	9-38	5.75	55.19	39.07	-25.13	0.42
5	X-ray Opaque Layer	17	66.18	271.68	5.09, 0.71-19.18	20.9	19.3	6-55	4.08	57.90	38.03	-24.91	0.37
6	Remnant Layer	1	7.67	38.68	-	-	No data	No data	No data	No data	No data	No data	No data

	# of Beds	Total Thickness of Units (cm)	Total Thickness of Units (yr)
Totals		2214.93	9390.51
Event Totals (excluding 1A-B, 2A-C)	59	324.89	1316.43
Total Tephra	12	67.69	417.88
Totals (Type 2)	61	1822.36	7656.20
Events - % of Whole, (Total excluding 1A-B, 2A-C)		[illegible]	[illegible]
% of Whole, Total Tephra		[illegible]	[illegible]

Table 4B - MD3004 – Southern Depocenter

Lithotype	Quick Reference Name	# of Beds	Total Thickness of Units (cm)	Total Thickness of Units (yr)	Thickness Avg., Range (cm)	Thickness Avg. (yr)	Mag. Sus. Avg. (SI)	Mag Sus. Range (SI)	% Sand	% Silt	% Clay	$\delta^{13}C$ Avg.	% Carbon
1A	Ashfall Tephra	1	9.63	4	9.63	4	147.0	No data	43.80	56.20	0.00	-25.33	0.08
1B	Mixed Mud & Tephra	4	11.07	35.58	3.69, 5.00-18.00	11.86	79.2	38-131.7	24.12	52.30	23.59	-29.51	0.12
2A	Bioturbated Olive Mud	32	1053.43	6890.36	32.92, 2.75-129.55	215.32	30.0	79.1-16	12.60	51.47	35.93	-25.23	0.41
2B	Bioturbated Olive Sandy Mud	11	265.54	2030.08	24.14, 3.95-75.54	184.55	46.7	20.1-71.4	31.78	42.49	25.71	-25.26	0.31
2C	Bioturbated Olive Muddy Sand	4	107.64	731.19	26.91, 15.28-40.28	40.28	67.9	65.5-72.2	55.66	25.04	19.27	No data	No data
3A	Low Density, Single Layer	12	27.91	236.85	2.33, 0.69-4.21	19.74	40.0	18-73	6.03	65.70	28.26	-25.36	0.49
3B	Wood-rich, Single Layer	-											
4	Normally Graded Layer	22	135.54	952.76	5.89, 1.40-10.96	41.69	29.5	17-92.5	6.99	53.51	39.51	-25.16	0.47
5	Single, X-ray Opaque Layer	6	28.32	103.13	4.27, 0.69-17.97	17.19	33.3	15.5-68	21.55	77.21	1.24	-25.30	0.16
6	Remnant Layer(s)	3	10.91	72.96	3.64, 2.09-4.77	24.32	21.6	15-34.3	No data	No data	No data	No data	No data

	# of Beds	Total Thickness of Units (cm)	Total Thickness of Units (yr)
Totals		1649.99	10984.35
Event Totals (excluding 1A-B, 2A-C)	43	202.68	1366.1
Total Tephra	5	20.7	39.58
Totals (Type 2)	46	1426.61	9651.63
Events - % of Whole, (Total excluding 1A-B, 2A-C)		[illegible]	[illegible]
% of Whole, Total Tephra		[illegible]	[illegible]
% of Whole, Totals (Type 2)		[illegible]	67.72

Table 4C - MD3006 – Shelf Break Depocenter

Lithotype	Quick Reference Name	# of Beds	Total Thickness of Units (cm)	Total Thickness of Units (yr)	Thickness Avg., Range (cm)	Thickness Avg. (yr)	Mag. Sus. Avg. (SI)	Mag Sus. Range (SI)	% Sand	% Silt	% Clay	$\delta^{13}C$ Avg.	% Carbon
1A	Ashfall Tephra	1	10.16	30.63	No data	No data	30	No data	18.82	46.92	34.25	No data	
1B	Mixed Mud & Tephra	1	2.77	11.52	No data	No data	9	No data	No data	No data	No data	No data	
2A	Bioturbated Olive Mud	15	2113	10396.50	140.87, 3.95-476.65	693.10, 16.44-1543.07	11	8-17	7.45	50.19	42.34	-23.58	
2B	Bioturbated Olive Sandy Mud	-											
2C	Bioturbated Olive Muddy Sand	5	168.73	3348.35	33.75, 1.57-57.56	669.67, 9.72-1376.29	46	26-55	50.51	33.54	15.94	-24.36	
3A	Low Density, Single Layer	-											
3B	Wood-rich, Single Layer	-											
4	Normally Graded Layer	-											
5	Single, X-ray Opaque Layer	3	15.49	406	5.16, 0.66-13.08	135.56, 1.64-357.39	38	10-54	No data	No data	No data	No data	
6	Remnant Layers	14	70.85	539.82	5.06, 0.33-11.84	38.56, 2.03-104.16	22	7-54	22.67	45.5	31.82	No data	

	# of Beds	Total Thickness of Units (cm)	Total Thickness of Units (yr)
Totals		**2381.00**	**14733.51**
Event Totals (excluding 1A-B, 2A-C)	17	**86.34**	**946.50**
Total Tephra	2	**12.93**	**42.15**
Totals (Type 2)	20	**2281.73**	**13744.86**
Events - % of Whole, (Total excluding 1A-B, 2A-C)		[illegible]	[illegible]
% of Whole, Total Tephra		[illegible]	0.20
% of Whole, Totals (Type 2)		[illegible]	93.29

Chapter 3 Figure Legend

Figure 1.
A. North Island, New Zealand with study area indicated by red box. TVZ = Taupo Volcanic Zone. RP = Raukumara Peninsula. EC = East Cape. ECC and arrows = East Cape Current and direction. LT and star = location of Lake Tutira. STC and arrows = Subtropical Convergence and flow direction. Gray shaded region denotes location of warm surface currents associated with the Subtropical Gyre (after Carter, 2001). **B.** Poverty Margin location map with Marion Dufresne (MD) cores indicated and underlying tectonics and tectonic subregions after Brown, 1995. Holocene sediment thickness is shown in overlay (after Gerber et al., 2010). W = Waipaoa River Mouth **C.** Interpretation of Poverty Bay shoreline position through time modified from Brown (1995) and Gerber et al. (2010). **D.** Post glacial sea level rise in the Western Pacific modified from Lui et al., 2004. Inset (red box) is Holocene sea level rise, modified from Cochran et al. (2006) and Gerber et al. (2010). Grey lines in inset highlight tephra occurrence. Mwp = meltwater pulse.

Figure 2.
A. Age models for MD3001, MD3007, MD3004 and MD3006, cores in this study, from Rose et al., In Prep. Colors correspond to core colors in Figure 1B. **B.** Point-to-Point accumulation rates from the same MD cores (Rose et al., In Prep.).

Figure 3.
Example of X-radiograph guiding MD core sampling from MD3001, section VI (777cm-807cm; 5239-5349yr BP). Survey (S) samples are 1cm thickness, every 10cm and Target (T) samples are 0.5cm in thickness. On the third panel, dots represent the location of a sample that was analyzed for $\delta^{13}C$ and textural properties (as seen subsequently in Figures 12 and 13).

Figure 4.
Comparison of $\delta^{13}C$ from splits of MD bulk sediment samples from the same depth interval within cores to ensure no degradation. One set was immediately frozen onboard and then processed post cruise in March, 2006, and the other set was dried after removal in August 2007 and processed in 2011.

Figure 5.
X-radiographic examples of lithotypes. **A.** Lithotype 1 - tephric units with companion photograph and MSCL profile. **B.** Lithotype 2 - non-event deposition. **C.** Lithotype 3 – low density units. **D.** Lithotype 4 – graded beds. **E.** Lithotype 5 – high density units. **F.** Lithotype 6 – remnant layers.

Figure 6.
Lithotype logs. Tephras identified with glass shard chemistry are indicated, along with the region of increased event preservation (4.6-7.4ka). Stars along the age axis indicate occurrences of known East Cape large magnitude earthquakes (Mw = 7.3 or greater) **A.** Northern Depocenter (MD3001) lithotype log. **B.** Southern Depocenter

(MD3004) lithotype log. **C.** Shelf Break Depocenter (MD3006) lithotype log. Only a portion of the record is presented in this figure for comparison with the other depocenters – the complete record is in Figure 7.

Figure 7.
Shelf Break Depocenter (MD3006) lithotype log and textural and geochemical profiles. Arrows color-coordinate to percent silt or sand, show general textural trends and indicate transitions between textural modes, as described in text. Lithotype key is found in Figure 6.

Figure 8.
Northern Depocenter (MD3001 and MD3007) core profiles. **A.** MD3001 texture. **B.** Magnetic susceptibility profiles (SI) from MSCL. **C.** MD3001 percent carbon. Note axis break. **D.** $\delta^{13}C$ profile showing original survey samples from MD3007 (red circles), subsequent Survey sampling of MD3001 (blue circles) and Target sampling (guided by X-radiographs) of MD3001 (black circles) and MD3007 (green circles). Bracketed sections indicate Figures 5A-F.

Figure 9.
Southern Depocenter (MD3004) core profiles. **A.** Texture. **B.** Magnetic susceptibility profiles (SI) from MSCL. C. $\delta^{13}C$ profile showing original survey samples from MD3006 (pink open circles) and Target sampling (guided by X-radiographs) of MD3004 (black circles).

Figure 10.
Plot of bulk $\delta^{13}C$ and N:C of original "skeleton" MD samples taken every 1.5m in 2006.

Figure 11.
Examples of the two most prominent reversals recorded in Marion DuFresne age models, both occurring in the Northern Deopocenter, with the location of nearly co-occurring earthquakes (yellow stars). **A.** MD3001. **B.** MD3007. All samples involved in the reversals are whole shell gastropods except for the grey diamond in MD3001, which is a piece of wood.

Figure 1.

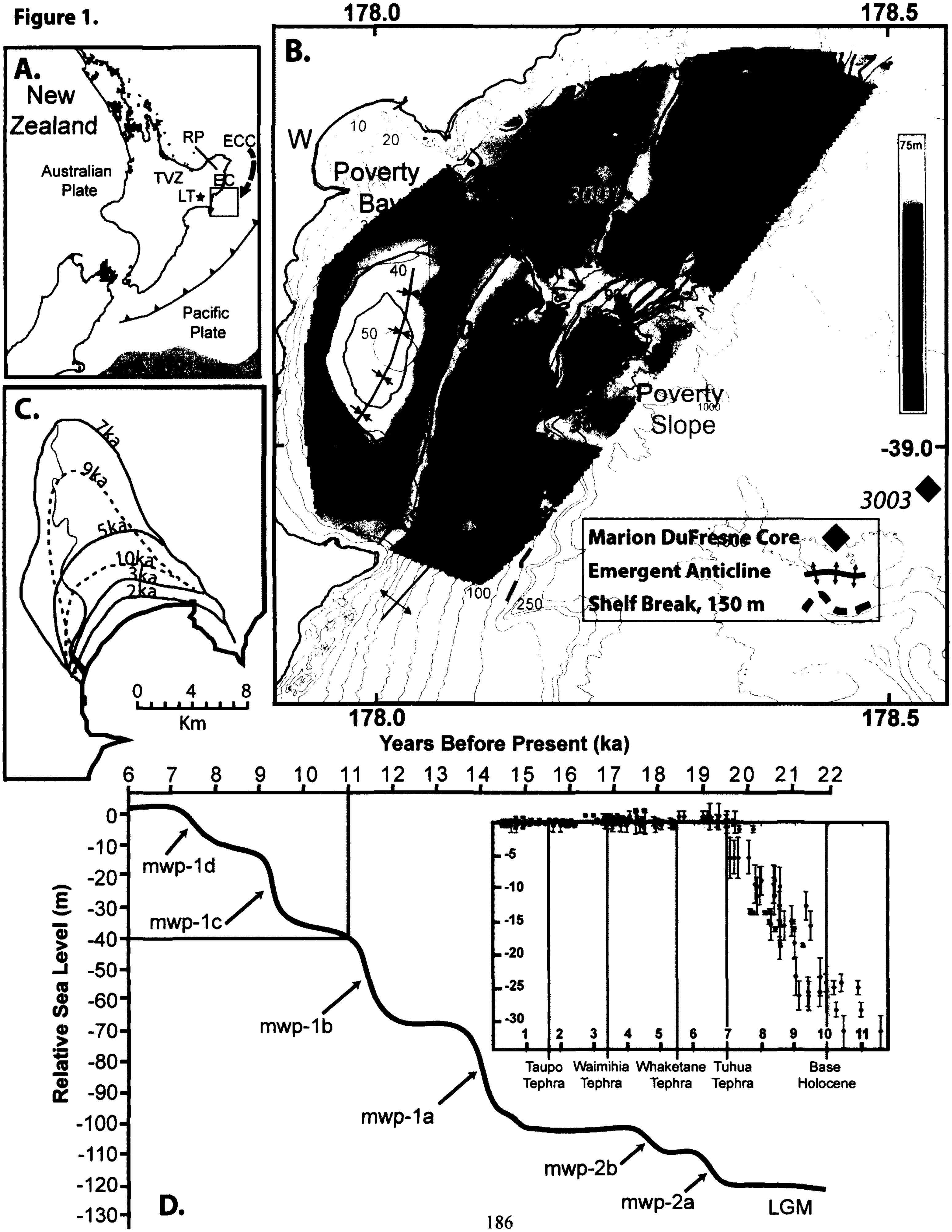
A.
New Zealand
Australian Plate
Pacific Plate
TVZ
RP
ECC
EC
LT
B.
178.0
178.5
W
Poverty Bay
3001
Poverty Slope
-39.0
3003
75m
Marion DuFresne Core
Emergent Anticline
Shelf Break, 150 m
10
20
40
50
100
250
1000
C.
7ka
9ka
5ka
10ka
3ka
2ka
0 4 8
Km
D.
Years Before Present (ka)
Relative Sea Level (m)
mwp-1d
mwp-1c
mwp-1b
mwp-1a
mwp-2b
mwp-2a
LGM
Taupo Tephra
Waimihia Tephra
Whaketane Tephra
Tuhua Tephra
Base Holocene

Figure 2

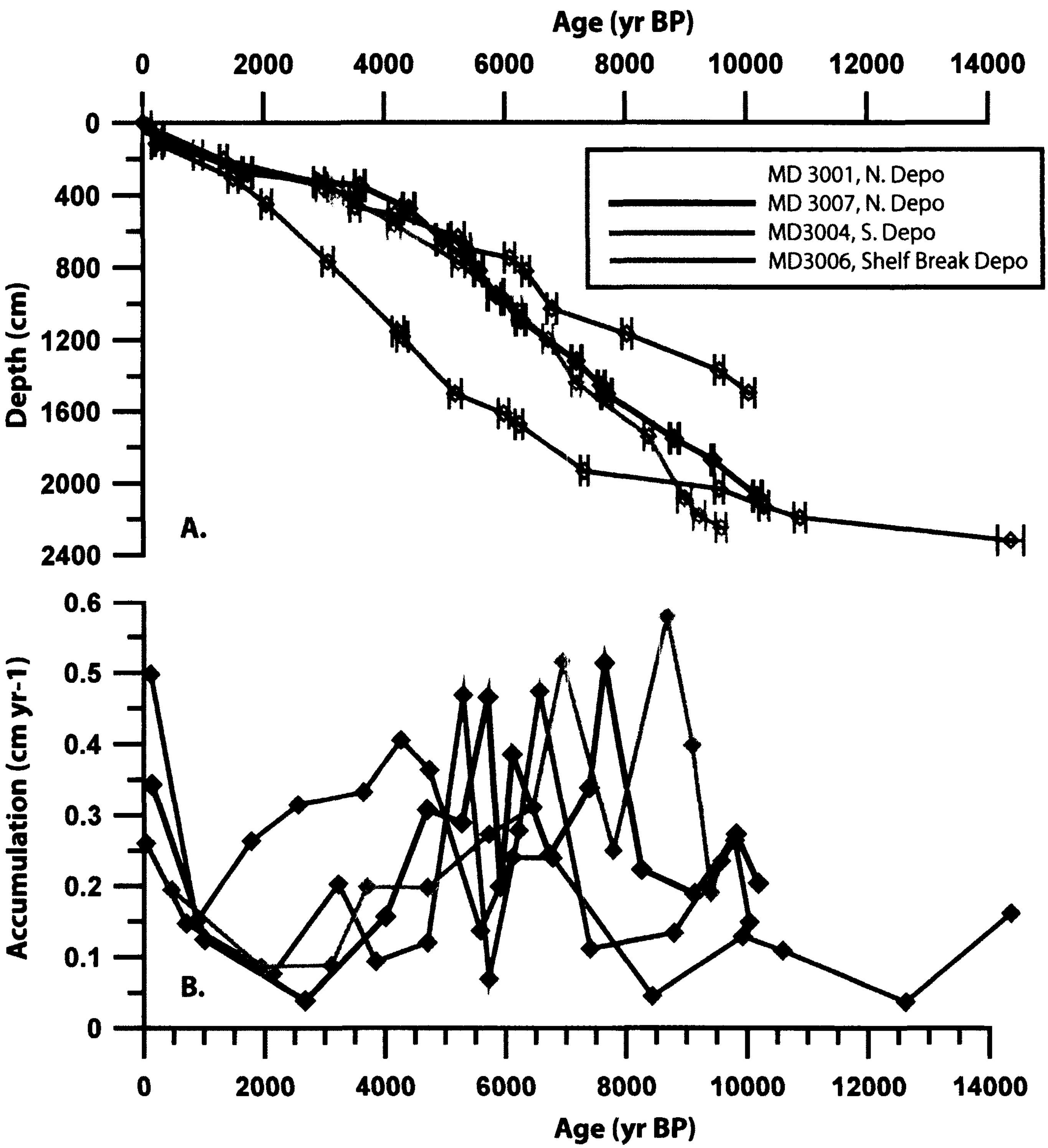
Age (yr BP)
0
2000
4000
6000
8000
10000
12000
14000
0
400
800
1200
1600
2000
2400
Depth (cm)
MD 3001, N. Depo
MD 3007, N. Depo
MD3004, S. Depo
MD3006, Shelf Break Depo
A.
0.6
0.5
0.4
0.3
0.2
0.1
0
Accumulation (cm yr-1)
B.
0
2000
4000
6000
8000
10000
12000
14000
Age (yr BP)

Figure 3

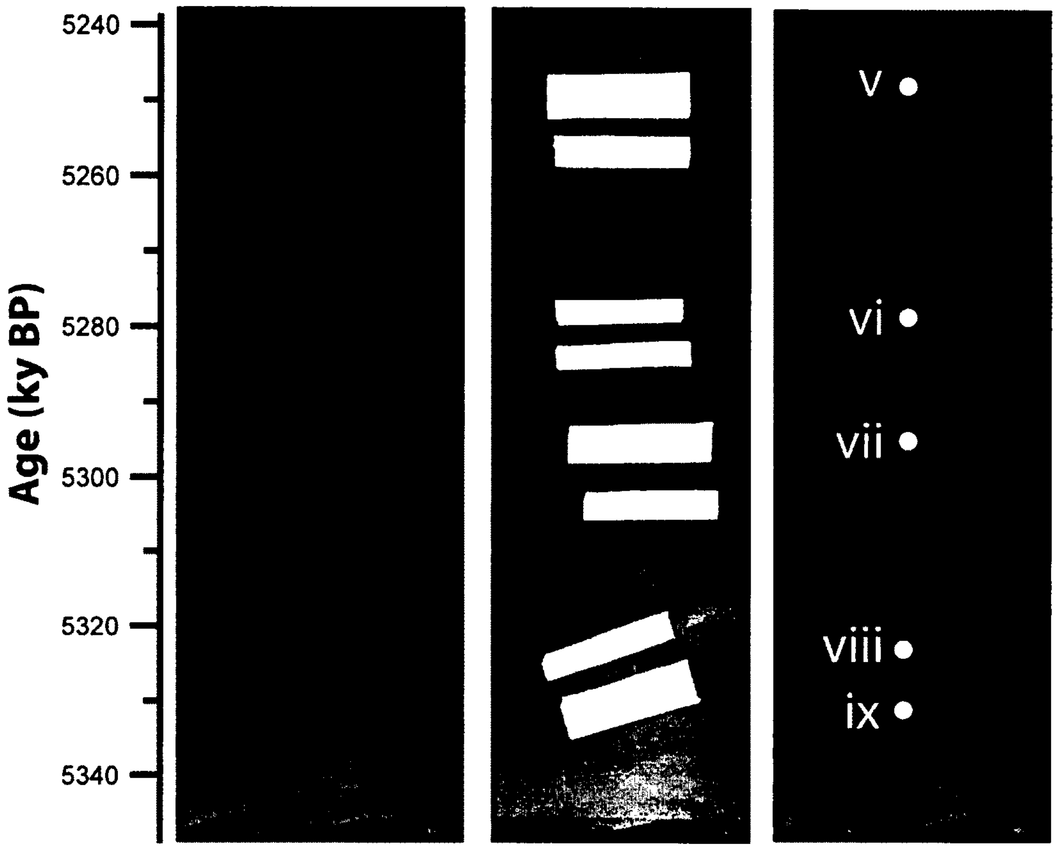

MD3001, VI 777-807cm, 5239-5349 yrBP

Figure 4

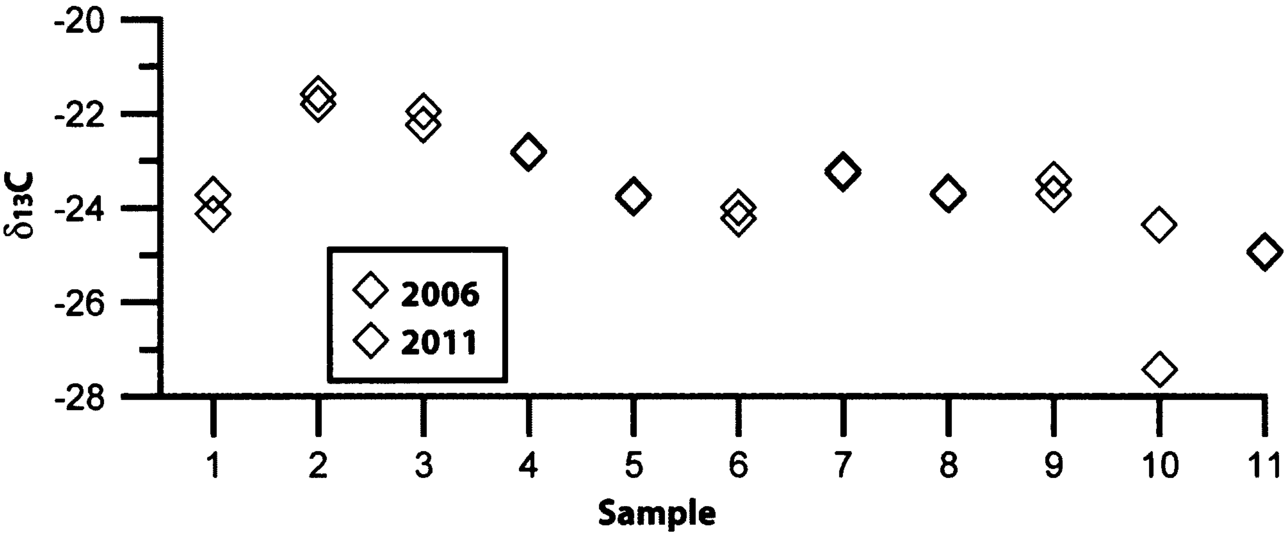

Figure 5

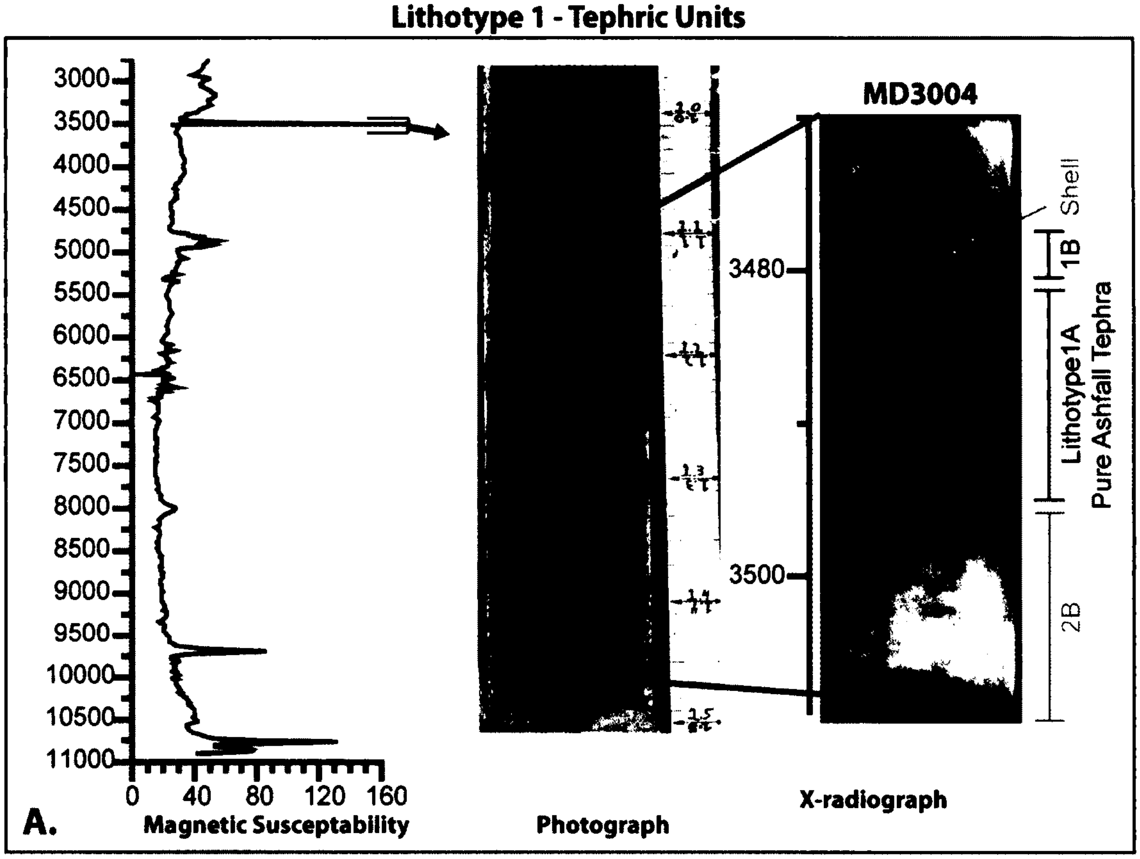

Lithotype 1 - Tephric Units
MD3004
Shell
3480
1B
Lithotype1A
Pure Ashfall Tephra
3500
2B
3000
3500
4000
4500
5000
5500
6000
6500
7000
7500
8000
8500
9000
9500
10000
10500
11000
0
40
80
120
160
A.
Magnetic Susceptability
Photograph
X-radiograph

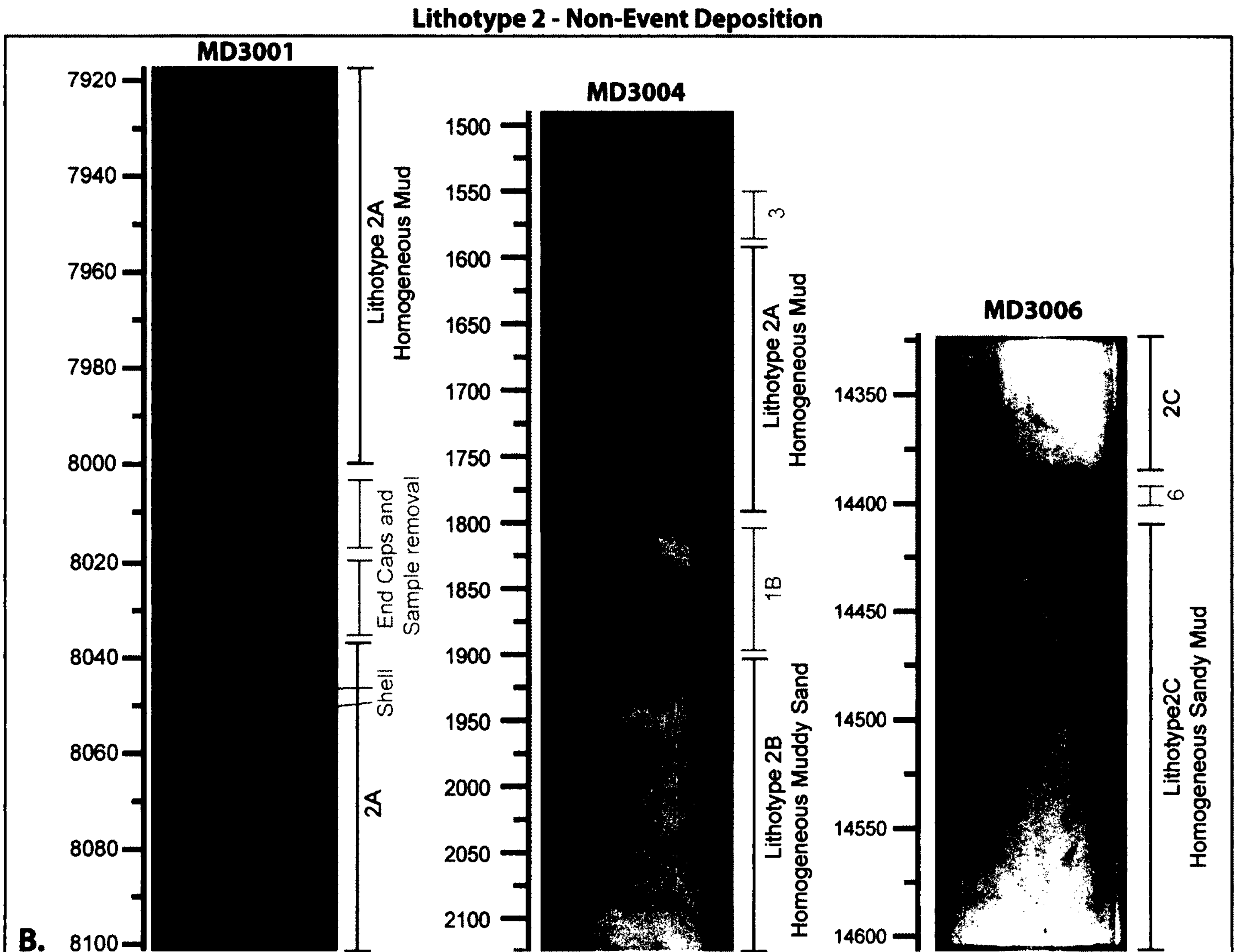

Lithotype 2 - Non-Event Deposition
MD3001
7920
7940
7960
7980
8000
8020
8040
8060
8080
8100
Lithotype 2A
Homogeneous Mud
End Caps and
Sample removal
Shell
2A
MD3004
1500
1550
1600
1650
1700
1750
1800
1850
1900
1950
2000
2050
2100
3
Lithotype 2A
Homogeneous Mud
1B
Lithotype 2B
Homogeneous Muddy Sand
MD3006
14350
14400
14450
14500
14550
14600
2C
6
Lithotype2C
Homogeneous Sandy Mud
B.

Lithotype 3- Low Density Units **Figure 5**

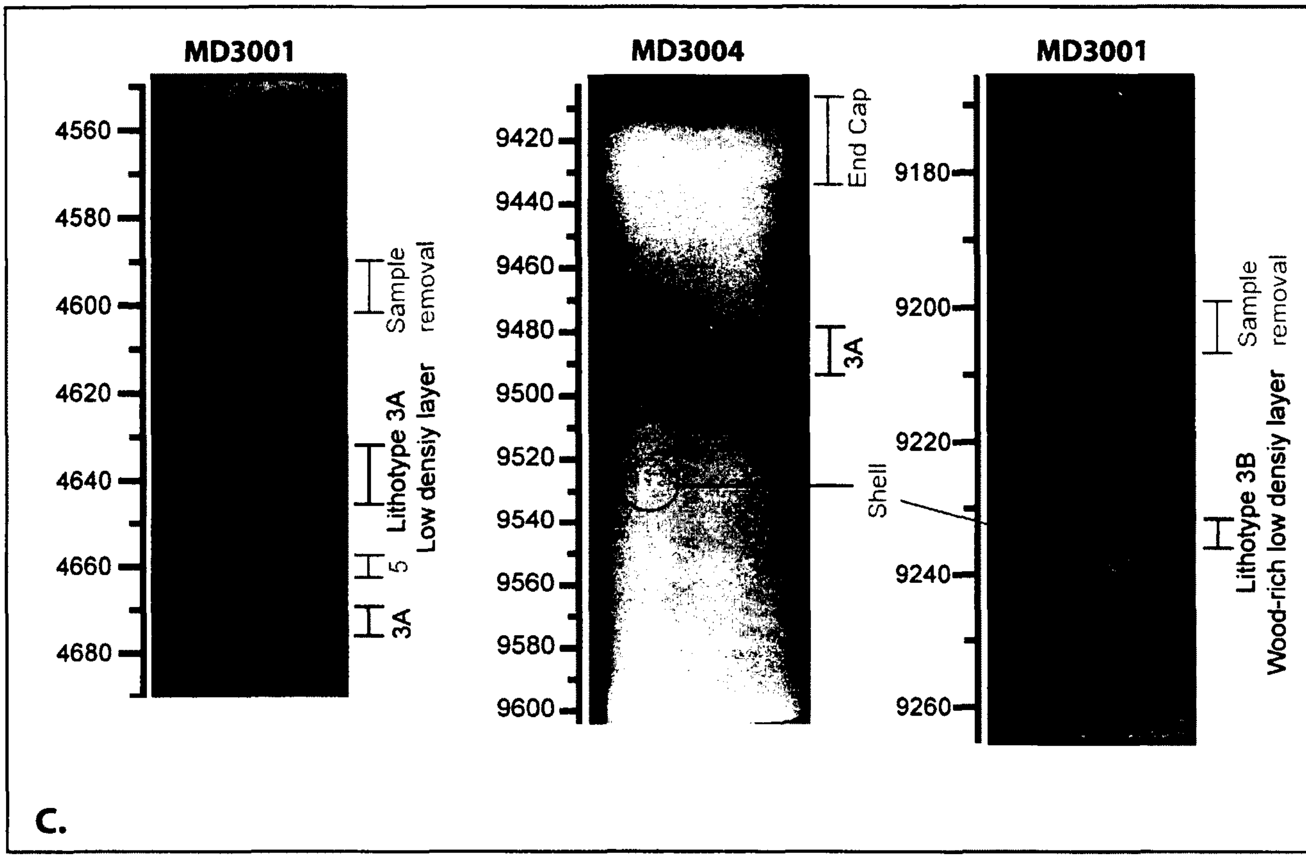

Lithotype 4 - Graded Beds

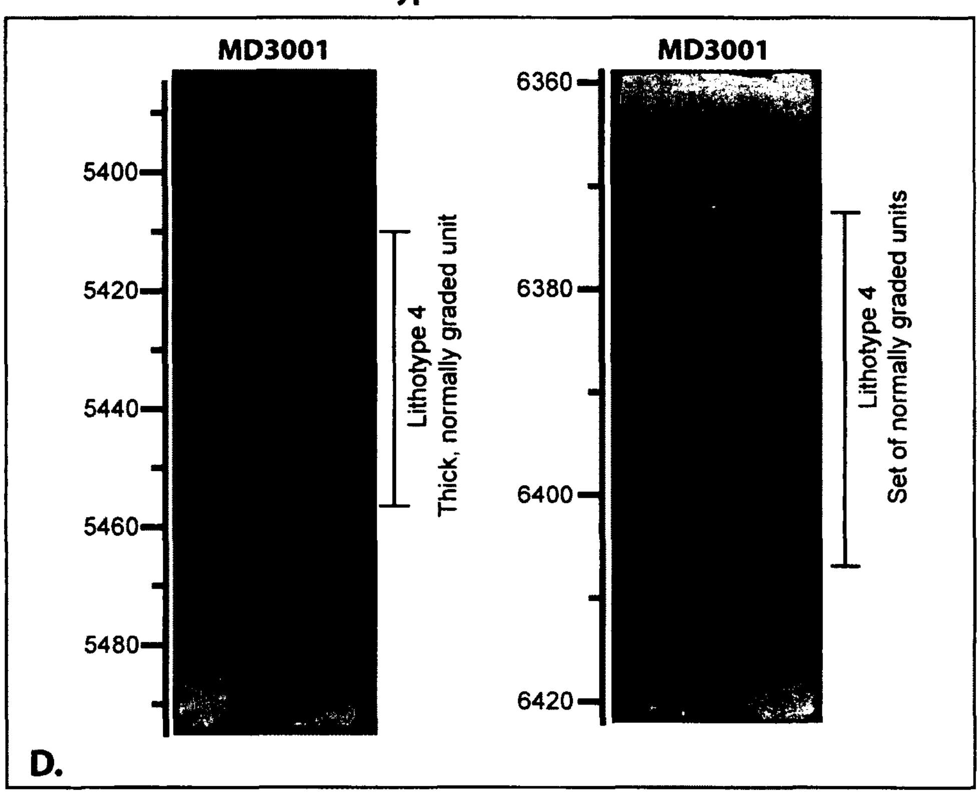

Figure 5

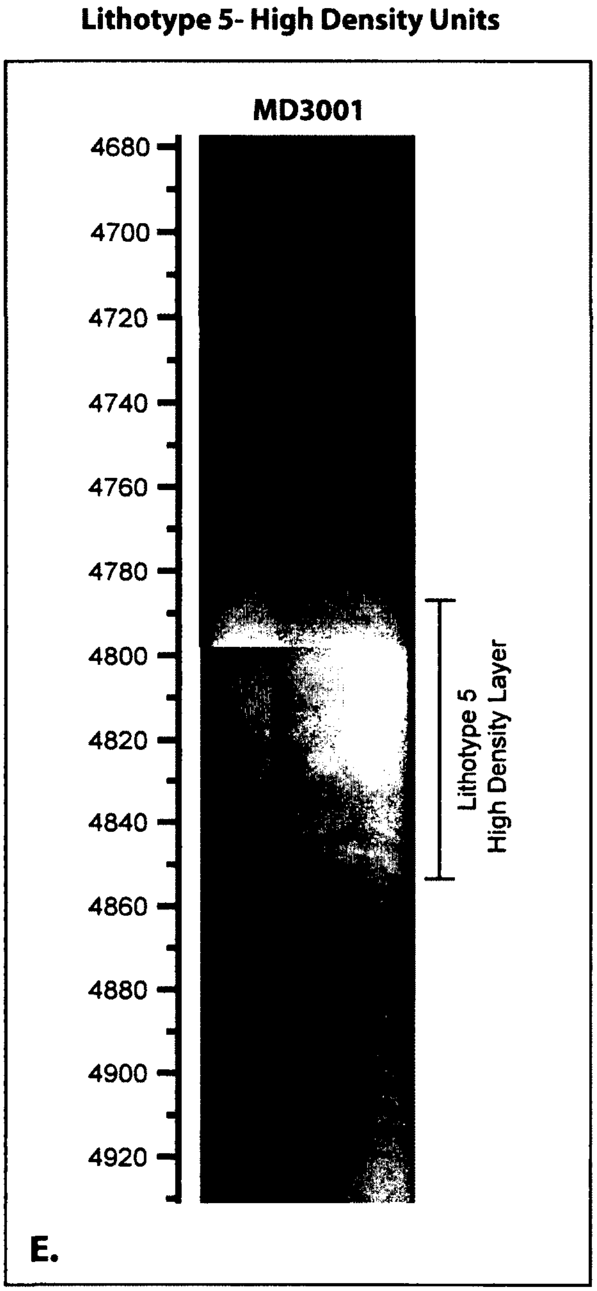

Lithotype 5- High Density Units
MD3001
4680
4700
4720
4740
4760
4780
4800
4820
4840
4860
4880
4900
4920
Lithotype 5
High Density Layer
E.

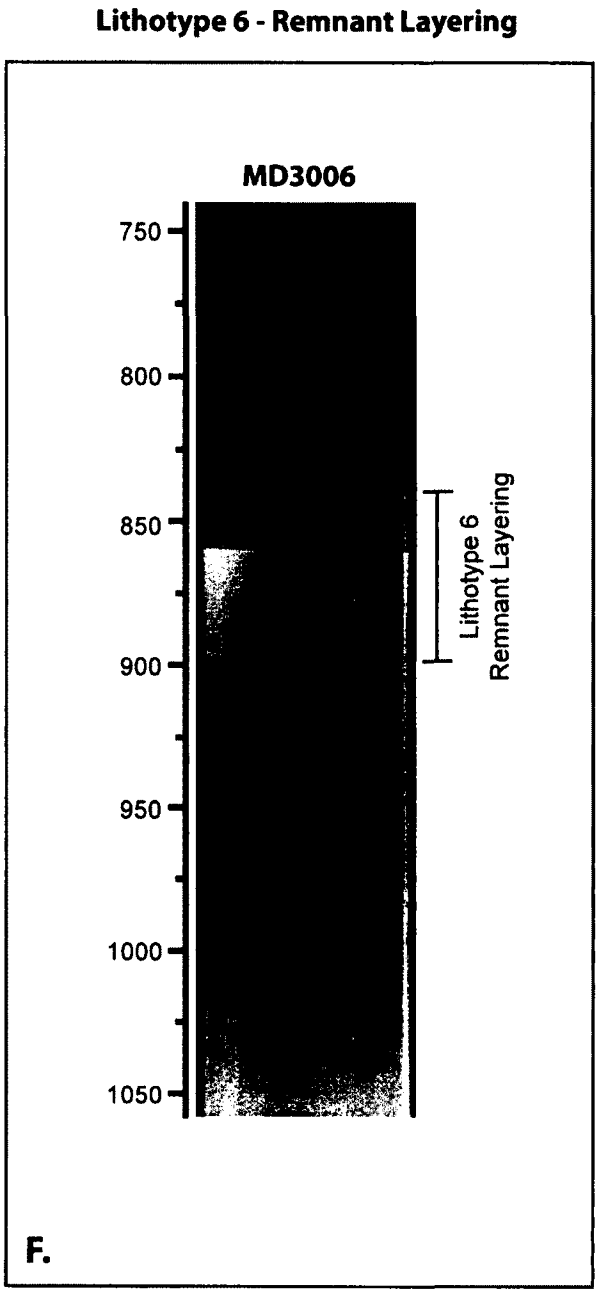

Lithotype 6 - Remnant Layering
MD3006
750
800
850
900
950
1000
1050
Lithotype 6
Remnant Layering
F.

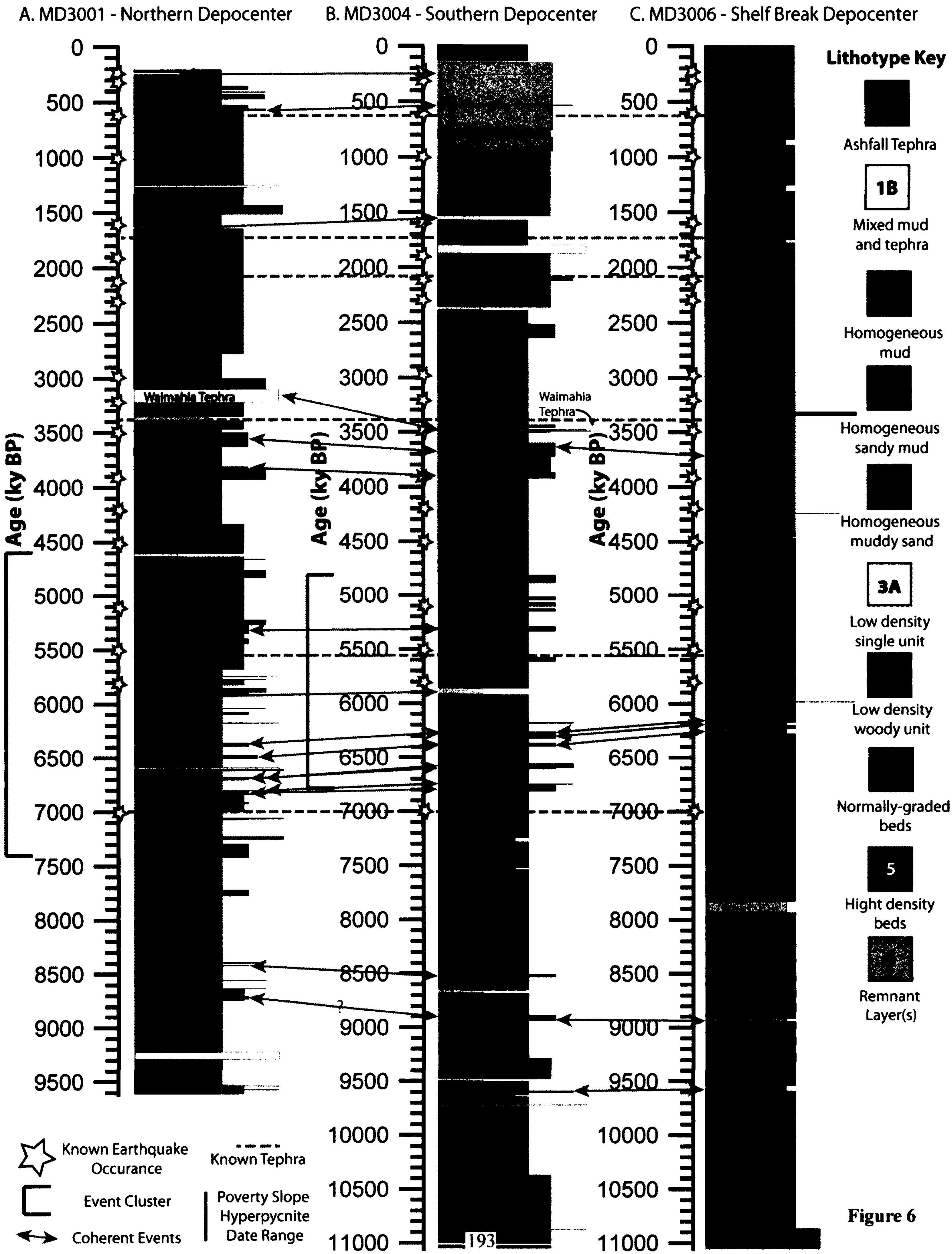
A. MD3001 - Northern Depocenter
B. MD3004 - Southern Depocenter
C. MD3006 - Shelf Break Depocenter
Age (ky BP)
Waimahia Tephra
Waimahia Tephra
Lithotype Key
Ashfall Tephra
1B
Mixed mud and tephra
Homogeneous mud
Homogeneous sandy mud
Homogeneous muddy sand
3A
Low density single unit
Low density woody unit
Normally-graded beds
5
Hight density beds
Remnant Layer(s)
Known Earthquake Occurance
Known Tephra
Event Cluster
Poverty Slope Hyperpycnite Date Range
Coherent Events

Figure 6

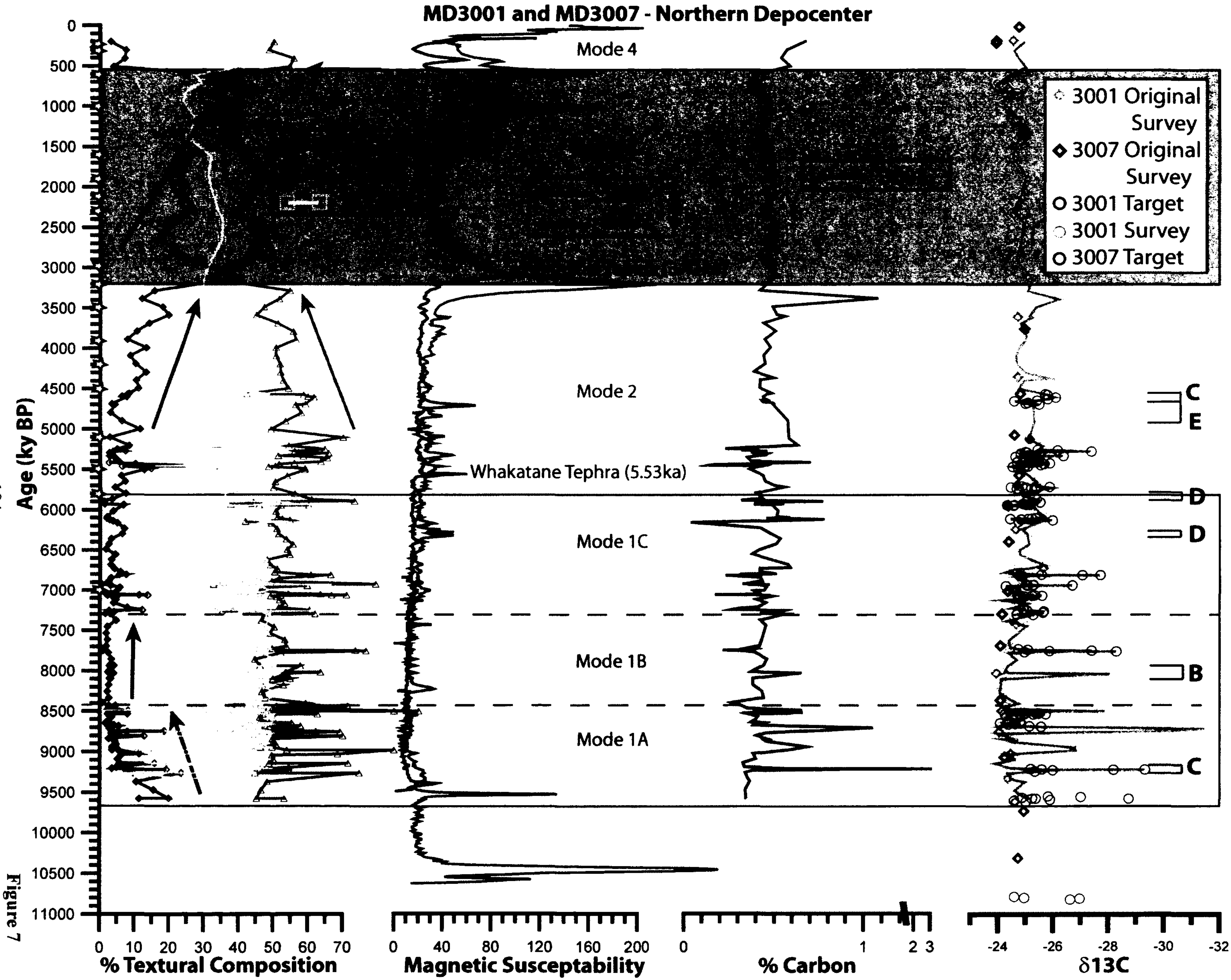
MD3001 and MD3007 - Northern Depocenter
Mode 4
Mode 2
Whakatane Tephra (5.53ka)
Mode 1C
Mode 1B
Mode 1A
C
E
D
D
B
C
3001 Original Survey
3007 Original Survey
3001 Target
3001 Survey
3007 Target
Age (ky BP)
% Textural Composition
Magnetic Susceptability
% Carbon
δ13C

Figure 7

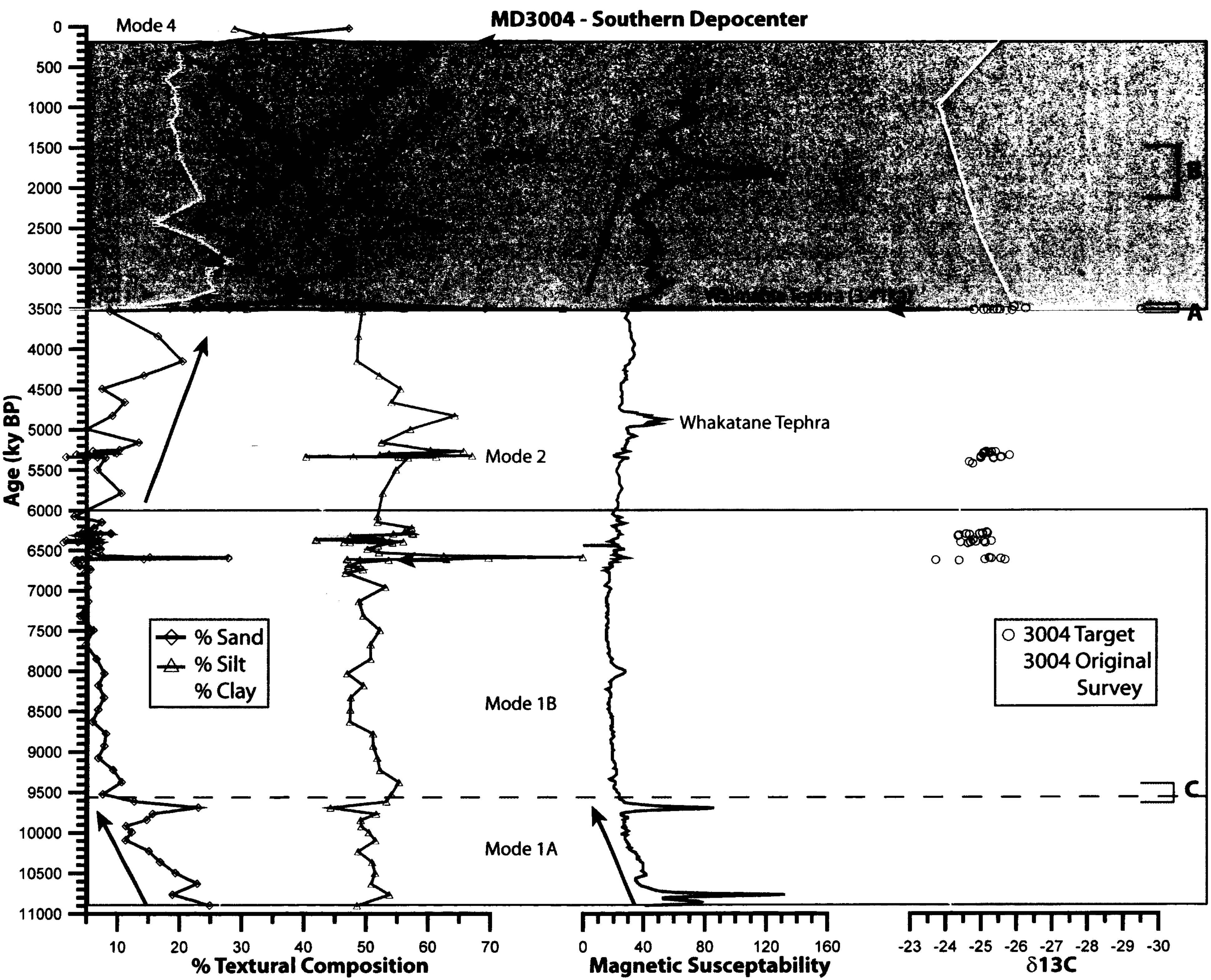
MD3004 - Southern Depocenter
Mode 4
Mode 2
Mode 1B
Mode 1A
Whakatane Tephra
A
B
C
% Sand
% Silt
% Clay
3004 Target
3004 Original Survey
Age (ky BP)
% Textural Composition
Magnetic Susceptibility
δ13C
0
500
1000
1500
2000
2500
3000
3500
4000
4500
5000
5500
6000
6500
7000
7500
8000
8500
9000
9500
10000
10500
11000
10 20 30 40 50 60 70
0 40 80 120 160
-23 -24 -25 -26 -27 -28 -29 -30

Figure 8

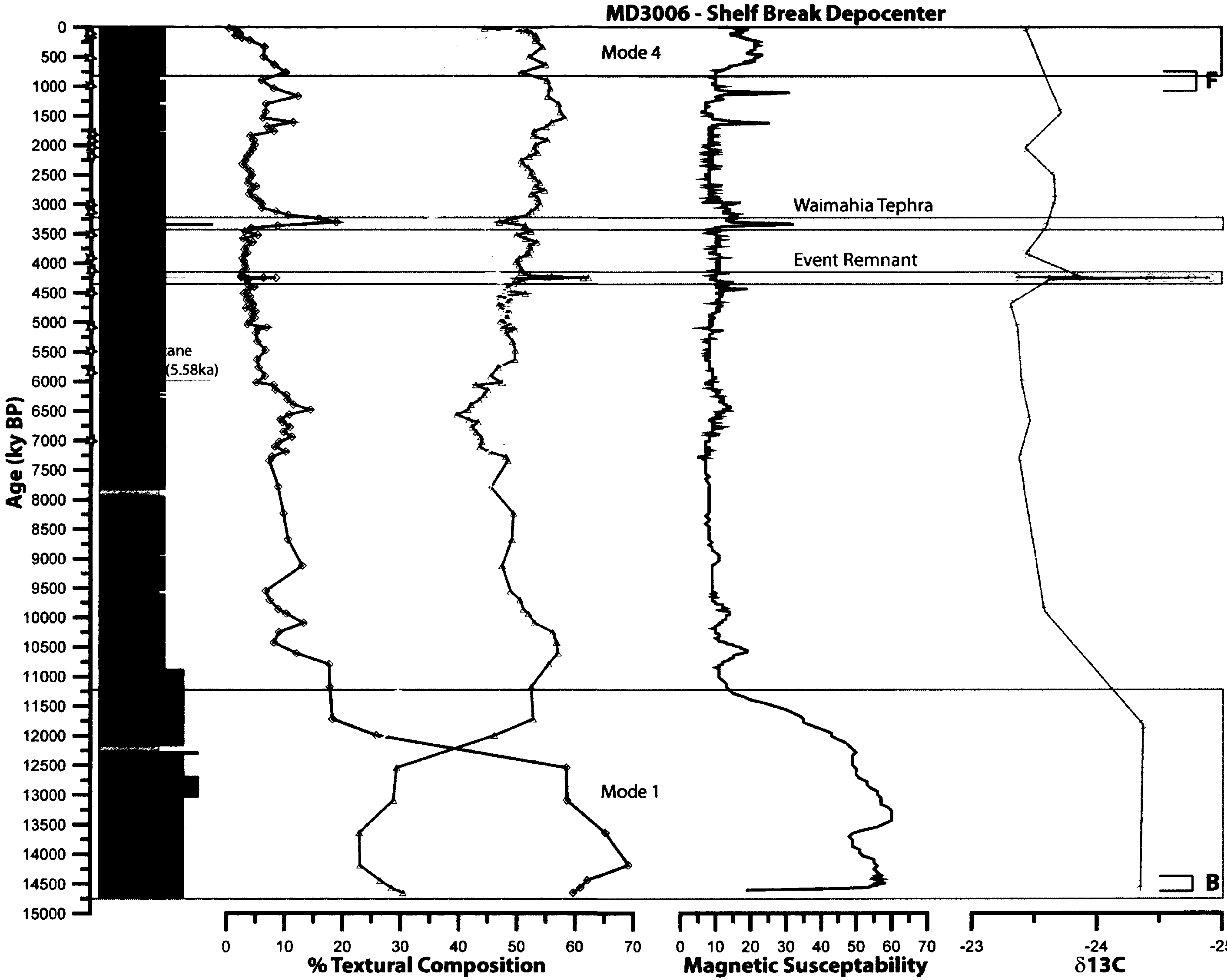

MD3006 - Shelf Break Depocenter
Age (ky BP)
Mode 4
F
Waimahia Tephra
Event Remnant
ane
(5.58ka)
Mode 1
B
% Textural Composition
Magnetic Susceptability
δ13C

Figure 9

Figure 10

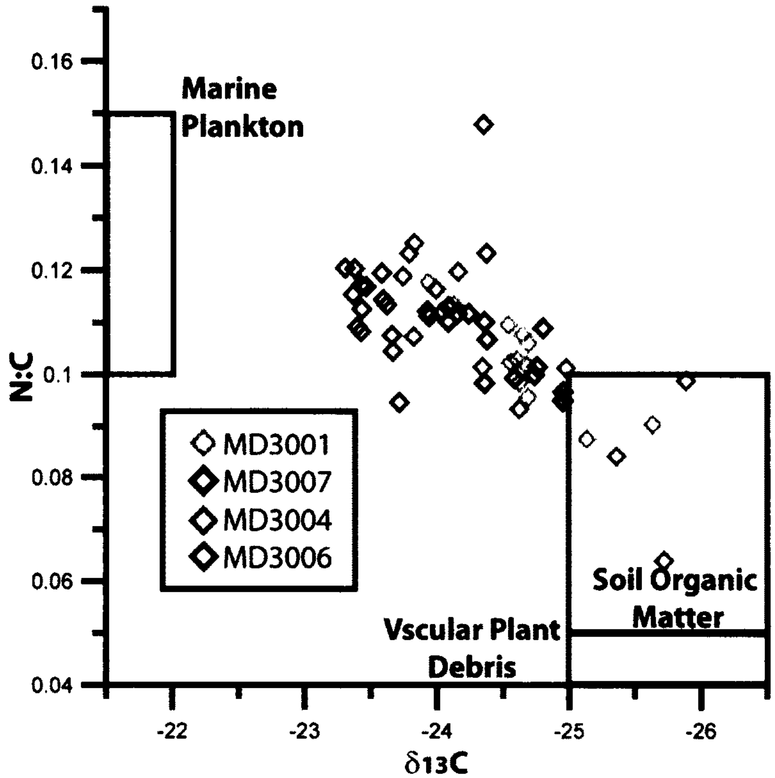
0.16
0.14
0.12
0.1
0.08
0.06
0.04
N:C
Marine
Plankton
MD3001
MD3007
MD3004
MD3006
Soil Organic
Matter
Vscular Plant
Debris
-22
-23
-24
-25
-26
δ13C

Figure 11

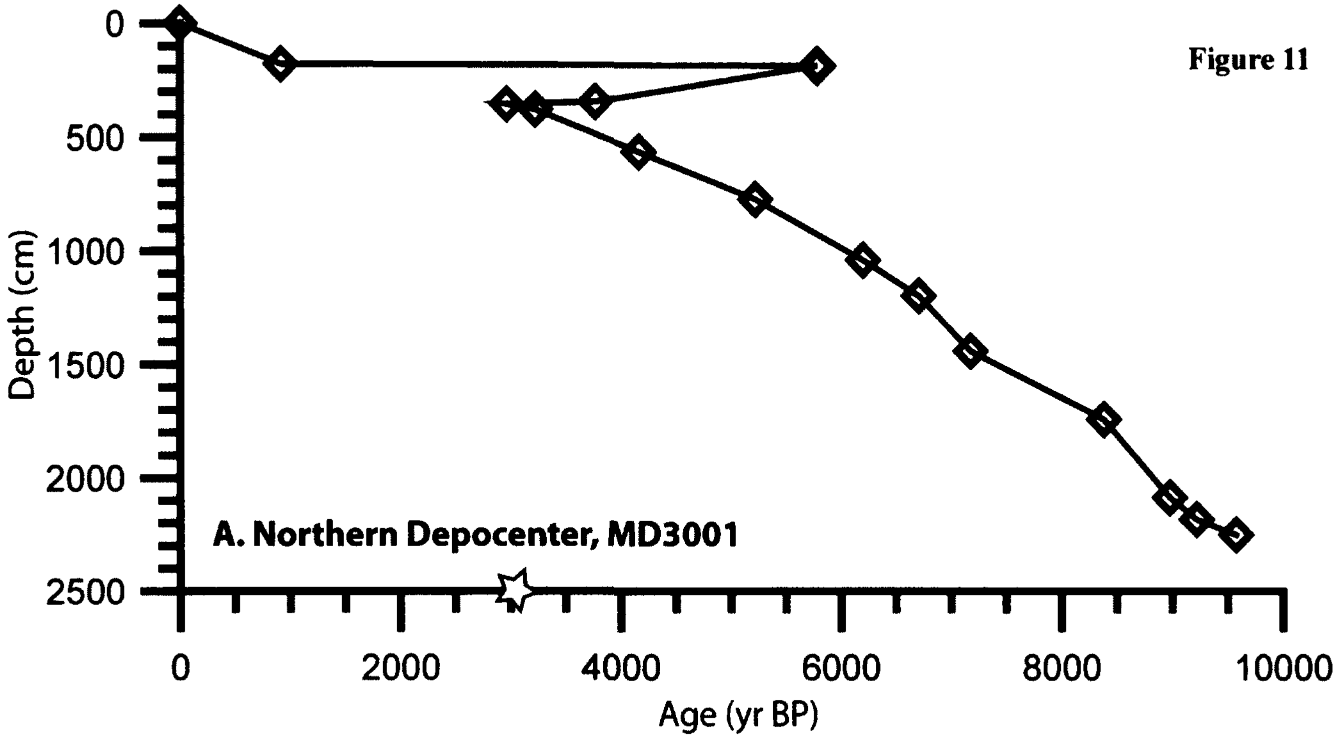

A. Northern Depocenter, MD3001
Depth (cm)
0
500
1000
1500
2000
2500
0
2000
4000
6000
8000
10000
Age (yr BP)

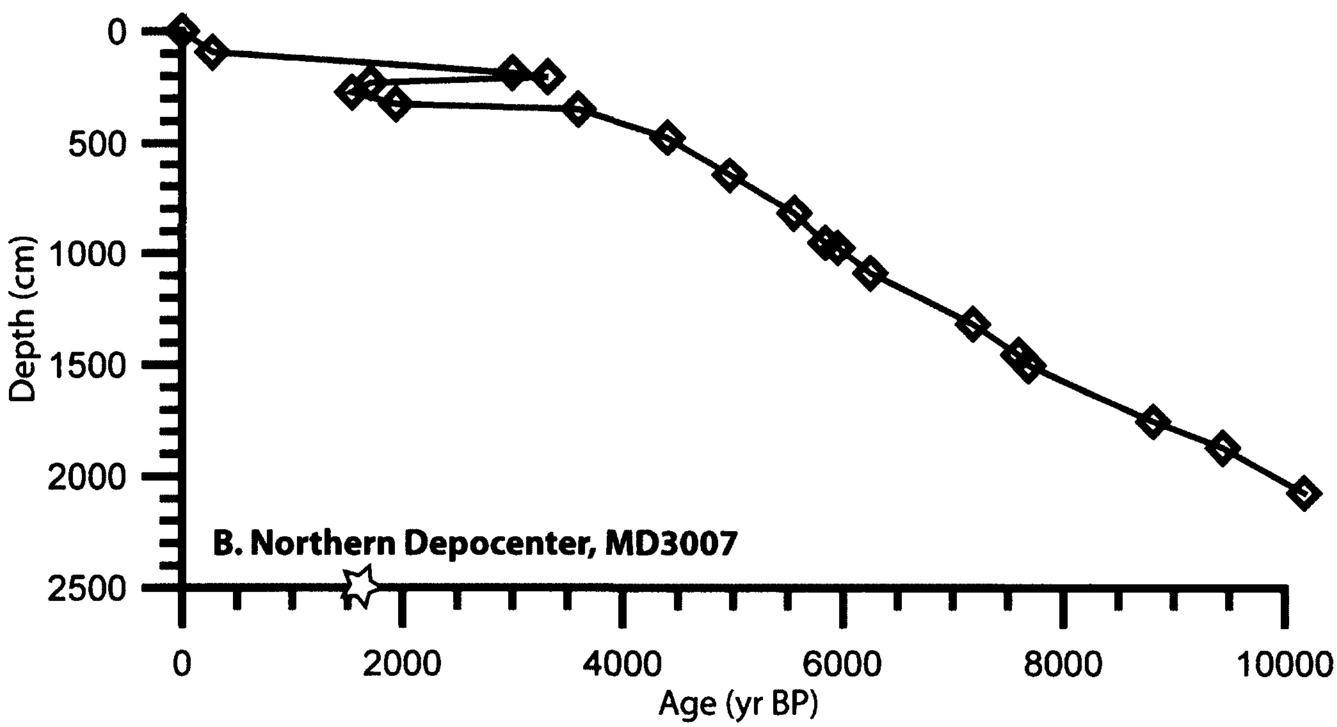

B. Northern Depocenter, MD3007
Depth (cm)
0
500
1000
1500
2000
2500
0
2000
4000
6000
8000
10000
Age (yr BP)

Appendix 1A: Marion DuFresne core and sample ID legend

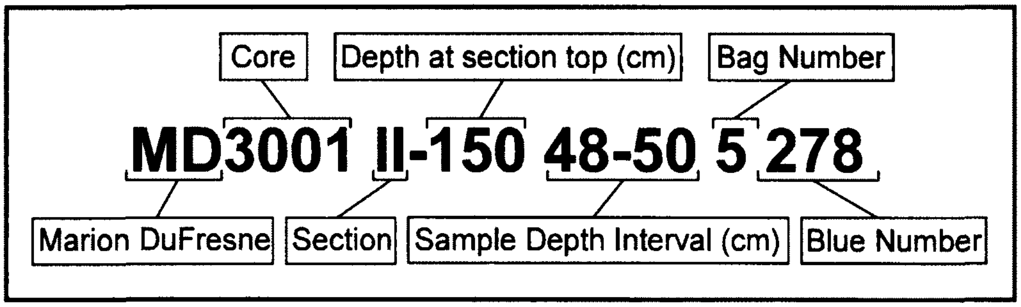

MD: Two letter ship code identifying *R/V Marion DuFresne.*
Core: Core ID number (see Figure – for locations)
Section: Cores were cut into roughly 1.5m sections, labled consecutively with roman numerals.
Depth at Section Top (cm): The depth at the top of the section indicated in cumulative depth within the core.
Sample Depth Interval (cm): Depth interval within the core section, measured from the top of the core section.
Bag Number: Unique identification number written in black ink on the sample bag. This number may not be part of the sample ID in subsequent appendices.
Blue Number: Unique and random reference number written in blue ink on the sample bag. This number may not be part of the sample ID in subsequent appendices.

Appendix 1B: Core gap correction

Core	Section	Interval (cm)	Gap (cm)	Cumulative Adjustment (cm)
3001	- No Gap Correction -			
3003	I	0-5	5	5
3004	- No Gap Correction -			
3006	V	143-150	7	7
3006	VI	0-150	150	157
3006	VII	0-16	16	173
3007	X	38-110	72	72

Gap (cm): Empty space in core (cm), noted post-extraction and core splitting.
Cumulative Adjustment (cm): Cumulative depth adjustment based on gaps in core (cm) applied to core as a "Gap Correction."

Appendix 1C: Core age equation

Standard IODP (http://www.iodp.org/) age equation protocol.

Appendix 2: Marion DuFresne ^{14}C sample list with raw and corrected ages and reversals indicated

Sample ID	Type of Sample	Depth in Core (cm)	Gap Corrected Depth (cm)	RAW ^{14}C Age (years)	RAW ^{14}C Age SD (years)	Calibrated Lower (cal yr BP)	Calibrated Upper (cal yr BP)	Average Calibrated ^{14}C Age	Error
MD3001									
MD 3001 II-150 28	gastropod	178	None	1370	30	838	994	916	78
MD 3001 II-150 37	**wood**	**187**		**5130**	**40**	**5750**	**5828**	**5789**	**39**
MD 3001 III-300 345, vial #5	gastropod	345		3820	30			3772	88
MD 3001 III-300 55	gastropod	355		3170	25	2874	3061	2967.5	93.5
MD 3001 III-300 378, vial #8	gastropod	378		3350	40			3227.5	93.5
MD 3001 IV-450 114	gastropod	564		4100	40	4057	4273	4165	108
MD 3001 VI-750 23	gastropod	773		4920	30	5116	5332	5224	108
MD 3001 VII-900 140	gastropod	1040		5780	45	6123	6282	6202.5	79.5
MD 3001 VIII-1050 146-148	scaphopod	1197		6250	40	6621	6794	6707.5	86.5
MD 3001 X-1350 74	**gastropod**	**1424**		**6650**	**40**	**7109**	**7268**	**7188.5**	**79.5**
MD 3001 X-1350, 1456, vial #6	**gastropod**	**1456**		**6630**	**30**			**7169.5**	**77.5**
MD 3001 XI-1500 113	gastropod	1613		8020	50	8399	8557	8478	79
MD 3001 XIII-1800 69	gastropod	1869		7820	40	8214	8360	8287	73
MD 3001 XIV-1950 135	gastropod	2085		8380	45	8862	9093	8977.5	115.5
MD 3001 XV-2100 2181.5, vial #7	gastropod	2181.5		8570	35			9220	102
MD 3001 XV-2100 82-83	**wood**	**2182.5**		**8150**	**75**	**8783**	**8831**	**8807**	**24**
MD 3001 XVI-2200 49-50	gastropod	2249.5		8910	45	9492	9662	9577	85
MD3003									
MD 3003 I-0 26	gastropod	26.0	21	1380	25	865	1014	939.5	74.5

Sample ID	Type of Sample	Depth in Core (cm)	Gap Corrected Depth (cm)	RAW ^{14}C Age (years)	RAW ^{14}C Age SD (years)	Calibrated Lower (cal yr BP)	Calibrated Upper (cal yr BP)	Average Calibrated ^{14}C Age	Error
MD152-3003 I 62.5-63.2	Foram	62.9	57.9	1415	45	889	1060	974	78
MD152-3003 I 136.5-137.2	AMS	136.9	131.9	1790	35	1272	1403	1337.5	65.5
MD152-3003 II-146 53-54	AMS	199.5	194.5	2440	40	1977	2197	2081.5	100.5
MD152-3003 II-146 120-122	AMS	267	262	2780	30	2434	2652	2543	109
MD152-3003 III-296 9.5-10.2	AMS	305.9	300.9	3170	35	2869	3065	2967	98
MD152-3003 III-296 103-104	AMS	399.5	394.5	3962	35	3858	4074	3968.5	94.5
MD 3003 IV-446 84	gastropod frgmt	530.0	525	6000	35	6330	6491	6410.5	80.5
MD152-3003 IV-446 96.5-97.2	AMS	542.9	537.9	7050	45	7467	7603	7535	64
MD152-3003 V-596 13-14	AMS	609.5	604.5	7846	35	8227	8389	8315.5	70.5
MD152-3003 V-596 121-122	AMS	717.5	712.5	9300	45	10037	10058	10047.5	10.5
MD152-3003 VI-746 10.0-11	AMS	756.5	751.5	9830	55	10583	10818	10700.5	117.5
MD152-3003 VI-746 146.2-147	AMS	892.6	887.6	12480	90	13382	13652	13525	149
MD152-3003 VII-896 25.5-26.7	AMS	922.1	917.1	12850	65	14159	14721	14440	281
MD 3003 VII-896 129-130	**echinoid frgmt**	**1025.5**	**1020.5**	**13350**	**45**	**15163**	**15660**	**15411.5**	**248.5**
MD152-3003 VII-896 131.5-132.2	Foram	1027.8	1022.8	12998	75	14602	15073	14838.5	259.5
MD152-3003 VIII-1046 107.5-108.5	Foram	1153.8	1148.8	13502	75	15550	16318	15937.5	398.5
MD 3003 IX-1196 88-89	gastropod	1284.5	1279.5	14800	65	17243	17336	17289.5	46.5
MD152-3003 IX-1196 88.5-89.5	**AMS**	**1285.0**	**1280**	**13800**	**65**	**16406**	**16778**	**16586**	**199**

Sample ID	Type of Sample	Depth in Core (cm)	Gap Corrected Depth (cm)	RAW ^{14}C Age (years)	RAW ^{14}C Age SD (years)	Calibrated Lower (cal yr BP)	Calibrated Upper (cal yr BP)	Average Calibrated ^{14}C Age	Error
MD3004									
MD 3004 I-0 19	gastropod	19.0	19	485	30	0	146	73	73
MD 3004 II-150 55	gastropod	205.0	205	1790	30	1274	1399	1336.5	62.5
MD 3004 III-300 26	gastropod	326.0	326	3130	30	2828	3011	2919.5	91.5
MD 3004 III-300 125	shell frgmt	425.0	425	3600	30	3418	3580	3499	81
MD 3004 IV-450, 465, vial #4	gastropod		465.0	3610	35			3515	84
MD 3004 IV-450 57-58	gastropod	507.5	507.5	4110	30	4074	4273	4173.5	99.5
MD 3004 V-600 34	gastropod	634.0	634	4920	45	5115	5334	5224.5	109.5
MD 3004 V-600, 696.5, vial #2	gastropod		696.5	4990	30			5358	74
MD 3004 V-600 145-147	gastropod	746.0	746	5660	35	5989	6160	6074.5	85.5
MD 3004 VI-750 71	gastropod	821.0	821	5930	35	6278	6410	6344	66
MD 3004 VII-900 125-127	shell frgmt	1026.0	1026	6310	30	6695	6859	6777	82
MD 3004 VIII-1050 69-70	**gastropod**	**1119.5**	**1119.5**	**7560**	**55**	**7947**	**8115**	**8031**	**84**
MD 3004 VIII-1150, 1151, vial #3	**gastropod**		**1151.0**	**7700**	**35**			**8185.5**	**87.5**
MD 3004 IX-1200 27-28	**gastropod**	**1227.5**	**1227.5**	**7400**	**40**	**7796**	**7938**	**7867**	**71**
MD 3004 X-1350 15	gastropod	1365.0	1365	6460	40	6866	7066	6966	100
MD 3004 X-1350, 1370, vial #1	gastropod		1370	8890	35			9552	75
MD 3004 X-1350 147-148	gastropod	1497.5	1497.5	9210	40	9928	10142	10035	107
MD3006									
MD 3006 I-0 116	gastropod	116.0	116	615	30	144	322	233	89
MD 3006 III-300 5-6	gastropod	305.5	305.5	1950	30	1412	1580	1496	84
MD 3006 III-300 105-106	**snail**	**405.5**	**405.5**	**2650**	**30**	**2276**	**2456**	**2366**	**90**
MD 3006 III-300, 427.5, vial #9	**gastropod**		**427.5**	[illegible]	[illegible]			**2263**	**79**

Sample ID	Type of Sample	Depth in Core (cm)	Gap Corrected Depth (cm)	RAW ^{14}C Age (years)	RAW ^{14}C Age SD (years)	Calibrated Lower (cal yr BP)	Calibrated Upper (cal yr BP)	Average Calibrated ^{14}C Age	Error
MD 3006 IV-450 68-69	**gastropod**	**518.5**	**518.5**	**1960**	**25**	**1428**	**1595**	**1511.5**	**83.5**
MD 3006 VII-900 40-41	gastropod	940.5	767.5	3230	25	2959	3150	3054.5	95.5
MD 3006 IX-1200, 1154, vial #14	gastropod		1154					4219.5	98.5
MD 3006 X-1350 8	gastropod	1358.0	1185	4190	30	4202	4390	4296	94
MD 3006 XII-1650 25	gastropod	1675.0	1502	4860	35	5069	5270	5169.5	100.5
MD 3006 XII-1650 135	gastropod frgmt	1785.0	1612	5570	40	5887	6061	5974	87
MD 3006 XIII-1800 46	gastropod	1846.0	1673	5800	30	6164	6292	6228	64
MD 3006 XV-2100 5	shell	2105.0	1932	6770	30	7245	7375	7310	65
MD 3006 XV-2100, 2012, vial #15	**gastropod**		**2012**					**9610.5**	**88.5**
MD 3006 XV-2100 126	**gastropod**	**2226.0**	**2053**	**8820**	**35**	**9425**	**9537**	**9481**	**56**
MD 3006 XVI-2250, 2128, vial #16	gastropod		2128					10286.5	81.5
MD 3006 XVI-2250 70	gastropod frgmt	2320.0	2147	10300	55	11180	11405	11292.5	112.5
MD 3006 XVII-2400 10-12	gastropod frgmt	2411.0	2238	9590	40	10385	10542	10463.5	78.5
MD 3006 XVII-2400, 2273.5, vial #18	**gastropod**		**2273.5**					**16261.5**	**326.5**
MD 3006 XVIII-2534.5	**gastropod**	**2539.0**	**2366**	**10900**	**40**	**12341**	**12554**	**12447.5**	**106.5**
MD3007									
MD 3007 I-0 65	**scaphopod**	**65.0**	**65**	**685**	**35**	**278**	**411**	**344.5**	**66.5**
MD 3007 II-71, 123.5, vial #12	**gastropod**		**123.5**					**205.5**	
MD 3007 II-71 115-116	gastropod	186.5	186.5	3190	35	2899	3102	3000.5	101.5
MD 3007 II-71, 205, vial#13	gastropod		205					3320	

Sample ID	Type of Sample	Depth in Core (cm)	Gap Corrected Depth (cm)	RAW ^{14}C Age (years)	RAW ^{14}C Age SD (years)	Calibrated Lower (cal yr BP)	Calibrated Upper (cal yr BP)	Average Calibrated ^{14}C Age	Error
MD 3007 III-221 230.5 vial #17	**gastropod**		**230.5**					**1711.5**	
MD 3007 III-221 51-52	**gastropod**	**272.5**	**272.5**	**1980**	**30**	**1455**	**1629**	**1542**	**87**
MD 3007 III-221 325.5 vial #11	**gastropod**		**325.5**					**1941**	
MD 3007 III-221 127	gastropod	348.0	348	3680	25	3510	3682	3596	86
MD 3007 IV-371 103-105	gastropods	475.0	475	4280	35	4309	4502	4405.5	96.5
MD 3007 V-521 127	olive shell	648.0	648	4740	35	4859	5077	4968	109
MD 3007 VI-671 147	olive shell	818.0	818	5200	30	5486	5626	5556	70
MD 3007 VII-821 131	gastropod	952.0	952	5470	95	5715	5973	5844	129
MD 3007 VIII-971 2-5	wood	974.5	974.5	5260	40	5940	5974	5957	17
MD 3007 VIII-971 61	**gastropod**	**1032.0**	**1032**	**5550**	**30**	**5867**	**6027**	**5947**	**80**
MD 3007 IX-1121 26	**gastropod**	**1147.0**	**1147**	**6130**	**35**	**6483**	**6646**	**6564.5**	**81.5**
MD 3007 X-1271 117	gastropod	1388.0	1316	6650	50	7097	7273	7185	88
MD 3007 XI-1421 1455 vial #10	gastropod		1455					7595.5	
MD 3007 XII-1571 3	gastropod	1574.0	1502	7220	40	7614	7760	7687	73
MD 3007 XIII-1721 104	gastropod	1825.0	1753	8360	60	8797	8828	8812.5	15.5
MD 3007 XIV-1871 73	gastropod	1944.0	1872	8760	50	9372	9514	9443	71
MD 3007 XV-2021 97	**wood**	**2118.0**	**2046**	**9110**	**60**	**10204**	**10298**	**10251**	**47**
MD 3007 XVI-2171 1	shell	2172.0	2100	9270	40	10009	10203	10106	97

RAW ^{14}C Age (years): AMS raw C-14 age of sample returned from Woods Hole NOSAMS facility (http://www.whoi.edu/nosams/) and GNS Science Rafter Laboratory (New Zealand).
RAW ^{14}C Age SD (years): Standard Deviation of RAW ^{14}C age returned from NOSAMS and GNS.

Calibrated Lower (cal yr BP): Calibrated lower limit of ^{14}C age determined using the INTCAL09 and MARINE09 radiocarbon age calibration curves with a delt-R (-5) and delta-R standard deviation (57).

Calibrated Upper (cal yr BP): Calibrated upper limit of ^{14}C age determined using the INTCAL09 and MARINE09 radiocarbon age calibration curves with a delt-R (-5) and delta-R standard deviation (57).

Average Calibrated ^{14}C Age: Average of above upper and lower limits.

Error: Average Calibrated ^{14}C Age error (in years).

Shaded Cells: Indicates samples that were either removed or averaged due to reversals to preserve age model integrity. See Chapter 1, Section 3.2 (pg. 11) for more detail.

Appendix 3: Marion DuFresne accumulation rate data

MD3001	
AR (cm/yr)	Age (yr BP)
0.19	458
0.09	1942
0.09	3098
0.20	3696
0.20	4695
0.27	5713
0.31	6455
0.52	6943
0.25	7781
0.58	8680
0.40	9099
0.19	9399
0.23	9577

MD3003	
AR (cm/yr)	Age (yr BP)
0.04	478
0.24	1147
0.08	1710
0.15	2312
0.09	2755
0.09	3468
0.05	5190
0.01	6973
0.09	7925
0.06	9182
0.06	10374
0.05	12113
0.03	13983
0.27	14639
0.11	15388
0.13	16437

MD3004	
AR (cm/yr)	Age (yr BP)
0.26	37
0.15	705
0.08	2128
0.20	3213
0.09	3840
0.12	4699
0.47	5291
0.07	5716
0.28	6209
0.47	6561
0.11	7402
0.13	8790
0.26	9794
0.15	10035

MD3006	
AR (cm/yr)	Age (yr BP)
0.50	117
0.15	865
0.26	1771
0.31	2551
0.33	3637
0.41	4258
0.36	4733
0.14	5572
0.24	6101
0.24	6769
0.04	8428
0.13	9916
0.11	10582
0.04	12616
0.16	14355

MD3007	
AR (cm/yr)	Age (yr BP)
0.34	138
0.12	1003
0.04	2664
0.16	4001
0.31	4687
0.29	5262
0.47	5700
0.20	5901
0.38	6106
0.24	6720
0.34	7390
0.51	7641
0.22	8250
0.19	9128
0.27	9811
0.20	10179

AR (cm/yr): Calculated linear Accumulation Rate (cm/yr).

Appendix 4A: Marion DuFresne grain size analyses (Sedigraph)

Core	Section	Interval	Midpoint Depth (cm)	Gap Corrected Midpoint Depth (cm)	Percent			Mean φ
					Sand	Silt	Clay	
MD3001	I-0	38-40	39	No Correction	3.12	50.19	46.7	8.21
MD3001	I-0	58-60	59		7.49	48.81	43.7	7.82
MD3001	I-0	78-80	79		7.11	55.83	37.07	7.46
MD3001	I-0	98-100	99		3.89	54.63	41.48	7.89
MD3001	I-0	118-120	119		37.98	34.6	27.42	6.24
MD3001	I-0	138-140	139		31.05	39.54	29.41	6.52
MD3001	II-150	8-10	159		44.25	30.81	24.94	5.99
MD3001	II-150	28-30	179		39.47	36.57	23.96	6.02
MD3001	II-150	48-50	199		32.58	39.92	27.5	6.34
MD3001	II-150	68-70	219		38.53	35.68	25.79	6.10
MD3001	II-150	88-90	239		25.5	42.44	32.04	6.74
MD3001	II-150	108-110	259		22.53	46.23	31.24	6.77
MD3001	II-150	128-130	279		23.78	43.7	32.52	6.87
MD3001	II-150	147-149	298		26.9	38.67	34.44	6.91
MD3001	III-300	8-10	309		19.25	45.22	35.53	7.15
MD3001	III-300	28-30	329		17.85	46.99	35.16	7.10
MD3001	III-300	48-50	349		24.96	42.82	32.21	6.79
MD3001	III-300	68-70	369		40.09	29.89	30.02	6.16
MD3001	III-300	88-90	389		15.66	54.7	29.64	6.78
MD3001	III-300	108-110	409		12.15	51.62	36.23	7.29
MD3001	III-300	128-130	429		18.07	47.32	34.51	7.08
MD3001	III-300	148-150	449		19.82	45.07	35.11	7.04
MD3001	IV-450	18-20	469		14.12	51.21	34.67	7.16
MD3001	IV-450	38-40	489		10.63	55.65	33.72	7.15
MD3001	IV-450	58-60	509		7.82	56.34	35.84	7.33
MD3001	IV-450	78-80	529		13.3	50.7	36	7.32
MD3001	IV-450	98-100	549		8.68	50.72	40.61	7.65
MD3001	IV-450	118-120	569		10.23	51.82	37.95	7.36
MD3001	IV-450	138-140	589		13.22	52	34.79	7.15
MD3001	V-600	8-10	609		10.43	52.77	36.8	7.34
MD3001	V-600	28-30	629		11.16	54.37	34.47	7.11
MD3001	V-600	48-50	649		6.34	59.97	33.7	7.22
MD3001	V-600	68-70	669		4.31	56.41	39.28	7.60
MD3001	V-600	88-90	689		3.1	58.02	38.88	7.63
MD3001	V-600	108-110	709		6.32	53.47	40.22	7.61
MD3001	V-600	128-130	729		11.63	49.34	39.03	7.46
MD3001	V-600	148-150	749		2.89	70.06	27.06	6.90
MD3001	VI-750	18-20	769		8.46	54.46	37.08	7.38
MD3001	VI-750	38-40	789		3.8	57.16	39.05	7.68
MD3001	VI-750	58-60	809		4.4	65.53	30.07	7.01
MD3001	VI-750	78-80	829		10.25	51.63	38.12	7.46
MD3001	VI-750	98-100	849		12.74	58.98	28.27	6.74
MD3001	VI-750	118-120	869		6.19	53.99	39.82	7.70
MD3001	VI-750	138-140	889		7.31	50.59	42.05	7.71

Core	Section	Interval	Midpoint Depth (cm)	Gap Corrected Midpoint Depth (cm)	Percent			Mean φ
					Sand	Silt	Clay	
MD3001	VII-900	8-10	909		4.44	50.08	45.48	8.04
MD3001	VII-900	28-30	929		7.44	56.16	36.4	7.39
MD3001	VII-900	48-50	949		3.58	60.98	35.44	7.35
MD3001	VII-900	68-70	969		6.73	52.17	41.1	7.67
MD3001	VII-900	88-90	989		3.88	50.8	45.32	8.04
MD3001	VII-900	108-110	1009		2.12	51.27	46.62	8.16
MD3001	VII-900	128-130	1029		4.99	49.43	45.58	8.00
MD3001	VII-900	148-150	1049		7.05	51.05	41.9	7.74
MD3001	VIII-1050	18-20	1069		6.41	51.55	42.04	7.76
MD3001	VIII-1050	38-40	1089		3.33	53.74	42.93	7.90
MD3001	VIII-1050	58-60	1109		2.61	55.61	41.78	7.87
MD3001	VIII-1050	78-80	1129		1.77	54.06	44.16	7.98
MD3001	VIII-1050	98-100	1149		4.49	54.74	40.77	7.64
MD3001	VIII-1050	118-120	1169		3.4	48.2	48.39	8.13
MD3001	VIII-1050	138-140	1189		3.18	49.29	47.53	8.13
MD3001	IX-1200	8-10	1209		4.23	51.08	44.69	7.90
MD3001	IX-1200	28-30	1229		5.95	50.41	43.64	7.96
MD3001	IX-1200	48-50	1249					
MD3001	IX-1200	68-70	1269		3.24	51.75	45	8.05
MD3001	IX-1200	88-90	1289		2.6	49.58	47.82	8.14
MD3001	IX-1200	108-110	1309					
MD3001	IX-1200	128-130	1329		5.72	46.8	47.48	8.06
MD3001	IX-1200	148-150	1349		5	46.52	48.48	8.16
MD3001	X-1350	18-20	1369		3.14	54.38	42.47	7.85
MD3001	X-1350	38-40	1389		4.89	51.14	43.96	7.93
MD3001	X-1350	58-60	1409		4.69	51.91	43.39	7.77
MD3001	X-1350	78-80	1429		4.05	53.24	42.71	7.81
MD3001	X-1350	98-100	1449		7.94	51.64	40.42	7.54
MD3001	X-1350	118-120	1469		3.1	47.67	49.23	8.21
MD3001	X-1350	138-140	1489		4.75	46.7	48.55	8.13
MD3001	XI-1500	8-10	1509		2.26	50.31	47.43	8.13
MD3001	XI-1500	28-30	1529		1.92	49.24	48.84	8.21
MD3001	XI-1500	48-50	1549		2.23	53.39	44.38	7.91
MD3001	XI-1500	68-70	1569		1.87	53.78	44.35	7.92
MD3001	XI-1500	88-90	1589		2.51	52.17	45.32	7.99
MD3001	XI-1500	108-110	1609		3.39	44.77	51.84	8.38
MD3001	XI-1500	128-130	1629		2.84	46.27	50.89	8.29
MD3001	XI-1500	148-150	1649		2.37	53.62	44.01	7.94
MD3001	XII-1650	18-20	1669		2.84	49.98	47.18	8.08
MD3001	XII-1650	38-40	1689		2.58	46.95	50.47	8.33
MD3001	XII-1650	58-60	1709		2.2	46.78	51.02	8.32
MD3001	XII-1650	78-80	1729		2.68	47.62	49.7	8.28
MD3001	XII-1650	98-100	1749		0.7	59.36	39.94	7.78
MD3001	XII-1650	118-120	1769		2.64	50.99	46.37	7.99
MD3001	XII-1650	138-140	1789		2.51	49.78	47.71	8.12
MD3001	XIII-1800	8-10	1809		2.62	48	49.37	8.24

Core	Section	Interval	Midpoint Depth (cm)	Gap Corrected Midpoint Depth (cm)	Percent			Mean φ
					Sand	Silt	Clay	
MD3001	XIII-1800	28-30	1829		2.34	47.02	50.64	8.23
MD3001	XIII-1800	48-50	1849		3.48	46.19	50.33	8.24
MD3001	XIII-1800	68-70	1869		2.73	46.58	50.69	8.33
MD3001	XIII-1800	88-90	1889		1.81	48.85	49.35	8.19
MD3001	XIII-1800	108-110	1909		4.14	47.68	48.17	8.09
MD3001	XIII-1800	128-130	1929		2.9	52.83	44.27	7.94
MD3001	XIII-1800	148-150	1949		3.59	46.84	49.57	8.22
MD3001	XIV-1950	13-15	1964		3.39	45.84	50.76	8.24
MD3001	XIV-1950	33-35	1984		4.87	45.19	49.69	8.18
MD3001	XIV-1950	53-55	2004		2.63	49.8	47.57	8.08
MD3001	XIV-1950	73-75	2024		4.39	50.02	45.59	7.89
MD3001	XIV-1950	93-95	2044		4.72	50.85	44.43	7.87
MD3001	XIV-1950	113-115	2064		3.61	46.34	50.05	8.23
MD3001	XIV-1950	133-135	2084		3.59	53.93	42.48	7.81
MD3001	XV-2100	8-10	2109		6.21	49.64	44.15	7.81
MD3001	XV-2100	28-30	2129		5.17	50.05	44.77	7.84
MD3001	XV-2100	48-50	2149		5.74	48.8	45.46	7.90
MD3001	XV-2100	68-70	2169		4.86	54.49	40.48	7.57
MD3001	XV-2100	88-90	2189		9.67	44.79	45.44	7.85
MD3001	XVI-2200	8-10	2209		10.54	48.25	41.21	7.49
MD3001	XVI-2200	28-30	2229		15.44	46.5	38.06	7.18
MD3001	XVI-2200	48-50	2249		19.87	45.22	34.91	6.87
MD3003	I-0	10-12	11	6	0.97	41.55	57.49	8.68
MD3003	I-0	30-32	31	26	1.66	43.46	54.88	8.50
MD3003	I-0	48-50	49	44	1.21	51.5	47.29	8.21
MD3003	I-0	70-72	71	66	18.1	43.24	38.66	7.19
MD3003	I-0	90-92	91	86	2.92	41.37	55.71	8.55
MD3003	I-0	110-112	111	106	1.92	46.87	51.21	8.37
MD3003	I-0	130-132	131	126	18.2	41.41	40.39	7.36
MD3003	II-146	0-2	147	142	9.75	44.27	45.98	7.81
MD3003	II-146	20-22	167	162	32.87	43.72	23.4	6.03
MD3003	II-146	40-42	187	182	4	45.34	50.63	8.24
MD3003	II-146	60-62	207	202	14.02	41.52	44.44	7.54
MD3003	II-146	80-82	227	222	1.55	45.49	52.93	8.42
MD3003	II-146	102-104	249	244	1.49	46.54	51.97	8.35
MD3003	II-146	122-124	269	264	1.03	45.61	53.36	8.42
MD3003	II-146	140-142	287	282	1.24	52.47	46.28	8.10
MD3003	III-296	5-7	302	297	37.4	38.87	23.71	5.90
MD3003	III-296	25-27	322	317	0.86	47.68	51.46	8.41
MD3003	III-296	45-47	342	337	1.7	47.58	50.72	8.30
MD3003	III-296	65-67	362	357	2.71	58.4	38.87	7.72
MD3003	III-296	85-87	382	377	73.36	17.31	9.33	4.35
MD3003	III-296	105-107	402	397	0.95	51.82	47.23	8.20
MD3003	III-296	125-127	422	417	1.96	46.81	51.23	8.34
MD3003	III-296	145-147	442	437	3.94	47.79	48.27	8.16

Core	Section	Interval	Midpoint Depth (cm)	Gap Corrected Midpoint Depth (cm)	Percent Sand	Percent Silt	Percent Clay	Mean φ
MD3003	IV-446	11-13	458	453	10.07	47.05	41.71	7.57
MD3003	IV-446	31-33	478	473	52.31	20.54	27.16	5.38
MD3003	IV-446	51-53	498	493	0.3	45.4	54.3	8.57
MD3003	IV-446	71-73	518	513	1.48	46.15	52.38	8.40
MD3003	IV-446	91-93	538	533	2.83	44.96	52.2	8.36
MD3003	IV-446	111-113	558	553	2.31	45.22	52.47	8.38
MD3003	IV-446	131-133	578	573	2.84	46.55	50.6	8.29
MD3003	V-596	5-7	602	597	4.22	43.85	51.93	8.23
MD3003	V-596	25-27	622	617	7.61	39.33	53.06	8.28
MD3003	V-596	45-47	642	637	25.77	39.39	34.83	6.87
MD3003	V-596	65-67	662	657	1.81	41.81	56.38	8.56
MD3003	V-596	85-87	682	677	14.11	44.98	40.91	7.40
MD3003	V-596	105-107	702	697	21.31	50.49	28.2	6.58
MD3003	V-596	125-127	722	717	1.59	44.48	53.93	8.44
MD3003	V-596	145-147	742	737	8.22	45.99	45.8	7.84
MD3003	VI-746	18-20	765	760	10.79	47.74	41.46	7.52
MD3003	VI-746	38-40	785	780	9.13	47.3	43.57	7.64
MD3003	VI-746	58-60	805	800	1.31	45.22	53.47	8.42
MD3003	VI-746	78-80	825	820	3.78	50.11	46.11	7.91
MD3003	VI-746	98-100	845	840	0.79	49.2	50.01	8.32
MD3003	VI-746	118-120	865	860	63.92	18.24	16.97	4.77
MD3003	VI-746	138-140	885	880	60.61	23	16.39	4.98
MD3003	VII-896	8-10	905	900	65.38	23.97	10.66	4.70
MD3003	VII-896	28-30	925	920	52.54	31.81	15.65	5.18
MD3003	VII-896	48-50	945	940	34.47	47.13	18.4	5.69
MD3003	VII-896	68-70	965	960	60.58	31.97	7.46	4.55
MD3003	VII-896	88-90	985	980	74.97	15.72	9.3	4.46
MD3003	VII-896	108-110	1005	1000	75.59	11.22	13.19	4.41
MD3003	VII-896	128-130	1025	1020	60.82	17.59	20.55	5.02
MD3003	VII-896	148-150	1045	1040	25.07	46.92	28.01	6.52
MD3003	VIII-1046	20-22	1067	1062	30.79	44.25	24.96	6.15
MD3003	VIII-1046	40-42	1087	1082	17.23	57.16	25.61	6.42
MD3003	VIII-1046	60-62	1107	1102	78.32	10.92	10.76	4.22
MD3003	VIII-1046	80-82	1127	1122	75.63	15.97	8.36	4.32
MD3003	VIII-1046	100-102	1147	1142	76.15	12.51	11.31	4.38
MD3003	VIII-1046	120-122	1167	1162	76.08	16.07	7.85	4.39
MD3003	VIII-1046	140-142	1187	1182	10.91	51.91	37.17	7.26
MD3003	IX-1196	10-12	1207	1202	71.01	16.03	12.95	4.66
MD3003	IX-1196	30-32	1227	1222	28.89	44.88	26.23	6.27
MD3003	IX-1196	50-52	1247	1242	84.82	7.19	7.88	3.82
MD3003	IX-1196	70-72	1267	1262	1.92	57.38	40.7	7.70
MD3003	IX-1196	90-92	1287	1282	2.44	50.83	46.62	8.07

MD3004	I-0	5-7	6	No Correction	47.29	28.92	23.79	5.81
MD3004	I-0	25-27	26		33.55	33.6	32.85	6.67
MD3004	I-0	45-47	46		60.36	19.9	19.74	5.34

Core	Section	Interval	Midpoint Depth (cm)	Gap Corrected Midpoint Depth (cm)	Percent			Mean φ
					Sand	Silt	Clay	
MD3004	I-0	65-67	66		58.47	21.41	20.12	5.37
MD3004	I-0	85-87	86		52.84	26.85	20.32	5.45
MD3004	I-0	105-107	106		56.43	25.65	17.8	5.29
MD3004	I-0	125-127	126		53.13	27.44	19.42	5.37
MD3004	I-0	145-147	146		50.18	30.49	19.32	5.48
MD3004	II-150	15-17	166		47.62	32.48	19.89	5.57
MD3004	II-150	35-37	186		50.72	30.54	18.54	5.40
MD3004	II-150	55-57	206		44.46	35.86	19.68	5.62
MD3004	II-150	75-77	226		42.36	37.55	20	5.60
MD3004	II-150	95-97	246					
MD3004	II-150	115-117	266		33.14	43.29	23.52	6.09
MD3004	II-150	138-140	289		22.26	61.51	16.23	5.80
MD3004	III-300	5-7	306		31.3	45.17	23.51	6.12
MD3004	III-300	25-27	326		24.59	47.28	28.13	6.53
MD3004	III-300	45-47	346		29.58	45.62	24.8	6.22
MD3004	III-300	65-67	366		37.54	37.93	24.53	6.03
MD3004	III-300	85-87	386		34.84	39.52	25.63	6.10
MD3004	III-300	105-107	406		43.16	35.81	21.01	5.51
MD3004	III-300	125-127	426		23.33	56	20.67	6.17
MD3004	III-300	145-147	446		22.29	47.19	30.52	6.74
MD3004	IV-450	15-17	466		8.73	49.34	41.93	7.75
MD3004	IV-450	35-37	486		16.48	48.74	34.78	7.14
MD3004	IV-450	55-57	506		20.47	48.57	30.96	6.80
MD3004	IV-450	75-77	526		14.25	52.12	33.62	7.07
MD3004	IV-450	95-97	546		7.47	55.48	37.05	7.51
MD3004	IV-450	115-117	566		11.13	54.04	34.61	7.17
MD3004	IV-450	135-137	586		9.14	64.26	26.6	6.73
MD3004	V-600	5-7	606		5.04	57.11	37.85	7.52
MD3004	V-600	25-27	626		13.42	52.47	34.11	7.12
MD3004	V-600	45-47	646		10.32	60.37	29.3	6.81
MD3004	V-600	65-67	666		9.84	53.67	36.49	7.31
MD3004	V-600	85-87	686		5.36	55.19	39.45	7.68
MD3004	V-600	105-107	706		6.77	54.79	38.43	7.50
MD3004	V-600	125-127	726		10.64	52.66	36.7	7.21
MD3004	V-600	145-147	746		3.04	51.84	45.12	8.00
MD3004	VI-750	15-17	766		7.43	51.83	40.74	7.64
MD3004	VI-750	35-37	786		6.23	57.34	36.43	7.38
MD3004	VI-750	55-57	806		8.96	54.37	36.67	7.39
MD3004	VI-750	75-77	826		6.55	52.65	40.8	7.53
MD3004	VI-750	95-97	846		3.62	46.48	49.9	8.14
MD3004	VI-750	115-117	866		5.4	51.91	42.65	7.72
MD3004	VI-750	135-137	886		7.22	50.23	42.5	7.72
MD3004	VII-900	5-7	906		5.76	52.04	42.09	7.66
MD3004	VII-900	24-26	925		7.4	62.47	30.13	6.94
MD3004	VII-900	45-47	946		5.13	46.97	47.91	8.13
MD3004	VII-900	65-67	966		3.02	48.68	48.3	8.09

Core	Section	Interval	Midpoint Depth (cm)	Gap Corrected Midpoint Depth (cm)	Percent Sand	Percent Silt	Percent Clay	Mean φ
MD3004	VII-900	85-87	986		3.88	47.12	49.01	8.15
MD3004	VII-900	105-107	1006		5.68	49.49	44.83	7.85
MD3004	VII-900	125-127	1026		4.68	46.74	48.59	8.13
MD3004	VII-900	145-147	1046		5.21	53.08	41.71	7.68
MD3004	VIII-1050	15-17	1066		5.28	48.86	45.86	7.97
MD3004	VIII-1050	35-37	1086		3.97	49.58	46.45	8.03
MD3004	VIII-1050	55-57	1106		6.12	52.19	41.69	7.65
MD3004	VIII-1050	75-77	1126		4.89	50.74	44.36	7.80
MD3004	VIII-1050	95-97	1146		6.66	50.73	42.6	7.67
MD3004	VIII-1050	115-117	1166		7.86	46.99	45.15	7.81
MD3004	VIII-1050	135-137	1186		6.95	49.58	43.47	7.70
MD3004	IX-1200	5-7	1206		7.84	47.58	44.58	7.80
MD3004	IX-1200	25-27	1226		6.91	47.48	45.6	7.88
MD3004	IX-1200	45-47	1246		6.03	47.42	46.55	7.92
MD3004	IX-1200	65-67	1266		8.14	51.14	40.72	7.57
MD3004	IX-1200	85-87	1286		7.88	51.15	40.97	7.54
MD3004	IX-1200	105-107	1306		6.94	51.81	41.25	7.49
MD3004	IX-1200	125-127	1326		9.31	52.24	38.45	7.29
MD3004	IX-1200	145-147	1346		10.73	55.3	33.97	7.02
MD3004	X-1350	15-17	1366		7.64	54.09	38.27	7.43
MD3004	X-1350	35-37	1386		12.69	53.3	34.01	7.02
MD3004	X-1350	55-57	1406		23.06	44.3	32.64	6.71
MD3004	X-1350	75-77	1426		15.75	51.65	32.6	6.87
MD3004	X-1350	95-97	1446		14.77	49.18	36.06	7.11
MD3004	X-1350	115-117	1466		11.42	49.31	39.2	7.40
MD3004	X-1350	135-137	1486		12.31	50.49	37.19	7.25
MD3004	XI-1500	5-7	1506		11.37	51.53	37.09	7.20
MD3004	XI-1500	25-27	1526		15.14	48.78	36.09	7.12
MD3004	XI-1500	45-47	1546		16.91	51.02	32.06	6.81
MD3004	XI-1500	65-67	1566		19.38	51.49	29.13	6.57
MD3004	XI-1500	85-87	1586		22.86	50.9	26.24	6.30
MD3004	XI-1500	105-107	1606		18.91	53.77	27.32	6.41
MD3004	XI-1500	125-127	1626		24.91	48.59	26.5	6.26

MD3006	I-0	10-12	11	11	0.36	44.43	55.2	8.72
MD3006	I-0	30-32	31	31	1.64	51.15	47.21	8.12
MD3006	I-0	50-52	51	51	2.1	52.49	45.41	8.13
MD3006	I-0	70-72	71	71	1.46	53.21	45.32	8.10
MD3006	I-0	90-93	91.5	91.5	2.54	53.35	44.11	7.91
MD3006	I-0	110-113	111.5	111.5	3.95	53.14	42.88	7.91
MD3006	I-0	130-133	131.5	131.5	6.47	54.35	39.18	7.57
MD3006	II-150	5-8	156.5	156.5	6.28	52.11	41.61	7.74
MD3006	II-150	25-28	176.5	176.5	8.16	54.9	36.94	7.38
MD3006	II-150	45-48	196.5	196.5	10.08	50.75	39.16	7.50
MD3006	II-150	65-68	216.5	216.5	5.92	55.19	38.89	7.59
MD3006	II-150	85-88	236.5	236.5	8.06	55.66	36.28	7.36

Core	Section	Interval	Midpoint Depth (cm)	Gap Corrected Midpoint Depth (cm)	Percent Sand	Percent Silt	Percent Clay	Mean φ
MD3006	II-150	105-108	256.5	256.5	12.23	55.3	32.43	7.03
MD3006	II-150	125-128	276.5	276.5	6.7	57.11	36.18	7.43
MD3006	II-150	145-148	296.5	296.5	6.65	57.39	35.96	7.42
MD3006	III-300	15-18	316.5	316.5	6.16	58.09	35.75	7.44
MD3006	III-300	35-38	336.5	336.5	11.4	55.9	32.64	7.10
MD3006	III-300	55-58	356.5	356.5	6.89	55.01	38.1	7.52
MD3006	III-300	75-78	376.5	376.5	8.1	52.92	38.98	7.50
MD3006	III-300	95-98	396.5	396.5	4.05	52.78	43.17	7.86
MD3006	III-300	115-118	416.5	416.5	4.59	55.14	40.23	7.67
MD3006	III-300	135-138	436.5	436.5	4.73	53.18	42.09	7.78
MD3006	IV-450	5-8	456.5	456.5	4.41	52.94	42.64	7.85
MD3006	IV-450	25-28	476.5	476.5	3.96	53.52	42.5	7.86
MD3006	IV-450	45-48	496.5	496.5	3.44	52.01	44.55	7.96
MD3006	IV-450	65-68	516.5	516.5	3.19	50.69	46.12	8.05
MD3006	IV-450	85-88	536.5	536.5	2.59	50.95	46.46	8.05
MD3006	IV-450	105-108	556.5	556.5	3.35	51.9	44.75	8.02
MD3006	IV-450	125-128	576.5	576.5	4.07	52.55	43.38	7.87
MD3006	IV-450	145-148	596.5	596.5	4.29	52.34	43.37	7.88
MD3006	V-600	15-18	616.5	616.5	3.8	53.09	43.11	7.88
MD3006	V-600	35-38	636.5	636.5	3.57	53.87	42.56	7.89
MD3006	V-600	55-58	656.5	656.5	5.03	53.12	41.85	7.73
MD3006	V-600	75-78	676.5	676.5	4.1	54.65	41.25	7.82
MD3006	V-600	95-98	696.5	696.5	3.77	52.5	43.72	7.93
MD3006	V-600	115-118	716.5	716.5	4.76	53.45	41.79	7.79
MD3006	V-600	135-138	736.5	736.5	5.58	53.63	40.79	7.66
MD3006	VII-900	22-25	923.5	750.5	5.99	53.86	40.15	7.68
MD3006	VII-900	42-45	943.5	770.5	5.96	53.3	40.74	7.69
MD3006	VII-900	62-65	963.5	790.5	8.4	52.37	39.23	7.50
MD3006	VII-900	82-85	983.5	810.5	10.52	51.74	37.75	7.36
MD3006	VII-900	102-105	1003.5	830.5	15.84	49.57	34.59	7.06
MD3006	VII-900	122-125	1023.5	850.5	18.82	46.92	34.25	6.93
MD3006	VII-900	142-145	1043.5	870.5	8.69	51.35	39.96	7.54
MD3006	VIII-1050	5-8	1056.5	883.5	4.17	51.34	44.49	7.95
MD3006	VIII-1050	25-28	1076.5	903.5	3.01	52.34	44.64	7.99
MD3006	VIII-1050	45-48	1096.5	923.5	5.27	49.89	44.84	7.86
MD3006	VIII-1050	65-68	1116.5	943.5	2.71	51.46	45.83	8.06
MD3006	VIII-1050	85-88	1136.5	963.5	4.41	53.35	42.24	7.82
MD3006	VIII-1050	105-108	1156.5	983.5	3.44	52.09	44.47	7.92
MD3006	VIII-1050	125-128	1176.5	1003.5	2.93	52.26	44.81	8.04
MD3006	VIII-1050	145-148	1196.5	1023.5	3.52	51.66	44.8	8.01
MD3006	IX-1200	5-8	1206.5	1033.5	3.01	52.03	44.96	8.02
MD3006	IX-1200	25-28	1226.5	1053.5	2.62	50.36	47.02	8.17
MD3006	IX-1200	45-48	1246.5	1073.5	2.93	49.77	47.3	8.16
MD3006	IX-1200	65-68	1266.5	1093.5	3.01	50.3	46.7	8.11
MD3006	IX-1200	85-88	1286.5	1113.5	3.26	50.7	46.04	8.11
MD3006	IX-1200	105-108	1306.5	1133.5	2.52	50.72	46.76	8.09

Core	Section	Interval	Midpoint Depth (cm)	Gap Corrected Midpoint Depth (cm)	Percent			Mean φ
					Sand	Silt	Clay	
MD3006	IX-1200	125-128	1326.5	1153.5	2.7	52.21	45.01	8.06
MD3006	IX-1200	145-148	1346.5	1173.5	3.59	49.88	46.53	8.14
MD3006	X-1350	5-8	1356.5	1183.5	3.53	50.82	45.65	8.08
MD3006	X-1350	25-28	1376.5	1203.5	3.46	49.3	47.24	8.13
MD3006	X-1350	45-48	1396.5	1223.5	4.64	48.3	47.06	8.07
MD3006	X-1350	65-68	1416.5	1243.5	3.54	47.84	48.62	8.18
MD3006	X-1350	85-88	1436.5	1263.5	2.84	51.36	45.8	8.01
MD3006	X-1350	105-108	1456.5	1283.5	3.96	47.18	48.86	8.18
MD3006	X-1350	125-128	1476.5	1303.5	3.35	48.81	47.84	8.15
MD3006	X-1350	145-148	1496.5	1323.5	4.32	48.18	47.51	8.09
MD3006	XI-1500	5-8	1506.5	1333.5	4.44	46.85	48.71	8.14
MD3006	XI-1500	25-28	1526.5	1353.5	3.16	47.21	49.63	8.21
MD3006	XI-1500	45-48	1546.5	1373.5	4.85	48.55	46.6	8.24
MD3006	XI-1500	62-65	1563.5	1390.5	4.3	47.56	48.14	8.11
MD3006	XI-1500	85-88	1586.5	1413.5	4.74	48.32	46.95	8.12
MD3006	XI-1500	105-108	1606.5	1433.5	3.94	47.12	48.92	8.26
MD3006	XI-1500	125-128	1626.5	1453.5	3.49	48.64	47.86	8.19
MD3006	XI-1500	145-148	1646.5	1473.5	6.82	47.53	45.65	7.94
MD3006	XII-1650	5-8	1656.5	1483.5	5.3	49.47	45.23	7.94
MD3006	XII-1650	25-28	1676.5	1503.5	4.96	48.08	46.95	8.07
MD3006	XII-1650	45-48	1696.5	1523.5	5.2	49.15	45.65	7.95
MD3006	XII-1650	65-68	1716.5	1543.5	6.6	49.6	43.8	7.85
MD3006	XII-1650	87-90	1738.5	1565.5	5.15	49.56	45.29	8.05
MD3006	XII-1650	105-108	1756.5	1583.5	5.43	46.64	47.93	8.15
MD3006	XII-1650	125-128	1776.5	1603.5	6.53	45.49	47.98	8.11
MD3006	XII-1650	145-148	1796.5	1623.5	5.04	47.35	47.61	8.13
MD3006	XIII-1800	5-8	1806.5	1633.5	8.02	42.84	49.14	8.13
MD3006	XIII-1800	25-28	1826.5	1653.5	8.33	44.91	46.76	7.99
MD3006	XIII-1800	45-48	1846.5	1673.5	10.16	44.28	45.56	7.82
MD3006	XIII-1800	65-68	1866.5	1693.5	10.37	43.41	46.22	7.84
MD3006	XIII-1800	85-88	1886.5	1713.5	11.41	42.01	46.58	7.85
MD3006	XIII-1800	105-108	1906.5	1733.5	14.38	41.54	44.08	7.65
MD3006	XIII-1800	125-128	1926.5	1753.5	10.67	39.61	49.72	8.09
MD3006	XIII-1800	145-148	1946.5	1773.5	9.19	41.7	49.09	8.10
MD3006	XIV-1950	5-8	1956.5	1783.5	9.56	43.2	47.23	7.98
MD3006	XIV-1950	25-28	1976.5	1803.5	10.75	42.22	47.03	7.90
MD3006	XIV-1950	45-48	1996.5	1823.5	9.69	42.94	47.38	8.00
MD3006	XIV-1950	65-68	2016.5	1843.5	11.13	43.68	45.19	7.83
MD3006	XIV-1950	85-88	2036.5	1863.5	8.97	43.86	47.18	7.96
MD3006	XIV-1950	105-108	2056.5	1883.5	8.25	43.58	48.17	8.10
MD3006	XIV-1950	125-128	2076.5	1903.5	10.09	45.05	44.86	7.83
MD3006	XIV-1950	145-148	2096.5	1923.5	7.74	48	44.26	7.86
MD3006	XV-2100	5-8	2106.5	1933.5	7.26	48.34	44.4	7.77
MD3006	XV-2100	25-28	2126.5	1953.5	8.83	45.54	45.63	7.88
MD3006	XV-2100	45-48	2146.5	1973.5	9.78	49.38	40.84	7.56
MD3006	XV-2100	65-68	2166.5	1993.5	10.54	49.12	40.34	7.54

Core	Section	Interval	Midpoint Depth (cm)	Gap Corrected Midpoint Depth (cm)	Percent Sand	Percent Silt	Percent Clay	Mean φ
MD3006	XV-2100	85-88	2186.5	2013.5	13.01	47.46	39.39	7.42
MD3006	XV-2100	105-108	2206.5	2033.5	6.74	48.92	44.33	7.86
MD3006	XV-2100	125-128	2226.5	2053.5	7.41	50.56	42.03	7.73
MD3006	XV-2100	145-148	2246.5	2073.5	8.91	51.14	39.96	7.56
MD3006	XVI-2250	5-8	2256.5	2083.5	10.24	52.03	37.73	7.37
MD3006	XVI-2250	25-28	2276.5	2103.5	13.29	53.06	33.65	7.04
MD3006	XVI-2250	45-48	2296.5	2123.5	9.02	56.18	34.81	7.23
MD3006	XVI-2250	65-68	2316.5	2143.5	8.12	56.85	34.84	7.19
MD3006	XVI-2250	85-88	2336.5	2163.5	12.02	57.03	30.71	6.99
MD3006	XVI-2250	105-108	2356.5	2183.5	17.7	55.48	26.81	6.57
MD3006	XVI-2250	125-128	2376.5	2203.5	17.81	52.52	29.65	6.77
MD3006	XVI-2250	145-148	2396.5	2223.5	18.29	52.82	28.88	6.71
MD3006	XVII-2400	5-8	2406.5	2233.5	25.89	46.19	27.91	6.49
MD3006	XVII-2400	25-28	2426.5	2253.5	58.49	29.32	12.19	4.94
MD3006	XVII-2400	45-48	2446.5	2273.5	58.6	28.77	12.6	4.93
MD3006	XVII-2400	65-68	2466.5	2293.5	65.22	22.91	11.86	4.78
MD3006	XVII-2400	85-88	2486.5	2313.5	69.15	23.04	7.8	4.46
MD3006	XVII-2400	105-108	2506.5	2333.5	62.19	26.57	11.23	4.78
MD3006	XVII-2400	125-128	2526.5	2353.5	60.98	28.46	10.54	4.75
MD3006	XVIII-2534	5-8	2540.5	2367.5	59.7	30.48	9.81	4.73
MD3007	I-0	2-5	3.5	3.5	10.17	45.66	44.17	7.81
MD3007	I-0	22-25	23.5	23.5	16.02	46.36	37.56	7.21
MD3007	I-0	42-45	43.5	43.5	12.07	56.12	31.72	7.00
MD3007	I-0	62-65	63.5	63.5	30.4	39.36	30.24	6.58
MD3007	II-71	12-14	84	84	36.9	37.37	25.69	6.12
MD3007	II-71	32-34	104	104	36.2	38.02	25.79	6.14
MD3007	II-71	52-54	124	124	41.13	33.07	25.69	6.06
MD3007	II-71	72-74	144	144	29.98	41.96	28.03	6.38
MD3007	II-71	92-94	164	164	36.67	35.32	27.97	6.24
MD3007	II-71	112-114	184	184	38.98	35.68	25.33	5.93
MD3007	II-71	132-134	204	204	18.31	48.34	33.32	7.00
MD3007	III-221	7-9	229	229	17.2	52.94	29.86	6.73
MD3007	III-221	27-29	249	249	24.21	44.32	31.47	6.71
MD3007	III-221	47-49	269	269	19.8	47.91	32.29	6.87
MD3007	III-221	67-69	289	289	24.83	43.71	31.45	6.68
MD3007	III-221	87-89	309	309	21.51	45.94	32.55	6.82
MD3007	III-221	107-109	329	329	37.81	31.57	30.62	6.22
MD3007	III-221	127-129	349	349	14.58	49.94	35.48	7.15
MD3007	III-221	147-149	369	369	12.6	51.74	35.66	7.25
MD3007	IV-371	5-7	377	377	15.39	49.04	35.53	7.10
MD3007	IV-371	25-27	397	397	13.59	51.05	35.36	7.17
MD3007	IV-371	45-47	417	417	8.61	55.52	35.87	7.33
MD3007	IV-371	65-67	437	437	7.47	59.45	33.07	7.11
MD3007	IV-371	85-87	457	457	10.23	57.6	32.17	6.99
MD3007	IV-371	105-107	477	477	10.31	52.28	36.02	7.12

Core	Section	Interval	Midpoint Depth (cm)	Gap Corrected Midpoint Depth (cm)	Percent Sand	Percent Silt	Percent Clay	Mean φ
MD3007	IV-371	125-127	497	497	9.69	52.96	37.35	7.39
MD3007	IV-371	145-147	517	517	10.57	55.74	33.68	7.15
MD3007	V-521	5-7	527	527	9.76	52.89	37.35	7.34
MD3007	V-521	25-27	547	547	7.74	59.68	32.58	7.04
MD3007	V-521	45-47	567	567	3.58	60.89	35.53	7.40
MD3007	V-521	65-67	587	587	5.04	59.81	35.15	7.35
MD3007	V-521	85-87	607	607	2.99	62.12	34.89	7.34
MD3007	V-521	105-107	627	627	2.28	64.72	33	7.31
MD3007	V-521	125-127	647	647	4	56.75	39.25	7.59
MD3007	V-521	145-147	667	667	5.19	64.57	30.24	6.98
MD3007	VI-671	7-9	679	679	6.65	61.18	32.17	7.06
MD3007	VI-671	25-27	697	697	7.86	53.79	38.35	7.48
MD3007	VI-671	45-47	717	717	4.95	53.36	41.5	7.69
MD3007	VI-671	65-67	737	737	9.35	52.39	38.26	7.39
MD3007	VI-671	85-87	757	757	9.63	55.11	35.26	7.27
MD3007	VI-671	105-107	777	777	5.96	54.64	39.4	7.55
MD3007	VI-671	125-127	797	797	7.95	62.67	29.38	6.87
MD3007	VI-671	145-147	817	817	5.25	57.59	37.16	7.44
MD3007	VII-821	5-7	827	827	18.09	50.66	31.26	6.78
MD3007	VII-821	25-27	847	847	5.41	52.95	41.64	7.63
MD3007	VII-821	45-47	867	867	3.36	61.94	34.7	7.33
MD3007	VII-821	65-67	887	887	2.64	52.14	45.23	8.02
MD3007	VII-821	85-87	907	907	4.71	56.95	38.35	7.50
MD3007	VII-821	105-107	927	927	2.42	54.34	43.24	7.91
MD3007	VII-821	125-127	947	947	6.37	51.23	42.4	7.69
MD3007	VII-821	145-147	967	967	7.08	56.9	36.02	7.29
MD3007	VIII-971	5-7	977	977	4.65	53.87	41.49	7.59
MD3007	VIII-971	25-27	997	997	4.2	56.46	39.34	7.57
MD3007	VIII-971	45-47	1017	1017	4.33	53.67	42.01	7.79
MD3007	VIII-971	65-67	1037	1037	4.19	57.62	38.19	7.63
MD3007	VIII-971	85-87	1057	1057	5.1	56.59	38.31	7.45
MD3007	VIII-971	105-107	1077	1077	3.98	60.85	35.17	7.29
MD3007	VIII-971	125-127	1097	1097	3.83	51.9	44.27	7.94
MD3007	VIII-971	145-147	1117	1117	3.05	56.69	40.26	7.69
MD3007	IX-1121	5-7	1127	1127	3.41	54.32	42.26	7.82
MD3007	IX-1121	25-27	1147	1147	4.91	51.06	44.04	7.85
MD3007	IX-1121	45-47	1167	1167	2.7	52.57	44.73	8.00
MD3007	IX-1121	65-67	1187	1187	2.96	50.18	46.86	8.10
MD3007	IX-1121	85-87	1207	1207	3.2	53.05	43.74	7.88
MD3007	IX-1121	105-107	1227	1227	4.31	49.3	46.38	8.04
MD3007	IX-1121	125-127	1247	1247	4.6	51.31	44.09	7.90
MD3007	IX-1121	145-147	1267	1267	4.3	53.15	42.54	7.77
MD3007	X-1271	5-7	1277	1277	2.26	53.59	44.15	7.94
MD3007	X-1271	25-27	1297	1297	4.46	52.19	43.35	7.85
MD3007	X-1271	120-122	1392	1320	4.41	50.19	45.39	7.99
MD3007	X-1271	140-142	1412	1340	7.54	51.17	41.29	7.68

Core	Section	Interval	Midpoint Depth (cm)	Gap Corrected Midpoint Depth (cm)	Percent Sand	Percent Silt	Percent Clay	Mean φ
MD3007	XI-1421	5-7	1427	1355	13.63	48.33	38.04	7.32
MD3007	XI-1421	25-27	1447	1375	3.65	46.72	49.63	8.21
MD3007	XI-1421	45-47	1467	1395	2.89	46.95	50.15	8.26
MD3007	XI-1421	65-67	1487	1415	2.59	49.3	48.1	8.15
MD3007	XI-1421	85-87	1507	1435	1.54	53.93	44.53	7.92
MD3007	XI-1421	105-107	1527	1455	3.15	46.42	50.42	8.30
MD3007	XI-1421	125-127	1547	1475	2.86	51.38	45.76	7.97
MD3007	XI-1421	145-147	1567	1495	3.02	48.93	48.06	8.13
MD3007	XII-1571	5-7	1577	1505	2.25	49.42	48.33	8.16
MD3007	XII-1571	25-27	1597	1525	1.8	46.16	52.05	8.38
MD3007	XII-1571	45-47	1617	1545	2.57	51.84	45.57	7.98
MD3007	XII-1571	65-67	1637	1565	2.4	50.76	46.84	8.00
MD3007	XII-1571	85-87	1657	1585	3.69	55.54	40.76	7.53
MD3007	XII-1571	105-107	1677	1605	4.05	47.2	48.74	8.09
MD3007	XII-1571	125-127	1697	1625	5.72	47.77	46.51	7.95
MD3007	XII-1571	145-147	1717	1645	2.64	55.68	41.69	7.71
MD3007	XIII-1721	5-7	1727	1655	3.06	53.85	43.08	7.76
MD3007	XIII-1721	25-28	1747.5	1675.5	2.78	58.47	38.75	7.57
MD3007	XIII-1721	45-47	1767	1695	2.85	51.15	46	7.96
MD3007	XIII-1721	65-67	1787	1715	3.93	51.39	44.68	7.90
MD3007	XIII-1721	85-87	1807	1735	3.85	50	46.16	7.95
MD3007	XIII-1721	105-107	1827	1755	4.01	48.43	47.56	8.04
MD3007	XIII-1721	125-127	1847	1775	4.71	52.36	42.94	7.77
MD3007	XIII-1721	145-147	1867	1795	4.99	54.39	40.57	7.63
MD3007	XIV-1871	5-7	1877	1805	8.62	60.82	30.55	6.87
MD3007	XIV-1871	25-27	1897	1825	5.02	62.25	29.73	6.83
MD3007	XIV-1871	45-47	1917	1845	9.38	47.59	43.02	7.70
MD3007	XIV-1871	65-67	1937	1865	14.43	44.78	40.8	7.42
MD3007	XIV-1871	85-87	1957	1885	6.47	56.4	37.13	7.32
MD3007	XIV-1871	105-107	1977	1905	2.7	71.27	26.03	6.57
MD3007	XIV-1871	125-127	1997	1925	6.07	64.66	29.27	6.85
MD3007	XIV-1871	145-147	2017	1945	2.93	58.14	38.92	7.63
MD3007	XV-2021	5-7	2027	1955	1.6	66.93	31.48	7.26
MD3007	XV-2021	25-27	2047	1975	8.11	50.48	41.41	7.63
MD3007	XV-2021	45-47	2067	1995	4.85	60.52	34.62	7.28
MD3007	XV-2021	65-67	2087	2015	3.43	52.29	44.29	7.89
MD3007	XV-2021	85-87	2107	2035	4.28	68.96	26.76	6.80
MD3007	XV-2021	105-107	2127	2055	11.77	46.43	41.8	7.63
MD3007	XV-2021	125-127	2147	2075	10.42	50.59	38.99	7.39
MD3007	XV-2021	145-147	2167	2095	11.74	54.43	33.83	7.03
MD3007	XVI-2171	5-7	2177	2105	8.6	60.02	31.34	6.93
MD3007	XVI-2171	25-27	2197	2125	14.42	58.66	26.93	6.55
MD3007	XVI-2171	45-47	2217	2145	9.33	54.01	36.66	7.25
MD3007	XVI-2171	65-67	2237	2165	13.58	50.31	36.1	7.17

Appendix 4B: Marion DuFresne grain size analyses (Sieve and Pipette)

Core	Sample Type	Sample Interval	Gap Corrected Depth (cm)	Percent			Age
				Sand	Silt	Clay	
MD3001	TARGET	42-42.5	642.25	8.44	42.37	49.18	4561
MD3001	TARGET	44-44.5	644.25	7.88	58.68	33.44	4572
MD3001	TARGET	50-51	650.5	7.72	61.69	30.60	4603
MD3001	TARGET	67-68	667.5	3.50	59.23	37.27	4689
MD3001	TARGET	29-30	779.5	5.02	64.83	30.16	5248
MD3001	TARGET	35.5-36	785.75	7.35	56.11	36.54	5271
MD3001	TARGET	42-43	792.5	2.80	65.92	31.28	5295
MD3001	TARGET	51-51.5	801.25	3.80	51.40	44.81	5328
MD3001	TARGET	53-54	803.5	2.93	58.60	38.47	5336
MD3001	TARGET	71-72	821.5	5.50	63.66	30.83	5402
MD3001	TARGET	75.5-76.5	825.75	2.72	55.99	41.29	5417
MD3001	TARGET	85.5-86	835.75	33.72	50.59	15.69	5454
MD3001	TARGET	87.5-88	837.75	6.46	48.65	44.89	5461
MD3001	TARGET	94-95	844.5	14.77	59.14	26.09	5486
MD3001	TARGET	53.5-54.5	954	0.49	73.31	26.20	5887
MD3001	TARGET	57-58	957.5	1.25	44.32	54.43	5900
MD3001	TARGET	62.5-63.5	963	1.14	43.49	55.37	5920
MD3001	TARGET	66.5-67	965.75	1.46	37.74	60.80	5930
MD3001	TARGET	67.5-68	967.75	6.86	45.94	47.20	5938
MD3001	TARGET	68-69	968.5	6.70	60.14	33.16	5940
MD3001	TARGET	113.5-114	1013.75	2.07	52.56	45.37	6106
MD3001	TARGET	118-119	1018.5	2.85	54.77	42.38	6124
MD3001	TARGET	123-123.5	1023.25	3.81	41.90	54.29	6141
MD3001	TARGET	46.5-47	1246.75	5.63	60.76	33.61	6804
MD3001	TARGET	47-47.5	1247.25	7.57	66.50	25.93	6805
MD3001	TARGET	107.5-108.5	1308	0.47	79.40	20.13	6923
MD3001	TARGET	109-109.5	1309.25	0.51	32.66	66.82	6925
MD3001	TARGET	116.5-117.5	1317	3.17	59.68	37.15	6940
MD3001	TARGET	22.5-23.5	1372.75	1.92	63.62	34.46	7049
MD3001	TARGET	28.5-29	1378.75	13.78	71.13	15.09	7060
MD3001	TARGET	29-29.5	1379.25	11.37	66.80	21.83	7061
MD3001	TARGET	30.5-31	1380.75	2.36	52.17	45.46	7064
MD3001	TARGET	34-34.5	1384.25	3.59	49.29	47.12	7071
MD3001	TARGET	106.5-107	1456.75	12.34	60.42	27.23	7246
MD3001	TARGET	109-109.5	1459.25	2.75	35.41	61.84	7256
MD3001	TARGET	113-114	1463.5	4.14	53.86	42.00	7273
MD3001	TARGET	118-119	1468.5	1.68	62.03	36.30	7293
MD3001	TARGET	76-76.5	1576.25	1.05	49.80	49.16	7724
MD3001	TARGET	81-81.5	1581.25	1.02	51.78	47.20	7744
MD3001	TARGET	82-82.5	1582.25	1.03	73.61	25.35	7748
MD3001	TARGET	83.5-84	1583.75	0.64	76.70	22.66	7754
MD3001	SURVEY	128-130	1629	4.11	57.76	38.12	7935
MD3001	SURVEY	148-150	1649	3.66	63.63	32.72	8015
MD3001	SURVEY	2-4	1653	4.01	53.88	42.11	8031

Core	Sample Type	Sample Interval	Gap Corrected Depth (cm)	Percent			Age
				Sand	Silt	Clay	
MD3001	SURVEY	18-20	1669	3.20	54.90	41.90	8095
MD3001	SURVEY	38-40	1689	2.62	52.97	44.41	8175
MD3001	SURVEY	118-120	1769	4.57	71.42	24.01	8431
MD3001	SURVEY	138-140	1789	3.30	57.04	39.66	8466
MD3001	SURVEY	2-4.5	1803.25	8.16	91.84	0.00	8490
MD3001	SURVEY	3-5	1804	4.18	84.78	11.04	8491
MD3001	SURVEY	8-10	1809	2.64	57.29	40.07	8500
MD3001	TARGET	27-28	1827.5	8.00	62.72	29.27	8532
MD3001	TARGET	89.5-90	1889.75	2.57	55.31	42.12	8640
MD3001	TARGET	98-99	1898.5	1.85	46.52	51.64	8655
MD3001	SURVEY	108-110	1909	3.55	51.22	45.23	8673
MD3001	TARGET	111-112	1911.5	3.25	57.82	38.94	8677
MD3001	TARGET	115-115.5	1915.25	5.49	48.89	45.61	8684
MD3001	SURVEY	128-130	1929	2.75	56.60	40.65	8708
MD3001	SURVEY	148-150	1949	18.59	62.25	19.15	8742
MD3001	SURVEY	3-5	1954	7.89	69.25	22.86	8751
MD3001	SURVEY	13-15	1964	5.10	57.68	37.22	8768
MD3001	SURVEY	33-35	1984	12.78	69.99	17.23	8803
MD3001	SURVEY	113-115	2064	3.74	49.73	46.53	8941
MD3001	SURVEY	133-135	2084	5.36	84.71	9.93	8976
MD3001	SURVEY	3-5	2104	11.40	68.53	20.06	9025
MD3001	SURVEY	48-50	2149	15.77	71.51	12.71	9138
MD3001	TARGET	75-75.5	2175.25	3.58	46.31	50.11	9204
MD3001	TARGET	78.5-79	2178.75	7.41	47.47	45.13	9213
MD3001	TARGET	79.5-80.5	2179.75	19.22	47.49	33.29	9216
MD3001	TARGET	81-81.5	2181.25	9.11	54.49	36.40	9219
MD3001	TARGET	84-84.5	2184.25	7.71	51.57	40.72	9234
MD3001	SURVEY	88-90	2189	23.43	74.69	1.88	9259
MD3001	SURVEY	48-50	2249	11.37	53.18	35.45	9574
MD3004	TARGET	122.5-123	422.75	22.72	66.61	10.67	3486
MD3004	SURVEY	128-128.5	428.25	18.46	81.54	0.00	3500
MD3004	TARGET	132.5-133	432.75	69.14	30.86	0.00	3502
MD3004	TARGET	142-143	442.5	28.03	47.58	24.39	3506
MD3004	TARGET	52.5-53	652.75	6.03	65.70	28.26	5265
MD3004	TARGET	61-61.5	661.25	9.39	61.27	29.34	5283
MD3004	TARGET	72.5-73	672.75	3.38	52.19	44.43	5307
MD3004	TARGET	79.5-80	679.75	4.89	67.06	28.04	5322
MD3004	TARGET	83-83.5	683.25	7.78	47.98	44.24	5330
MD3004	TARGET	85-85.5	685.25	4.58	40.36	55.06	5334
MD3004	TARGET	86.5-87.5	687	1.71	61.28	37.01	5338
MD3004	TARGET	89-89.5	689.25	6.71	55.56	37.73	5343
MD3004	TARGET	91.5-92	691.75	8.01	56.74	35.25	5348
MD3004	TARGET	48-49	798.5	4.49	56.21	39.30	6263
MD3004	TARGET	55-55.5	805.25	8.81	57.42	33.77	6287
MD3004	TARGET	57-57.5	807.25	7.22	57.59	35.19	6295

Core	Sample Type	Sample Interval	Gap Corrected Depth (cm)	Percent			Age
				Sand	Silt	Clay	
MD3004	TARGET	62-63	812.5	3.47	47.47	49.05	6313
MD3004	TARGET	80.5-81.5	831	4.43	41.97	53.60	6365
MD3004	TARGET	85-85.5	835.25	1.73	50.79	47.48	6374
MD3004	TARGET	90-90.5	840.25	6.06	53.76	40.19	6385
MD3004	TARGET	92-92.5	842.25	5.78	56.00	38.22	6389
MD3004	TARGET	95.5-96.5	846	1.29	47.41	51.30	6397
MD3004	TARGET	98.5-99	848.75	7.24	54.23	38.53	6403
MD3004	TARGET	33.5-34.5	934	15.26	84.74	0.00	6583
MD3004	TARGET	38-38.5	938.25	27.85	69.67	2.47	6592
MD3004	TARGET	45.5-46	945.75	14.25	62.90	22.85	6607
MD3004	TARGET	47-47.5	947.25	4.30	49.03	46.67	6611
MD3004	TARGET	50-51	950.5	3.35	53.60	43.05	6618
MD3006	TARGET	129-130	1027	2.34	55.88	41.78	4226
MD3006	TARGET	134-135	1027	2.35	55.17	42.48	4238
MD3006	TARGET	137.5-138	1027	6.25	62.24	31.51	4246
MD3006	TARGET	138.5-139	1027	8.38	61.36	30.26	4248
MD3006	TARGET	99.5-100.5	1899	4.23	59.04	36.74	9542
MD3006	TARGET	104.5-105	1903.75	4.67	87.28	8.05	9559
MD3006	TARGET	111.5-112.5	1911	4.22	61.81	33.97	9586
MD3006	TARGET	114-115	1913.25	3.22	69.06	27.72	9594
MD3006	TARGET	117.5-118.5	1917	3.64	52.43	43.93	9608
MD3006	TARGET	96-97	2195.5	14.51	57.20	28.29	10780
MD3006	TARGET	99-99.5	2198.25	5.52	64.46	30.02	10793
MD3006	TARGET	103-104	2202.5	13.00	56.84	30.16	10814

Appendix 4A: Analyses performed at Skidaway Institute of Oceanography using a Sedigraph® 5100. See Chapter 1, Section 3.4 (pg. 12).

Appendix 4B: Analyses performed at the Virginia Institute of Marine Science using standard wet sieve and pipette technique. See Chapter 3, section 2.5 (pg. 137).

Appendix 5A: Marion DuFresne elemental and stable isotopic carbon and nitrogen data (Chapter 1 and 3)

Core	Depth (cm)	Gap Corrected Depth (cm)	Original Sample Size (mg)	Age	$\delta^{13}C$	Carbon (ug)	$\delta^{15}N$	Nitrogen (ug)
MD3003	1	1	31.85	45	-21.74	208.75	4.54	31.14
MD3003	45	40	30.27	962	-22.73	158.30	4.65	21.94
MD3003	95	90	35.95	1156	-21.95	195.28	5.89	30.25
MD3003	141	136	25.54	1446	-22.17	129.21	6.03	19.17
MD3003	191	186	26.21	2040	-22.05	111.48	5.33	15.68
MD3003	241	236	33.91	2399	-22.44	176.22	5.34	26.07
MD3003	291	286	27.60	2859	-22.41	152.70	5.81	22.18
MD3003	341	336	32.92	3396	-22.20	148.23	6.25	22.59
MD3003	391	386	29.91	3931	-22.75	138.16	5.68	20.31
MD3003	445	440	29.15	4913	-22.31	144.87	5.23	21.12
MD3003	495	490	29.95	5849	-22.69	166.14	5.71	22.83
MD3003	545	540	31.80	7618	-22.03	152.87	5.99	22.24
MD3003	591	586	30.92	8157	-22.33	121.39	5.21	18.43
MD3003	641	636	33.96	8901	-22.15	135.85	5.87	20.32
MD3003	686	681	30.17	9623	-22.80	128.10	6.12	18.84
MD3003	741	736	36.80	10525	-22.43	186.31	6.35	26.95
MD3003	791	786	28.99	11520	-22.83	120.27	5.82	17.45
MD3003	841	836	32.75	12558	-22.79	146.06	6.16	20.48
MD3003	894	889	27.14	13724	-22.50	114.69	5.89	16.80
MD3003	945	940	34.95	14545	-22.85	124.74	5.75	18.43
MD3003	995	990	38.53	14734	-24.00	55.70	4.45	9.23
MD3003	1046	1041	33.90	15041	-23.63	132.57	5.31	17.94
MD3003	1106	1101	38.32	15564	-23.33	157.41	5.64	21.20
MD3003	1159	1154	33.22	16015	-24.35	90.40	4.78	12.07
MD3003	1195	1190	34.57	16290	-24.17	135.92	5.74	18.11
MD3003	1281	1276	31.09	16954	-24.03	121.39	4.55	16.55

MD3004	0	None	37.52	0	-25.89	340.58	4.32	39.25
MD3004	150		38.54	963	-23.82	104.11	5.00	13.03
MD3004	300		28.29	2579	-24.98	98.10	4.57	11.59
MD3004	450		37.07	3509	-25.72	223.29	5.21	16.64
MD3004	600		33.39	4942	-25.36	200.56	4.37	19.68
MD3004	750		30.21	6089	-24.34	110.12	4.21	13.03
MD3004	900		35.41	6511	-24.62	160.81	4.61	17.52
MD3004	1050		26.64	6991	-23.79	86.21	5.69	12.39
MD3004	1200		39.79	8282	-23.74	119.98	6.37	16.64
MD3004	1350		40.18	9403	-23.99	103.09	4.11	14.00
MD3004	1500		36.17	10052	-23.83	87.57	6.22	12.79
MD3004	1630		35.69	10923	-24.16	65.15	4.48	9.10

MD3006	1	1	33.43	2	-23.43	241.33	5.54	32.98
MD3006	300	300	36.41	1459	-23.71	177.34	5.13	19.58
MD3006	450	450	29.18	2045	-23.42	144.01	4.54	18.18

Core	Depth (cm)	Gap Corrected Depth (cm)	Original Sample Size (mg)	Age	$\delta^{13}C$	Carbon (ug)	$\delta^{15}N$	Nitrogen (ug)
MD3006	600	600	28.71	2522	-23.66	148.23	5.68	18.60
MD3006	901	728	32.48	2929	-23.66	156.28	5.29	19.04
MD3006	1050	877	30.53	3385	-23.59	131.45	5.48	17.54
MD3006	1200	1027	28.98	3837	-23.43	129.21	5.58	16.96
MD3006	1350	1177	31.63	4276	-23.62	138.16	4.95	18.27
MD3006	1500	1327	30.00	4687	-23.30	122.51	5.85	17.21
MD3006	1650	1477	30.69	5101	-23.36	123.07	5.37	16.56
MD3006	1800	1627	27.72	6036	-23.40	114.31	5.65	14.56
MD3006	1950	1777	32.02	6662	-23.46	110.27	4.05	15.03
MD3006	2100	1927	25.67	7289	-23.38	81.10	4.03	11.38
MD3006	2250	2077	31.19	9891	-23.58	89.49	4.78	12.47
MD3006	2400	2227	30.61	11821	-24.37	65.94	3.94	9.48
MD3006	2534	2361	46.73	14610	-24.35	40.23	2.55	6.94
MD3007*		2		6	-24.76			
MD3007	61	61	35.94	178	-23.94	131.32	4.65	17.04
MD3007	71	71	36.63	207	-23.93	129.05	5.19	16.88
MD3007	224	224	28.52	1314	-24.95	129.05	4.47	14.56
MD3007	372	372	27.25	3749	-24.95	117.71	5.04	13.03
MD3007	521	521	34.86	4555	-24.80	117.71	4.12	14.96
MD3007	676	676	33.84	5065	-24.58	154.01	5.54	17.84
MD3007	821	821	32.90	5562	-24.76	125.65	5.66	14.88
MD3007	971	971	29.10	5939	-24.36	132.45	5.03	15.20
MD3007	1121	1121	26.24	6385	-24.38	118.84	5.44	14.80
MD3007	1272	1272	37.51	7004	-24.36	149.47	5.11	19.20
MD3007	1423	1351	36.58	7288	-24.15	144.93	4.78	18.88
MD3007	1571	1499	32.44	7681	-24.09	133.59	5.41	17.60
MD3007	1723	1651	29.86	8355	-24.08	118.84	4.73	15.28
MD3007	1871	1799	28.75	9056	-24.24	109.89	4.77	14.32
MD3007	2021	1949	29.91	9725	-24.95	129.05	4.51	14.32
MD3007	2171	2099	37.86	10306	-24.73	132.45	4.68	15.44

* Surface value for MD3007 from:

Brulet, B.R. Environmental Change of the Waipaoa watershed shown by marine sedimentary signals; North Island, New Zealand. 2009. Master's Thesis, North Carolina State University, 101 pgs.

Appendix 5B: Marion DuFresne survey and target elemental and stable isotopic carbon and nitrogen data (Chapter 3)

Sample ID	Sample Type	Midpoint Depth (cm)	Gap Corrected Depth (cm)	Original Sample Size (mg)	Age	$\delta^{13}C$	C (ug)	$\delta^{15}N$	N (ug)
3001 I-0 38-40 45 284	SURVEY	39	39	60.4	201	-24.93	404.94	3.98	55.75
3001 I-0 58-60 70 285	SURVEY	59	59	68.3	304	-24.57	390.12	3.42	65.67
3001 I-0 78-80 46 286	SURVEY	79	79	70.4	407	-24.76	378.93	1.82	49.77
3001 I-0 98-100 65 287	SURVEY	99	99	65	509	-25.00	381.80	2.27	51.62
3001 I-0 118-120 48 288	SURVEY	119	119	53.1	612	-24.36	205.13	3.68	31.78
3001 I-0 138-140 71 289	SURVEY	139	139	70.5	715	-23.96	280.55	3.33	52.45
3001 II-150 5-7 118 275	SURVEY	6	156	66.9	803	-24.15	254.85	2.65	40.15
3001 II-150 8-10 3 276	SURVEY	9	159	54.9	818	-24.65	190.57	4.28	23.01
3001 II-150 28-30 1 277	SURVEY	29	179	65.5	928	-24.13	299.66	2.67	45.96
3001 II-150 48-50 5 278	SURVEY	49	199	43.2	1159	-24.78	190.36	3.31	34.27
3001 II-150 68-70 6 279	SURVEY	69	219	67	1391	-24.73	273.15	3.30	44.58
3001 II-150 88-90 4 280	SURVEY	89	239	65.1	1623	-24.51	299.79	3.33	46.55
3001 II-150 108-110 2 281	SURVEY	109	259	61.4	1855	-24.98	299.72	3.69	47.60
3001 II-150 128-130 8 282	SURVEY	129	279	67.8	2087	-24.85	339.76	3.68	47.86
3001 II-150 147-149 7 283	SURVEY	148	298	71.5	2307	-24.51	329.39	4.49	41.64
3001 III-300 2 5-5 5 117 264	SURVEY	4	304	68.6	2376	-24.80	295.96	4.27	32.64
3001 III-300 8-10 30 265	SURVEY	9	309	45.7	2434	-24.91	227.33	2.83	30.95
3001 III-300 28-30 40 268	SURVEY	29	329	51.8	2666	-24.83	259.19	2.66	36.87
3001 III-300 48-50 17 269	SURVEY	49	349	62.1	2898	-24.64	286.66	3.06	46.88
3001 III-300 68-70 44 270	SURVEY	69	369	64.9	3126	-25.23	321.14	2.62	50.14
3001 III-300 88-90 9 271	SURVEY	89	389	51.2	3283	-25.06	214.29	1.99	36.65
3001 III-300 108-110 15 272	SURVEY	109	409	61.1	3384	-26.20	657.43	2.25	52.67
3001 III-300 128-130 43 273	SURVEY	129	429	58.7	3485	-25.34	286.47	3.49	41.43
3001 III-300 148-150 41 274	SURVEY	149	449	62.3	3585	-25.13	319.87	3.55	35.19
3001 IV-450 2-4 112 256	SURVEY	3	453	67	3606	-25.23	374.61	2.20	48.03
3001 IV-450 18-20 14 257	SURVEY	19	469	71.3	3686	-24.79	311.63	3.83	49.06
3001 IV-450 38-40 13 258	SURVEY	39	489	54.7	3787	-25.06	276.55	2.92	35.19
3001 IV-450 58-60 12 259	SURVEY	59	509	58.6	3888	-24.98	260.25	3.09	42.32
3001 IV-450 78-80 39 260	SURVEY	79	529	66.1	3989	-24.75	314.10	2.45	48.15
3001 IV-450 98-100 42 261	SURVEY	99	549	63.3	4089	-24.63	277.06	3.63	48.16
3001 IV-450 118-120 10 262	SURVEY	119	569	52.2	4190	-24.67	233.13	2.91	39.47
3001 IV-450 138-140 11 263	SURVEY	139	589	53.7	4292	-24.96	206.98	3.43	37.92
3001 V-600 2 5-5 5 109 254	SURVEY	4	604	50.5	4368	-25.87	249.73	3.74	30.78
3001 V-600 8-10 32 255	SURVEY	9	609	69.2	4393	-24.93	289.67	4.42	39.90
3001 V-600 28-30 31 266	SURVEY	29	629	47.1	4494	-24.75	196.44	4.10	30.78
3001 V 42-42 5 147 140	TARGET	42.25	642.25	64.5	4561	-25.70	313.11	4.03	46.22
3001 V 44-44 5 148 139	TARGET	44.25	644.25	55.3	4572	-25.79	253.92	4.30	39.80

Sample ID	Sample Type	Midpoint Depth (cm)	Gap Corrected Depth (cm)	Original Sample Size (mg)	Age	$\delta^{13}C$	C (ug)	$\delta^{15}N$	N (ug)
3001 V 50-51 149 138	TARGET	50.5	650.5	58.4	4603	-26.08	255.40	4.29	31.35
3001 V 54-55 150 137	TARGET	54.5	654.5	53.7	4624	-25.79	236.18	4.94	30.38
3001 V 57 5-58 151 136	TARGET	57.75	657.75	50.6	4640	-25.40	230.90	2.44	49.91
3001 V 59-59 5 152 135	TARGET	59.25	659.25	54.8	4648	-24.58	233.52	2.87	46.46
3001 V 63-63 5 153 134	TARGET	63.25	663.25	45.4	4668	-25.07	197.50	4.29	31.52
3001 V 65-65 5 154 133	TARGET	65.25	665.25	42.8	4678	-24.99	209.19	2.87	39.40
3001 V 67-68 155 132	TARGET	67.5	667.5	64	4689	-25.48	317.55	2.90	63.46
3001 V-600 68-70 36 267	SURVEY	69	669	66.9	4697	-25.25	328.52	3.83	36.98
3001 V-600 108-110 16 239	SURVEY	109	709	62	4900	-25.31	356.75	4.41	45.19
3001 VI-750 1 5-3 114 248	SURVEY	2.25	752.25	66	5119	-25.11	383.24	3.42	49.30
3001 VI-750 18-20 27 249	SURVEY	19	769	49.6	5204	-25.61	312.66	2.76	35.07
3001 VI 29-30 131 131	TARGET	29.5	779.5	64.9	5248	-25.43	147.78	4.61	28.04
3001 VI 31 5-32 132 130	TARGET	31.75	781.75	61.3	5256	-26.15	218.44	3.84	40.12
3001 VI 35 5-36 133 129	TARGET	35.75	785.75	50.2	5271	-27.38	159.33	4.88	22.96
3001 VI 37 5-38 134 128	TARGET	37.75	787.75	58.6	5278	-24.99	268.72	2.89	46.50
3001 VI 39 5-40 135 127	TARGET	39.75	789.75	58.9	5285	-25.04	244.88	6.41	28.88
3001 VI 42-43 136 126	TARGET	42.5	792.5	44.1	5295	-24.81	162.93	3.32	34.41
3001 VI 45-45 5 137 124	TARGET	45.25	795.25	59	5306	-24.82	272.22	3.27	49.38
3001 VI 48 5-49 138 125	TARGET	48.75	798.75	50	5318	-25.07	222.54	4.88	31.52
3001 VI 51-51 5 139 122	TARGET	51.25	801.25	57.9	5328	-26.36	219.91	3.00	40.12
3001 VI 53-54 140 123	TARGET	53.5	803.5	54.9	5336	-24.62	226.72	4.86	31.16
3001 VI-750 58-68 25 250	SURVEY	59	809	55.6	5356	-25.69	193.97	2.53	34.07
3001 VI 71-72 112 121	TARGET	71.5	821.5	66.9	5402	-24.67	247.84	2.74	53.01
3001 VI 75 5-76 5 113 120	TARGET	75.75	825.75	66.6	5417	-25.87	467.36	3.24	54.23
3001 VI 78-78 5 114 119	TARGET	78.25	828.25	61.1	5426	-25.65	268.66	3.98	37.15
3001 VI 81 5-82 115 118	TARGET	81.75	831.75	49.6	5439	-25.53	202.04	2.73	35.96
3001 VI 83 5-84 116 117	TARGET	83.75	833.75	65.6	5447	-24.96	100.35	1.42	41.59
3001 VI 85 5-86 117 116	TARGET	85.75	835.75	64.7	5454	-25.07	87.40	1.77	31.84
3001 VI 86-86 5 118 115	TARGET	86.25	836.25	66.5	5456	-24.96	118.00	2.20	33.21
3001 VI 87 5-88 119 114	TARGET	87.75	837.75	56	5461	-24.52	243.54	2.61	47.16
3001 VI 94-95 120 113	TARGET	94.5	844.5	43.4	5486	-24.72	167.75	3.75	29.69
3001 VI-750 98-100 19 251	SURVEY	99	849	62.4	5503	-24.83	226.58	3.14	40.45
3001 VI-750 118-120 23 252	SURVEY	119	869	66.7	5576	-25.13	291.00	3.17	49.42
3001 VI-750 138-140 33 253	SURVEY	139	889	64.6	5649	-25.39	289.55	2.65	45.96
3001 VII-900 1-4 110 240	SURVEY	2.5	902.5	65.1	5699	-25.36	323.23	3.93	42.54
3001 VII-900 8-10 72 241	SURVEY	9	909	49.7	5722	-25.95	277.99	5.18	25.86
3001 VII-900 28-30 21 242	SURVEY	29	929	62.6	5796	-24.72	249.73	5.22	34.51
3001 VII-900 48-50 28 243	SURVEY	49	949	69.2	5869	-25.40	302.55	3.39	39.13
3001 VII 53 5-54 5 156 112	TARGET	54	954	57.8	5887	-25.03	182.03	2.25	46.81

Sample ID	Sample Type	Midpoint Depth (cm)	Gap Corrected Depth (cm)	Original Sample Size (mg)	Age	$\delta^{13}C$	C (ug)	$\delta^{15}N$	N (ug)
3001 VII 57-58 157 111	TARGET	57.5	957.5	60	5900	-25.51	461.29	3.49	60.59
3001 VII 60-60 5 158 109	TARGET	60.25	960.25	53.3	5910	-25.18	207.22	3.58	41.41
3001 VII 62 5-63 5 159 110	TARGET	63	963	50.9	5920	-24.90	251.84	4.26	34.95
3001 VII 65-65 5 160 108	TARGET	65.25	965.25	60.2	5929	-25.00	256.09	3.52	44.20
3001 VII 66 5-67 162 106	TARGET	65.75	965.75	71.5	5930	-25.06	330.90	3.49	57.23
3001 VII 65 5-66 161 107	TARGET	65.75	965.75	61.7	5930	-25.16	341.19	3.12	63.31
3001 VII 67-67 5 163 105	TARGET	67	967	67	5935	-24.57	361.97	4.92	54.32
3001 VII 67 5-68 164 103	TARGET	67.75	967.75	71	5938	-24.32	283.51	3.76	48.08
3001 VII 68-69 165 104	TARGET	68.5	968.5	52.9	5940	-24.55	204.90	3.57	46.35
3001 VII-900 68-70 26 244	SURVEY	69	969	58.2	5942	-25.24	282.33	3.75	33.51
3001 VII-900 88-90 24 245	SURVEY	89	989	66.7	6016	-25.45	347.26	4.02	45.73
3001 VII-900 108-110 22 246	SURVEY	109	1009	65.8	6089	-25.74	337.17	3.87	36.42
3001 VII 111-111 5 165 5 93	TARGET	111.25	1011.25	67.3	6097	-25.36	380.37	3.72	47.11
3001 VII 112 5-113 166 94	TARGET	112.75	1012.75	54.1	6103	-25.21	317.55	3.46	50.81
3001 VII 113-113 5 167 95	TARGET	113.25	1013.25	64.8	6104	-25.09	335.31	4.11	48.84
3001 VII 113 5-114 168 96	TARGET	113.75	1013.75	57.4	6106	-24.43	261.32	4.33	38.71
3001 VII 115-115 5 169 97	TARGET	115.25	1015.25	69	6112	-24.82	378.27	4.16	53.22
3001 VII 118-119 170 98	TARGET	118.5	1018.5	64.9	6124	-25.97	502.83	3.82	55.97
3001 VII 123-123 5 171 99	TARGET	123.25	1023.25	44.9	6141	-24.73	221.39	4.54	28.22
3001 VII-900 128-130 20 247	SURVEY	129	1029	774.7	6162	-25.42	273.65	2.54	44.59
3001 VII-900 148-150 29 238	SURVEY	149	1049	42.7	6231	-24.86	182.30	4.22	27.70
3001 VIII-1050 18-20 37 232	SURVEY	19	1069	60.2	6296	-25.06	286.47	5.14	36.97
3001 VIII-1050 38-40 85 233	SURVEY	39	1089	54.3	6360	-25.08	289.43	5.22	34.70
3001 VIII-1050 58-68 75 234	SURVEY	59	1109	50.2	6424	-25.12	256.88	3.98	41.64
3001 VIII-1050 78-80 58 235	SURVEY	79	1129	52.5	6489	-24.78	223.50	3.98	37.45
3001 VIII-1050 98-100 76 236	SURVEY	99	1149	63.5	6553	-24.79	239.25	3.20	46.81
3001 VIII-1050 138-140 38 237	SURVEY	139	1189	63.2	6682	-25.72	364.54	3.88	39.35
3001 IX-1200 3-5 113 225	SURVEY	4	1204	46.6	6721	-25.12	274.63	4.92	36.11
3001 IX-1200 8-10 59 226	SURVEY	9	1209	51.3	6731	-24.61	214.91	3.81	37.68
3001 IX-1200 28-30 55 227	SURVEY	29	1229	54.5	6770	-24.26	227.79	3.75	48.44
3001 IX 44-44 5 1 100	TARGET	44.25	1244.25	69.4	6799	-25.58	354.46	4.37	40.03
3001 IX 46 5-47 2 101	TARGET	46.75	1246.75	57.2	6804	-27.72	182.36	3.48	21.60
3001 IX 47-47 5 3 102	TARGET	47.25	1247.25	65	6805	-27.07	201.23	2.34	34.18

Sample ID	Sample Type	Midpoint Depth (cm)	Gap Corrected Depth (cm)	Original Sample Size (mg)	Age	$\delta^{13}C$	C (ug)	$\delta^{15}N$	N (ug)
3001 IX 50 5-51 4 89	TARGET	50.75	1250.75	67.5	6812	-24.78	249.28	4.52	43.91
3001 IX 53-53 5 5 90	TARGET	53.25	1253.25	69	6817	-24.84	295.18	2.47	70.62
3001 IX 53 5-54 6 91	TARGET	53.75	1253.75	69.8	6818	-24.82	181.49	4.57	31.13
3001 IX 54-54 5 7 92	TARGET	54.25	1254.25	65.5	6819	-24.88	150.47	4.03	34.81
3001 IX-1200 68-70 56 228	SURVEY	69	1269	57.5	6847	-24.86	243.48	4.34	42.38
3001 IX-1200 88-90 57 229	SURVEY	89	1289	41.5	6886	-24.90	179.50	4.77	29.96
3001 IX 107 5-108 5 8 82	TARGET	108	1308	70.9	6923	-25.05	243.54	3.22	57.37
3001 IX 108 5-109 9 83	TARGET	109	1309	71.4	6925	-25.03	230.65	2.89	60.33
3001 IX 109-109 5 10 84	TARGET	109.25	1309.25	53.9	6925	-25.28	237.81	2.09	56.66
3001 IX 111-111 5 11 85	TARGET	111.25	1311.25	55.9	6929	-25.27	204.45	2.67	51.00
3001 IX 112 5-113 12 86	TARGET	112.75	1312.75	66.1	6932	-26.70	311.21	3.09	34.85
3001 IX 114-114 5 13 87	TARGET	114.25	1314.25	62.1	6935	-25.07	218.36	3.27	44.93
3001 IX 116 5-117 5 14 88	TARGET	117	1317	52.9	6940	-24.28	228.78	5.20	35.13
3001 IX-1200 128-130 63 230	SURVEY	129	1329	60.8	6964	-24.78	276.52	3.69	51.84
3001 IX-1200 148-150 64 231	SURVEY	149	1349	48.5	7002	-24.69	214.91	2.50	59.86
3001 X-1350 3-5 107 218	SURVEY	4	1354	50.6	7012	-24.54	196.12	3.58	35.37
3001 X-1350 18-20 52 219	SURVEY	19	1369	63.2	7041	-24.76	261.32	6.00	35.35
3001 X 22 5-23 37 76	TARGET	22.75	1372.75	66.7	7049	-24.70	260.64	2.93	41.51
3001 X 26 5-27 38 77	TARGET	26.75	1376.75	63.6	7056	-25.33	238.92	1.47	38.90
3001 X 28 5-29 39 78	TARGET	28.75	1378.75	51.5	7060	-25.23	123.98	2.03	36.18
3001 X 29-29 5 40 79	TARGET	29.25	1379.25	60.9	7061	-25.59	104.70	3.79	29.02
3001 X 30 5-31 41 80	TARGET	30.75	1380.75	72	7064	-24.78	279.39	3.64	51.02
3001 X 33 5-34 42 55	TARGET	33.75	1383.75	52.3	7070	-24.94	251.84	3.43	37.81
3001 X 34-34 5 43 81	TARGET	34.25	1384.25	58.3	7071	-24.97	249.28	2.95	51.02
3001 X-1350 38-40 54 220	SURVEY	39	1389	43	7080	-25.33	209.57	7.05	26.50
3001 X-1350 58-60 60 221	SURVEY	59	1409	51.8	7119	-24.07	207.76	4.42	38.25
3001 X-1350 78-80 53 222	SURVEY	79	1429	45.6	7158	-25.05	206.61	5.18	31.13
3001 X-1350 98-100 51 223	SURVEY	99	1449	64.2	7215	-24.51	263.61	3.49	50.78
3001 X 102 5-103 125 54	TARGET	102.75	1452.75	45.3	7230	-24.92	139.84	2.72	33.19
3001 X 106 5-107 126 53	TARGET	106.75	1456.75	70.3	7246	-25.04	189.62	2.33	29.95
3001 X 109-109 5 127 52	TARGET	109.25	1459.25	53.6	7256	-25.65	299.66	3.87	30.06
3001 X 113-114 128 51	TARGET	113.5	1463.5	68.7	7273	-25.63	363.10	5.62	36.31
3001 X 118-119 129 50	TARGET	118.5	1468.5	67.2	7293	-24.67	283.37	4.43	47.06
3001 X 120-120 5 130 49	TARGET	120.25	1470.25	60.3	7300	-25.27	340.05	2.86	51.62
3001 X-1350 138-140 49 224	SURVEY	139	1489	64.3	7375	-24.30	270.78	4.77	50.31
3001 XI-1500 3 5-5 5 108 211	SURVEY	4.5	1504.5	49.3	7437	-25.05	223.93	5.94	30.20
3001 XI-1500 48-50 62 212	SURVEY	49	1549	44.9	7615	-24.39	193.46	2.54	50.90

Sample ID	Sample Type	Midpoint Depth (cm)	Gap Corrected Depth (cm)	Original Sample Size (mg)	Age	$\delta^{13}C$	C (ug)	$\delta^{15}N$	N (ug)
3001 XI-1500 68-70 80 213	SURVEY	69	1569	51.4	7695	-24.43	214.91	4.38	41.02
3001 XI 76-76 5 44 75	TARGET	76.25	1576.25	55.9	7724	-24.73	195.17	4.22	34.62
3001 XI 78-79 45 74	TARGET	78.5	1578.5	65.9	7733	-25.08	264.45	3.42	42.21
3001 XI 81-81 5 46 73	TARGET	81.25	1581.25	66.2	7744	-27.39	253.40	4.03	26.63
3001 XI 82-82 5 47 72	TARGET	82.25	1582.25	62.7	7748	-25.87	135.83	3.00	28.51
3001 XI 83 5-84 48 71	TARGET	83.75	1583.75	64.8	7754	-28.29	191.07	1.74	27.74
3001 XI 85 5-86 49 70	TARGET	85.75	1585.75	65.8	7762	-24.96	227.33	2.01	43.45
3001 XI-1500 88-90 84 214	SURVEY	89	1589	56.3	7775	-24.37	221.14	6.03	31.52
3001 XI-1500 108-110 61 215	SURVEY	109	1609	55.4	7855	-24.67	253.92	5.78	38.06
3001 XI-1500 128-130 69 216	SURVEY	129	1629	51.9	7935	-24.35	228.78	5.29	34.59
3001 XI-1500 148-150 50 217	SURVEY	149	1649	59.5	8015	-24.22	220.63	3.39	56.66
3001 XII-1650 2-4 115 203	SURVEY	3	1653	70.9	8031	-28.08	460.74	4.40	48.61
3001 XII-1650 18-20 81 204	SURVEY	19	1669	58.6	8095	-24.11	223.50	4.48	45.18
3001 XII-1650 38-40 79 205	SURVEY	39	1689	59.8	8175	-24.10	227.79	5.31	40.90
3001 XII-1650 58-60 66 206	SURVEY	59	1709	58.1	8255	-24.05	250.71	4.86	50.31
3001 XII-1650 78-80 78 207	SURVEY	79	1729	44.8	8335	-24.39	197.74	4.58	36.54
3001 XII-1650 98-100 77 208	SURVEY	99	1749	45.8	8396	-24.74	120.90	4.38	22.53
3001 XII-1650 118-120 74 209	SURVEY	119	1769	46.3	8431	-24.24	146.41	5.56	26.48
3001 XII-1650 138-140 82 210	SURVEY	139	1789	56.3	8466	-24.27	196.12	4.98	32.60
3001 XIII-1800 2-4 5 111 194	SURVEY	3.25	1803.25	58.2	8490	-27.45	380.37	3.38	37.77
3001 XIII-1800 3-5 105 193	SURVEY	4	1804	66.3	8491	-27.89	407.67	4.09	48.15
3001 XIII-1800 8-10 86 195	SURVEY	9	1809	70.8	8500	-24.22	271.53	5.98	37.79
3001 XIII 17 5-18 52 68	TARGET	17.75	1817.75	61.2	8515	-24.99	309.77	3.43	35.19
3001 XIII 20-20 5 53 69	TARGET	20.25	1820.25	56.1	8520	-24.77	250.71	3.90	41.94
3001 XIII 21-21 5 54 48	TARGET	21.25	1821.25	52.2	8521	-25.47	342.94	3.20	42.19
3001 XIII 21 5-22 55 47	TARGET	21.75	1821.75	58.7	8522	-25.40	322.75	4.07	35.97
3001 XIII 24-24 5 56 46	TARGET	24.25	1824.25	65.8	8526	-24.78	214.29	1.54	41.05
3001 XIII 25-25 5 57 45	TARGET	25.25	1825.25	64.7	8528	-24.95	334.29	2.90	53.95
3001 XIII 25 5-26 58 44	TARGET	25.75	1825.75	65.7	8529	-24.26	282.79	4.15	52.71
3001 XIII 25 5-26 58 44 5	TARGET	25.75	1825.75	63.3	8529	-25.72	374.61	2.59	46.54
3001 XIII 27-28 59 43	TARGET	27.5	1827.5	50.3	8532	-25.28	237.48	3.46	32.61
3001 XIII-1800 28-30 96 196	SURVEY	29	1829	46.1	8535	-24.36	161.55	4.89	28.04
3001 XIII-1800 48-50 95 197	SURVEY	49	1849	49.4	8569	-24.30	202.18	3.80	37.08
3001 XIII-1800 68-70 94 198	SURVEY	69	1869	43.9	8604	-24.80	174.10	5.92	27.47

Sample ID	Sample Type	Midpoint Depth (cm)	Gap Corrected Depth (cm)	Original Sample Size (mg)	Age	$\delta^{13}C$	C (ug)	$\delta^{15}N$	N (ug)
3001 XIII-1800 88-90 93 199	SURVEY	89	1889	47.7	8638	-24.49	176.73	4.95	27.80
3001 XIII 89 5-90 121 64	TARGET	89.75	1889.75	61.8	8640	-24.08	252.44	3.86	46.55
3001 XIII 92-92 5 122 65	TARGET	92.25	1892.25	54.8	8644	-24.82	243.27	2.52	39.35
3001 XIII 95-95 5 123 66	TARGET	95.25	1895.25	63.5	8649	-24.62	277.06	3.69	43.97
3001 XIII 98-99 124 67	TARGET	98.5	1898.5	63.7	8655	-24.37	253.94	4.47	42.65
3001 XIII-1800 108-110 97 200	SURVEY	109	1909	57.5	8673	-24.12	222.37	5.41	38.69
3001 XIII 111-112 50 42	TARGET	111.5	1911.5	65.9	8677	-25.13	325.64	3.74	37.55
3001 XIII 115-115 5 51 41	TARGET	115.25	1915.25	64.1	8684	-25.56	367.42	4.32	37.10
3001 XIII-1800 128-130 83 201	SURVEY	129	1929	63	8708	-31.48	661.68	2.37	44.59
3001 XIII-1800 148-150 73 202	SURVEY	149	1949	49	8742	-30.13	371.73	4.06	28.95
3001 XIV-1950 3-5 119 186	SURVEY	4	1954	69.1	8751	-27.26	424.90	3.93	47.46
3001 XIV-1950 13-15 90 187	SURVEY	14	1964	55.5	8768	-24.02	251.95	3.56	41.17
3001 XIV-1950 33-35 91 188	SURVEY	34	1984	54.6	8803	-24.37	218.36	5.48	29.48
3001 XIV-1950 53-55 88 189	SURVEY	54	2004	59.1	8837	-24.56	266.42	2.74	49.19
3001 XIV-1950 53-55 88 189 5	SURVEY	54	2004	65.4	8837	-24.15	282.33	3.88	44.47
3001 XIV-1950 73-75 89 190	SURVEY	74	2024	44.2	8872	-24.57	200.28	3.88	33.33
3001 XIV-1950 113-115 92 191	SURVEY	114	2064	55.1	8941	-26.79	376.05	4.32	38.11
3001 XIV-1950 133-135 87 192	SURVEY	134	2084	64.3	8976	-26.82	380.37	3.63	38.90
3001 XV-2100 3-5 106 176	SURVEY	4	2104	41.7	9025	-24.10	159.19	4.72	29.91
3001 XV-2100 8-10 99 177	SURVEY	9	2109	60.2	9038	-24.50	232.90	3.83	40.78
3001 XV-2100 28-30 103 178	SURVEY	29	2129	58.2	9088	-24.60	230.90	5.07	40.20
3001 XV-2100 48-50 101 179	SURVEY	49	2149	52	9138	-23.86	169.18	2.95	41.02
3001 XV-2100 68-70 98 180	SURVEY	69	2169	53.2	9189	-24.41	177.75	4.74	31.62
3001 XV 75-75 5 141 63	TARGET	75.25	2175.25	49.7	9204	-25.18	256.30	3.22	33.40
3001 XV 77 5-78 142 62	TARGET	77.75	2177.75	43.1	9211	-25.58	245.53	4.70	25.72
3001 XV 78 5-79 143 61	TARGET	78.75	2178.75	60.4	9213	-29.31	695.68	2.54	43.45
3001 XV 79 5-80 5 144 60	TARGET	79.75	2179.75	55.9	9216	-28.19	1724.00	3.00	67.67
3001 XV 81-81 5 145 59	TARGET	81.25	2181.25	55.1	9219	-25.98	466.47	3.11	44.93
3001 XV 84-84 5 146 58	TARGET	84.25	2184.25	58	9234	-25.33	218.64	2.23	30.72
3001 XV-2100 88-90 100 181	SURVEY	89	2189	45.4	9259	-24.34	153.48	3.61	35.38
3001 XVI-2200 2-4 116 182	SURVEY	3	2203	65.1	9333	-24.48	230.26	6.60	29.30
3001 XVI-2200 8-10 104 183	SURVEY	9	2209	60.8	9364	-24.98	221.39	6.09	29.30

Sample ID	Sample Type	Midpoint Depth (cm)	Gap Corrected Depth (cm)	Original Sample Size (mg)	Age	$\delta^{13}C$	C (ug)	$\delta^{15}N$	N (ug)
3001 XVI-2200 28-30 104 5 184	SURVEY	29	2229	57	9469	-24.58	193.31	4.74	28.87
3001 XVI-2200 48-50 102 185	SURVEY	49	2249	54.3	9574	-25.07	185.92	4.93	26.93
3004 III 118 5-119 172 39	TARGET	418.75	No Gap Correction	56.1	3462	-25.94	232.09	1.96	47.63
3004 III 122 5-123 173 290	TARGET	422.75		47.7	3486	-26.26	164.99	1.54	31.32
3004 III 128-128 5 174 291	TARGET	428.25		54.2	3500	-29.51	63.39	1.54	28.55
3004 III 130-130 5 175 292	TARGET	430.25		57.8	3501	-25.46	44.93	0.51	38.83
3004 III 130 5-131 176 293	TARGET	430.75		64.9	3501	-25.54	37.84	0.70	33.90
3004 III 132-132 5 177 294	TARGET	432.25		65.2	3502	-25.19	54.16	1.11	32.41
3004 III 132 5-133 178 295	TARGET	432.75		65.3	3502	-25.36	30.46	1.12	22.47
3004 III 138-138 5 179 296	TARGET	438.25		70.1	3504	-25.08	77.59	1.30	31.28
3004 III 139-139 5 180 56	TARGET	439.25		66.2	3505	-24.81	203.06	4.53	27.44
3004 III 139 5-140 181 57	TARGET	439.75		46.8	3505	-25.08	138.36	2.63	27.81
3004 III 142-143 182 40	TARGET	442.5		64.5	3506	-25.88	203.61	1.50	37.48
3004 V 52 5-53 75 38	TARGET	652.75		63.7	5265	-25.14	247.68	5.58	29.48
3004 V 53 5-54 76 37	TARGET	653.75		61.8	5267	-25.41	274.35	4.04	33.21
3004 V 54 5-55 77 36	TARGET	654.75		40.4	5269	-25.31	216.96	4.87	28.88
3004 V 59 5-60 78 35	TARGET	659.75		54.3	5280	-25.08	210.00	4.95	30.32
3004 V 60-60 5 79 34	TARGET	660.25		65.4	5281	-25.08	151.91	3.44	28.52
3004 V 61-61 5 80 33	TARGET	661.25		69.9	5283	-25.25	355.59	4.23	42.05
3004 V 66 5-67 5 81 32	TARGET	667		58.1	5295	-25.06	289.67	4.45	34.84
3004 V 72 5-73 82 31	TARGET	672.75		47.7	5307	-25.81	388.01	3.44	44.56
3004 V 79 5-80 100 20	TARGET	679.75		56.7	5322	-25.00	233.70	3.02	41.53
3004 V 83-83 5 101 21	TARGET	683.25		56.6	5330	-25.58	377.66	2.97	53.01
3004 V 85-85 5 102 22	TARGET	685.25		60.2	5334	-25.56	367.11	2.84	66.05
3004 V 86 5-87 5 103 26	TARGET	687		56.5	5338	-25.36	309.62	4.58	29.60
3004 V 89-89 5 104 27	TARGET	689.25		56.5	5343	-25.00	268.66	3.62	40.45
3004 V 91 5-92 105 28	TARGET	691.75		52	5348	-25.36	261.70	4.53	34.29
3004 V 98 5-99 106 29	TARGET	698.75		56.4	5391	-24.68	259.31	3.47	53.01
3004 V 100-100 5 107 30	TARGET	700.25		53.7	5412	-24.77	244.88	4.19	35.86
3004 VI 48-49 15 14	TARGET	798.5		64.6	6263	-25.16	314.85	4.65	40.12
3004 VI 52-52 5 16 15	TARGET	802.25		47.9	6277	-25.19	240.68	5.07	30.68
3004 VI 53-53 5 17 16	TARGET	803.25		61	6280	-25.04	237.89	3.49	31.28
3004 VI 54 5-55 18 17	TARGET	804.75		47.1	6286	-24.96	140.91	4.19	20.02
3004 VI 55-55 5 19 18	TARGET	805.25		44.6	6287	-24.59	175.34	5.54	28.03
3004 VI 57057 5 20 23	TARGET	807.25		53.9	6295	-24.68	185.03	4.53	24.09
3004 VI 58 5-61 21 24	TARGET	808.75		59.3	6300	-24.38	207.22	4.07	39.60
3004 VI 62-63 22 25	TARGET	812.5		56.9	6313	-24.35	203.06	3.93	26.12

Sample ID	Sample Type	Midpoint Depth (cm)	Gap Corrected Depth (cm)	Original Sample Size (mg)	Age	$\delta^{13}C$	C (ug)	$\delta^{15}N$	N (ug)
3004 VI 80 5-81 5 23 19	TARGET	831		43.2	6365	-24.78	176.73	4.15	32.96
3004 VI 85-85 5 24 12	TARGET	835.25		57.4	6374	-25.30	288.43	4.67	39.24
3004 VI 88-88 5 25 10	TARGET	838.25		59	6380	-25.09	289.67	3.41	45.30
3004 VI 90-90 5 26 8	TARGET	840.25		59.2	6385	-24.85	243.42	3.47	45.41
3004 VI 92-92 5 27 6	TARGET	842.25		60.6	6389	-24.43	226.72	4.96	35.13
3004 VI 92 5-93 28 4	TARGET	842.75		48.6	6390	-24.71	186.41	5.26	30.80
3004 VI 95 5-96 5 29 2	TARGET	846		47.8	6397	-25.12	219.75	5.00	26.36
3004 VI 98 5-99 30 1	TARGET	848.75		51.1	6403	-24.64	188.21	5.00	26.71
3004 VII 33 5-34 5 83 13	TARGET	934		54.8	6583	-25.24	71.07	4.26	13.24
3004 VII 38-38 5 84 11	TARGET	938.25		61	6592	-25.30	102.91	1.73	32.64
3004 VII 38-38 5 84 11 5	TARGET	938.25		63.1	6592	-25.56	110.63	2.98	26.16
3004 VII 44-44 5 85 9	TARGET	944.25		55.2	6604	-25.11	88.44	2.37	24.80
3004 VII 45 5-46 86 5	TARGET	945.75		49.6	6607	-25.68	191.96	5.08	27.32
3004 VII 47-47 5 87 7	TARGET	947.25		64.7	6611	-23.73	237.81	2.76	62.47
3004 VII 50-51 88 3	TARGET	950.5		50.2	6618	-24.38	185.03	5.88	28.52
3006 IX 129-130 69 146	TARGET	129.5	1156.5	44.7	4226	-23.86	191.96	7.12	23.85
3006 IX 134-135 70 145	TARGET	134.5	1161.5	47.8	4238	-23.35	208.61	3.88	48.08
3006 IX 137 5-138 71 144	TARGET	137.75	1164.75	61.4	4246	-24.54	293.87	5.53	40.99
3006 IX 138-138 5 72 143	TARGET	138.25	1165.25	61.1	4247	-24.43	280.55	4.19	56.96
3006 IX 138 5-139 73 142	TARGET	138.75	1165.75	46.5	4248	-24.91	197.74	5.87	29.73
3006 IX 139-139 5 74 141	TARGET	139.25	1166.25	44.9	4250	-24.76	312.46	5.83	28.40
3007 VII 63-64 89 175	TARGET	884.5	884.5	53.1	5699	-24.86	222.07	3.20	39.75
3007 VII 66-67 90 174	TARGET	887.5	887.5	66	5705	-25.86	320.51	5.17	47.53
3007 VII 68 5-69 91 173	TARGET	889.75	889.75	61.6	5710	-24.98	183.36	2.54	40.01
3007 VII 69-69 5 92 172	TARGET	890.25	890.25	67.6	5711	-24.45	240.61	3.34	49.72
3007 VII 73-73 5 93 171	TARGET	894.25	894.25	56.5	5720	-25.33	193.70	3.05	37.59
3007 VII 74-74 5 94 170	TARGET	895.25	895.25	58.7	5722	-25.03	154.91	2.32	38.37
3007 VII 75 5-76 95 169	TARGET	896.75	896.75	47.7	5725	-25.40	279.07	4.03	39.69
3007 VII 76 5-77 96 168	TARGET	897.75	897.75	64.7	5727	-25.33	216.96	2.56	63.13
3007 VII 77-77 5 97 167	TARGET	898.25	898.25	66.7	5728	-25.20	163.76	6.13	22.32
3007 VII 77 5-78 98	TARGET	898.75	898.75	65.2	5730	-24.67	262.80	4.96	38.71
3007 VII 81-82 99 165	TARGET	902.5	902.5	60.2	5738	-24.75	228.78	5.02	38.71
3007 XIV 99 5-100 5 60 164	TARGET	1971	1899	67.6	9542	-25.81	228.78	4.47	35.57
3007 XIV 102-102 5 61 154	TARGET	1973.25	1901.25	63	9550	-27.00	153.42	3.30	35.67
3007 XIV 104 5-105 62 163	TARGET	1975.75	1903.75	51.3	9559	-24.88	132.53	2.41	32.53
3007 XIV 107-107 5 63 162	TARGET	1978.25	1906.25	55.5	9568	-25.24	129.11	2.46	36.99
3007 XIV 107 5-108 64 161	TARGET	1978.75	1906.75	44.7	9570	-25.37	122.98	1.32	35.38
3007 XIV 108-108 5 65 160	TARGET	1979.25	1907.25	50	9572	-28.75	109.43	4.36	20.07
3007 XIV 111 5-112 5 66 152	TARGET	1983	1911	65.8	9586	-25.89	256.88	4.97	30.81

Sample ID	Sample Type	Midpoint Depth (cm)	Gap Corrected Depth (cm)	Original Sample Size (mg)	Age	$\delta^{13}C$	C (ug)	$\delta^{15}N$	N (ug)
3007 XIV 114-115 67 159	TARGET	1985.25	1913.25	42.1	9594	-24.59	108.32	1.39	39.06
3007 XIV 117 5-118 5 68 158	TARGET	1989	1917	55	9608	-25.02	211.05	5.44	28.98
3007 XVI 96-97 108 157	TARGET	2267.5	2195.5	57.1	10780	-24.60	200.70	4.66	30.06
3007 XVI 99-99 5 109 156	TARGET	2270.25	2198.25	50.6	10793	-24.96	194.89	2.30	36.07
3007 XVI 101-101 5 110 155	TARGET	2272.25	2200.25	61.6	10803	-26.97	175.58	3.90	33.73
3007 XVI 103-104 111 153	TARGET	2274.5	2202.5	55.7	10814	-26.63	231.74	3.53	31.46

All samples were prepared at the Virginia Institute of Marine Science (see Chapter 1, Section 3.2 (pg. 11) and Chapter 3, Section 2.4, (pg. 136)) and sent for analysis to the UC Davis Stable Isotope Facility: http://stableisotopefacility.ucdavis.edu/index.html.

Analytical standard deviation is 0.2 permil for ^{13}C and 0.3 permil for ^{15}N.

Appendix 6A: Marion DuFresne carbon and nitrogen sample verification data.

2006

Sample ID	Sample Size (mg)	N (ug)	^{15}N	C (ug)	$\delta^{13}C$
3001 XIII T1800 MD 23 298	34.965	18.72	5.13	141.53	-24.13
3002 I 0-150 MD 58 304	30.383	21.12	6.69	140.39	-21.80
3002 III @50 MD 63 300	33.726	22.91	6.22	147.11	-22.24
3003 VII 896-1046 MD 130 306	34.947	18.43	5.75	124.74	-22.85
3004 VII T1050-1200 MD 35 307	26.639	12.39	5.69	86.21	-23.79
3004 X 1350-1500 MD 37 308	40.18	14.00	4.11	103.09	-23.99
3005 II T150 MD 2 305	30.978	19.04	5.00	148.33	-23.27
3005 V T600 MD 5 297	26.44	16.48	5.79	127.91	-23.67
3006 III 300-450 MD 94 301	36.408	19.58	5.13	177.34	-23.71
3006 XVIII 2534-2554 MD 108 302	46.729	6.94	2.55	40.23	-24.35
3007 III T221-371 MD 42 299	28.522	14.56	4.47	129.05	-24.95

2011

3001 XIII T1800 MD 23 298	65.9	53.72	3.98	233.52	-23.72
3002 I 0-150 MD 58 304	56.5	60.93	4.51	234.95	-21.59
3002 III @50 MD 63 300	51.8	64.62	3.32	227.79	-21.96
3003 VII 896-1046 MD 130 306	55.7	42.75	4.11	222.07	-22.79
3004 VII T1050-1200 MD 35 307	64.8	33.33	5.39	213.48	-23.73
3004 X 1350-1500 MD 37 308	55.2	29.02	4.27	152.52	-24.23
3005 II T150 MD 2 305	61.5	70.86	3.39	312.42	-23.20
3005 V T600 MD 5 297	42.6	42.38	4.25	205.83	-23.72
3006 III 300-450 MD 94 301	44	34.24	5.16	212.05	-23.40
3006 XVIII 2534-2554 MD 108 302	67.2	12.49	6.12	78.44	-27.42
3007 III T221-371 MD 42 299	66.6	59.50	2.51	321.05	-24.90

See Chapter 3, Section 2.4 (pg. 136).

Appendix 6B: Kilo Moana carbon and nitrogen sample verification data.

Chilled

Sample Number	Sample ID	Sample Size (mg)	N (ug)	^{15}N	C (ug)	$\delta^{13}C$
136	1 KM	33.782	17.3	4.52	122.5	-24.64
154	2 KM	33.484	14.4	3.65	110.6	-24.85
139	3 KM	34.166	14.4	5.38	91.7	-23.26
148	4 KM	38.387	16.6	4.50	110.4	-23.59
156	5 KM	31.107	3.8	1.94	16.7	-22.95
115	6 KM	36.922	8.7	7.18	45.2	-22.50
114	7 KM	38.750	36.4	5.80	251.5	-23.02
105	8 KM	40.158	35.3	5.32	241.3	-23.24
110	9 KM	29.105	24.8	5.09	166.1	-23.21
167	10 KM	37.126	18.9	5.54	113.6	-22.71
145	11 KM	38.436	39.5	5.57	277.4	-23.24
127	12 KM	33.836	23.4	4.33	168.4	-23.77
125	13 KM	35.305	28.3	4.49	209.9	-23.66

Dried

150	15 KM	35.244	19.4	4.26	138.2	-24.65
162	16 KM	30.645	15.0	4.16	107.5	-24.68
122	17 KM	32.274	19.2	4.80	128.1	-23.31
109	18 KM	36.624	20.9	4.28	142.6	-23.50
138	19 KM	34.124	4.1	5.75	18.2	-22.77
77	20 KM	35.719	8.78	4.52	51.68	-22.41
126	21 KM	33.370	28.6	5.28	189.7	-23.10
149	22 KM	28.585	25.2	4.82	170.6	-23.34
111	23 KM	39.791	21.9	4.94	143.8	-23.05
112	24 KM	39.457	19.2	4.86	120.3	-23.03
143	25 KM	32.072	24.0	4.49	168.4	-23.54
134	26 KM	31.017	30.8	5.10	213.2	-22.99
152	27 KM	36.642	30.7	4.95	207.6	-23.37

See Chapter 2, Section 2.8 (pg. 63).

Appendix 7: Marion DuFresne magnetic susceptibility data

MD3001

Depth (cm)	Age (yr BP)	MS (SI)
0.3	2	1033
2.3	12	2152
4.3	22	4392
6.3	32	7676
8.3	43	793
10.3	53	1474
12.3	63	8635
14.3	74	4814
16.3	84	2334
18.3	94	1168
20.3	104	706
22.3	115	624
24.3	125	725
26.3	135	762
28.3	146	528
30.3	156	
32.3	166	116
34.3	177	68
36.3	187	52
38.3	197	50
40.3	207	48
42.3	218	41
44.3	228	31
46.3	238	25
48.3	249	22
50.3	259	21
52.3	269	19
54.3	279	18
56.3	290	16
58.3	300	15
60.3	310	16
62.3	321	17
64.3	331	19
66.3	341	21
68.3	351	23
70.3	362	25
72.3	372	27
74.3	382	30
76.3	393	34
78.3	403	40
80.3	413	47
82.3	424	55
84.3	434	58
86.3	444	53
88.3	454	44
90.3	465	36
92.3	475	31
94.3	485	26
96.3	496	24
98.3	506	24
100.3	516	25
102.3	526	27
104.3	537	31
106.3	547	36
108.3	557	39
110.3	568	40
112.3	578	39
114.3	588	40
116.3	598	42
118.3	609	44
120.3	619	47
122.3	629	47
124.3	640	46
126.3	650	45
128.3	660	45
130.3	671	47
132.3	681	47
134.3	691	49
136.3	701	50
138.3	712	51
140.3	722	51
142.3	732	52
144.3	743	50
146.3	753	47
148.3	763	45
149.1	767	52
151.1	778	56
153.1	788	58
155.1	798	60
157.1	808	61
159.1	819	61
161.1	829	61
163.1	839	61
165.1	850	63
167.1	860	66
169.1	870	69
171.1	880	67
173.1	891	66
175.1	901	71
177.1	911	76
179.1	929	83
181.1	952	88
183.1	975	96
185.1	998	94
187.1	1021	94
189.1	1045	97
191.1	1068	84
193.1	1091	79
195.1	1114	78
197.1	1137	79
199.1	1161	83
201.1	1184	86
203.1	1207	85
205.1	1230	87
207.1	1253	82
209.1	1276	72
211.1	1300	68
213.1	1323	67
215.1	1346	67
217.1	1369	67
219.1	1392	69
221.1	1416	73
223.1	1439	78
225.1	1462	81
227.1	1485	82
229.1	1508	76
231.1	1531	69
233.1	1555	61
235.1	1578	54
237.1	1601	49
239.1	1624	46
241.1	1647	46
243.1	1671	47
245.1	1694	46
247.1	1717	43
249.1	1740	41
251.1	1763	38
253.1	1786	37
255.1	1810	38
257.1	1833	38
259.1	1856	37
261.1	1879	34
263.1	1902	32
265.1	1926	31
267.1	1949	32
269.1	1972	31
271.1	1995	31
273.1	2018	31
275.1	2041	32
277.1	2065	32
279.1	2088	32
281.1	2111	32
283.1	2134	31
285.1	2157	31
287.1	2181	30
289.1	2204	29
291.1	2227	30
293.1	2250	31
295.1	2273	29
297.1	2296	29
297.4	2300	27
299.4	2323	30
301.4	2346	30
303.4	2369	30
305.4	2393	29
307.4	2416	30
309.4	2439	31
311.4	2462	33
313.4	2485	35
315.4	2509	35
317.4	2532	34
319.4	2555	32
321.4	2578	30
323.4	2601	31
325.4	2624	32
327.4	2648	35
329.4	2671	36
331.4	2694	37

Depth (cm)	Age (yr BP)	MS (SI)
333.4	2717	38
335.4	2740	40
337.4	2764	42
339.4	2787	43
341.4	2810	43
343.4	2833	46
345.4	2856	48
347.4	2879	51
349.4	2903	56
351.4	2926	62
353.4	2949	67
355.4	2972	69
357.4	2995	73
359.4	3017	75
361.4	3040	77
363.4	3062	82
365.4	3085	89
367.4	3108	92
369.4	3130	85
371.4	3153	68
373.4	3176	54
375.4	3198	46
377.4	3221	33
379.4	3235	37
381.4	3245	37
383.4	3255	35
385.4	3265	34
387.4	3275	31
389.4	3285	29
391.4	3295	28
393.4	3305	28
395.4	3315	26
397.4	3325	26
399.4	3335	26
401.4	3345	26
403.4	3356	25
405.4	3366	24
407.4	3376	24
409.4	3386	24
411.4	3396	26
413.4	3406	28
415.4	3416	28
417.4	3426	27
419.4	3436	27
421.4	3446	26
423.4	3456	24
425.4	3466	22

Depth (cm)	Age (yr BP)	MS (SI)
427.4	3476	21
429.4	3487	21
431.4	3497	20
433.4	3507	21
435.4	3517	24
437.4	3527	25
439.4	3537	26
441.4	3547	25
451.4	3597	25
453.4	3608	26
455.4	3618	26
457.4	3628	27
459.4	3638	27
461.4	3648	26
463.4	3658	25
465.4	3668	25
467.4	3678	23
469.4	3688	23
471.4	3698	23
473.4	3708	23
475.4	3718	22
477.4	3729	22
479.4	3739	22
481.4	3749	22
483.4	3759	21
485.4	3769	22
487.4	3779	22
489.4	3789	22
491.4	3799	22
493.4	3809	22
495.4	3819	23
497.4	3829	22
499.4	3839	22
501.4	3849	22
503.4	3860	22
505.4	3870	21
507.4	3880	21
509.4	3890	20
511.4	3900	21
513.4	3910	21
515.4	3920	21
517.4	3930	22
519.4	3940	22
521.4	3950	21
523.4	3960	21
525.4	3970	21
527.4	3981	21

Depth (cm)	Age (yr BP)	MS (SI)
529.4	3991	20
531.4	4001	20
533.4	4011	20
535.4	4021	19
537.4	4031	19
539.4	4041	19
541.4	4051	20
543.4	4061	19
545.4	4071	20
547.4	4081	21
549.4	4091	21
551.4	4101	20
553.4	4112	21
555.4	4122	22
557.4	4132	22
559.4	4142	21
561.4	4152	21
563.4	4162	21
565.4	4172	21
567.4	4182	21
569.4	4192	21
571.4	4202	21
573.4	4213	
575.4	4223	23
577.4	4233	24
579.4	4243	23
581.4	4253	23
583.4	4263	23
585.4	4273	24
587.4	4284	23
589.4	4294	24
591.4	4304	23
598.7	4341	22
600.7	4351	22
602.7	4361	22
604.7	4371	21
606.7	4381	22
608.7	4391	22
610.7	4402	22
612.7	4412	22
614.7	4422	21
616.7	4432	20
618.7	4442	20
620.7	4452	20
622.7	4462	20
624.7	4473	20
626.7	4483	20

Depth (cm)	Age (yr BP)	MS (SI)
628.7	4493	21
630.7	4503	20
632.7	4513	20
634.7	4523	21
636.7	4533	21
638.7	4544	21
640.7	4554	21
642.7	4564	20
644.7	4574	21
646.7	4584	21
648.7	4594	21
650.7	4604	20
652.7	4614	23
654.7	4625	24
656.7	4635	25
658.7	4645	26
660.7	4655	27
662.7	4665	29
664.7	4675	32
666.7	4685	37
668.7	4696	45
670.7	4706	60
672.7	4716	67
674.7	4726	55
676.7	4736	42
678.7	4746	32
680.7	4756	27
682.7	4766	25
684.7	4777	24
686.7	4787	24
688.7	4797	23
690.7	4807	15
692.7	4817	22
694.7	4827	21
696.7	4837	20
698.7	4848	19
700.7	4858	18
702.7	4868	18
704.7	4878	19
706.7	4888	19
708.7	4898	19
710.7	4908	18
712.7	4918	18
714.7	4929	18
716.7	4939	19
718.7	4949	20
720.7	4959	20

Depth (cm)	Age (yr BP)	MS (SI)
722.7	4969	21
724.7	4979	20
726.7	4989	19
728.7	5000	19
730.7	5010	11
732.7	5020	18
734.7	5030	19
736.7	5040	19
738.7	5050	19
742.7	5070	20
743.4	5074	18
745.4	5084	20
747.4	5094	21
749.4	5104	23
751.4	5115	24
753.4	5125	23
755.4	5135	22
757.4	5145	21
759.4	5155	21
761.4	5165	20
763.4	5175	20
765.4	5185	20
767.4	5196	20
769.4	5206	21
771.4	5216	21
773.4	5225	20
775.4	5233	21
777.4	5240	19
779.4	5247	19
781.4	5255	19
783.4	5262	18
785.4	5269	18
787.4	5277	18
789.4	5284	19
791.4	5291	20
793.4	5299	21
795.4	5306	20
797.4	5313	21
799.4	5321	21
801.4	5328	21
803.4	5335	22
805.4	5343	22
807.4	5350	21
809.4	5357	22
811.4	5365	21
813.4	5372	20
815.4	5379	20

Depth (cm)	Age (yr BP)	MS (SI)
817.4	5387	20
819.4	5394	23
821.4	5401	24
823.4	5409	26
825.4	5416	26
827.4	5423	25
829.4	5431	24
831.4	5438	23
833.4	5445	24
835.4	5453	24
837.4	5460	24
839.4	5467	24
841.4	5475	23
843.4	5482	23
845.4	5489	23
847.4	5497	23
849.4	5504	22
851.4	5511	
853.4	5519	21
855.4	5526	22
857.4	5533	21
859.4	5541	21
861.4	5548	22
863.4	5555	23
865.4	5563	27
867.4	5570	28
869.4	5577	29
871.4	5585	26
873.4	5592	21
875.4	5599	18
877.4	5607	18
879.4	5614	17
881.4	5621	17
883.4	5629	17
885.4	5636	16
887.4	5643	15
889.4	5651	14
891.4	5658	14
891.9	5660	15
893.9	5667	16
895.9	5674	16
897.9	5682	15
899.9	5689	15
901.9	5696	16
903.9	5704	15
905.9	5711	16
907.9	5718	16

Depth (cm)	Age (yr BP)	MS (SI)
909.9	5726	15
911.9	5733	16
913.9	5740	17
915.9	5748	17
917.9	5755	18
919.9	5762	18
921.9	5770	18
923.9	5777	17
925.9	5784	16
927.9	5792	16
929.9	5799	16
931.9	5806	15
933.9	5814	16
935.9	5821	16
937.9	5828	17
939.9	5836	17
941.9	5843	16
943.9	5850	15
945.9	5858	15
947.9	5865	14
949.9	5872	15
951.9	5880	14
953.9	5887	14
955.9	5894	16
957.9	5902	17
959.9	5909	17
961.9	5916	18
963.9	5924	17
965.9	5931	16
967.9	5938	15
969.9	5946	15
971.9	5953	15
973.9	5960	15
975.9	5968	15
977.9	5975	16
979.9	5982	15
981.9	5990	15
983.9	5997	15
985.9	6004	15
987.9	6012	15
989.9	6019	15
991.9	6026	15
993.9	6034	15
995.9	6041	15
997.9	6048	14
999.9	6056	14
1001.9	6063	14

Depth (cm)	Age (yr BP)	MS (SI)
1003.9	6070	14
1005.9	6078	14
1007.9	6085	15
1009.9	6092	15
1011.9	6100	15
1013.9	6107	15
1015.9	6114	16
1017.9	6122	16
1019.9	6129	17
1021.9	6136	16
1023.9	6143	17
1025.9	6151	16
1027.9	6158	17
1029.9	6165	17
1031.9	6173	17
1033.9	6180	17
1035.9	6187	16
1037.9	6195	16
1039.9	6202	15
1040.1	6203	16
1042.1	6209	16
1044.1	6216	16
1046.1	6222	16
1048.1	6229	15
1050.1	6235	15
1052.1	6241	15
1054.1	6248	15
1056.1	6254	16
1058.1	6261	15
1060.1	6267	15
1062.1	6274	14
1064.1	6280	15
1066.1	6286	15
1068.1	6293	16
1070.1	6299	15
1072.1	6306	15
1074.1	6312	16
1076.1	6319	15
1078.1	6325	15
1080.1	6331	15
1082.1	6338	15
1084.1	6344	15
1086.1	6351	15
1088.1	6357	16
1090.1	6364	16
1092.1	6370	17
1094.1	6377	17

Depth (cm)	Age (yr BP)	MS (SI)
1096.1	6383	19
1098.1	6389	20
1100.1	6396	22
1102.1	6402	24
1104.1	6409	21
1106.1	6415	19
1108.1	6422	17
1110.1	6428	16
1112.1	6434	15
1114.1	6441	15
1116.1	6447	15
1118.1	6454	14
1120.1	6460	15
1122.1	6467	15
1124.1	6473	15
1126.1	6479	15
1128.1	6486	16
1130.1	6492	16
1132.1	6499	16
1134.1	6505	16
1136.1	6512	16
1138.1	6518	16
1140.1	6524	15
1142.1	6531	16
1144.1	6537	16
1146.1	6544	15
1148.1	6550	15
1150.1	6557	14
1152.1	6563	14
1154.1	6570	14
1156.1	6576	14
1158.1	6582	14
1160.1	6589	15
1162.1	6595	15
1164.1	6602	16
1166.1	6608	14
1168.1	6615	16
1170.1	6621	16
1172.1	6627	15
1174.1	6634	15
1176.1	6640	14
1178.1	6647	14
1180.1	6653	15
1182.1	6660	15
1184.1	6666	15
1186.1	6672	15
1188.1	6679	14

Depth (cm)	Age (yr BP)	MS (SI)
1189.4	6683	14
1191.4	6689	14
1193.4	6696	14
1195.4	6702	14
1197.4	6708	14
1199.4	6712	14
1201.4	6716	14
1203.4	6720	15
1205.4	6724	14
1207.4	6728	14
1209.4	6732	14
1211.4	6735	13
1213.4	6739	14
1215.4	6743	14
1217.4	6747	14
1219.4	6751	15
1221.4	6755	15
1223.4	6759	16
1225.4	6763	16
1227.4	6766	16
1229.4	6770	15
1231.4	6774	15
1233.4	6778	16
1235.4	6782	15
1237.4	6786	15
1239.4	6790	14
1241.4	6794	15
1243.4	6798	15
1245.4	6801	15
1247.4	6805	14
1249.4	6809	14
1251.4	6813	14
1253.4	6817	14
1255.4	6821	13
1257.4	6825	13
1259.4	6829	13
1261.4	6832	14
1263.4	6836	14
1265.4	6840	14
1267.4	6844	6
1269.4	6848	14
1271.4	6852	14
1273.4	6856	14
1275.4	6860	14
1277.4	6864	14
1279.4	6867	14
1281.4	6871	13

Depth (cm)	Age (yr BP)	MS (SI)
1283.4	6875	14
1285.4	6879	14
1287.4	6883	13
1289.4	6887	14
1291.4	6891	14
1293.4	6895	13
1295.4	6898	14
1297.4	6902	14
1299.4	6906	15
1301.4	6910	17
1303.4	6914	18
1305.4	6918	17
1307.4	6922	16
1309.4	6926	15
1311.4	6929	15
1313.4	6933	15
1315.4	6937	15
1317.4	6941	15
1319.4	6945	14
1321.4	6949	15
1323.4	6953	15
1325.4	6957	14
1327.4	6961	14
1329.4	6964	14
1331.4	6968	15
1333.4	6972	14
1335.4	6976	14
1337.4	6980	14
1337.6	6980	15
1339.6	6984	16
1341.6	6988	16
1343.6	6992	16
1345.6	6996	17
1347.6	7000	16
1349.6	7004	16
1351.6	7007	16
1353.6	7011	16
1355.6	7015	16
1357.6	7019	16
1359.6	7023	18
1361.6	7027	19
1363.6	7031	19
1365.6	7035	19
1367.6	7039	17
1369.6	7042	16
1371.6	7046	15
1373.6	7050	15

Depth (cm)	Age (yr BP)	MS (SI)
1375.6	7054	15
1377.6	7058	14
1379.6	7062	15
1381.6	7066	14
1383.6	7070	15
1385.6	7073	15
1387.6	7077	14
1389.6	7081	14
1391.6	7085	15
1393.6	7089	14
1395.6	7093	14
1397.6	7097	14
1399.6	7101	14
1401.6	7104	14
1403.6	7108	14
1405.6	7112	15
1407.6	7116	14
1409.6	7120	14
1411.6	7124	13
1413.6	7128	14
1415.6	7132	13
1417.6	7136	13
1419.6	7139	14
1421.6	7143	13
1423.6	7147	14
1425.6	7151	14
1427.6	7155	13
1429.6	7159	13
1431.6	7163	13
1433.6	7167	14
1435.6	7170	13
1437.6	7174	15
1439.6	7178	16
1441.6	7185	16
1443.6	7193	
1445.6	7201	14
1447.6	7209	12
1449.6	7217	12
1451.6	7225	12
1453.6	7233	12
1455.6	7241	12
1457.6	7249	12
1459.6	7257	12
1461.6	7265	12
1463.6	7273	11
1465.6	7281	11
1467.6	7289	12

Depth (cm)	Age (yr BP)	MS (SI)
1469.6	7297	12
1471.6	7305	12
1473.6	7313	12
1475.6	7321	12
1477.6	7329	12
1479.6	7337	12
1481.6	7345	11
1483.6	7353	10
1485.6	7361	10
1487.1	7367	12
1489.1	7375	12
1491.1	7383	13
1493.1	7391	13
1495.1	7399	13
1497.1	7407	12
1499.1	7415	11
1501.1	7423	11
1503.1	7431	12
1505.1	7439	11
1507.1	7447	11
1509.1	7455	12
1511.1	7463	11
1513.1	7471	11
1515.1	7479	11
1517.1	7487	11
1519.1	7495	11
1521.1	7503	11
1523.1	7511	11
1525.1	7519	12
1527.1	7527	12
1529.1	7535	12
1531.1	7543	12
1533.1	7551	12
1535.1	7559	13
1537.1	7567	13
1539.1	7575	12
1541.1	7583	12
1543.1	7591	12
1545.1	7599	13
1547.1	7607	13
1549.1	7615	13
1551.1	7623	12
1553.1	7631	12
1555.1	7639	11
1557.1	7647	11
1559.1	7655	12
1561.1	7663	12
1563.1	7671	13
1565.1	7679	14
1567.1	7687	14
1569.1	7695	14
1571.1	7703	13
1573.1	7711	12
1575.1	7719	11
1577.1	7727	10
1579.1	7735	10
1581.1	7743	10
1583.1	7751	11
1585.1	7759	11
1587.1	7767	11
1589.1	7775	12
1591.1	7783	11
1593.1	7791	11
1595.1	7799	12
1597.1	7807	11
1599.1	7815	11
1601.1	7823	11
1603.1	7831	11
1605.1	7839	11
1607.1	7847	12
1609.1	7855	10
1611.1	7863	11
1613.1	7871	10
1615.1	7879	10
1617.1	7887	10
1619.1	7895	11
1621.1	7903	11
1623.1	7911	11
1625.1	7919	11
1627.1	7927	10
1629.1	7935	11
1631.1	7943	11
1633.1	7951	11
1635.1	7959	11
1636.7	7965	11
1638.7	7973	11
1640.7	7981	11
1642.7	7989	10
1644.7	7997	10
1646.7	8005	10
1648.7	8013	11
1650.7	8021	11
1652.7	8029	11
1654.7	8037	11
1656.7	8045	11
1658.7	8053	11
1660.7	8061	11
1662.7	8069	11
1664.7	8077	11
1666.7	8085	12
1668.7	8093	11
1670.7	8101	11
1672.7	8109	11
1674.7	8117	10
1676.7	8125	10
1678.7	8133	11
1680.7	8141	11
1682.7	8149	11
1684.7	8157	11
1686.7	8165	11
1688.7	8173	11
1690.7	8181	11
1692.7	8189	10
1694.7	8197	10
1696.7	8205	10
1698.7	8213	10
1700.7	8221	10
1702.7	8229	10
1704.7	8237	10
1706.7	8245	10
1708.7	8253	3
1710.7	8261	11
1712.7	8269	10
1714.7	8277	10
1716.7	8285	11
1718.7	8293	11
1720.7	8301	11
1722.7	8309	10
1724.7	8317	10
1726.7	8325	11
1728.7	8333	11
1730.7	8341	11
1732.7	8349	10
1734.7	8357	9
1736.7	8365	10
1738.7	8373	10
1740.7	8381	9
1742.7	8385	9
1744.7	8389	10
1746.7	8392	10
1748.7	8396	10
1750.7	8399	9
1752.7	8403	10
1754.7	8406	10
1756.7	8410	9
1758.7	8413	10
1760.7	8417	10
1762.7	8420	9
1764.7	8423	9
1766.7	8427	10
1768.7	8430	10
1770.7	8434	9
1772.7	8437	9
1774.7	8441	9
1776.7	8444	9
1778.7	8448	9
1780.7	8451	9
1782.7	8455	9
1783.7	8456	9
1785.7	8460	9
1787.7	8463	9
1789.7	8467	9
1791.7	8470	8
1793.7	8474	8
1795.7	8477	9
1797.7	8481	9
1799.7	8484	10
1801.7	8487	9
1803.7	8491	10
1805.7	8494	9
1807.7	8498	10
1809.7	8501	10
1811.7	8505	10
1813.7	8508	10
1815.7	8512	10
1817.7	8515	11
1819.7	8519	11
1821.7	8522	12
1823.7	8526	11
1825.7	8529	12
1827.7	8532	12
1829.7	8536	13
1831.7	8539	15
1833.7	8543	17
1835.7	8546	19
1837.7	8550	19
1839.7	8553	18
1841.7	8557	16

Depth (cm)	Age (yr BP)	MS (SI)
1843.7	8560	13
1845.7	8564	12
1847.7	8567	11
1849.7	8571	11
1851.7	8574	11
1853.7	8577	10
1855.7	8581	10
1857.7	8584	10
1859.7	8588	10
1861.7	8591	10
1863.7	8595	10
1865.7	8598	9
1867.7	8602	9
1869.7	8605	10
1871.7	8609	10
1873.7	8612	10
1875.7	8615	10
1877.7	8619	9
1879.7	8622	11
1881.7	8626	10
1883.7	8629	11
1885.7	8633	10
1887.7	8636	10
1889.7	8640	10
1891.7	8643	10
1893.7	8647	10
1895.7	8650	10
1897.7	8654	10
1899.7	8657	10
1901.7	8660	10
1903.7	8664	10
1905.7	8667	10
1907.7	8671	10
1909.7	8674	10
1911.7	8678	10
1913.7	8681	9
1915.7	8685	10
1917.7	8688	9
1919.7	8692	9
1921.7	8695	9
1923.7	8699	9
1925.7	8702	9
1927.7	8705	9
1929.7	8709	9
1931.7	8712	9
1931.9	8713	8
1933.9	8716	9

Depth (cm)	Age (yr BP)	MS (SI)
1935.9	8720	10
1937.9	8723	9
1939.9	8727	9
1941.9	8730	9
1943.9	8733	9
1945.9	8737	8
1947.9	8740	7
1949.9	8744	7
1951.9	8747	6
1953.9	8751	7
1955.9	8754	7
1957.9	8758	8
1959.9	8761	8
1961.9	8765	9
1963.9	8768	10
1965.9	8771	10
1967.9	8775	10
1969.9	8778	9
1971.9	8782	9
1973.9	8785	10
1975.9	8789	9
1977.9	8792	9
1979.9	8796	9
1981.9	8799	9
1983.9	8803	8
1985.9	8806	7
1987.9	8810	5
1989.9	8813	3
1991.9	8816	6
1993.9	8820	7
1995.9	8823	8
1997.9	8827	8
1999.9	8830	9
2001.9	8834	10
2003.9	8837	9
2005.9	8841	9
2007.9	8844	9
2009.9	8848	9
2011.9	8851	8
2013.9	8855	9
2015.9	8858	
2017.9	8861	9
2019.9	8865	9
2021.9	8868	8
2023.9	8872	9
2025.9	8875	9
2027.9	8879	8

Depth (cm)	Age (yr BP)	MS (SI)
2029.9	8882	8
2031.9	8886	8
2033.9	8889	7
2035.9	8893	7
2037.9	8896	8
2039.9	8899	7
2041.9	8903	8
2043.9	8906	7
2045.9	8910	8
2047.9	8913	8
2049.9	8917	7
2051.9	8920	7
2053.9	8924	7
2055.9	8927	7
2057.9	8931	8
2059.9	8934	8
2061.9	8938	7
2063.9	8941	8
2065.9	8944	8
2067.9	8948	9
2069.9	8951	9
2071.9	8955	9
2073.9	8958	8
2075.9	8962	8
2077.9	8965	7
2079.9	8969	7
2080	8969	7
2082	8972	7
2084	8976	7
2086	8980	7
2088	8985	6
2090	8990	7
2092	8995	7
2094	9000	10
2096	9005	9
2098	9010	7
2100	9015	7
2102	9020	7
2104	9025	7
2106	9030	7
2108	9035	7
2110	9040	7
2112	9045	7
2114	9050	7
2116	9055	7
2118	9060	8
2120	9065	7

Depth (cm)	Age (yr BP)	MS (SI)
2122	9070	8
2124	9076	8
2126	9081	8
2128	9086	8
2130	9091	8
2132	9096	8
2134	9101	8
2136	9106	8
2138	9111	8
2140	9116	9
2142	9121	9
2144	9126	9
2146	9131	9
2148	9136	8
2150	9141	9
2152	9146	9
2154	9151	9
2156	9156	9
2158	9161	10
2160	9166	12
2162	9171	12
2164	9176	12
2166	9181	12
2168	9186	11
2170	9191	10
2172	9196	9
2174	9201	8
2176	9206	8
2178	9211	8
2178.5	9212	9
2180.5	9217	10
2182.5	9225	11
2184.5	9236	11
2186.5	9246	11
2188.5	9257	11
2190.5	9267	11
2192.5	9278	11
2194.5	9288	12
2196.5	9299	12
2198.5	9309	12
2200.5	9320	12
2202.5	9330	13
2204.5	9341	13
2206.5	9351	14
2208.5	9362	14
2210.5	9372	17
2212.5	9383	26

Depth (cm)	Age (yr BP)	MS (SI)
2214.5	9393	35
2216.5	9404	32
2218.5	9414	26
2220.5	9425	20
2222.5	9435	15
2224.5	9446	13
2226.5	9456	15
2228.5	9467	15
2230.5	9477	9
2232.5	9488	2

MD3004

Depth (cm)	Age (yr BP)	MS (SI)
0.4	2	31
2.4	9	29
4.4	17	33
6.4	25	38
8.4	32	40
10.4	40	43
12.4	48	45
14.4	55	49
16.4	63	54
18.4	71	59
20.4	83	62
22.4	96	58
24.4	110	55
26.4	123	55
28.4	137	57
30.4	150	54
32.4	164	54
34.4	178	58
36.4	191	63
38.4	205	65
40.4	218	69
42.4	232	73
44.4	246	73
46.4	259	73
48.4	273	73
50.4	286	75
52.4	300	77
54.4	313	74
56.4	327	70
58.4	341	67
60.4	354	69
62.4	368	71
64.4	381	73
66.4	395	72
68.4	409	70
70.4	422	69
72.4	436	72
74.4	449	73
76.4	463	74
78.4	477	74
80.4	490	74
82.4	504	73
84.4	517	72
86.4	531	72
88.4	544	68
90.4	558	67
92.4	572	69
94.4	585	68
96.4	599	63
98.4	612	61
100.4	626	62
102.4	640	63
104.4	653	63
106.4	667	64
108.4	680	64
110.4	694	65
112.4	707	66
114.4	721	67
116.4	735	68
118.4	748	68
120.4	762	70
122.4	775	71
124.4	789	69
126.4	803	70
128.4	816	72
130.4	830	74
132.4	843	74
134.4	857	73
136.4	870	71
138.4	884	70
140.4	898	70
142.4	911	69
144.4	925	65
146.4	938	60
148.4	952	61
149.2	957	65
151.2	971	67
153.2	985	68
155.2	998	68
157.2	1012	70
159.2	1025	71
161.2	1039	74
163.2	1053	76
165.2	1066	77
167.2	1080	75
169.2	1093	72
171.2	1107	70
173.2	1120	70
175.2	1134	70
177.2	1148	71
179.2	1161	72
181.2	1175	72
183.2	1188	69
185.2	1202	66
187.2	1216	64
189.2	1229	62
191.2	1243	60
193.2	1256	59
195.2	1270	57
197.2	1284	54
199.2	1297	51
201.2	1311	51
203.2	1324	52
205.2	1339	52
207.2	1365	52
209.2	1391	53
211.2	1418	55
213.2	1444	55
215.2	1470	56
217.2	1496	58
219.2	1522	61
221.2	1548	62
223.2	1575	63
225.2	1601	64
227.2	1627	66
229.2	1653	69
231.2	1679	75
233.2	1705	79
235.2	1732	85
237.2	1758	92
239.2	1784	103
241.2	1810	125
243.2	1836	129
245.2	1862	103
247.2	1889	77
249.2	1915	64
251.2	1941	57
253.2	1967	53
255.2	1993	50
257.2	2019	50
259.2	2046	50
261.2	2072	49
263.2	2098	45
265.2	2124	43
267.2	2150	41
269.2	2176	41
271.2	2203	40
273.2	2229	36
275.2	2255	32
277.2	2281	32
279.2	2307	33
281.2	2333	37
283.2	2360	38
285.2	2386	36
287.2	2412	36
289.2	2438	39
291.2	2464	45
293.2	2490	46
295.2	2517	42
297.2	2543	38
300	2579	43
302	2606	46
304	2632	47
306	2658	48
308	2684	49
310	2710	49
312	2736	49
314	2763	49
316	2789	48
318	2815	46
320	2841	46
322	2867	45
324	2893	43
326	2920	41
328	2931	39
330	2943	41
332	2955	46
334	2966	50
336	2978	50
338	2990	48
340	3001	46
342	3013	46
344	3025	45
346	3037	44
348	3048	44

Depth (cm)	Age (yr BP)	MS (SI)
350	3060	44
352	3072	46
354	3083	47
356	3095	48
358	3107	50
360	3119	51
362	3130	51
364	3142	52
366	3154	54
368	3165	54
370	3177	54
372	3189	53
374	3200	52
376	3212	51
378	3224	49
380	3236	49
382	3247	49
384	3259	50
386	3271	50
388	3282	51
390	3294	49
392	3306	48
394	3318	46
396	3329	44
398	3341	43
400	3353	43
402	3364	42
404	3376	39
406	3388	35
408	3399	35
410	3411	35
412	3423	33
414	3435	31
416	3446	31
418	3458	35
420	3470	43
422	3481	61
424	3493	92
426	3507	140
428	3524	163
430	3540	168
432	3556	179
434	3573	170
436	3589	129
438	3605	89
440	3622	63
442	3638	48

Depth (cm)	Age (yr BP)	MS (SI)
444	3654	38
446	3671	32
448.8	3694	34
450.8	3710	33
452.8	3726	32
454.8	3743	28
456.8	3759	27
458.8	3775	25
460.8	3792	26
462.8	3808	28
464.8	3824	29
466.8	3841	30
468.8	3857	29
470.8	3873	28
472.8	3890	30
474.8	3906	31
476.8	3923	31
478.8	3939	31
480.8	3955	31
482.8	3972	32
484.8	3988	32
486.8	4004	32
488.8	4021	33
490.8	4037	34
492.8	4053	34
494.8	4070	33
496.8	4086	33
498.8	4102	34
500.8	4119	34
502.8	4135	33
504.8	4151	31
506.8	4168	31
508.8	4184	30
510.8	4201	28
512.8	4218	28
514.8	4234	28
516.8	4251	27
518.8	4267	29
520.8	4284	28
522.8	4301	28
524.8	4317	29
526.8	4334	29
528.8	4350	28
530.8	4367	29
532.8	4384	27
534.8	4400	27
536.8	4417	25

Depth (cm)	Age (yr BP)	MS (SI)
538.8	4434	25
540.8	4450	25
542.8	4467	25
544.8	4483	25
546.8	4500	25
548.8	4517	26
550.8	4533	26
552.8	4550	26
554.8	4566	26
556.8	4583	25
558.8	4600	26
560.8	4616	26
562.8	4633	26
564.8	4650	26
566.8	4666	26
568.8	4683	25
570.8	4699	24
572.8	4716	24
574.8	4733	24
576.8	4749	25
578.8	4766	27
580.8	4782	36
582.8	4799	36
584.8	4816	44
586.8	4832	42
588.8	4849	47
590.8	4866	55
592.8	4882	50
594.8	4899	43
596.8	4915	42
597.6	4922	49
599.6	4939	44
601.6	4955	31
603.6	4972	29
605.6	4989	29
607.6	5005	30
609.6	5022	30
611.6	5038	30
613.6	5055	33
615.6	5072	35
617.6	5088	32
619.6	5105	30
621.6	5121	29
623.6	5138	30
625.6	5155	29
627.6	5171	29
629.6	5188	28

Depth (cm)	Age (yr BP)	MS (SI)
631.6	5205	28
633.6	5221	28
635.6	5237	27
637.6	5252	26
639.6	5267	26
641.6	5282	27
643.6	5297	27
645.6	5313	28
647.6	5328	28
649.6	5343	29
651.6	5358	30
653.6	5373	29
655.6	5388	28
657.6	5404	27
659.6	5419	27
661.6	5434	26
663.6	5449	24
665.6	5464	22
667.6	5480	22
669.6	5495	22
671.6	5510	22
673.6	5525	21
675.6	5540	20
677.6	5555	20
679.6	5571	20
681.6	5586	21
683.6	5601	23
685.6	5616	25
687.6	5631	28
689.6	5646	30
691.6	5662	30
693.6	5677	27
695.6	5692	27
697.6	5707	26
699.6	5722	24
701.6	5738	24
703.6	5753	
705.6	5768	22
707.6	5783	22
709.6	5798	23
711.6	5813	24
713.6	5829	24
715.6	5844	24
717.6	5859	24
719.6	5874	25
721.6	5889	26
723.6	5905	25

Depth (cm)	Age (yr BP)	MS (SI)
725.6	5920	24
727.6	5935	23
729.6	5950	23
731.6	5965	22
733.6	5980	23
735.6	5996	23
737.6	6011	23
739.6	6026	21
741.6	6041	20
743.6	6056	19
745.6	6071	21
746.4	6076	24
748.4	6083	25
750.4	6090	24
752.4	6097	23
754.4	6105	23
756.4	6112	22
758.4	6119	22
760.4	6126	23
762.4	6133	24
764.4	6141	25
766.4	6148	26
768.4	6155	28
770.4	6162	27
772.4	6169	25
774.4	6177	22
776.4	6184	20
778.4	6191	21
780.4	6198	20
782.4	6205	21
784.4	6212	21
786.4	6220	22
788.4	6227	22
790.4	6234	22
792.4	6241	22
794.4	6248	22
796.4	6256	24
798.4	6263	24
800.4	6270	24
802.4	6277	24
804.4	6284	24
806.4	6292	25
808.4	6299	23
810.4	6306	23
812.4	6313	23
814.4	6320	23
816.4	6327	23

Depth (cm)	Age (yr BP)	MS (SI)
818.4	6335	23
820.4	6342	22
822.4	6347	21
824.4	6351	20
826.4	6355	20
828.4	6360	19
830.4	6364	19
832.4	6368	19
834.4	6372	18
836.4	6377	18
838.4	6381	17
840.4	6385	18
842.4	6389	19
844.4	6393	20
846.4	6398	20
848.4	6402	20
850.4	6406	20
852.4	6410	20
854.4	6415	21
856.4	6419	20
858.4	6423	20
860.4	6427	20
862.4	6431	0
864.4	6436	20
866.4	6440	21
868.4	6444	22
870.4	6448	24
872.4	6453	24
874.4	6457	24
876.4	6461	24
878.4	6465	24
880.4	6469	26
882.4	6474	27
884.4	6478	27
886.4	6482	26
888.4	6486	24
890.4	6491	22
892.4	6495	20
894.4	6499	20
897.2	6505	22
899.2	6509	22
901.2	6513	22
903.2	6518	22
905.2	6522	21
907.2	6526	21
909.2	6530	21
911.2	6535	21

Depth (cm)	Age (yr BP)	MS (SI)
913.2	6539	20
915.2	6543	20
917.2	6547	21
919.2	6551	20
921.2	6556	21
923.2	6560	23
925.2	6564	25
927.2	6568	25
929.2	6573	26
931.2	6577	27
933.2	6581	
935.2	6585	29
937.2	6589	26
939.2	6594	25
941.2	6598	23
943.2	6602	21
945.2	6606	22
947.2	6611	21
949.2	6615	21
951.2	6619	21
953.2	6623	21
955.2	6627	21
957.2	6632	20
959.2	6636	21
961.2	6640	19
963.2	6644	19
965.2	6649	18
967.2	6653	17
969.2	6657	17
971.2	6661	17
973.2	6665	18
975.2	6670	18
977.2	6674	18
979.2	6678	18
981.2	6682	19
983.2	6687	19
985.2	6691	19
987.2	6695	19
989.2	6699	18
991.2	6703	18
993.2	6708	16
995.2	6712	17
997.2	6716	17
999.2	6720	17
1001.2	6725	16
1003.2	6729	15
1005.2	6733	15

Depth (cm)	Age (yr BP)	MS (SI)
1007.2	6737	15
1009.2	6742	14
1011.2	6746	15
1013.2	6750	15
1015.2	6754	15
1017.2	6758	16
1019.2	6763	16
1021.2	6767	16
1023.2	6771	17
1025.2	6775	17
1027.2	6793	17
1029.2	6820	17
1031.2	6847	17
1033.2	6874	17
1035.2	6900	17
1037.2	6927	17
1039.2	6954	16
1041.2	6981	15
1043.2	7008	14
1046	7045	17
1048	7072	18
1050	7099	17
1052	7126	17
1054	7153	16
1056	7179	16
1058	7206	16
1060	7233	15
1062	7260	15
1064	7287	15
1066	7313	15
1068	7340	15
1070	7367	16
1072	7394	15
1074	7421	16
1076	7448	16
1078	7474	16
1080	7501	16
1082	7528	15
1084	7555	16
1086	7582	15
1088	7609	15
1090	7635	16
1092	7662	16
1094	7689	16
1096	7716	16
1098	7743	15
1100	7769	15

Depth (cm)	Age (yr BP)	MS (SI)
1102	7796	16
1104	7823	15
1106	7850	15
1108	7877	15
1110	7904	15
1112	7930	15
1114	7957	15
1116	7984	15
1118	8011	15
1120	8030	15
1122	8027	16
1124	8024	16
1126	8021	16
1128	8018	16
1130	8015	16
1132	8012	17
1134	8009	17
1136	8006	17
1138	8003	16
1140	8000	17
1142	7997	17
1144	7994	18
1146	7991	19
1148	7988	18
1150	7985	18
1152	7982	19
1154	7979	20
1156	7976	21
1158	7973	23
1160	7970	26
1162	7966	28
1164	7963	28
1166	7960	27
1168	7957	25
1170	7954	23
1172	7951	21
1174	7948	20
1176	7945	19
1178	7942	18
1180	7939	17
1182	7936	18
1184	7933	18
1186	7930	18
1188	7927	18
1190	7924	17
1192	7921	15
1194.8	7917	17

Depth (cm)	Age (yr BP)	MS (SI)
1196.8	7914	17
1198.8	7911	18
1200.8	7908	18
1202.8	7905	18
1204.8	7901	18
1206.8	7898	17
1208.8	7895	17
1210.8	7892	17
1212.8	7889	17
1214.8	7886	16
1216.8	7883	16
1218.8	7880	17
1220.8	7877	17
1222.8	7874	17
1224.8	7871	16
1226.8	7868	17
1228.8	7858	17
1230.8	7845	17
1232.8	7832	18
1234.8	7819	18
1236.8	7806	19
1238.8	7793	18
1240.8	7780	19
1242.8	7767	19
1244.8	7754	19
1246.8	7741	19
1248.8	7727	19
1250.8	7714	19
1252.8	7701	18
1254.8	7688	19
1256.8	7675	18
1258.8	7662	18
1260.8	7649	19
1262.8	7636	20
1264.8	7623	19
1266.8	7609	19
1268.8	7596	20
1270.8	7583	20
1272.8	7570	19
1274.8	7557	18
1276.8	7544	18
1278.8	7531	18
1280.8	7518	18
1282.8	7505	19
1284.8	7492	19
1286.8	7478	19
1288.8	7465	19

Depth (cm)	Age (yr BP)	MS (SI)
1290.8	7452	19
1292.8	7439	20
1294.8	7426	19
1296.8	7413	19
1298.8	7400	19
1300.8	7387	19
1302.8	7374	19
1304.8	7360	19
1306.8	7347	19
1308.8	7334	19
1310.8	7321	20
1312.8	7308	20
1314.8	7295	21
1316.8	7282	21
1318.8	7269	21
1320.8	7256	21
1322.8	7243	20
1324.8	7229	22
1326.8	7216	22
1328.8	7203	22
1330.8	7190	22
1332.8	7177	22
1334.8	7164	21
1336.8	7151	20
1338.8	7138	19
1340.8	7125	17
1342.8	7111	18
1343.6	7106	20
1345.6	7093	21
1347.6	7080	21
1349.6	7067	21
1351.6	7054	20
1353.6	7041	20
1355.6	7028	20
1357.6	7014	21
1359.6	7001	22
1361.6	6988	22
1363.6	6975	23
1365.6	6980	24
1367.6	7026	24
1369.6	7073	24
1371.6	7119	24
1373.6	7165	24
1375.6	7212	24
1377.6	7258	24
1379.6	7304	25
1381.6	7350	26

Depth (cm)	Age (yr BP)	MS (SI)
1383.6	7397	27
1385.6	7443	27
1387.6	7489	27
1389.6	7536	28
1391.6	7582	31
1393.6	7628	34
1395.6	7675	38
1397.6	7721	43
1399.6	7767	47
1401.6	7814	54
1403.6	7860	67
1405.6	7906	80
1407.6	7953	86
1409.6	7999	81
1411.6	8045	66
1413.6	8092	51
1415.6	8138	41
1417.6	8184	35
1419.6	8231	32
1421.6	8277	28
1423.6	8323	26
1425.6	8370	25
1427.6	8416	25
1429.6	8462	25
1431.6	8509	26
1433.6	8555	27
1435.6	8601	29
1437.6	8648	30
1439.6	8694	30
1441.6	8740	28
1443.6	8787	28
1445.6	8833	27
1447.6	8879	28
1449.6	8926	28
1451.6	8972	28
1453.6	9018	27
1455.6	9065	27
1457.6	9111	27
1459.6	9157	27
1461.6	9203	27
1463.6	9250	28
1465.6	9296	28
1467.6	9342	27
1469.6	9389	28
1471.6	9435	27
1473.6	9481	28
1475.6	9528	28

Depth (cm)	Age (yr BP)	MS (SI)
1477.6	9574	29
1479.6	9620	29
1481.6	9667	30
1483.6	9713	29
1485.6	9759	29
1487.6	9806	28
1489.6	9852	27
1491.6	9898	28
1492.4	9917	25
1494.4	9963	28
1496.4	10010	29
1498.4	10041	28
1500.4	10054	28
1502.4	10068	28
1504.4	10081	28
1506.4	10095	29
1508.4	10108	29
1510.4	10121	30
1512.4	10135	30
1514.4	10148	31
1516.4	10162	31
1518.4	10175	30
1520.4	10188	32
1522.4	10202	31
1524.4	10215	32
1526.4	10229	33
1528.4	10242	35
1530.4	10255	35
1532.4	10269	36
1534.4	10282	36
1536.4	10296	37
1538.4	10309	36
1540.4	10322	36
1542.4	10336	38
1544.4	10349	38
1546.4	10363	39
1548.4	10376	40
1550.4	10389	40
1552.4	10403	40
1554.4	10416	40
1556.4	10430	40
1558.4	10443	40
1560.4	10457	40
1562.4	10470	39
1564.4	10483	40
1566.4	10497	41
1568.4	10510	42
1570.4	10524	42
1572.4	10537	39
1574.4	10550	37
1576.4	10564	35
1578.4	10577	35
1580.4	10591	35
1582.4	10604	36
1584.4	10617	36
1586.4	10631	37
1588.4	10644	38
1590.4	10658	39
1592.4	10671	42
1594.4	10684	44
1596.4	10698	46
1598.4	10711	48
1600.4	10725	52
1602.4	10738	61
1604.4	10751	84
1606.4	10765	132
1608.4	10778	112
1610.4	10792	68
1612.4	10805	53
1614.4	10818	53
1616.4	10832	63
1618.4	10845	75
1620.4	10859	78
1622.4	10872	77
1624.4	10885	68
1626.4	10899	42

MD3006

Depth (cm)	Age (yr BP)	MS (SI)
0.4	1	11
2.4	5	14
4.4	9	15
6.4	13	15
8.4	17	16
10.4	21	16
12.4	25	15
14.4	29	16
16.4	33	18
18.4	37	19
20.4	41	19
22.4	45	19
24.4	49	18
26.4	53	18
28.4	57	17
30.4	61	16
32.4	65	16
34.4	69	16
36.4	73	17
38.4	77	17
40.4	81	17
42.4	85	17
44.4	89	16
46.4	93	18
48.4	97	17
50.4	101	16
52.4	105	
54.4	109	14
56.4	113	15
58.4	117	15
60.4	121	15
62.4	125	14
64.4	129	15
66.4	133	14
68.4	137	15
70.4	141	16
72.4	145	16
74.4	149	16
76.4	153	17
78.4	157	17
80.4	161	17
82.4	166	17
84.4	170	17
86.4	174	17
88.4	178	18
90.4	182	17
92.4	186	18
94.4	190	18
96.4	194	19
98.4	198	19
100.4	202	18
102.4	206	19
104.4	210	19
106.4	214	20
108.4	218	20
110.4	222	20
112.4	226	21
114.4	230	21
116.4	236	21
118.4	249	22
120.4	262	21
122.4	276	21
124.4	289	21
126.4	302	21
128.4	316	22
130.4	329	21
132.4	342	21
134.4	356	21
136.4	369	21
138.4	382	21
140.4	396	20
142.4	409	20
144.4	422	20
146.4	436	19
148.4	449	19
151.6	470	23
153.6	484	23
155.6	497	22
157.6	510	22
159.6	524	21
161.6	537	21
163.6	550	21
165.6	564	20
167.6	577	19
169.6	590	20
171.6	604	19
173.6	617	18
175.6	630	17
177.6	644	16
179.6	657	14
181.6	670	14
183.6	684	14
185.6	697	13
187.6	710	13
189.6	724	12
191.6	737	10
193.6	750	11
195.6	764	10
197.6	777	10
199.6	790	10
201.6	804	10
203.6	817	10
205.6	830	10
207.6	844	10
209.6	857	9
211.6	870	10
213.6	883	10
215.6	897	10
217.6	910	10

Depth (cm)	Age (yr BP)	MS (SI)
219.6	923	10
221.6	937	10
223.6	950	9
225.6	963	9
227.6	977	9
229.6	990	10
231.6	1003	12
233.6	1017	10
235.6	1030	10
237.6	1043	10
239.6	1057	10
241.6	1070	11
243.6	1083	14
245.6	1097	22
247.6	1110	31
249.6	1123	26
251.6	1137	17
253.6	1150	12
255.6	1163	11
257.6	1177	10
259.6	1190	10
261.6	1203	11
263.6	1217	12
265.6	1230	12
267.6	1243	10
269.6	1257	9
271.6	1270	8
273.6	1283	7
275.6	1297	7
277.6	1310	7
279.6	1323	7
281.6	1337	8
283.6	1350	8
285.6	1363	7
287.6	1377	7
289.6	1390	7
291.6	1403	7
293.6	1417	7
295.6	1430	6
297.6	1443	6
299.6	1457	
300.5	1463	8
302.5	1476	9
304.5	1489	9
306.5	1500	9
308.5	1507	8
310.5	1515	9

Depth (cm)	Age (yr BP)	MS (SI)
312.5	1523	9
314.5	1530	9
316.5	1538	9
318.5	1545	9
320.5	1553	9
322.5	1561	10
324.5	1568	11
326.5	1576	12
328.5	1583	13
330.5	1591	14
332.5	1599	16
334.5	1606	18
336.5	1614	21
338.5	1621	25
340.5	1629	25
342.5	1637	19
344.5	1644	15
346.5	1652	11
348.5	1659	10
350.5	1667	9
352.5	1675	9
354.5	1682	9
356.5	1690	9
358.5	1697	8
360.5	1705	8
362.5	1713	9
364.5	1720	8
366.5	1728	8
368.5	1735	9
370.5	1743	9
372.5	1751	9
374.5	1758	9
376.5	1766	8
378.5	1773	8
380.5	1781	9
382.5	1789	9
384.5	1796	8
386.5	1804	8
388.5	1811	8
390.5	1819	8
392.5	1827	9
394.5	1834	8
396.5	1842	8
398.5	1849	8
400.5	1857	9
402.5	1864	8
404.5	1872	8

Depth (cm)	Age (yr BP)	MS (SI)
406.5	1880	9
408.5	1887	9
410.5	1895	8
412.5	1902	8
414.5	1910	8
416.5	1918	9
418.5	1925	9
420.5	1933	8
422.5	1940	8
424.5	1948	9
426.5	1956	8
428.5	1963	8
430.5	1971	8
432.5	1978	8
434.5	1986	9
436.5	1994	8
438.5	2001	9
440.5	2009	8
442.5	2016	8
444.5	2024	8
446.5	2032	8
448.5	2039	7
455.4	2062	8
457.4	2069	8
459.4	2075	9
461.4	2081	8
463.4	2088	8
465.4	2094	8
467.4	2101	8
469.4	2107	8
471.4	2113	9
473.4	2120	8
475.4	2126	9
477.4	2132	9
479.4	2139	9
481.4	2145	9
483.4	2151	8
485.4	2158	9
487.4	2164	8
489.4	2170	9
491.4	2177	9
493.4	2183	8
495.4	2190	8
497.4	2196	9
499.4	2202	9
501.4	2209	8
503.4	2215	8

Depth (cm)	Age (yr BP)	MS (SI)
505.4	2221	9
507.4	2228	9
509.4	2234	9
511.4	2240	8
513.4	2247	9
515.4	2253	
517.4	2259	9
519.4	2266	9
521.4	2272	9
523.4	2279	8
525.4	2285	9
527.4	2291	9
529.4	2298	8
531.4	2304	8
533.4	2310	8
535.4	2317	8
537.4	2323	8
539.4	2329	9
541.4	2336	9
543.4	2342	8
545.4	2348	9
547.4	2355	8
549.4	2361	9
551.4	2368	8
553.4	2374	8
555.4	2380	8
557.4	2387	8
559.4	2393	8
561.4	2399	8
563.4	2406	9
565.4	2412	8
567.4	2418	8
569.4	2425	8
571.4	2431	8
573.4	2438	8
575.4	2444	8
577.4	2450	8
579.4	2457	8
581.4	2463	8
583.4	2469	8
585.4	2476	8
587.4	2482	8
589.4	2488	8
591.4	2495	7
593.4	2501	7
595.4	2507	7
597.4	2514	7

Depth (cm)	Age (yr BP)	MS (SI)
599.4	2520	7
600.3	2523	8
602.3	2529	8
604.3	2536	8
606.3	2542	8
608.3	2548	8
610.3	2555	8
612.3	2561	8
614.3	2568	8
616.3	2574	7
618.3	2580	8
620.3	2587	8
622.3	2593	8
624.3	2599	8
626.3	2606	8
628.3	2612	8
630.3	2618	8
632.3	2625	8
634.3	2631	8
636.3	2637	8
638.3	2644	8
640.3	2650	8
642.3	2657	8
644.3	2663	8
646.3	2669	9
648.3	2676	8
650.3	2682	9
652.3	2688	8
654.3	2695	8
656.3	2701	8
658.3	2707	9
660.3	2714	8
662.3	2720	9
664.3	2726	9
666.3	2733	8
670.3	2746	8
672.3	2752	8
674.3	2758	8
676.3	2765	9
678.3	2771	8
680.3	2777	8
682.3	2784	8
684.3	2790	9
686.3	2796	9
688.3	2803	8
690.3	2809	8
692.3	2815	9

Depth (cm)	Age (yr BP)	MS (SI)
694.3	2822	8
696.3	2828	8
698.3	2835	8
700.3	2841	8
702.3	2847	8
704.3	2854	8
706.3	2860	9
708.3	2866	9
710.3	2873	9
712.3	2879	10
714.3	2885	11
716.3	2892	9
718.3	2898	8
720.3	2904	9
722.3	2911	8
724.3	2917	8
726.3	2924	8
728.3	2930	8
730.3	2936	9
732.3	2943	8
734.3	2949	8
736.3	2955	8
738.3	2962	7
740.3	2968	7
742.3	2974	6
742.7	2976	17
744.7	2982	15
746.7	2988	13
748.7	2995	13
750.7	3001	12
752.7	3007	12
754.7	3014	13
756.7	3020	12
758.7	3027	12
760.7	3033	12
668.3	2739	8
762.7	3039	12
764.7	3046	13
766.7	3052	13
768.7	3058	12
770.7	3064	13
772.7	3070	13
774.7	3076	13
776.7	3082	13
778.7	3088	14
780.7	3094	14
782.7	3100	14

Depth (cm)	Age (yr BP)	MS (SI)
784.7	3106	14
786.7	3112	14
788.7	3118	13
790.7	3124	12
792.7	3130	12
794.7	3136	12
796.7	3143	12
798.7	3149	12
800.7	3155	13
802.7	3161	14
804.7	3167	15
806.7	3173	14
808.7	3179	14
810.7	3185	14
812.7	3191	14
814.7	3197	15
816.7	3203	15
818.7	3209	16
820.7	3215	16
822.7	3221	16
824.7	3227	16
826.7	3233	16
828.7	3239	16
830.7	3245	14
832.7	3251	13
834.7	3257	13
836.7	3263	13
838.7	3269	13
840.7	3275	13
842.7	3281	13
844.7	3287	15
846.7	3293	14
848.7	3299	14
850.7	3305	15
852.7	3311	18
854.7	3317	20
858.7	3329	29
860.7	3335	31
862.7	3341	32
864.7	3347	30
866.7	3354	27
868.7	3360	24
870.7	3366	19
872.7	3372	15
874.7	3378	12
876.7	3384	11
877.5	3386	11

Depth (cm)	Age (yr BP)	MS (SI)
879.5	3392	10
881.5	3398	10
883.5	3404	10
885.5	3410	10
887.5	3416	10
889.5	3422	9
891.5	3428	10
893.5	3434	9
895.5	3440	10
897.5	3446	11
899.5	3452	10
901.5	3458	11
903.5	3464	11
905.5	3470	10
907.5	3476	10
909.5	3483	9
911.5	3489	10
913.5	3495	10
915.5	3501	9
917.5	3507	10
919.5	3513	10
921.5	3519	10
923.5	3525	10
925.5	3531	10
927.5	3537	11
929.5	3543	10
931.5	3549	10
933.5	3555	11
935.5	3561	11
937.5	3567	11
939.5	3573	11
941.5	3579	10
943.5	3585	10
945.5	3591	10
947.5	3597	10
949.5	3603	11
856.7	3323	26
951.5	3609	10
953.5	3615	10
955.5	3621	10
957.5	3627	11
959.5	3633	11
961.5	3639	11
963.5	3645	11
965.5	3651	10
967.5	3657	10
969.5	3663	11

Depth (cm)	Age (yr BP)	MS (SI)
971.5	3669	11
973.5	3675	11
975.5	3681	11
977.5	3687	11
979.5	3694	11
981.5	3700	11
983.5	3706	11
985.5	3712	10
987.5	3718	11
989.5	3724	10
991.5	3730	10
993.5	3736	10
995.5	3742	10
997.5	3748	10
999.5	3754	9
1001.5	3760	10
1003.5	3766	10
1005.5	3772	10
1007.5	3778	10
1009.5	3784	10
1011.5	3790	10
1013.5	3796	10
1015.5	3802	10
1017.5	3808	10
1019.5	3814	10
1021.5	3820	9
1023.5	3826	8
1025.5	3832	8
1028.2	3840	9
1030.2	3846	10
1032.2	3852	10
1034.2	3858	11
1036.2	3864	11
1038.2	3870	11
1040.2	3876	11
1042.2	3883	11
1044.2	3889	11
1048.2	3901	11
1050.2	3907	12
1052.2	3913	11
1054.2	3919	11
1056.2	3925	10
1058.2	3931	11
1060.2	3937	11
1062.2	3943	11
1064.2	3949	11
1066.2	3955	11

Depth (cm)	Age (yr BP)	MS (SI)
1068.2	3961	11
1070.2	3967	11
1072.2	3973	11
1074.2	3979	11
1076.2	3985	10
1078.2	3991	10
1080.2	3997	11
1082.2	4003	11
1084.2	4009	11
1086.2	4015	11
1088.2	4021	10
1090.2	4027	10
1092.2	4033	11
1094.2	4039	11
1096.2	4045	11
1098.2	4051	11
1100.2	4057	11
1102.2	4063	10
1104.2	4069	10
1106.2	4075	11
1108.2	4081	11
1110.2	4087	11
1112.2	4094	11
1114.2	4100	11
1116.2	4106	11
1118.2	4112	11
1120.2	4118	10
1122.2	4124	11
1124.2	4130	10
1126.2	4136	10
1128.2	4142	10
1130.2	4148	10
1132.2	4154	10
1134.2	4160	11
1136.2	4166	10
1138.2	4172	10
1140.2	4178	11
1046.2	3895	11
1142.2	4184	10
1144.2	4190	10
1146.2	4196	10
1148.2	4202	10
1150.2	4208	9
1152.2	4214	10
1154.2	4220	10
1156.2	4225	9
1158.2	4230	10

Depth (cm)	Age (yr BP)	MS (SI)
1160.2	4235	10
1162.2	4240	9
1164.2	4245	10
1166.2	4250	10
1168.2	4255	10
1170.2	4259	9
1172.2	4264	9
1174.2	4269	8
1176.2	4274	9
1177.2	4277	9
1179.2	4282	10
1181.2	4287	10
1183.2	4292	10
1185.2	4297	10
1187.2	4302	11
1189.2	4308	11
1191.2	4313	12
1193.2	4319	15
1195.2	4324	13
1197.2	4330	11
1199.2	4335	11
1201.2	4341	11
1203.2	4346	11
1205.2	4352	10
1207.2	4357	10
1209.2	4363	10
1211.2	4368	10
1213.2	4374	11
1215.2	4379	10
1217.2	4385	11
1219.2	4390	10
1221.2	4396	10
1223.2	4401	11
1225.2	4407	10
1227.2	4412	10
1229.2	4418	11
1231.2	4423	12
1233.2	4429	16
1237.2	4440	16
1239.2	4445	17
1241.2	4451	16
1243.2	4456	13
1245.2	4462	12
1247.2	4467	11
1249.2	4473	11
1251.2	4478	11
1253.2	4484	12

Depth (cm)	Age (yr BP)	MS (SI)
1255.2	4489	12
1257.2	4495	12
1259.2	4500	11
1261.2	4506	10
1263.2	4511	10
1265.2	4517	11
1267.2	4523	11
1269.2	4528	11
1271.2	4534	11
1273.2	4539	12
1275.2	4545	11
1277.2	4550	11
1279.2	4556	12
1281.2	4561	11
1283.2	4567	11
1285.2	4572	11
1287.2	4578	11
1289.2	4583	11
1291.2	4589	11
1293.2	4594	11
1295.2	4600	11
1297.2	4605	11
1299.2	4611	11
1301.2	4616	11
1303.2	4622	10
1305.2	4627	10
1307.2	4633	11
1309.2	4638	11
1311.2	4644	11
1313.2	4649	10
1315.2	4655	10
1317.2	4660	11
1319.2	4666	10
1321.2	4671	10
1323.2	4677	10
1325.2	4682	9
1328.1	4690	10
1330.1	4696	11
1235.2	4434	19
1332.1	4701	11
1334.1	4707	11
1336.1	4712	11
1338.1	4718	11
1340.1	4723	12
1342.1	4729	11
1344.1	4734	11
1346.1	4740	11

Depth (cm)	Age (yr BP)	MS (SI)
1348.1	4745	11
1350.1	4751	11
1352.1	4756	10
1354.1	4762	10
1356.1	4767	10
1358.1	4773	11
1360.1	4778	10
1362.1	4784	10
1364.1	4790	10
1366.1	4795	10
1368.1	4801	10
1370.1	4806	11
1372.1	4812	11
1374.1	4817	10
1376.1	4823	10
1378.1	4828	10
1380.1	4834	10
1382.1	4839	10
1384.1	4845	10
1386.1	4850	9
1388.1	4856	9
1390.1	4861	9
1392.1	4867	9
1394.1	4872	8
1396.1	4878	8
1398.1	4883	8
1400.1	4889	8
1402.1	4894	8
1404.1	4900	8
1406.1	4905	9
1408.1	4911	9
1410.1	4916	9
1412.1	4922	9
1414.1	4927	10
1416.1	4933	9
1418.1	4938	9
1420.1	4944	9
1422.1	4949	9
1424.1	4955	9
1428.1	4966	8
1430.1	4971	8
1432.1	4977	9
1434.1	4982	9
1436.1	4988	8
1438.1	4993	9
1440.1	4999	9
1442.1	5004	8

Depth (cm)	Age (yr BP)	MS (SI)
1444.1	5010	8
1446.1	5015	8
1448.1	5021	9
1450.1	5026	8
1452.1	5032	8
1454.1	5038	9
1456.1	5043	9
1458.1	5049	9
1460.1	5054	8
1462.1	5060	8
1464.1	5065	9
1466.1	5071	8
1468.1	5076	8
1470.1	5082	8
1472.1	5087	8
1474.1	5093	7
1476.1	5098	6
1478.8	5106	7
1480.8	5111	7
1482.8	5117	8
1484.8	5122	8
1486.8	5128	8
1488.8	5133	9
1490.8	5139	12
1492.8	5144	11
1494.8	5150	11
1496.8	5155	9
1498.8	5161	9
1500.8	5166	9
1502.8	5175	9
1504.8	5190	9
1506.8	5205	8
1508.8	5219	8
1510.8	5234	8
1512.8	5248	8
1514.8	5263	8
1516.8	5278	9
1518.8	5292	7
1520.8	5307	8
1426.1	4960	8
1522.8	5322	8
1524.8	5336	7
1526.8	5351	8
1528.8	5366	8
1530.8	5380	8
1532.8	5395	8
1534.8	5409	8

Depth (cm)	Age (yr BP)	MS (SI)
1536.8	5424	8
1538.8	5439	8
1540.8	5453	8
1542.8	5468	7
1544.8	5483	8
1546.8	5497	8
1548.8	5512	8
1550.8	5526	7
1552.8	5541	8
1554.8	5556	8
1556.8	5570	7
1558.8	5585	8
1560.8	5600	8
1562.8	5614	7
1564.8	5629	7
1566.8	5643	7
1568.8	5658	8
1570.8	5673	8
1572.8	5687	8
1574.8	5702	8
1576.8	5717	8
1578.8	5731	8
1580.8	5746	
1582.8	5760	8
1584.8	5775	8
1586.8	5790	9
1588.8	5804	9
1590.8	5819	8
1592.8	5834	9
1594.8	5848	9
1596.8	5863	9
1598.8	5877	9
1600.8	5892	9
1602.8	5907	9
1604.8	5921	9
1606.8	5936	10
1608.8	5951	10
1610.8	5965	9
1612.8	5977	9
1614.8	5986	9
1618.8	6002	8
1620.8	6011	9
1622.8	6019	8
1624.8	6027	7
1626.8	6036	7
1628.6	6043	7
1630.6	6051	8

Depth (cm)	Age (yr BP)	MS (SI)
1632.6	6060	9
1634.6	6068	9
1636.6	6076	9
1638.6	6085	9
1640.6	6093	
1642.6	6101	9
1644.6	6110	9
1646.6	6118	8
1648.6	6126	9
1650.6	6135	9
1652.6	6143	10
1654.6	6151	9
1656.6	6160	9
1658.6	6168	10
1660.6	6176	11
1662.6	6185	11
1664.6	6193	10
1666.6	6201	
1668.6	6210	10
1670.6	6218	10
1672.6	6226	10
1674.6	6235	10
1676.6	6243	10
1678.6	6251	11
1680.6	6260	10
1682.6	6268	11
1684.6	6276	11
1686.6	6285	11
1688.6	6293	12
1690.6	6302	12
1692.6	6310	12
1694.6	6318	12
1696.6	6327	12
1698.6	6335	12
1700.6	6343	11
1702.6	6352	11
1704.6	6360	12
1706.6	6368	12
1708.6	6377	12
1710.6	6385	12
1616.8	5994	8
1712.6	6393	13
1714.6	6402	13
1716.6	6410	13
1718.6	6418	13
1720.6	6427	14
1722.6	6435	14

Depth (cm)	Age (yr BP)	MS (SI)
1724.6	6444	14
1726.6	6452	14
1728.6	6460	13
1730.6	6469	13
1732.6	6477	13
1734.6	6485	12
1736.6	6494	12
1738.6	6502	13
1740.6	6510	12
1742.6	6519	11
1744.6	6527	12
1746.6	6535	12
1748.6	6544	11
1750.6	6552	11
1752.6	6561	11
1754.6	6569	10
1756.6	6577	10
1758.6	6586	10
1760.6	6594	11
1762.6	6602	10
1764.6	6611	10
1766.6	6619	9
1768.6	6627	9
1770.6	6636	10
1772.6	6644	9
1774.6	6652	8
1776.6	6661	8
1782.9	6687	9
1784.9	6695	9
1786.9	6704	10
1788.9	6712	9
1790.9	6721	9
1792.9	6729	9
1794.9	6737	9
1796.9	6746	9
1798.9	6754	9
1800.9	6762	9
1802.9	6771	11
1804.9	6779	10
1806.9	6787	9
1808.9	6796	9
1812.9	6812	9
1814.9	6821	9
1816.9	6829	9
1818.9	6838	9
1820.9	6846	9
1822.9	6854	9

Depth (cm)	Age (yr BP)	MS (SI)
1824.9	6863	9
1826.9	6871	8
1828.9	6879	9
1830.9	6888	8
1832.9	6896	8
1834.9	6904	9
1836.9	6913	8
1838.9	6921	9
1840.9	6929	8
1842.9	6938	8
1844.9	6946	8
1846.9	6954	8
1848.9	6963	8
1850.9	6971	8
1852.9	6980	8
1854.9	6988	8
1856.9	6996	8
1858.9	7005	8
1860.9	7013	8
1862.9	7021	7
1864.9	7030	7
1866.9	7038	7
1868.9	7046	7
1870.9	7055	7
1872.9	7063	7
1874.9	7071	7
1876.9	7080	7
1878.9	7088	7
1880.9	7097	7
1882.9	7105	7
1884.9	7113	7
1886.9	7122	8
1888.9	7130	8
1890.9	7138	7
1892.9	7147	7
1894.9	7155	7
1896.9	7163	7
1898.9	7172	8
1900.9	7180	7
1902.9	7188	7
1904.9	7197	7
1810.9	6804	10
1906.9	7205	8
1908.9	7213	8
1910.9	7222	8
1912.9	7230	8
1914.9	7239	8

Depth (cm)	Age (yr BP)	MS (SI)
1916.9	7247	7
1918.9	7255	7
1920.9	7264	7
1922.9	7272	6
1924.9	7280	5
1926.9	7289	5
1927.6	7292	6
1929.6	7300	7
1931.6	7308	6
1933.6	7346	7
1935.6	7390	7
1937.6	7435	7
1939.6	7479	7
1941.6	7524	7
1943.6	7568	7
1945.6	7613	8
1947.6	7657	7
1949.6	7702	
1951.6	7746	8
1953.6	7791	8
1955.6	7835	8
1957.6	7880	8
1959.6	7924	8
1961.6	7968	8
1963.6	8013	8
1965.6	8057	8
1967.6	8102	8
1969.6	8146	8
1971.6	8191	8
1973.6	8235	8
1975.6	8280	7
1977.6	8324	8
1979.6	8369	8
1981.6	8413	7
1983.6	8458	8
1985.6	8502	8
1987.6	8547	8
1989.6	8591	8
1991.6	8636	8
1993.6	8680	8
1995.6	8725	9
1997.6	8769	8
2001.6	8858	9
2003.6	8903	10
2005.6	8947	11
2007.6	8992	11
2009.6	9036	11

Depth (cm)	Age (yr BP)	MS (SI)
2011.6	9081	10
2013.6	9125	9
2015.6	9170	9
2017.6	9214	9
2019.6	9259	9
2021.6	9303	9
2023.6	9348	9
2025.6	9392	9
2027.6	9437	9
2029.6	9481	9
2031.6	9526	9
2033.6	9554	9
2035.6	9570	
2037.6	9585	10
2039.6	9601	9
2041.6	9616	10
2043.6	9632	10
2045.6	9647	9
2047.6	9663	10
2049.6	9678	9
2051.6	9694	9
2053.6	9709	9
2055.6	9725	9
2057.6	9740	10
2059.6	9756	10
2061.6	9771	10
2063.6	9787	12
2065.6	9802	12
2067.6	9818	12
2069.6	9834	12
2071.6	9849	13
2073.6	9865	12
2075.6	9880	11
2077.6	9896	12
2077.7	9896	13
2079.7	9912	14
2081.7	9927	14
2083.7	9943	14
2085.7	9958	14
2087.7	9974	13
2089.7	9989	13
2091.7	10005	13
1999.6	8814	9
2093.7	10020	13
2095.7	10036	13
2097.7	10051	12
2099.7	10067	12

Depth (cm)	Age (yr BP)	MS (SI)
2101.7	10083	12
2103.7	10098	11
2105.7	10114	11
2107.7	10129	11
2109.7	10145	10
2111.7	10160	10
2113.7	10176	10
2115.7	10191	9
2117.7	10207	10
2119.7	10222	10
2121.7	10238	10
2123.7	10253	10
2125.7	10269	10
2127.7	10284	11
2129.7	10302	11
2131.7	10320	11
2133.7	10339	11
2135.7	10357	10
2137.7	10375	
2139.7	10394	11
2141.7	10412	11
2143.7	10430	13
2145.7	10449	13
2147.7	10467	15
2149.7	10486	15
2151.7	10504	17
2153.7	10522	17
2155.7	10541	18
2157.7	10559	19
2159.7	10577	19
2161.7	10596	19
2163.7	10614	
2165.7	10632	16
2167.7	10651	15
2169.7	10669	15
2171.7	10687	15
2173.7	10706	14
2175.7	10724	14
2177.7	10742	13
2179.7	10761	12
2181.7	10779	12
2183.7	10797	12
2185.7	10816	11
2189.7	10852	10
2191.7	10871	11
2193.7	10911	11
2195.7	10965	11

Depth (cm)	Age (yr BP)	MS (SI)
2197.7	11020	11
2199.7	11075	12
2201.7	11129	13
2203.7	11184	13
2205.7	11239	14
2207.7	11293	15
2209.7	11348	18
2211.7	11403	20
2213.7	11457	24
2215.7	11512	27
2217.7	11566	30
2219.7	11621	32
2221.7	11676	34
2223.7	11730	35
2225.7	11785	35
2232.1	11960	43
2234.1	12015	43
2236.1	12069	45
2238.1	12124	47
2240.1	12178	48
2242.1	12233	49
2244.1	12288	50
2246.1	12342	49
2248.1	12397	49
2250.1	12452	49
2252.1	12506	49
2254.1	12561	50
2256.1	12616	50
2258.1	12670	50
2260.1	12725	51
2262.1	12779	53
2264.1	12834	53
2266.1	12889	54
2268.1	12943	56
2270.1	12998	56
2272.1	13053	57
2274.1	13107	57
2276.1	13162	57
2278.1	13217	59
2280.1	13271	60
2282.1	13326	60
2284.1	13381	60
2286.1	13435	60
2187.7	10834	11
2288.1	13490	58
2290.1	13544	56
2292.1	13599	52

Depth (cm)	Age (yr BP)	MS (SI)
2294.1	13654	49
2296.1	13708	48
2298.1	13763	49
2300.1	13818	49
2302.1	13872	49
2304.1	13927	51
2306.1	13982	51
2308.1	14036	52
2310.1	14091	55
2312.1	14146	55
2314.1	14200	56
2316.1	14255	55
2318.1	14309	56
2320.1	14357	57
2322.1	14369	56
2324.1	14381	57
2326.1	14394	57
2328.1	14406	57
2330.1	14419	54
2332.1	14431	57
2334.1	14443	56
2336.1	14456	56
2338.1	14468	56
2340.1	14480	57
2342.1	14493	56
2344.1	14505	57
2346.1	14518	56
2348.1	14530	56
2350.1	14542	54
2352.1	14555	54
2354.1	14567	53
2356.1	14579	47
2358.1	14592	36
2360.1	14604	19

MD3007

1.7	5	144
3.7	11	154
5.7	17	154
7.7	22	154
9.7	28	166
11.7	34	185
13.7	40	205
15.7	46	187
17.7	52	147
19.7	57	120

Depth (cm)	Age (yr BP)	MS (SI)
21.7	63	109
23.7	69	116
25.7	75	129
27.7	81	134
29.7	87	121
31.7	92	117
33.7	98	125
35.7	104	125
37.7	110	114
39.7	116	98
41.7	122	82
43.7	128	62
45.7	133	52
47.7	139	49
49.7	145	51
51.7	151	57
53.7	157	68
55.7	163	70
57.7	168	61
59.7	174	50
61.7	180	45
63.7	186	43
65.7	192	41
67.7	198	37
69.7	203	39
70.5	206	44
72.5	212	46
74.5	217	45
76.5	223	44
78.5	229	45
80.5	235	47
82.5	241	50
84.5	247	52
86.5	252	51
88.5	258	51
90.5	264	52
92.5	270	53
94.5	277	52
96.5	293	52
98.5	309	52
100.5	325	53
102.5	341	54
104.5	357	55
106.5	373	58
108.5	389	62
110.5	405	66
112.5	421	74

Depth (cm)	Age (yr BP)	MS (SI)
114.5	437	85
116.5	453	88
118.5	469	80
120.5	485	75
122.5	501	72
124.5	517	79
126.5	533	92
128.5	549	107
130.5	565	136
132.5	581	161
134.5	597	143
136.5	613	101
138.5	629	76
140.5	645	68
142.5	661	67
144.5	677	68
146.5	693	70
148.5	709	74
150.5	725	76
152.5	741	75
154.5	757	74
156.5	773	77
158.5	789	80
160.5	805	87
162.5	821	90
164.5	837	88
166.5	853	88
168.5	869	87
170.5	885	86
172.5	902	87
174.5	918	84
176.5	934	80
178.5	950	77
180.5	966	87
182.5	982	110
184.5	998	146
186.5	1014	173
188.5	1030	145
190.5	1046	113
192.5	1062	93
194.5	1078	77
196.5	1094	63
198.5	1110	55
200.5	1126	51
202.5	1142	47
204.5	1158	43
206.5	1174	42

Depth (cm)	Age (yr BP)	MS (SI)
208.5	1190	43
210.5	1206	44
212.5	1222	47
214.5	1238	45
216.5	1254	41
218.5	1270	39
221.3	1292	40
223.3	1308	41
225.3	1324	41
227.3	1340	40
229.3	1356	40
231.3	1372	40
233.3	1388	43
235.3	1404	42
237.3	1420	40
239.3	1436	39
241.3	1452	35
243.3	1468	36
245.3	1484	36
247.3	1500	36
249.3	1516	35
251.3	1532	38
253.3	1548	36
255.3	1564	40
257.3	1580	43
259.3	1596	44
261.3	1612	38
263.3	1628	39
265.3	1644	41
267.3	1661	38
269.3	1677	37
271.3	1693	35
273.3	1709	35
275.3	1725	36
277.3	1761	36
279.3	1813	39
281.3	1865	37
283.3	1917	37
285.3	1969	36
287.3	2020	37
289.3	2072	38
291.3	2124	37
293.3	2176	33
295.3	2228	32
297.3	2280	33
299.3	2332	36
301.3	2384	36

Depth (cm)	Age (yr BP)	MS (SI)
303.3	2436	37
305.3	2488	40
307.3	2540	41
309.3	2592	45
311.3	2643	45
313.3	2695	47
315.3	2747	51
317.3	2799	54
319.3	2851	57
321.3	2903	60
323.3	2955	66
325.3	3007	74
327.3	3059	80
329.3	3111	120
331.3	3163	174
333.3	3214	215
335.3	3266	156
337.3	3318	89
339.3	3370	58
341.3	3422	44
343.3	3474	37
345.3	3526	34
347.3	3578	33
349.3	3604	35
351.3	3617	45
353.3	3630	44
355.3	3643	35
357.3	3655	31
359.3	3668	30
361.3	3681	31
363.3	3694	31
365.3	3706	29
367.3	3719	30
370.1	3737	40
372.1	3750	41
374.1	3762	40
376.1	3775	38
378.1	3788	37
380.1	3801	35
382.1	3813	37
384.1	3826	40
386.1	3839	35
388.1	3852	36
390.1	3864	34
392.1	3877	32
394.1	3890	34
396.1	3903	33

Depth (cm)	Age (yr BP)	MS (SI)
398.1	3915	32
400.1	3928	30
402.1	3941	30
404.1	3954	30
406.1	3966	31
408.1	3979	31
410.1	3992	29
412.1	4005	29
414.1	4017	28
416.1	4030	29
418.1	4043	30
420.1	4056	30
422.1	4068	30
424.1	4081	32
426.1	4094	30
428.1	4107	25
430.1	4119	24
432.1	4132	23
434.1	4145	24
436.1	4158	26
438.1	4170	27
440.1	4183	27
442.1	4196	24
444.1	4209	23
446.1	4221	23
448.1	4234	23
450.1	4247	25
452.1	4260	24
454.1	4272	25
456.1	4285	26
458.1	4298	27
460.1	4311	27
462.1	4323	26
464.1	4336	25
466.1	4349	24
468.1	4362	25
470.1	4374	24
472.1	4387	24
474.1	4400	24
476.1	4409	23
478.1	4416	23
480.1	4422	24
482.1	4429	24
484.1	4435	26
486.1	4442	26
488.1	4448	27
490.1	4455	26

Depth (cm)	Age (yr BP)	MS (SI)
492.1	4461	27
494.1	4468	29
496.1	4474	30
498.1	4481	28
500.1	4487	26
502.1	4494	28
504.1	4500	30
506.1	4507	30
508.1	4513	28
510.1	4520	28
512.1	4526	28
514.1	4533	28
516.1	4539	27
518.1	4546	27
518.9	4548	27
520.9	4555	24
522.9	4561	24
524.9	4568	24
526.9	4574	23
528.9	4581	22
530.9	4587	23
532.9	4594	23
534.9	4600	25
536.9	4607	25
538.9	4613	24
540.9	4620	23
542.9	4626	24
544.9	4633	25
546.9	4639	25
548.9	4646	22
550.9	4652	21
552.9	4659	22
554.9	4665	23
556.9	4672	22
558.9	4678	21
560.9	4685	21
562.9	4691	22
564.9	4698	22
566.9	4704	21
568.9	4711	20
570.9	4717	20
572.9	4724	20
574.9	4730	20
576.9	4737	22
578.9	4743	26
580.9	4750	29
582.9	4756	28

Depth (cm)	Age (yr BP)	MS (SI)
584.9	4763	26
586.9	4769	27
588.9	4776	30
590.9	4782	31
592.9	4789	29
594.9	4795	28
596.9	4802	28
598.9	4808	29
600.9	4815	29
602.9	4821	31
604.9	4828	34
606.9	4834	38
608.9	4841	39
610.9	4847	39
612.9	4854	36
614.9	4860	29
616.9	4867	25
618.9	4873	23
620.9	4880	23
622.9	4886	22
624.9	4893	23
626.9	4899	22
628.9	4906	21
630.9	4912	22
632.9	4919	22
634.9	4925	24
636.9	4932	23
638.9	4938	22
640.9	4945	22
642.9	4951	24
644.9	4958	24
646.9	4964	27
648.9	4971	29
650.9	4978	28
652.9	4985	28
654.9	4992	25
656.9	4999	22
658.9	5006	22
660.9	5013	22
662.9	5020	21
664.9	5026	19
666.9	5033	20
667.7	5036	21
669.7	5043	27
671.7	5050	29
673.7	5057	27
675.7	5064	26

Depth (cm)	Age (yr BP)	MS (SI)
677.7	5071	26
679.7	5078	28
681.7	5085	35
683.7	5091	41
685.7	5098	41
687.7	5105	37
689.7	5112	29
691.7	5119	27
693.7	5126	28
695.7	5133	30
697.7	5140	27
699.7	5147	29
701.7	5154	30
703.7	5161	29
705.7	5168	30
707.7	5174	30
709.7	5181	33
711.7	5188	28
713.7	5195	27
715.7	5202	30
717.7	5209	30
719.7	5216	30
721.7	5223	26
723.7	5230	26
725.7	5237	28
727.7	5244	28
729.7	5251	27
731.7	5258	26
733.7	5264	25
735.7	5271	25
737.7	5278	26
739.7	5285	27
741.7	5292	30
743.7	5299	35
745.7	5306	39
747.7	5313	40
749.7	5320	47
751.7	5327	48
753.7	5334	45
755.7	5341	40
757.7	5347	37
759.7	5354	36
761.7	5361	31
763.7	5368	28
765.7	5375	31
767.7	5382	35
769.7	5389	33

Depth (cm)	Age (yr BP)	MS (SI)
771.7	5396	32
773.7	5403	32
775.7	5410	29
777.7	5417	28
779.7	5424	28
781.7	5430	27
783.7	5437	26
785.7	5444	27
787.7	5451	31
789.7	5458	35
791.7	5465	39
793.7	5472	34
795.7	5479	33
797.7	5486	33
799.7	5493	34
801.7	5500	34
803.7	5507	33
805.7	5513	32
807.7	5520	31
809.7	5527	30
811.7	5534	29
813.7	5541	30
815.7	5548	35
818.5	5557	54
820.5	5561	60
822.5	5566	53
824.5	5570	45
826.5	5574	39
828.5	5579	33
830.5	5583	30
832.5	5587	29
834.5	5591	31
836.5	5596	28
838.5	5600	26
840.5	5604	26
842.5	5609	25
844.5	5613	25
846.5	5617	25
848.5	5622	25
850.5	5626	25
852.5	5630	25
854.5	5634	25
856.5	5639	25
858.5	5643	26
860.5	5647	27
862.5	5652	28
864.5	5656	26

Depth (cm)	Age (yr BP)	MS (SI)
866.5	5660	25
868.5	5665	24
870.5	5669	25
872.5	5673	26
874.5	5677	26
876.5	5682	25
878.5	5686	25
880.5	5690	25
882.5	5695	26
884.5	5699	25
886.5	5703	25
888.5	5708	24
890.5	5712	25
892.5	5716	24
894.5	5720	25
896.5	5725	25
898.5	5729	25
900.5	5733	25
902.5	5738	26
904.5	5742	27
906.5	5746	25
908.5	5751	23
910.5	5755	21
912.5	5759	22
914.5	5763	21
916.5	5768	22
918.5	5772	20
920.5	5776	20
922.5	5781	19
924.5	5785	20
926.5	5789	20
928.5	5793	20
930.5	5798	20
932.5	5802	21
934.5	5806	21
936.5	5811	22
938.5	5815	22
940.5	5819	22
942.5	5824	21
944.5	5828	21
946.5	5832	22
948.5	5836	22
950.5	5841	21
952.5	5847	21
954.5	5857	21
956.5	5867	21
958.5	5877	21

Depth (cm)	Age (yr BP)	MS (SI)
960.5	5887	22
962.5	5897	21
964.5	5907	21
967.3	5921	25
969.3	5931	25
971.3	5941	23
973.3	5951	21
975.3	5959	20
977.3	5964	19
979.3	5969	19
981.3	5975	19
983.3	5980	21
985.3	5985	20
987.3	5990	21
989.3	5995	21
991.3	6001	21
993.3	6006	21
995.3	6011	21
997.3	6016	20
999.3	6021	20
1001.3	6027	19
1003.3	6032	20
1005.3	6037	20
1007.3	6042	21
1009.3	6047	21
1011.3	6053	21
1013.3	6058	20
1015.3	6063	20
1017.3	6068	20
1019.3	6073	21
1021.3	6079	20
1023.3	6084	19
1025.3	6089	19
1027.3	6094	20
1029.3	6099	23
1031.3	6105	22
1033.3	6110	22
1035.3	6115	21
1037.3	6120	20
1039.3	6125	21
1041.3	6131	21
1043.3	6136	23
1045.3	6141	24
1047.3	6146	25
1049.3	6151	27
1051.3	6157	28
1053.3	6162	29

Depth (cm)	Age (yr BP)	MS (SI)
1055.3	6167	32
1057.3	6172	33
1059.3	6177	30
1061.3	6182	26
1063.3	6188	25
1065.3	6193	29
1067.3	6198	26
1069.3	6203	21
1071.3	6208	19
1073.3	6214	21
1075.3	6219	23
1077.3	6224	22
1079.3	6229	24
1081.3	6234	25
1083.3	6240	28
1085.3	6245	37
1087.3	6250	37
1089.3	6255	30
1091.3	6263	29
1093.3	6271	34
1095.3	6280	49
1097.3	6288	37
1099.3	6296	27
1101.3	6304	29
1103.3	6312	42
1105.3	6321	49
1107.3	6329	44
1109.3	6337	38
1111.3	6345	30
1113.3	6353	24
1115.3	6362	23
1116.1	6365	22
1118.1	6373	22
1120.1	6381	22
1122.1	6389	22
1124.1	6398	23
1126.1	6406	23
1128.1	6414	24
1130.1	6422	23
1132.1	6431	23
1134.1	6439	23
1136.1	6447	23
1138.1	6455	24
1140.1	6463	23
1142.1	6472	23
1144.1	6480	21
1146.1	6488	21

Depth (cm)	Age (yr BP)	MS (SI)
1148.1	6496	23
1150.1	6504	22
1152.1	6513	21
1154.1	6521	20
1156.1	6529	18
1158.1	6537	18
1160.1	6545	17
1162.1	6554	17
1164.1	6562	17
1166.1	6570	16
1168.1	6578	17
1170.1	6586	18
1172.1	6595	18
1174.1	6603	18
1176.1	6611	18
1178.1	6619	17
1180.1	6627	17
1182.1	6636	17
1184.1	6644	17
1186.1	6652	19
1188.1	6660	19
1190.1	6668	21
1192.1	6677	23
1194.1	6685	23
1196.1	6693	21
1198.1	6701	19
1200.1	6710	18
1202.1	6718	18
1204.1	6726	18
1206.1	6734	19
1208.1	6742	19
1210.1	6751	20
1212.1	6759	22
1214.1	6767	22
1216.1	6775	22
1218.1	6783	21
1220.1	6792	20
1222.1	6800	19
1224.1	6808	19
1226.1	6816	19
1228.1	6824	19
1230.1	6833	20
1232.1	6841	20
1234.1	6849	19
1236.1	6857	20
1238.1	6865	20
1240.1	6874	20

Depth (cm)	Age (yr BP)	MS (SI)
1242.1	6882	19
1244.1	6890	20
1246.1	6898	22
1248.1	6906	23
1250.1	6915	23
1252.1	6923	21
1254.1	6931	20
1256.1	6939	18
1258.1	6947	20
1260.1	6956	21
1262.1	6964	22
1264.1	6972	22
1264.9	6975	22
1266.9	6984	24
1268.9	6992	27
1270.9	7000	29
1272.9	7008	29
1274.9	7016	28
1276.9	7025	25
1278.9	7033	25
1280.9	7041	24
1282.9	7049	22
1284.9	7057	21
1286.9	7066	21
1288.9	7074	21
1290.9	7082	23
1292.9	7090	21
1294.9	7098	18
1296.9	7107	15
1298.9	7115	9
1300.9	7123	5
1374.9	7131	24
1376.9	7139	20
1378.9	7148	18
1380.9	7156	17
1382.9	7164	17
1384.9	7172	17
1386.9	7180	16
1388.9	7188	16
1390.9	7194	16
1392.9	7199	16
1394.9	7205	15
1396.9	7211	16
1398.9	7217	15
1400.9	7223	16
1402.9	7229	16
1404.9	7235	16

Depth (cm)	Age (yr BP)	MS (SI)
1406.9	7241	17
1408.9	7247	16
1410.9	7253	16
1412.9	7259	14
1413.7	7261	14
1415.7	7267	14
1417.7	7273	13
1419.7	7279	13
1421.7	7285	14
1423.7	7290	14
1425.7	7296	15
1427.7	7302	16
1429.7	7308	16
1431.7	7314	17
1433.7	7320	17
1435.7	7326	17
1437.7	7332	17
1439.7	7338	16
1441.7	7344	16
1443.7	7349	17
1445.7	7355	16
1447.7	7361	19
1449.7	7367	17
1451.7	7373	15
1453.7	7379	15
1455.7	7385	15
1457.7	7391	14
1459.7	7397	14
1461.7	7403	14
1463.7	7409	14
1465.7	7414	14
1467.7	7420	17
1469.7	7426	22
1471.7	7432	31
1473.7	7438	23
1475.7	7444	20
1477.7	7450	17
1479.7	7456	15
1481.7	7462	16
1483.7	7468	15
1485.7	7474	14
1487.7	7479	13
1489.7	7485	13
1491.7	7491	12
1493.7	7497	12
1495.7	7503	12
1497.7	7509	14

Depth (cm)	Age (yr BP)	MS (SI)
1499.7	7515	13
1501.7	7521	13
1503.7	7527	13
1505.7	7533	13
1507.7	7539	14
1509.7	7544	14
1511.7	7550	15
1513.7	7556	16
1515.7	7562	15
1517.7	7568	14
1519.7	7574	14
1521.7	7580	15
1523.7	7586	17
1525.7	7592	16
1527.7	7597	14
1529.7	7601	13
1531.7	7605	15
1533.7	7609	13
1535.7	7612	13
1537.7	7616	14
1539.7	7620	15
1541.7	7624	14
1543.7	7628	13
1545.7	7632	11
1547.7	7636	11
1549.7	7640	12
1551.7	7644	12
1553.7	7647	11
1555.7	7651	11
1557.7	7655	10
1559.7	7659	9
1561.7	7663	0
1564.5	7669	11
1566.5	7672	10
1568.5	7676	11
1570.5	7680	11
1572.5	7684	10
1574.5	7689	11
1576.5	7698	11
1578.5	7707	12
1580.5	7716	12
1582.5	7725	12
1584.5	7734	14
1586.5	7743	16
1588.5	7752	15
1590.5	7761	13
1592.5	7770	14

Depth (cm)	Age (yr BP)	MS (SI)
1594.5	7779	13
1596.5	7788	14
1598.5	7797	12
1600.5	7806	13
1602.5	7815	13
1604.5	7824	13
1606.5	7833	13
1608.5	7842	14
1610.5	7851	15
1612.5	7860	18
1614.5	7869	16
1616.5	7878	13
1618.5	7887	13
1620.5	7896	10
1622.5	7904	13
1624.5	7913	13
1626.5	7922	13
1628.5	7931	16
1630.5	7940	18
1632.5	7949	15
1634.5	7958	13
1636.5	7967	12
1638.5	7976	10
1640.5	7985	10
1642.5	7994	11
1644.5	8003	11
1646.5	8012	13
1648.5	8021	16
1650.5	8030	18
1652.5	8039	15
1654.5	8048	12
1656.5	8057	11
1658.5	8066	12
1660.5	8075	11
1662.5	8084	14
1664.5	8093	15
1666.5	8102	14
1668.5	8111	15
1670.5	8120	15
1672.5	8129	14
1674.5	8138	14
1676.5	8147	15
1678.5	8156	15
1680.5	8165	16
1682.5	8174	18
1684.5	8182	20
1686.5	8191	23

Depth (cm)	Age (yr BP)	MS (SI)
1688.5	8200	26
1690.5	8209	30
1692.5	8218	31
1694.5	8227	33
1696.5	8236	31
1698.5	8245	26
1700.5	8254	22
1702.5	8263	18
1704.5	8272	14
1706.5	8281	12
1708.5	8290	11
1710.5	8299	10
1713.3	8312	12
1715.3	8321	12
1717.3	8330	13
1719.3	8339	14
1721.3	8348	13
1723.3	8356	12
1725.3	8365	13
1727.3	8374	13
1729.3	8383	12
1731.3	8392	12
1733.3	8401	12
1735.3	8410	11
1737.3	8419	11
1739.3	8428	11
1741.3	8437	12
1743.3	8446	11
1745.3	8455	12
1747.3	8464	11
1749.3	8473	11
1751.3	8482	10
1753.3	8491	11
1755.3	8500	10
1757.3	8509	11
1759.3	8518	10
1761.3	8527	10
1763.3	8536	10
1765.3	8545	10
1767.3	8554	12
1769.3	8563	12
1771.3	8572	11
1773.3	8581	12
1775.3	8590	14
1777.3	8599	13
1779.3	8608	13
1781.3	8617	14

Depth (cm)	Age (yr BP)	MS (SI)
1783.3	8626	14
1785.3	8634	14
1787.3	8643	14
1789.3	8652	13
1791.3	8661	14
1793.3	8670	14
1795.3	8679	14
1797.3	8688	15
1799.3	8697	14
1801.3	8706	14
1803.3	8715	13
1805.3	8724	13
1807.3	8733	14
1809.3	8742	15
1811.3	8751	14
1813.3	8760	13
1815.3	8769	12
1817.3	8778	12
1819.3	8787	14
1821.3	8796	14
1823.3	8805	12
1825.3	8814	12
1827.3	8825	12
1829.3	8835	11
1831.3	8846	11
1833.3	8856	10
1835.3	8867	11
1837.3	8878	11
1839.3	8888	11
1841.3	8899	10
1843.3	8909	11
1845.3	8920	10
1847.3	8931	11
1849.3	8941	11
1851.3	8952	11
1853.3	8962	10
1855.3	8973	10
1857.3	8984	11
1859.3	8994	11
1862.1	9009	14
1864.1	9020	18
1866.1	9030	16
1868.1	9041	13
1870.1	9051	12
1872.1	9062	12
1874.1	9073	12
1876.1	9083	13

Depth (cm)	Age (yr BP)	MS (SI)
1878.1	9094	14
1880.1	9104	15
1882.1	9115	16
1884.1	9126	18
1886.1	9136	17
1888.1	9147	16
1890.1	9157	16
1892.1	9168	17
1894.1	9179	16
1896.1	9189	17
1898.1	9200	18
1900.1	9210	20
1902.1	9221	22
1904.1	9232	24
1906.1	9242	24
1908.1	9253	24
1910.1	9263	25
1912.1	9274	23
1914.1	9285	22
1916.1	9295	22
1918.1	9306	24
1920.1	9316	25
1922.1	9327	26
1924.1	9338	26
1926.1	9348	25
1928.1	9359	25
1930.1	9369	22
1932.1	9380	20
1934.1	9391	19
1936.1	9401	18
1938.1	9412	19
1940.1	9422	18
1942.1	9433	16
1944.1	9443	17
1946.1	9451	17
1948.1	9458	18
1950.1	9465	18
1952.1	9473	20
1954.1	9480	22
1956.1	9487	25
1958.1	9495	30
1960.1	9502	38
1962.1	9509	55
1964.1	9517	86
1966.1	9524	134
1968.1	9531	124
1970.1	9539	77

Depth (cm)	Age (yr BP)	MS (SI)
1972.1	9546	49
1974.1	9553	34
1976.1	9560	28
1978.1	9568	25
1980.1	9575	24
1982.1	9582	25
1984.1	9590	26
1986.1	9597	25
1988.1	9604	22
1990.1	9612	23
1992.1	9619	22
1994.1	9626	20
1996.1	9634	20
1998.1	9641	18
2000.1	9648	18
2002.1	9656	17
2004.1	9663	16
2006.1	9670	
2008.1	9678	18
2010.9	9688	24
2012.9	9695	21
2014.9	9702	19
2016.9	9710	20
2018.9	9717	21
2020.9	9724	23
2022.9	9732	22
2024.9	9739	21
2026.9	9746	20
2028.9	9754	18
2030.9	9761	19
2032.9	9768	21
2034.9	9776	21
2036.9	9783	20
2038.9	9790	24
2040.9	9798	24
2042.9	9805	22
2044.9	9812	23
2046.9	9820	19
2048.9	9827	17
2050.9	9834	16
2052.9	9841	19
2054.9	9849	20
2056.9	9856	20
2058.9	9863	22
2060.9	9871	20
2062.9	9878	18
2064.9	9885	17

Depth (cm)	Age (yr BP)	MS (SI)
2066.9	9893	18
2068.9	9900	19
2070.9	9907	19
2072.9	9915	18
2074.9	9922	16
2076.9	9929	15
2078.9	9937	15
2080.9	9944	16
2082.9	9951	16
2084.9	9959	17
2086.9	9966	18
2088.9	9973	17
2090.9	9981	15
2092.9	9988	16
2094.9	9995	16
2096.9	10002	17
2098.9	10010	22
2100.9	10017	23
2102.9	10024	23
2104.9	10032	20
2106.9	10039	17
2108.9	10046	17
2110.9	10054	17
2112.9	10061	18
2114.9	10068	21
2116.9	10076	23
2118.9	10083	23
2120.9	10090	23
2122.9	10098	21
2124.9	10105	19
2126.9	10112	19
2128.9	10120	19
2130.9	10127	20
2132.9	10134	21
2134.9	10142	19
2136.9	10149	19
2138.9	10156	18
2140.9	10163	18
2142.9	10171	18
2144.9	10178	19
2146.9	10188	21
2148.9	10198	24
2150.9	10207	23
2152.9	10217	21
2154.9	10227	20
2156.9	10237	19
2159.7	10251	26

Depth (cm)	Age (yr BP)	MS (SI)
2161.7	10260	25
2163.7	10270	22
2165.7	10280	24
2167.7	10290	24
2169.7	10300	25
2171.7	10310	29
2173.7	10319	34
2175.7	10329	37
2177.7	10339	33
2179.7	10349	33
2181.7	10359	42
2183.7	10369	40
2185.7	10378	40
2187.7	10388	48
2189.7	10398	65
2191.7	10408	94
2193.7	10418	138
2195.7	10427	184
2197.7	10437	237
2199.7	10447	260
2201.7	10457	267
2203.7	10467	260
2205.7	10477	227
2207.7	10486	171
2209.7	10496	128
2211.7	10506	110
2213.7	10516	96
2215.7	10526	71
2217.7	10535	48
2219.7	10545	42
2221.7	10555	50
2223.7	10565	82
2225.7	10575	113
2227.7	10585	95
2229.7	10594	86
2231.7	10604	73
2233.7	10614	54
2235.7	10624	15

MS (SI): Magnetic susceptibility in Standard International units.

Appendix 8: Marion DuFresne lithotype log information

Core	From Corrected Depth (cm)	To Corrected Depth (cm)	From Age (yr BP)	To Age (yr BP)	Thickness (depth)	Thickness (age)	Lithotype
MD3001	0.0	43.6	0.00	224.32	43.6	224.32	None
MD3001	43.6	48.7	224.32	250.71	5.1	26.39	2A
MD3001	48.7	52.6	250.71	270.50	3.8	19.79	3A
MD3001	52.6	72.4	270.50	372.76	19.9	102.26	2A
MD3001	72.4	78.2	372.76	402.45	5.8	29.69	4A
MD3001	78.2	82.1	402.45	422.24	3.8	19.79	2A
MD3001	82.1	83.3	422.24	428.84	1.3	6.60	5A
MD3001	83.3	87.2	428.84	448.63	3.8	19.79	2A
MD3001	87.2	94.9	448.63	488.22	7.7	39.59	5B
MD3001	94.9	105.8	488.22	544.30	10.9	56.08	2A
MD3001	105.8	110.3	544.30	567.39	4.5	23.09	4A
MD3001	110.3	112.2	567.39	577.28	1.9	9.90	2A
MD3001	112.2	115.4	577.28	593.78	3.2	16.49	5A
MD3001	115.4	208.0	593.78	1263.71	92.6	669.93	2B
MD3001	208.0	210.0	1263.71	1286.89	2.0	23.18	1B
MD3001	210.0	224.0	1286.89	1449.16	14.0	162.27	2B
MD3001	224.0	231.0	1449.16	1530.29	7.0	81.13	1A
MD3001	231.0	240.9	1530.29	1645.14	9.9	114.85	2A
MD3001	240.9	242.2	1645.14	1660.19	1.3	15.05	3A
MD3001	242.2	339.8	1660.19	2790.98	97.6	1130.78	2B
MD3001	339.8	359.3	2790.98	3016.13	19.5	225.16	2A
MD3001	359.3	367.7	3016.13	3110.78	8.4	94.64	5A
MD3001	367.7	380.2	3110.78	3238.75	12.6	127.98	1B
MD3001	380.2	405.3	3238.75	3365.35	25.1	126.59	2B
MD3001	405.3	413.0	3365.35	3404.03	7.7	38.68	6A
MD3001	413.0	428.4	3404.03	3481.39	15.3	77.36	2B
MD3001	428.4	429.1	3481.39	3484.91	0.7	3.52	3A
MD3001	429.1	434.7	3484.91	3513.04	5.6	28.13	2A
MD3001	434.7	459.6	3513.04	3638.74	24.9	125.70	4A
MD3001	459.6	496.6	3638.74	3825.16	37.0	186.42	2A
MD3001	496.6	500.0	3825.16	3842.42	3.4	17.26	4A
MD3001	500.0	519.2	3842.42	3939.08	19.2	96.66	5A
MD3001	519.2	600.0	3939.08	4347.41	80.8	408.33	2A
MD3001	600.0	642.6	4347.41	4563.05	42.6	215.64	2B
MD3001	642.6	644.0	4563.05	4570.12	1.4	7.07	3A
MD3001	644.0	652.3	4570.12	4612.54	8.4	42.42	2B
MD3001	652.3	658.6	4612.54	4644.36	6.3	31.82	3A
MD3001	658.6	662.8	4644.36	4665.57	4.2	21.21	2B
MD3001	662.8	663.5	4665.57	4669.11	0.7	3.54	5A
MD3001	663.5	667.7	4669.11	4690.32	4.2	21.21	2B
MD3001	667.7	668.4	4690.32	4693.85	0.7	3.54	3A
MD3001	668.4	683.0	4693.85	4768.09	14.7	74.24	2B
MD3001	683.0	697.0	4768.09	4838.79	14.0	70.70	5A
MD3001	697.0	739.5	4838.79	5054.43	42.6	215.64	2B

Core	From Corrected Depth (cm)	To Corrected Depth (cm)	From Age (yr BP)	To Age (yr BP)	Thickness (depth)	Thickness (age)	Lithotype
MD3001	739.5	740.9	5054.43	5061.50	1.4	7.07	3A
MD3001	740.9	776.7	5061.50	5237.71	35.8	176.20	2B
MD3001	776.7	788.5	5237.71	5280.72	11.7	43.02	5A
MD3001	788.5	793.0	5280.72	5297.46	4.6	16.73	4A
MD3001	793.0	795.7	5297.46	5307.02	2.6	9.56	4A
MD3001	795.7	800.2	5307.02	5323.75	4.6	16.73	4A
MD3001	800.2	810.7	5323.75	5361.99	10.4	38.24	4A
MD3001	810.7	822.4	5361.99	5405.01	11.7	43.02	2B
MD3001	822.4	834.8	5405.01	5450.42	12.4	45.41	4A
MD3001	834.8	853.7	5450.42	5519.73	18.9	69.31	2B
MD3001	853.7	855.7	5519.73	5526.90	2.0	7.17	3A
MD3001	855.7	900.0	5526.90	5689.43	44.3	162.53	2B
MD3001	900.0	915.8	5689.43	5747.38	15.8	57.95	2A
MD3001	915.8	918.4	5747.38	5756.89	2.6	9.51	1B
MD3001	918.4	924.5	5756.89	5779.38	6.1	22.49	2A
MD3001	924.5	925.9	5779.38	5784.38	1.4	5.00	5A
MD3001	925.9	938.9	5784.38	5831.86	13.0	47.48	2B
MD3001	938.9	947.7	5831.86	5864.34	8.9	32.48	2A
MD3001	947.7	958.0	5864.34	5901.82	10.2	37.48	5A
MD3001	958.0	962.7	5901.82	5919.31	4.8	17.49	4A
MD3001	962.7	966.8	5919.31	5934.30	4.1	14.99	2A
MD3001	966.8	968.9	5934.30	5941.80	2.0	7.50	3A
MD3001	968.9	997.5	5941.80	6046.75	28.6	104.95	2A
MD3001	997.5	998.2	6046.75	6049.24	0.7	2.50	5A
MD3001	998.2	1008.4	6049.24	6086.73	10.2	37.48	2A
MD3001	1008.4	1013.9	6086.73	6106.72	5.5	19.99	4A
MD3001	1013.9	1033.6	6106.72	6179.18	19.8	72.46	2A
MD3001	1033.6	1036.4	6179.18	6189.17	2.7	9.99	1B
MD3001	1036.4	1091.5	6189.17	6368.06	55.1	178.88	2A
MD3001	1091.5	1094.9	6368.06	6379.19	3.5	11.13	4A
MD3001	1094.9	1101.2	6379.19	6399.20	6.2	20.01	4A
MD3001	1101.2	1109.4	6399.20	6425.88	8.3	26.68	2A
MD3001	1109.4	1110.8	6425.88	6430.33	1.4	4.45	3A
MD3001	1110.8	1126.0	6430.33	6479.24	15.2	48.92	2A
MD3001	1126.0	1136.4	6479.24	6512.59	10.4	33.35	4C
MD3001	1136.4	1161.3	6512.59	6592.64	24.9	80.04	2A
MD3001	1161.3	1167.5	6592.64	6612.65	6.2	20.01	1B
MD3001	1167.5	1172.4	6612.65	6628.21	4.8	15.56	1A
MD3001	1172.4	1190.3	6628.21	6686.02	18.0	57.81	2A
MD3001	1190.3	1193.1	6686.02	6694.92	2.8	8.89	5A
MD3001	1193.1	1197.2	6694.92	6707.96	4.1	13.04	4A
MD3001	1197.2	1200.0	6707.96	6713.32	2.8	5.36	2B
MD3001	1200.0	1247.4	6713.32	6805.30	47.4	91.98	2A
MD3001	1247.4	1250.9	6805.30	6812.17	3.5	6.86	5A
MD3001	1250.9	1262.3	6812.17	6834.13	11.3	21.97	4A
MD3001	1262.3	1265.8	6834.13	6841.00	3.5	6.86	2A

Core	From Corrected Depth (cm)	To Corrected Depth (cm)	From Age (yr BP)	To Age (yr BP)	Thickness (depth)	Thickness (age)	Lithotype
MD3001	1265.8	1267.2	6841.00	6843.74	1.4	2.75	5A
MD3001	1267.2	1305.4	6843.74	6917.88	38.2	74.14	2B
MD3001	1305.4	1307.5	6917.88	6922.00	2.1	4.12	4A
MD3001	1307.5	1312.5	6922.00	6931.61	5.0	9.61	4A
MD3001	1312.5	1350.0	6931.61	7004.37	37.5	72.76	2B
MD3001	1350.0	1379.1	7004.37	7060.92	29.1	56.55	2A
MD3001	1379.1	1384.1	7060.92	7070.58	5.0	9.66	1A
MD3001	1384.1	1387.7	7070.58	7077.48	3.6	6.90	4A
MD3001	1387.7	1393.4	7077.48	7088.51	5.7	11.04	2A
MD3001	1393.4	1394.8	7088.51	7091.27	1.4	2.76	3A
MD3001	1394.8	1421.1	7091.27	7142.31	26.3	51.04	2A
MD3001	1421.1	1422.5	7142.31	7145.07	1.4	2.76	3A
MD3001	1422.5	1428.2	7145.07	7156.10	5.7	11.04	2A
MD3001	1428.2	1429.6	7156.10	7158.86	1.4	2.76	3A
MD3001	1429.6	1453.8	7158.86	7234.14	24.2	75.28	2A
MD3001	1453.8	1460.9	7234.14	7262.57	7.1	28.42	1A
MD3001	1460.9	1470.9	7262.57	7302.36	10.0	39.79	2A
MD3001	1470.9	1501.4	7302.36	7424.59	30.6	122.22	4A
MD3001	1501.4	1577.1	7424.59	7727.26	75.7	302.68	2A
MD3001	1577.1	1586.3	7727.26	7764.04	9.2	36.78	4A
MD3001	1586.3	1589.9	7764.04	7778.19	3.5	14.15	4A
MD3001	1589.9	1747.4	7778.19	8393.62	157.6	615.44	2A
MD3001	1747.4	1751.6	8393.62	8400.90	4.2	7.27	5A
MD3001	1751.6	1762.9	8400.90	8420.29	11.2	19.40	2A
MD3001	1762.9	1767.1	8420.29	8427.57	4.2	7.27	4A
MD3001	1767.1	1844.3	8427.57	8561.16	77.2	133.59	2A
MD3001	1844.3	1846.4	8561.16	8564.85	2.1	3.70	5A
MD3001	1846.4	1889.3	8564.85	8638.98	42.9	74.13	2A
MD3001	1889.3	1890.0	8638.98	8640.22	0.7	1.24	5A
MD3001	1890.0	1929.3	8640.22	8708.17	39.3	67.95	2B
MD3001	1929.3	1932.9	8708.17	8714.35	3.6	6.18	4A
MD3001	1932.9	1936.4	8714.35	8720.52	3.6	6.18	4A
MD3001	1936.4	1939.3	8720.52	8725.47	2.9	4.94	4A
MD3001	1939.3	1945.0	8725.47	8735.35	5.7	9.88	4A
MD3001	1945.0	1951.4	8735.35	8746.47	6.4	11.12	2B
MD3001	1951.4	2119.3	8746.47	9063.59	167.8	317.13	2A
MD3001	2119.3	2123.0	9063.59	9072.90	3.7	9.31	3B
MD3001	2123.0	2183.0	9072.90	9227.68	60.0	154.78	2A
MD3001	2183.0	2196.3	9227.68	9297.68	13.3	70.00	1B
MD3001	2196.3	2241.1	9297.68	9533.06	44.8	235.38	2A
MD3001	2241.1	2244.0	9533.06	9548.19	2.9	15.13	1B
MD3001	2244.0	2248.3	9548.19	9570.92	4.3	22.73	2B
MD3001	2248.3	2249.8	9570.92	9578.21	1.4	7.29	1B
MD3001	2249.8	2258.4	9578.21	9615.07	8.7	36.86	2B

Core	From Corrected Depth (cm)	To Corrected Depth (cm)	From Age (yr BP)	To Age (yr BP)	Thickness (depth)	Thickness (age)	Lithotype
MD3004	0.0	29.9	0	147	29.9	146.78	2A
MD3004	29.9	31.9	147	161	2.1	14.15	3A
MD3004	31.9	47.2	161	265	15.3	103.78	2C
MD3004	47.2	47.9	265	269	0.7	4.72	3A
MD3004	47.9	88.2	269	543	40.3	273.61	2C
MD3004	88.2	88.9	543	548	0.7	4.72	5A
MD3004	88.9	121.5	548	769	32.6	221.72	2C
MD3004	121.5	130.6	769	831	9.0	61.33	2B
MD3004	130.6	150.0	831	963	19.4	132.09	2C
MD3004	150.0	180.8	963	1172	30.8	209.37	2B
MD3004	180.8	182.2	1172	1182	1.4	9.31	3A
MD3004	182.2	221.2	1182	1549	39.0	367.31	2B
MD3004	221.2	224.0	1549	1585	2.7	35.84	3A
MD3004	224.0	241.1	1585	1809	17.1	224.02	2A
MD3004	241.1	247.9	1809	1898	6.8	89.27	1B
MD3004	252.1	263.0	1952	2095	11.0	143.37	2B
MD3004	263.0	265.8	2095	2131	2.7	35.84	5A
MD3004	265.8	284.2	2131	2373	18.5	241.94	2B
MD3004	284.2	286.3	2373	2400	2.1	26.88	3A
MD3004	286.3	295.9	2400	2526	9.6	125.45	2A
MD3004	295.9	305.5	2526	2651	9.6	125.45	4A
MD3004	305.5	416.3	2651	3448	110.8	796.95	2A
MD3004	416.3	420.4	3448	3472	4.1	24.17	4A
MD3004	420.4	423.2	3472	3488	2.8	16.11	2A
MD3004	423.2	428.7	3488	3500	5.5	12.21	1B
MD3004	428.7	438.3	3500	3504	9.6	3.85	1A
MD3004	438.3	460.3	3504	3513	22.0	8.81	2B
MD3004	460.3	471.0	3513	3609	10.7	95.47	2A
MD3004	471.0	479.2	3609	3735	8.1	126.20	4A
MD3004	479.2	488.7	3735	3882	9.5	147.23	2B
MD3004	488.7	492.1	3882	3935	3.4	52.58	4A
MD3004	492.1	585.1	3935	4818	93.0	883.35	2A
MD3004	585.1	593.9	4818	4891	8.8	73.31	4A
MD3004	593.9	610.2	4891	5027	16.3	135.34	2A
MD3004	610.2	614.0	5027	5058	3.8	31.88	4A
MD3004	614.0	616.8	5058	5082	2.8	23.29	2A
MD3004	616.8	621.0	5082	5117	4.2	34.94	4A
MD3004	621.0	623.8	5117	5140	2.8	23.29	2A
MD3004	623.8	626.6	5140	5163	2.8	23.29	4A
MD3004	626.6	644.9	5163	5248	18.2	84.38	2A
MD3004	644.9	647.7	5248	5254	2.8	5.99	3A
MD3004	647.7	653.3	5254	5266	5.6	11.98	2A
MD3004	653.3	656.1	5266	5272	2.8	5.99	3A
MD3004	656.1	670.1	5272	5302	14.0	29.94	2A
MD3004	670.1	679.2	5302	5321	9.1	19.46	4A
MD3004	679.2	689.7	5321	5344	10.5	22.46	4A

Core	From Corrected Depth (cm)	To Corrected Depth (cm)	From Age (yr BP)	To Age (yr BP)	Thickness (depth)	Thickness (age)	Lithotype
MD3004	689.7	712.1	5344	5585	22.4	241.01	2A
MD3004	712.1	715.0	5585	5625	2.8	40.58	4A
MD3004	715.0	731.8	5625	5869	16.8	243.50	2A
MD3004	731.8	736.0	5869	5929	4.2	60.88	3A
MD3004	736.0	758.4	5929	6119	22.4	189.62	2A
MD3004	758.4	759.9	6119	6124	1.5	5.37	3A
MD3004	759.9	776.9	6124	6185	17.0	61.02	2A
MD3004	776.9	779.0	6185	6193	2.1	7.63	5A
MD3004	779.0	800.2	6193	6269	21.2	76.27	2A
MD3004	800.2	803.8	6269	6282	3.5	12.71	4A
MD3004	803.8	808.0	6282	6297	4.2	15.25	4A
MD3004	808.0	817.9	6297	6333	9.9	35.59	4C
MD3004	817.9	836.3	6333	6376	18.4	43.41	2A
MD3004	836.3	844.8	6376	6394	8.5	17.93	4A
MD3004	844.8	850.5	6394	6406	5.7	11.96	4A
MD3004	850.5	926.9	6406	6568	76.4	161.40	2A
MD3004	926.9	944.9	6568	6606	18.0	37.96	5A
MD3004	944.9	950.5	6606	6617	5.6	11.84	4A
MD3004	950.5	1015.7	6617	6755	65.2	137.69	2A
MD3004	1015.7	1016.4	6755	6757	0.7	1.48	5A
MD3004	1016.4	1021.3	6757	6767	4.9	10.36	2A
MD3004	1021.3	1031.1	6767	6822	9.8	55.35	4A
MD3004	1031.1	1079.4	6822	7254	48.4	432.11	2A
MD3004	1079.4	1083.5	7254	7291	4.0	36.18	6A
MD3004	1083.5	1110.0	7291	7528	26.5	236.87	2A
MD3004	1110.0	1112.1	7528	7546	2.1	18.70	6A
MD3004	1112.1	1231.4	7546	8516	119.3	970.23	2A
MD3004	1231.4	1234.3	8516	8538	3.0	22.04	4A
MD3004	1234.3	1251.2	8538	8664	16.8	125.69	2A
MD3004	1251.2	1254.7	8664	8690	3.5	26.18	3A
MD3004	1254.7	1282.0	8690	8895	27.3	204.24	2A
MD3004	1282.0	1284.8	8895	8916	2.8	20.95	4A
MD3004	1284.8	1287.6	8916	8936	2.8	20.95	4A
MD3004	1287.6	1289.0	8936	8947	1.4	10.47	4A
MD3004	1289.0	1335.3	8947	9293	46.3	345.64	2A
MD3004	1335.3	1363.3	9293	9489	28.0	196.40	2B
MD3004	1363.3	1364.3	9489	9510	1.0	20.38	3A
MD3004	1364.3	1381.4	9510	9595	17.0	85.50	2A
MD3004	1381.4	1385.5	9595	9611	4.1	15.50	5A
MD3004	1385.5	1390.9	9611	9631	5.5	20.66	2A
MD3004	1390.9	1395.7	9631	9649	4.8	18.08	6A
MD3004	1395.7	1414.1	9649	9719	18.4	69.74	2A
MD3004	1414.1	1418.9	9719	9737	4.8	18.08	1B
MD3004	1418.9	1548.4	9737	10376	129.5	639.04	2A
MD3004	1548.4	1623.9	10376	10882	75.5	506.19	2B
MD3004	1623.9	1624.7	10882	10888	0.8	5.29	1B

Core	From Corrected Depth (cm)	To Corrected Depth (cm)	From Age (yr BP)	To Age (yr BP)	Thickness (depth)	Thickness (age)	Lithotype
MD3004	1624.7	1642.9	10888	11009	18.2	121.68	2B
MD3004	1642.9	1646.1	11009	11030	3.2	21.16	3A
MD3004	1646.1	1650.0	11030	11057	3.9	26.45	2B

Core	From Corrected Depth (cm)	To Corrected Depth (cm)	From Age (yr BP)	To Age (yr BP)	Thickness (depth)	Thickness (age)	Lithotype
MD3006	0.0	208.1	0	847	846.8	846.84	2A
MD3006	208.1	216.0	847	900	52.8	52.84	6B
MD3006	216.0	270.6	900	1263	363.5	363.54	2A
MD3006	270.6	279.2	1263	1321	57.4	57.40	6B
MD3006	279.2	374.0	1321	1756	435.6	435.60	2A
MD3006	374.0	381.4	1756	1785	28.3	28.29	6B
MD3006	381.4	858.1	1785	3328	1542.5	1543.07	2A
MD3006	858.1	868.3	3328	3358	31.2	30.63	1A
MD3006	868.3	877.0	3358	3713	354.8	26.34	2A
MD3006	877.0	990.2	3713	3726	12.7	341.16	6A
MD3006	990.2	1166.2	3726	4250	523.9	523.89	2A
MD3006	1166.2	1166.9	4250	4251	1.6	1.64	5A
MD3006	1166.9	1245.1	4251	4462	209.8	210.36	2A
MD3006	1245.1	1249.9	4462	4475	13.9	13.27	6A
MD3006	1249.9	1327.0	4475	5985	1510.1	212.40	2A
MD3006	1327.0	1617.4	5985	5996	11.3	1309.06	1B
MD3006	1617.4	1657.3	5996	6163	165.7	166.28	2A
MD3006	1657.3	1658.6	6163	6168	6.0	5.33	6A
MD3006	1658.6	1662.5	6168	6184	16.4	16.44	2A
MD3006	1662.5	1669.1	6184	6212	27.4	27.39	6B
MD3006	1669.1	1675.7	6212	6239	27.4	27.43	2A
MD3006	1675.7	1687.5	6239	6289	49.5	49.47	6B
MD3006	1687.5	1777.0	6289	7839	1550.3	373.79	2A
MD3006	1777.0	1960.5	7839	7944	104.6	1281.15	6A
MD3006	1960.5	2004.7	7944	8927	983.2	983.21	2A
MD3006	2004.7	2006.0	8927	8957	29.8	29.79	6A
MD3006	2006.0	2032.8	8957	9548	591.5	591.48	2A
MD3006	2032.8	2039.5	9548	9600	51.9	51.94	6B
MD3006	2039.5	2077.0	9600	10872	1272.0	290.87	2A
MD3006	2077.0	2227.0	10872	12178	1306.0	1929.63	2C
MD3006	2227.0	2243.6	12178	12273	95.2	452.69	6A
MD3006	2243.6	2245.3	12273	12321	47.7	47.65	5A
MD3006	2245.3	2258.4	12321	12678	357.4	357.39	2C
MD3006	2258.4	2271.5	12678	13036	357.4	357.39	5A
MD3006	2271.5	2329.0	13036	14412	1376.3	1376.29	2C
MD3006	2329.0	2330.8	14412	14423	10.8	10.79	6A
MD3006	2330.8	2377.0	14423	14722	299.3	286.01	2C
MD3006	2377.0	2379.4	14722	14724	1.8	15.03	6A
MD3006	2379.4	2381.0	14724	14734	9.7	9.72	2C

From Corrected Depth (cm): Starting depth in centimeters of lithotype horizon. "Corrected" refers to gap correction plus a correction factor for transferring printed 2-D X-radiographic images to the correct length based on core section measurements.
To Corrected Depth (cm): As above, but for ending depth (in centimeters) of lithotype horizon.
From Age (yr BP): Age of upper (younger) contact of lithotype using *Appendix 1C* equation.
To Age (yr BP): Age of lower (older) contact of lithotype using *Appendix 1C* equation.
Thickness (depth): Thickness of lithotypic unit in depth (cm).
Thickness (age): Thickness of lithotypic unit in age (years).
Lithotype: Numerical identification of lithotypes. See section Chapter 3, Section 3.1 (pg. 138) and Chapter 3, Table 4 (pg. 177) for lithotype key and descriptions.

Appendix 9A: Kilo Moana survey (S) and target (T) samples, stable isotopes and grain size data

Core	Sample ID	Midpoint Depth (cm)	z'	Sample Weight for C & N analyses (mg)	C (mg)	N (mg)	Delta PDB	% C weight	% N weight	%C/%N	%N/%C	mass C/N	mass N/C	% Clay	% Silt	% Sand
B3	S10	5.5	5.16	32.07	0.0909	0.0110	-24.94	0.2834	0.0344	8.2285	0.1215	9.6000	0.1042	25.94	29.45	44.61
B3	S11	10.5	9.86	39.85	0.2152	0.0248	-25.29	0.5400	0.0622	8.6779	0.1152	10.1243	0.0988	29.74	36.55	33.71
B3	S12	15.5	14.55	38.66	0.1295	0.0175	-24.66	0.3351	0.0453	7.3944	0.1352	8.6268	0.1159	26.01	47.98	26.00
B3	S13	20.5	19.25	36.58	0.0584	0.0099	-25.18	0.1597	0.0272	5.8735	0.1703	6.8525	0.1459	17.27	24.82	57.91
B3	S9	0.5	0.47	35.72	0.0751	0.0110	-24.60	0.2173	0.0319	6.8107	0.1468	7.9458	0.1259	17.22	20.04	62.74
B3	T10	7.25	6.81	38.02	0.0792	0.0102	-24.13	0.2252	0.0289	7.7844	0.1285	9.0818	0.1101	11.61	39.95	48.44
B3	T11	12.25	11.50	31.20	0.1506	0.0197	-25.01	0.3960	0.0518	7.6403	0.1309	8.9137	0.1122	35.08	45.76	19.16
B3	T12	12.75	11.97	32.34	0.1908	0.0235	-25.00	0.6114	0.0752	8.1343	0.1229	9.4900	0.1054	46.78	39.37	13.85
B3	T13	13.25	12.44	39.82	0.1664	0.0199	-24.49	0.5145	0.0616	8.3477	0.1198	9.7390	0.1027	50.19	41.42	8.39
B3	T14	14.75	13.85	30.76	0.1300	0.0158	-24.90	0.3266	0.0397	8.2204	0.1216	9.5905	0.1043	38.43	41.72	19.86
B3	T15	16.25	15.26	35.95	0.1098	0.0136	-24.31	0.3569	0.0441	8.1023	0.1234	9.4527	0.1058	40.56	40.56	18.87
B3	T16	16.75	15.73	32.92	0.1346	0.0180	-24.62	0.3744	0.0502	7.4604	0.1340	8.7038	0.1149	39.72	37.15	23.13
B3	T17	17.25	16.20	31.94	0.1360	0.0164	-24.44	0.4132	0.0500	8.2709	0.1209	9.6494	0.1036	36.50	45.84	17.66
B6	S14	0.5	0.48	36.24	0.0686	0.0112	-24.55	0.1893	0.0308	6.1377	0.1629	7.1607	0.1397	15.01	66.99	18.00
B6	S15	5.5	5.23	38.65	0.0626	0.0097	-24.25	0.1619	0.0250	6.4786	0.1544	7.5584	0.1323	13.65	85.04	1.31
B6	S16	10.5	9.98	32.92	0.1462	0.0148	-24.74	0.4440	0.0451	9.8530	0.1015	11.4952	0.0870	34.91	55.52	9.57
B6	S17	15.5	14.73	35.45	0.0771	0.0126	-24.72	0.2174	0.0354	6.1349	0.1630	7.1574	0.1397	15.10	83.81	1.09
B6	S18	20.5	19.49	29.93	0.1058	0.0127	-25.28	0.3536	0.0424	8.3419	0.1199	9.7322	0.1028	15.16	36.85	47.99
B6	S19	25.5	24.24	36.97	0.1396	0.0169	-24.78	0.3777	0.0458	8.2509	0.1212	9.6260	0.1039	38.88	35.84	25.28
B6	T18	7.25	6.89	33.82	0.0449	0.0078	-24.58	0.1407	0.0244	5.7670	0.1734	6.7281	0.1486	15.92	77.62	6.46
B6	T19	9.25	8.79	33.12	0.0572	0.0092	-24.80	0.1692	0.0272	6.2085	0.1611	7.2432	0.1381	18.53	56.52	24.95
B6	T20	9.75	9.27	30.60	0.1061	0.0121	-24.60	0.3356	0.0383	8.7511	0.1143	10.2096	0.0979	31.12	47.32	21.55
B6	T21	12.25	11.64	35.62	0.1391	0.0140	-25.33	0.4544	0.0458	9.9239	0.1008	11.5778	0.0864	39.75	59.12	1.14
B6	T22	12.75	12.12	34.71	0.1344	0.0158	-25.01	0.3772	0.0445	8.4845	0.1179	9.8986	0.1010	32.76	66.01	1.23
B6	T23	18.25	17.35	37.09	0.0534	0.0095	-24.69	0.1537	0.0274	5.6055	0.1784	6.5398	0.1529	21.52	28.70	49.78
B6	T24	18.75	17.82	39.19	0.1000	0.0147	-24.30	0.2697	0.0396	6.8035	0.1470	7.9374	0.1260	25.70	31.14	43.16

Core	Sample ID	Midpoint Depth (cm)	z'	Sample Weight for C & N analyses (mg)	C (mg)	N (mg)	Delta PDB	% C weight	% N weight	%C/%N	%N/%C	mass C/N	mass N/C	% Clay	% Silt	% Sand
B6	T25	19.25	18.30	38.09	0.1815	0.0233	-24.67	0.4631	0.0595	7.7856	0.1284	9.0832	0.1101	38.18	42.56	19.27
B6	T26	19.75	18.77	35.84	0.1770	0.0217	-23.92	0.4648	0.0569	8.1669	0.1224	9.5280	0.1050	38.81	42.25	18.94
B6	T27	21.25	20.20	30.33	0.1268	0.0179	-25.01	0.3537	0.0499	7.0878	0.1411	8.2691	0.1209	36.75	39.55	23.70
B6	T28	21.75	20.67	31.79	0.1827	0.0230	-25.38	0.6022	0.0759	7.9320	0.1261	9.2540	0.1081	66.57	22.59	10.84
B6	T29	22.25	21.15	35.61	0.2216	0.0284	-25.46	0.6971	0.0893	7.8093	0.1281	9.1108	0.1098	66.22	29.46	4.32
B18	S1	0.5	0.54	39.14	0.1945	0.0277	-23.99	0.4970	0.0707	7.0329	0.1422	8.2051	0.1219	33.59	45.22	21.20
B18	S2	5.5	6.00	31.00	0.1575	0.0210	-24.24	0.5082	0.0679	7.4892	0.1335	8.7374	0.1145	37.66	55.48	6.86
B18	S3	10.5	11.45	33.87	0.1752	0.0238	-24.83	0.5172	0.0702	7.3718	0.1357	8.6005	0.1163	47.73	50.02	2.25
B18	S4	15.5	16.91	32.06	0.1481	0.0159	-25.02	0.3824	0.0411	9.3067	0.1075	10.8578	0.0921	28.97	70.19	0.84
B18	S5	20.5	22.36	35.26	0.1620	0.0192	-24.24	0.4155	0.0492	8.4374	0.1185	9.8436	0.1016	41.41	53.68	4.91
B18	S6	25.5	27.82	28.64	0.1860	0.0260	-24.43	0.5400	0.0754	7.1608	0.1396	8.3543	0.1197	43.62	50.22	6.15
B18	S7	30.5	33.27	33.25	0.0919	0.0133	-24.18	0.3208	0.0463	6.9248	0.1444	8.0789	0.1238	24.83	67.96	7.21
B18	S8	32.5	35.45	34.58	0.0694	0.0115	-24.87	0.2086	0.0345	6.0421	0.1655	7.0491	0.1419	19.96	72.41	7.63
B18	T1	8.25	9.00	35.15	0.1768	0.0221	-24.41	0.4949	0.0620	7.9822	0.1253	9.3125	0.1074	37.65	58.34	4.00
B18	T2	17.25	18.82	31.61	0.1482	0.0200	-23.98	0.4475	0.0604	7.4124	0.1349	8.6478	0.1156	45.45	52.74	1.81
B18	T3	19.25	21.00	28.07	0.1434	0.0161	-25.05	0.5109	0.0573	8.9188	0.1121	10.4053	0.0961	56.35	43.18	0.47
B18	T4	19.75	21.55	37.30	0.1802	0.0218	-24.96	0.4831	0.0585	8.2610	0.1211	9.6378	0.1038	39.88	59.63	0.49
B18	T5	21.75	23.73	32.15	0.2076	0.0239	-25.00	0.6459	0.0743	8.6948	0.1150	10.1440	0.0986	45.26	50.92	3.82
B18	T6	23.75	25.91	32.27	0.1513	0.0220	-25.17	0.4671	0.0679	6.8781	0.1454	8.0244	0.1246	40.47	58.16	1.37
B18	T7	24.25	26.45	32.22	0.1515	0.0186	-24.31	0.4702	0.0576	8.1616	0.1225	9.5219	0.1050	35.61	62.22	2.17
B18	T8	24.75	27.00	28.62	0.1442	0.0167	-25.07	0.5038	0.0584	8.6241	0.1160	10.0615	0.0994	54.34	44.27	1.39
B18	T9	28.75	31.36	33.55	0.1319	0.0160	-24.67	0.3932	0.0478	8.2317	0.1215	9.6036	0.1041	27.17	65.01	7.82
B24	S20	0.5	0.51	31.23	0.1667	0.0200	-25.11	0.5339	0.0641	8.3316	0.1200	9.7202	0.1029	27.61	62.07	10.32
B24	S21	5.5	5.66	33.90	0.1575	0.0203	-24.98	0.4648	0.0598	7.7779	0.1286	9.0742	0.1102	46.31	53.11	0.58
B24	S22	10.5	10.81	36.89	0.1702	0.0195	-24.49	0.4614	0.0528	8.7422	0.1144	10.1992	0.0980	33.71	61.81	4.48
B24	S23	15.5	15.96	35.27	0.1887	0.0212	-24.97	0.5350	0.0602	8.8870	0.1125	10.3682	0.0964	34.03	61.07	4.90
B24	S24	20.5	21.10	36.35	0.0813	0.0123	-24.11	0.2238	0.0337	6.6308	0.1508	7.7360	0.1293	19.30	79.88	0.82

Core	Sample ID	Midpoint	z'	Sample Weight for C & N analyses (mg)	C (mg)	N (mg)	Delta PDB	% C weight	% N weight	%C/%N	%N/%C	mass C/N	mass N/C	% Clay	% Silt	% Sand
B24	S25	25.5	26.25	25.85	0.1280	0.0147	-24.29	0.4952	0.0569	8.7047	0.1149	10.1555	0.0985	40.22	59.36	0.43
B24	S26	30.5	31.40	34.28	0.1721	0.0205	-24.56	0.5021	0.0599	8.3794	0.1193	9.7759	0.1023	52.59	46.72	0.69
B24	S27A	33.5	34.49	37.82	0.1099	0.0144	-24.73	0.2905	0.0381	7.6342	0.1310	8.9066	0.1123	65.29	34.54	0.17
B24	T31	6.75	6.95	30.46	0.1082	0.0136	-24.10	0.3450	0.0432	7.9812	0.1253	9.3114	0.1074	32.74	65.65	1.61
B24	T32	8.25	8.49	35.40	0.2335	0.0220	-25.84	0.7665	0.0722	10.6108	0.0942	12.3793	0.0808	64.06	34.82	1.12
B24	T33	8.75	9.01	33.85	0.2521	0.0261	-25.35	0.7122	0.0737	9.6687	0.1034	11.2802	0.0887	54.31	44.75	0.94
B24	T34	13.25	13.64	39.74	0.1840	0.0203	-24.95	0.5435	0.0598	9.0841	0.1101	10.5982	0.0944	37.11	61.55	1.34
B24	T35	16.75	17.24	38.89	0.1376	0.0175	-24.73	0.3463	0.0439	7.8851	0.1268	9.1992	0.1087	32.33	66.19	1.48
B24	T36	17.25	17.76	36.70	0.1371	0.0176	-24.79	0.3526	0.0454	7.7690	0.1287	9.0638	0.1103	32.25	64.16	3.59
B24	T37	17.75	18.27	33.51	0.1401	0.0171	-24.08	0.3819	0.0467	8.1856	0.1222	9.5499	0.1047	30.74	66.39	2.88
B24	T38	18.25	18.79	37.26	0.1401	0.0154	-24.58	0.4182	0.0461	9.0773	0.1102	10.5902	0.0944	30.86	65.95	3.19
B24	T39	23.25	23.93	39.49	0.1060	0.0133	-24.78	0.2684	0.0336	7.9788	0.1253	9.3086	0.1074	21.07	74.11	4.82
B24	T40	23.75	24.45	33.55	0.1134	0.0151	-25.00	0.3381	0.0450	7.5181	0.1330	8.7711	0.1140	29.30	68.24	2.46
B24	T41	27.25	28.05	36.61	0.0826	0.0122	-24.50	0.2257	0.0333	6.7834	0.1474	7.9140	0.1264	35.98	52.00	12.02
B25	S27B	0.5	0.39	37.45	0.1250	0.0163	-24.66	0.3337	0.0435	7.6789	0.1302	8.9587	0.1116	21.21	67.57	11.23
B25	S28	5.5	4.33	37.79	0.2019	0.0241	-24.88	0.5342	0.0637	8.3803	0.1193	9.7771	0.1023	18.91	69.70	11.39
B25	S29	10.5	8.27	37.85	0.1010	0.0135	-24.65	0.2667	0.0356	7.5003	0.1333	8.7504	0.1143	29.22	60.76	10.02
B25	S30	15.5	12.21	30.46	0.1468	0.0160	-25.58	0.4820	0.0526	9.1631	0.1091	10.6903	0.0935	29.83	62.99	7.19
B25	S31	20.5	16.15	37.04	0.1506	0.0143	-25.49	0.4067	0.0387	10.5142	0.0951	12.2666	0.0815	15.60	60.65	23.75
B25	S32	25.5	20.09	36.53	0.0819	0.0114	-25.25	0.2242	0.0311	7.2089	0.1387	8.4104	0.1189	11.13	61.26	27.61
B25	S33	30.5	24.03	33.61	0.1653	0.0195	-25.54	0.4919	0.0579	8.4941	0.1177	9.9098	0.1009	41.23	56.66	2.12
B25	T42	11.25	8.86	36.97	0.0653	0.0122	-24.59	0.1765	0.0330	5.3428	0.1872	6.2332	0.1604	19.94	65.11	14.94
B25	T43	13.25	10.44	33.65	0.2098	0.0220	-26.35	0.6236	0.0653	9.5447	0.1048	11.1355	0.0898	33.42	59.58	7.00
B25	T44	22.75	17.92	38.29	0.0666	0.0098	-25.00	0.1739	0.0257	6.7619	0.1479	7.8888	0.1268	17.63	65.77	16.60
B25	T45	27.25	21.47	35.89	0.1778	0.0199	-24.82	0.4954	0.0553	8.9545	0.1117	10.4470	0.0957	39.00	51.54	9.46
B25	T46	27.75	21.86	29.72	0.1444	0.0178	-24.37	0.4860	0.0598	8.1236	0.1231	9.4776	0.1055	46.86	50.78	2.36
B25	T47	31.25	24.62	38.48	0.1801	0.0207	-25.43	0.4680	0.0539	8.6863	0.1151	10.1340	0.0987	41.75	54.93	3.31
B25	T48	31.75	25.02	35.36	0.2145	0.0239	-24.96	0.6067	0.0675	8.9905	0.1112	10.4889	0.0953	35.57	59.03	5.40

Core	Sample ID	Midpoint Depth (cm)	z'	Sample Weight for C & N analyses (mg)	C (mg)	N (mg)	Delta PDB	% C weight	% N weight	%C/%N	%N/%C	mass C/N	mass N/C	% Clay	% Silt	% Sand
B52	S42	0.5	0.53	35.99	0.1777	0.0260	-23.38	0.5610	0.0822	6.8261	0.1465	7.9638	0.1256	38.44	57.59	3.97
B52	S43	5.5	5.81	37.43	0.2024	0.0263	-22.97	0.5622	0.0730	7.6975	0.1299	8.9804	0.1114	37.82	60.49	1.69
B52	S44	10.5	11.08	32.66	0.1855	0.0266	-23.39	0.4956	0.0711	6.9704	0.1435	8.1322	0.1230	38.38	58.98	2.64
B52	S45	15.5	16.36	35.72	0.1321	0.0200	-23.65	0.4045	0.0613	6.6010	0.1515	7.7012	0.1298	36.93	60.72	2.35
B52	S46	20.5	21.64	34.81	0.1665	0.0252	-23.74	0.4662	0.0705	6.6081	0.1513	7.7095	0.1297	46.30	50.16	3.54
B52	S47	25.5	26.92	33.67	0.1677	0.0230	-23.46	0.4818	0.0662	7.2814	0.1373	8.4949	0.1177			
B52	S48	30.5	32.19	35.84	0.1395	0.0198	-23.27	0.4144	0.0588	7.0478	0.1419	8.2225	0.1216	31.85	63.10	5.05
B52	S49	34.5	36.42	38.99	0.1558	0.0204	-23.72	0.4346	0.0569	7.6416	0.1309	8.9152	0.1122	33.91	60.60	5.49
B52	T56	13.75	14.51	31.94	0.1639	0.0265	-23.52	0.5133	0.0830	6.1823	0.1618	7.2127	0.1386	46.61	51.23	2.16
B52	T57	19.75	20.85	37.59	0.1972	0.0230	-23.07	0.5245	0.0613	8.5545	0.1169	9.9803	0.1002	41.53	55.44	3.03
B61	S34	0.5	0.61	37.55	0.1962	0.0237	-23.62	0.5224	0.0631	8.2839	0.1207	9.6646	0.1035	35.12	56.01	8.87
B61	S35	5.5	6.76	38.60	0.1998	0.0276	-24.71	0.5178	0.0715	7.2414	0.1381	8.4483	0.1184	44.71	51.39	3.91
B61	S36	10.5	12.90	37.41	0.2117	0.0287	-25.28	0.5659	0.0767	7.3829	0.1354	8.6133	0.1161	53.20	46.65	0.14
B61	S37	15.5	19.04	36.42	0.1618	0.0221	-25.10	0.4444	0.0608	7.3090	0.1368	8.5271	0.1173	51.37	48.53	0.11
B61	S38	20.5	25.19	33.26	0.2940	0.0347	-25.31	0.7891	0.0930	8.4810	0.1179	9.8945	0.1011	63.17	36.31	0.53
B61	S39	25.5	31.33	38.73	0.2918	0.0344	-25.75	0.8773	0.1033	8.4927	0.1177	9.9081	0.1009	69.49	29.91	0.61
B61	S40	30.5	37.47	35.21	0.2468	0.0318	-25.61	0.7699	0.0993	7.7528	0.1290	9.0450	0.1106	67.10	32.81	0.09
B61	S41	34.5	42.39	31.68	0.1442	0.0188	-24.47	0.4095	0.0533	7.6864	0.1301	8.9675	0.1115	68.68	31.24	0.08
B61	T49	13.25	16.28	30.17	0.1327	0.0184	-25.61	0.4397	0.0609	7.2212	0.1385	8.4247	0.1187	55.41	44.32	0.27
B61	T50	13.75	16.89	38.58	0.1951	0.0245	-24.93	0.5057	0.0636	7.9486	0.1258	9.2734	0.1078	56.59	43.17	0.24
B61	T51	14.25	17.51	32.20	0.1504	0.0189	-25.27	0.4671	0.0586	7.9784	0.1253	9.3081	0.1074	60.21	39.69	0.11
B61	T52	14.75	18.12	39.34	0.1754	0.0207	-24.60	0.4459	0.0526	8.4837	0.1179	9.8977	0.1010	59.14	40.23	0.63
B61	T53	17.75	21.81	36.22	0.1330	0.0171	-24.34	0.3674	0.0471	7.8011	0.1282	9.1013	0.1099	32.28	66.23	1.48
B61	T54	18.25	22.42	29.27	0.1796	0.0211	-24.87	0.6136	0.0721	8.5075	0.1175	9.9254	0.1008	53.32	44.91	1.77
B61	T55	18.75	23.04	33.14	0.2201	0.0242	-25.20	0.6640	0.0729	9.1043	0.1098	10.6217	0.0941	46.36	52.31	1.33
B85	S50	0.5	0.56	36.82	0.1374	0.0199	-24.09	0.3897	0.0564	6.9080	0.1448	8.0594	0.1241	24.42	50.20	25.72
B85	S51	5.5	6.13	34.70	0.1598	0.0174	-24.73	0.4340	0.0472	9.1907	0.1088	10.7225	0.0933	28.39	56.93	14.68

Core	Sample ID	Midpoint Depth (cm)	z'	Sample Weight for C & N analyses (mg)	C (mg)	N (mg)	Delta PDB	% C weight	% N weight	%C/%N	%N/%C	mass C/N	mass N/C	% Clay	% Silt	% Sand
B85	S52	10.5	11.70	30.44	0.1393	0.0191	-24.98	0.4016	0.0550	7.2958	0.1371	8.5118	0.1175	29.41	59.37	11.22
B85	S53	15.5	17.27	37.01	0.0969	0.0124	-24.30	0.3184	0.0409	7.7938	0.1283	9.0928	0.1100	26.31	55.61	18.07
B85	S54	20.5	22.84	31.50	0.1350	0.0178	-25.14	0.3648	0.0480	7.6007	0.1316	8.8675	0.1128	28.06	59.32	12.62
B85	S55	25.5	28.41	32.76	0.1241	0.0141	-24.89	0.3940	0.0449	8.7794	0.1139	10.2426	0.0976	30.91	55.40	13.69
B85	S56	30.5	33.99	38.13	0.1206	0.0139	-24.85	0.3680	0.0424	8.6819	0.1152	10.1289	0.0987	31.34	46.16	22.50
B85	S57	34.5	38.44	34.45	0.1317	0.0170	-24.34	0.3454	0.0447	7.7325	0.1293	9.0212	0.1108	33.67	44.72	21.60
B85	T58	8.25	9.19	32.61	0.1379	0.0186	-23.97	0.4228	0.0571	7.4015	0.1351	8.6350	0.1158	30.33	59.20	10.47
B85	T59	9.75	10.86	36.63	0.1379	0.0174	-24.24	0.3765	0.0475	7.9235	0.1262	9.2440	0.1082	32.67	59.43	7.91
B85	T60	11.75	13.09	34.16	0.1232	0.0150	-24.65	0.3819	0.0465	8.2047	0.1219	9.5722	0.1045	35.64	53.13	11.24
B85	T61	13.25	14.76	34.47	0.2205	0.0275	-25.77	0.6453	0.0804	8.0305	0.1245	9.3689	0.1067	25.35	62.83	11.82
B85	T62	17.75	19.78	38.42	0.1315	0.0186	-24.81	0.3814	0.0540	7.0637	0.1416	8.2410	0.1213	33.01	54.91	12.08
B85	T63	22.75	25.35	32.40	0.1293	0.0182	-24.84	0.3366	0.0473	7.1099	0.1406	8.2949	0.1206	23.80	60.69	15.51

z': Corrected midpoint depth (cm) – see Chapter 2, *Equation 1*, pg. 61.

Appendix 9B: Kilo Moana survey (S) and target (T) ^{210}Pb analyses.

Core	Sample ID	^{210}Pb Total Activity (dpm/g)	^{210}Pb Error (dpm/g)	Supported ^{210}Pb Activity (dpm/g)	^{210}Pb Excess Activity (dpm/g)	^{210}Pb Excess Activity Error (dpm/g)
B3	S10	1.19	0.03	-	-	-
B3	S11	1.11	0.02	-	-	-
B3	S12	0.89	0.05	-	-	-
B3	S13	0.80	0.10	-	-	-
B3	S9	1.68	0.04	-	-	-
B3	T10	0.88	0.02	-	-	-
B3	T11	1.08	0.02	-	-	-
B3	T12	1.45	0.03	-	-	-
B3	T13	1.57	0.03	-	-	-
B3	T14	1.07	0.09	-	-	-
B3	T15	1.08	0.07	-	-	-
B3	T16	1.04	0.03	-	-	-
B3	T17	1.22	0.04	-	-	-
B6	S14	1.07	0.03	-	-	-
B6	S15	0.80	0.02	-	-	-
B6	S16	1.23	0.03	-	-	-
B6	S17	0.79	0.05	-	-	-
B6	S18	1.67	0.17	-	-	-
B6	S19	0.85	0.06	-	-	-
B6	T18	0.89	0.03	-	-	-
B6	T19	0.96	0.02	-	-	-
B6	T20	0.90	0.06	-	-	-
B6	T21	1.08	0.04	-	-	-
B6	T22	1.11	0.07	-	-	-
B6	T23	1.06	0.09	-	-	-
B6	T24	1.55	0.04	-	-	-
B6	T25	2.62	0.07	-	-	-
B6	T26	2.23	0.05	-	-	-
B6	T27	1.39	0.12	-	-	-
B6	T28	1.56	0.07	-	-	-
B6	T29	1.42	0.11	-	-	-
B18	S1	4.31	0.09	-	-	-
B18	S2	2.95	0.06	-	-	-
B18	S3	2.23	0.03	-	-	-
B18	S4	1.20	0.03	-	-	-
B18	S5	1.49	0.07	-	-	-
B18	S6	2.80	0.08	-	-	-
B18	S7	1.56	0.13	-	-	-
B18	S8	0.99	0.04	-	-	-
B18	T1	2.23	0.05	-	-	-
B18	T2	1.63	0.06	-	-	-
B18	T3	1.33	0.03	-	-	-

Core	Sample ID	^{210}Pb Total Activity (dpm/g)	^{210}Pb Error (dpm/g)	Supported ^{210}Pb Activity (dpm/g)	^{210}Pb Excess Activity (dpm/g)	^{210}Pb Excess Activity Error (dpm/g)
B18	T4	1.20	0.03	-	-	-
B18	T5	1.52	0.12	-	-	-
B18	T6	1.43	0.10	-	-	-
B18	T7	1.99	0.06	-	-	-
B18	T8	2.23	0.10	-	-	-
B18	T9	1.65	0.05	-	-	-
B24	S20	3.00	0.08	-	-	-
B24	S21	1.66	0.04	-	-	-
B24	S22	1.67	0.04	-	-	-
B24	S23	1.71	0.04	-	-	-
B24	S24	0.86	0.03	-	-	-
B24	S25	1.70	0.07	-	-	-
B24	S26	1.28	0.06	-	-	-
B24	S27A	1.19	0.06	-	-	-
B24	T31	1.50	0.04	-	-	-
B24	T32	1.45	0.04	-	-	-
B24	T33	1.48	0.02	-	-	-
B24	T34	1.61	0.03	-	-	-
B24	T35	1.27	0.11	-	-	-
B24	T36	1.59	0.07	-	-	-
B24	T37	1.49	0.10	-	-	-
B24	T38	1.45	0.11	-	-	-
B24	T39	1.21	0.07	-	-	-
B24	T40	1.17	0.05	-	-	-
B24	T41	1.76	0.05	-	-	-
B25	S27B	2.03	0.06	-	-	-
B25	S28	1.81	0.04	-	-	-
B25	S29	1.87	0.04	-	-	-
B25	S30	1.51	0.02	-	-	-
B25	S31	1.07	0.03	-	-	-
B25	S32	0.89	0.22	-	-	-
B25	S33	1.35	0.04	-	-	-
B25	T42	1.57	0.04	-	-	-
B25	T43	1.71	0.03	-	-	-
B25	T44	1.03	0.08	-	-	-
B25	T45	1.19	0.06	-	-	-
B25	T46	1.15	0.04	-	-	-
B25	T47	1.24	0.05	-	-	-
B25	T48	1.17	0.03	-	-	-
B52	S42	4.86	0.10	0.80	4.25	0.23
B52	S43	4.95	0.10	0.80	4.34	0.23
B52	S44	4.39	0.09	0.80	3.75	0.22
B52	S45	3.36	0.08	0.80	2.88	0.20

Core	Sample ID	^{210}Pb Total Activity (dpm/g)	^{210}Pb Error (dpm/g)	Supported ^{210}Pb Activity (dpm/g)	^{210}Pb Excess Activity (dpm/g)	^{210}Pb Excess Activity Error (dpm/g)
B52	S46	3.56	0.05	0.80	1.65	0.18
B52	S47	2.59	0.04	0.80	1.33	0.17
B52	S48	2.38	0.12	0.80	3.14	0.25
B52	S49	2.07	0.06	0.80	2.23	0.19
B52	T56	3.80	0.07	0.80	2.67	0.20
B52	T57	2.94	0.05	0.80	1.87	0.18
B61	S34	4.20	0.09	-	-	-
B61	S35	3.31	0.07	-	-	-
B61	S36	1.43	0.03	-	-	-
B61	S37	1.27	0.03	-	-	-
B61	S38	1.85	0.10	-	-	-
B61	S39	1.44	0.04	-	-	-
B61	S40	1.37	0.11	-	-	-
B61	S41	1.40	0.09	-	-	-
B61	T49	1.39	0.04	-	-	-
B61	T50	1.31	0.04	-	-	-
B61	T51	1.25	0.04	-	-	-
B61	T52	1.31	0.03	-	-	-
B61	T53	1.76	0.10	-	-	-
B61	T54	2.74	0.04	-	-	-
B61	T55	2.69	0.05	-	-	-
B85	S50	2.99	0.06	0.58	2.51	0.19
B85	S51	2.98	0.06	0.58	2.51	0.19
B85	S52	2.01	0.03	0.58	0.96	0.16
B85	S53	1.93	0.02	0.58	0.55	0.15
B85	S54	1.50	0.05	0.58	1.89	0.18
B85	S55	1.46	0.05	0.58	1.55	0.17
B85	S56	1.22	0.05	0.58	1.28	0.18
B85	S57	1.11	0.03	0.58	0.81	0.16
B85	T58	2.64	0.05	0.58	1.49	0.17
B85	T59	2.39	0.05	0.58	1.41	0.18
B85	T60	2.07	0.04	0.58	0.92	0.16
B85	T61	2.07	0.03	0.58	0.67	0.15
B85	T62	1.81	0.07	0.58	2.15	0.20
B85	T63	1.35	0.06	0.58	1.55	0.18

Appendix 9C: Kilo Moana bulk density data

	B3			B6			B18			B24			B25			B52			B61			B85		
Depth (cm)	A	B	C	A	B	C	A	B	C	A	B	C	A	B	C	A	B	C	A	B	C	A	B	C
0	1.86	0.48	1.44	1.84	0.52	1.34	1.46	0.73	0.77	1.73	0.58	1.17	1.84	0.52	1.34	1.51	0.72	0.81	1.49	0.72	0.81	1.73	0.59	1.15
1	1.76	0.54	1.28	2.11	0.37	1.74	1.48	0.73	0.79	1.75	0.57	1.20	1.88	0.50	1.40	1.55	0.70	0.87	1.59	0.66	0.96	1.73	0.59	1.15
2	1.85	0.48	1.44	2.16	0.33	1.83	1.55	0.69	0.89	1.73	0.58	1.17	1.94	0.47	1.48	1.60	0.67	0.95	1.61	0.65	0.99	1.75	0.58	1.18
3	1.97	0.41	1.62	2.14	0.35	1.79	1.57	0.67	0.93	1.72	0.59	1.16	1.91	0.48	1.45	1.60	0.67	0.94	1.61	0.65	0.98	1.78	0.56	1.22
4	1.83	0.50	1.40	2.16	0.34	1.82	1.59	0.66	0.95	1.71	0.59	1.15	1.86	0.51	1.37	1.60	0.67	0.95	1.58	0.67	0.94	1.77	0.57	1.21
5	1.96	0.42	1.61	2.16	0.34	1.82	1.63	0.64	1.01	1.76	0.57	1.21	1.79	0.55	1.27	1.65	0.64	1.03	1.56	0.68	0.91	1.78	0.56	1.23
6	1.83	0.50	1.40	2.20	0.32	1.88	1.60	0.66	0.97	1.81	0.54	1.29	1.79	0.55	1.26	1.67	0.63	1.05	1.53	0.70	0.87	1.70	0.61	1.10
7	1.92	0.44	1.54	2.22	0.30	1.92	1.56	0.68	0.91	1.69	0.60	1.11	1.84	0.52	1.34	1.63	0.65	1.00	1.58	0.67	0.95	1.78	0.56	1.22
8	1.77	0.53	1.30	2.06	0.39	1.67	1.59	0.66	0.96	1.75	0.57	1.20	1.85	0.52	1.35	1.63	0.65	1.00	1.55	0.68	0.91	1.80	0.55	1.25
9	1.76	0.54	1.29	1.81	0.54	1.30	1.59	0.66	0.95	1.81	0.54	1.29	1.89	0.49	1.41	1.59	0.67	0.93	1.59	0.66	0.96	1.77	0.57	1.21
10	1.95	0.43	1.59	1.82	0.53	1.30	1.58	0.67	0.94	1.80	0.54	1.28	1.85	0.51	1.36	1.61	0.66	0.97	1.60	0.65	0.98	1.74	0.59	1.16
11	1.80	0.51	1.36	1.89	0.49	1.42	1.60	0.66	0.97	1.81	0.54	1.29	1.87	0.50	1.39	1.63	0.65	1.00	1.61	0.65	0.99	1.71	0.60	1.12
12	1.96	0.42	1.61	1.99	0.43	1.57	1.58	0.67	0.94	1.75	0.57	1.20	1.89	0.49	1.41	1.66	0.63	1.04	1.60	0.66	0.98	1.74	0.59	1.16
13	1.96	0.42	1.61	2.08	0.38	1.70	1.61	0.65	0.99	1.74	0.58	1.18	1.92	0.47	1.47	1.62	0.65	0.99	1.60	0.65	0.98	1.73	0.59	1.15
14	1.94	0.43	1.58	2.10	0.37	1.73	1.61	0.65	0.98	1.78	0.55	1.25	1.92	0.47	1.47	1.66	0.63	1.04	1.57	0.68	0.93	1.75	0.58	1.18
15	1.98	0.41	1.64	2.10	0.37	1.74	1.70	0.60	1.13	1.83	0.53	1.32	1.94	0.46	1.49	1.66	0.63	1.04	1.66	0.62	1.07	1.79	0.56	1.24
16	1.98	0.40	1.64	2.09	0.38	1.72	1.74	0.58	1.19	1.90	0.49	1.43	1.93	0.47	1.47	1.62	0.66	0.97	1.57	0.67	0.93	1.79	0.56	1.24
17	2.04	0.37	1.74	2.12	0.36	1.76	1.57	0.67	0.93	1.99	0.44	1.56	1.94	0.46	1.48	1.67	0.63	1.06	1.53	0.70	0.87	1.76	0.58	1.19
18	2.08	0.35	1.80	1.90	0.48	1.43	1.59	0.66	0.96	2.03	0.41	1.62	1.81	0.54	1.29	1.66	0.63	1.04	1.48	0.72	0.80	1.79	0.55	1.25
19	2.14	0.31	1.89	1.92	0.47	1.46	1.62	0.64	1.01	2.04	0.41	1.64	1.70	0.60	1.13	1.66	0.63	1.04	1.48	0.72	0.80	1.79	0.56	1.24
20	2.11	0.33	1.85	2.07	0.39	1.68	1.63	0.64	1.01	2.03	0.41	1.63	1.74	0.58	1.19	1.65	0.64	1.03	1.48	0.72	0.80	1.74	0.58	1.17
21				1.85	0.51	1.36	1.65	0.63	1.05	1.98	0.44	1.56	1.84	0.52	1.34	1.66	0.63	1.05	1.52	0.70	0.85	1.74	0.59	1.16
22				1.80	0.54	1.28	1.60	0.66	0.98	1.87	0.50	1.38	1.86	0.51	1.37	1.69	0.62	1.08	1.51	0.71	0.83	1.74	0.59	1.16
23				1.71	0.60	1.14	1.53	0.69	0.88	1.79	0.55	1.27	1.66	0.62	1.07	1.73	0.59	1.14	1.51	0.71	0.84	1.76	0.57	1.20
24				1.72	0.59	1.16	1.59	0.66	0.97	1.82	0.53	1.30	1.75	0.57	1.20	1.68	0.62	1.08	1.50	0.71	0.83	1.79	0.55	1.25
25				1.69	0.60	1.11	1.57	0.67	0.93	1.81	0.54	1.30	1.68	0.61	1.09	1.70	0.61	1.10	1.50	0.71	0.83	1.82	0.54	1.29

	B3			B6			B18			B24			B25			B52			B61			B85		
Depth (cm)	A	B	C	A	B	C	A	B	C	A	B	C	A	B	C	A	B	C	A	B	C	A	B	C
26							1.49	0.72	0.81	1.75	0.57	1.20	1.59	0.66	0.96	1.74	0.58	1.17	1.56	0.68	0.91	1.80	0.55	1.25
27							1.65	0.63	1.04	1.74	0.58	1.19				1.72	0.60	1.13	1.53	0.70	0.87	1.87	0.51	1.37
28							1.73	0.58	1.18	1.78	0.56	1.24				1.67	0.63	1.06	1.55	0.69	0.89	1.83	0.53	1.31
29							1.84	0.52	1.34	1.74	0.58	1.19				1.69	0.62	1.08	1.53	0.70	0.87	1.81	0.55	1.27
30							1.88	0.50	1.39	1.70	0.60	1.13				1.71	0.60	1.12	1.52	0.70	0.85	1.85	0.52	1.34
31							1.84	0.52	1.34	1.70	0.60	1.13				1.70	0.61	1.10	1.53	0.70	0.87	1.78	0.56	1.22
32							1.87	0.50	1.38	1.81	0.54	1.29				1.71	0.60	1.12	1.54	0.69	0.88	1.76	0.58	1.19
33							1.93	0.47	1.47	1.70	0.60	1.12				1.69	0.62	1.08	1.56	0.68	0.91	1.81	0.54	1.28
34							1.96	0.45	1.51	1.70	0.60	1.13				1.68	0.62	1.07	1.54	0.69	0.88	1.84	0.53	1.32
35							1.99	0.44	1.56	1.79	0.55	1.26				1.64	0.65	1.00	1.55	0.69	0.89	1.85	0.52	1.34
36							1.76	0.56	1.22							1.60	0.67	0.94	1.54	0.69	0.89	1.87	0.51	1.36
37																1.60	0.67	0.95	1.55	0.68	0.91	1.85	0.52	1.33
38																1.63	0.65	0.99	1.54	0.69	0.88	1.84	0.53	1.31
39																			1.53	0.70	0.86	1.80	0.55	1.25
40																			1.54	0.69	0.88			
41																			1.52	0.70	0.85			
42																			1.50	0.72	0.82			
43																			1.49	0.72	0.81			

Depth: Depth into core (cm) accounting for foam spacer.
A: Multi-sensor Core Logger (MSCL) bulk density.
B: MSCL fractional porosity.
C: Calculated dry bulk density (g cc^{-1}). See Chapter 2, Section 2.2 (pg. 59).

VITA

Lila Eve Rose Pierce

Born in Portchester, N.Y., February 23, 1981. Graduated from Pelham Memorial High School in 1999. Earned a M.A. in Geology and English Language and Literature from Smith College in 2003. Her Highest Honors thesis was entitled "Stress Bands in Belizean Patch Reef Corals: Their Use as Paleoclimate Indicators." Received a M.S. in Marine Sciences from The College of William & Mary, Virginia Institute of Marine Science, School of Marine Sciences in 2008. Her thesis was entitled "Recent Sedimentation Patterns and Facies Distribution on the Waipaoa River Shelf, N.Z." Entered the doctoral program at The College of William & Mary, Virginia Institute of Marine Science, School of Marine Sciences in 2008.